ISSN 1007-9327 (print)
ISSN 2219-2840 (online)

World Journal of *Gastroenterology*

World J Gastroenterol 2019 November 28; 25(44): 6483-6578

Published by Baishideng Publishing Group Inc

World Journal of Gastroenterology

Contents

Weekly Volume 25 Number 44 November 28, 2019

MINIREVIEWS

ORIGINAL ARTICLE

Basic Study

Retrospective Study

Observational Study

SYSTEMATIC REVIEW

CASE REPORT

Contents

World Journal of Gastroenterology

Volume 25 Number 44 November 28, 2019

ABOUT COVER

Editorial board member of *World Journal of Gastroenterology*, Alfred Gangl, MD, Professor, Department of Medicine III, Division of Gastroenterology and Hepatology, Medical University of Vienna, Allgemeines Krankenhaus, Vienna A-1090, Austria

AIMS AND SCOPE

The primary aim of *World Journal of Gastroenterology* (*WJG*, *World J Gastroenterol*) is to provide scholars and readers from various fields of gastroenterology and hepatology with a platform to publish high-quality basic and clinical research articles and communicate their research findings online.

WJG mainly publishes articles reporting research results and findings obtained in the field of gastroenterology and hepatology and covering a wide range of topics including gastroenterology, hepatology, gastrointestinal endoscopy, gastrointestinal surgery, gastrointestinal oncology, and pediatric gastroenterology.

INDEXING/ABSTRACTING

The *WJG* is now indexed in Current Contents®/Clinical Medicine, Science Citation Index Expanded (also known as SciSearch®), Journal Citation Reports®, Index Medicus, MEDLINE, PubMed, PubMed Central, and Scopus. The 2019 edition of Journal Citation Report® cites the 2018 impact factor for *WJG* as 3.411 (5-year impact factor: 3.579), ranking *WJG* as 35th among 84 journals in gastroenterology and hepatology (quartile in category Q2). CiteScore (2018): 3.43.

RESPONSIBLE EDITORS FOR THIS ISSUE

Responsible Electronic Editor: *Yan-Liang Zhang*

Proofing Production Department Director: *Xiang Li*

NAME OF JOURNAL
World Journal of Gastroenterology

ISSN
ISSN 1007-9327 (print) ISSN 2219-2840 (online)

LAUNCH DATE
October 1, 1995

FREQUENCY
Weekly

EDITORS-IN-CHIEF
Subrata Ghosh, Andrzej S Tarnawski

EDITORIAL BOARD MEMBERS
http://www.wjgnet.com/1007-9327/editorialboard.htm

EDITORIAL OFFICE
Ze-Mao Gong, Director

PUBLICATION DATE
November 28, 2019

INSTRUCTIONS TO AUTHORS
https://www.wjgnet.com/bpg/gerinfo/204

GUIDELINES FOR ETHICS DOCUMENTS
https://www.wjgnet.com/bpg/GerInfo/287

GUIDELINES FOR NON-NATIVE SPEAKERS OF ENGLISH
https://www.wjgnet.com/bpg/gerinfo/240

PUBLICATION MISCONDUCT
https://www.wjgnet.com/bpg/gerinfo/208

ARTICLE PROCESSING CHARGE
https://www.wjgnet.com/bpg/gerinfo/242

STEPS FOR SUBMITTING MANUSCRIPTS
https://www.wjgnet.com/bpg/GerInfo/239

ONLINE SUBMISSION
https://www.f6publishing.com

World Journal of Gastroenterology

Submit a Manuscript: https://www.f6publishing.com

World J Gastroenterol 2019 November 28; 25(44): 6483-6494

DOI: 10.3748/wjg.v25.i44.6483

ISSN 1007-9327 (print) ISSN 2219-2840 (online)

MINIREVIEWS

Inositol 1,4,5-trisphosphate receptor in the liver: Expression and function

Fernanda de Oliveira Lemos, Rodrigo M Florentino, Antônio Carlos Melo Lima Filho, Marcone Loiola dos Santos, M Fatima Leite

ORCID number: Fernanda de Oliveira Lemos (0000-0002-7070-4412); Rodrigo M Florentino (0000-0001-7033-176X); Antônio Carlos Melo Lima Filho (0000-0002-8185-669X); Marcone Loiola dos Santos (0000-0001-8835-2104); M Fatima Leite (0000-0001-9709-8865).

Author contributions: All authors contributed to this paper with literature review and analysis, drafting and critical revision and editing, and approval of the final version.

Conflict-of-interest statement: No potential conflicts of interest. No financial support.

Manuscript source: Unsolicited manuscript

Received: August 18, 2019
Peer-review started: August 18, 2019
First decision: October 14, 2019

Fernanda de Oliveira Lemos, Rodrigo M Florentino, Antônio Carlos Melo Lima Filho, M Fatima Leite, Department of Physiology and Biophysics, Universidade Federal de Minas Gerais, Belo Horizonte, Minas Gerais 31270-901, Brazil

Marcone Loiola dos Santos, Department of Cell Biology, Universidade Federal de Minas Gerais, Belo Horizonte, Minas Gerais 31270-901, Brazil

Corresponding author: M Fatima Leite, PhD, Full Professor, Department of Physiology and Biophysics, Federal University of Minas Gerais, Av. Antônio Carlos 6627, Belo Horizonte, Minas Gerais 31270-901, Brazil. leitemd@ufmg.br
Telephone: +55-31-34092518
Fax: +55-31-34092947

Abstract

The liver is a complex organ that performs several functions to maintain homeostasis. These functions are modulated by calcium, a second messenger that regulates several intracellular events. In hepatocytes and cholangiocytes, which are the epithelial cell types in the liver, inositol 1,4,5-trisphosphate ($InsP_3$) receptors (ITPR) are the only intracellular calcium release channels. Three isoforms of the ITPR have been described, named type 1, type 2 and type 3. These ITPR isoforms are differentially expressed in liver cells where they regulate distinct physiological functions. Changes in the expression level of these receptors correlate with several liver diseases and hepatic dysfunctions. In this review, we highlight how the expression level, modulation, and localization of ITPR isoforms in hepatocytes and cholangiocytes play a role in hepatic homeostasis and liver pathology.

Key words: Inositol 1,4,5-trisphosphate receptor; Liver; Calcium signaling; Hepatocytes and cholangiocytes

Core tip: Calcium regulates a variety of functions in our body. In the liver, inositol 1,4,5-trisphosphate receptors (ITPR) are the only expressed intracellular calcium release channels. ITPR regulates liver functions under healthy situation, but they can also be involved in liver diseases, depending for instance, in which isoform is expressed in a specific cell type, level of expression and where inside the cell each isoform is expressed. In this review, we discuss about ITPR roles in hepatic cells in physiological

Revised: October 22, 2019
Accepted: November 13, 2019
Article in press: November 13, 2019
Published online: November 28, 2019

P-Reviewer: Morales-González JA, Sun XT
S-Editor: Wang J
L-Editor: A
E-Editor: Zhang YL

and pathological conditions.

Citation: Lemos FO, Florentino RM, Lima Filho ACM, Santos MLD, Leite MF. Inositol 1,4,5-trisphosphate receptor in the liver: Expression and function. *World J Gastroenterol* 2019; 25(44): 6483-6494
URL: https://www.wjgnet.com/1007-9327/full/v25/i44/6483.htm
DOI: https://dx.doi.org/10.3748/wjg.v25.i44.6483

INTRODUCTION

The liver is an important and vital organ that regulates several functions, ranging from drug and macronutrient metabolism to immune system support[1-5]. Essentially all liver functions are at some point regulated by intracellular calcium (Ca^{2+}). In hepatocytes and cholangiocytes, the principal epithelial cell types of the liver, inositol 1,4,5-trisphosphate ($InsP_3$) receptors (ITPR) are the only intracellular Ca^{2+} release channels[6,7]. There are three types of ITPR: type 1 (ITPR1), type 2 (ITPR2) and type 3 (ITPR3)[8,9], and these receptors are expressed mainly along the endoplasmic and nucleoplasmic reticulum[10,11].

Dysregulation in the expression of ITPR can be a cause of several liver disorders, or can be involved in the development of diseases, such as cholestasis[12] and non-alcoholic fatty liver disease (NAFLD)[13]. In this review, we will discuss the expression and the physiological functions of each isoform of ITPR present in liver hepatocytes and cholangiocytes as well as their role in disease (Table 1).

LIVER

The liver is the largest internal organ[5] and is responsible for drug metabolism, albumin production, glycogen storage, cholesterol synthesis, bile secretion, and many other functions[14]. The liver is mostly composed of hepatocytes, which account for 80% of all cells in this organ[15]. The remaining 20% is composed mostly of cholangiocytes, Kupffer cells, stellate cells and liver sinusoidal endothelial cells[15]. Macroscopically, the liver is divided in four anatomic lobes, called the left, right, caudate and quadrate lobe[16,17]. In each lobe the cells are organized in a specific conformation, constituting a microscopic functional and structural unit, the lobule[14,18] (Figure 1). In the lobule, the hepatocytes are arranged in cords, connecting the portal triad to the central vein. In the space formed among the hepatocyte cords are the liver sinusoidal endothelial cells, the Kupffer cells, which are the resident macrophages in the liver, and the stellate cells, a cell type that stores vitamin A in its cytosol and secrets hepatocyte growth factor (HGF)[14,19,20].

As an epithelial cell, the hepatocyte is polarized, with a basolateral membrane in contact with the sinusoids and an apical side forming the biliary canaliculus. The biliary canaliculus is a virtual space between two hepatocytes, into which hepatocytes secrete bile acids[4]. The biliary canaliculi join to form the bile duct, which is lined by cholangiocytes, specialized cells that secrete electrolytes and fluids into the bile, altering bile composition and viscosity. The bile duct conducts the bile to the gallbladder, where it is stored until its content are needed to help lipid digestion[21,22].

Blood from the portal vein passes throughout the sinusoids and drains into the central vein[14,23]. Near the portal vein there are two other important structures: the hepatic artery and the bile duct. Together, these structures form the portal triad. The hepatocytes around this area are more highly oxygenated than those that are closer to the central vein, because the blood reaches the portal triad first[14]. This region in the lobule is called zone 1, while zone 2 is the transitional zone, and zone 3 is the region near the central vein[24,25] (Figure 2). It has been shown that based on their zonal position, hepatocytes regulate specific liver functions. For example, hepatocytes in zone 1 are more involved in producing albumin and proteins of both the complement system and coagulation pathway, while hepatocytes from zone 3 are more important for drug metabolism and bile production[26].

Due to the key role of the liver in metabolism, hepatic tissue is continuously exposed to insults from xenobiotics, toxic metabolites and infectious agents[2]. As result of this, the liver has a remarkable capacity for regeneration. In mice, liver functions are restored within days of removing two-thirds of the organ. This capacity

Table 1 Functions of inositol 1,4,5-trisphosphate receptor isoforms in hepatocytes and cholangiocytes

ITPR isoform	Cell type	Function	Ref.
ITPR1	Hepatocytes	Glucose secretion	[64]
		Lipid metabolism	[63,65]
		Liver regeneration	[66,67]
	Cholangiocytes	Bicarbonate secretion	[12,61]
ITPR2	Hepatocytes	Organic anion secretion	[6,62,69]
		Liver regeneration	[13,71]
	Cholangiocytes	bicarbonate secretion	[12,61]
ITPR3	Hepatocytes	Physiologically absent	[6]
		Proliferation and survival of hepatocellular carcinoma	[74]
	Cholangiocytes	Bicarbonate secretion	[12,61]
		Proliferation, migration, and survival of cholangiocarcinoma	[82]

ITPR: Inositol 1,4,5-trisphosphate receptor; ITPR1: ITPR isoform 1; ITPR2: ITPR isoform 2; ITPR3: ITPR isoform 3.

is also observed in humans for which liver function after partial hepatectomy is reestablished within a few weeks[27]. In many cases of liver disease, for which partial hepatectomy is indicated as a treatment, a small piece of healthy liver is implanted to drive hepatic tissue regeneration[27,28]. The path to regeneration depends on the extent of liver loss. When 1/3 of the liver is removed, the primary response is hepatocyte cellular hypertrophy, *i.e.*, an increase in cell size. When liver loss reaches 2/3, hepatocyte hyperplasia, an increase of the number of hepatocytes occurs to reestablish liver function. When 80-90 % of the liver is removed, the biliary epithelial cells (BEC) turn into progenitor cells, which differentiate into hepatocytes or BEC[28] that are able to regenerate the tissue. Liver regeneration is a complex process and the mechanism by which the hepatocytes stop proliferating after reestablishment of liver function is poorly understood. It is important to highlight that Ca^{2+} signaling, and consequently the ITPR isoforms, play an essential role in liver regeneration, as discussed below.

CALCIUM SIGNALING AND ITPRs

Many biological functions are regulated by intracellular Ca^{2+}. These include cell proliferation, gene expression, secretion, motility and cell death, among others[29-33]. As in other tissues, Ca^{2+} signaling in the liver starts with the binding of an agonist to a receptor, which may be a G protein-coupled receptor (GPCR) (Figure 3) or a tyrosine kinase receptor (RTK). Upon agonist-receptor binding, phospholipase C (PLC) is activated (typically isoform PLCβ when GPCR is activated or isoform PLCγ after RTK activation), causing breakdown of the membrane phospholipid phosphatidylinositol 4,5-bisphosphate (PIP_2), that generates diacylglycerol (DAG) and $InsP_3$. DAG remains at the plasma membrane while $InsP_3$ diffuses into the cytoplasm where it can bind to the $InsP_3$ receptor (ITPR) localized along the endoplasmic reticulum membrane, nuclear envelope or nucleoplasmic reticulum. $InsP_3$-ITPR binding causes a conformational change in the ITPR, leading to the release of internal Ca^{2+} stores[32,34]. $InsP_3$ is inactivated either after conversion to inositol 1,2-bisphosphate ($InsP_2$) by type I inositol polyphosphate 5-phosphatase or by $InsP_3$3-kinase mediated phosphorylation, forming inositol 1,3,4,5-tetrakisphosphate ($InsP_4$)[35,36].

Because of the toxic effect of high concentrations of Ca^{2+} to the cells, this ion is promptly removed from the cytosol after its release. Different mechanisms are involved in this process, including the activation of plasma membrane Ca^{2+}-ATPase or Na^+/Ca^{2+} exchanger that exports Ca^{2+} out of the cell, while sarco-/endoplasmic Ca^{2+}-ATPase (SERCA) and mitochondrial Ca^{2+} uptake 1 (MCU1) move Ca^{2+} into the endoplasmic reticulum and mitochondria, respectively[37,38].

The ITPRs are formed by approximately 2700 amino acids[39,40] and are organized in three domains: a N-terminal domain, which includes the $InsP_3$-binding region, a C-terminal domain, which forms the channel pore, and a regulatory domain between the other regions (Figure 4). ITPR is an intrinsic membrane protein, with 6 transmembrane segments[41,42]. There are some sites along the ITPR structure that regulate the activity of the receptor, or determine its localization by posttranslational modifications (phosphorylation, ubiquitination, oxidation, and proteolytic frag-

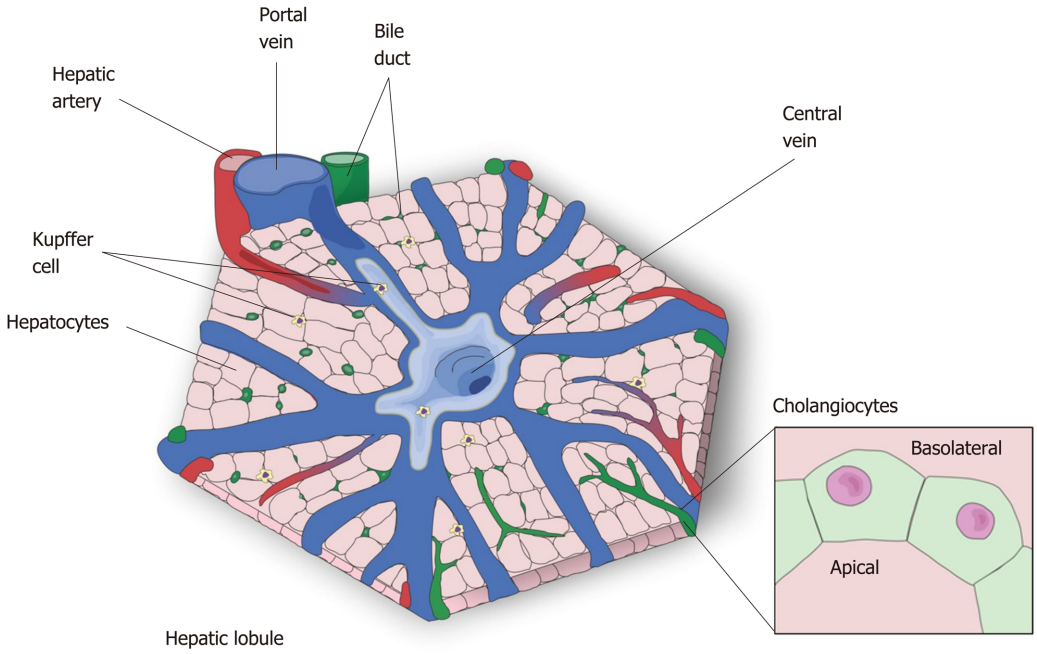

Figure 1 The hepatic lobule-the microscopic functional structure of the liver. The hepatocytes are arranged in cordon, connecting the central vein to the portal triad, which is formed by a hepatic artery, a portal vein and a bile duct. The other represented cell types are: *Kupffer cell*, resident macrophages responsible for the immunologic response in the liver, and *cholangiocytes* which form the bile duct that transport bile to the gallbladder.

mentation) or by interaction with modulatory proteins, such as chromogranin A and B, neuronal Ca^{2+} sensor 1, cytochrome c, and antiapoptotic Bcl-2 family members[43-46]. There are three isoforms of ITPR: type 1 (ITPR1), type 2 (ITPR2) and type 3 (ITPR3)[8,9]. They share 70% homology[47], however each isoform of ITPR displays a distinct affinity to $InsP_3$: ITPR2 has the highest affinity, ITPR1 has an intermediate affinity, and ITPR3 has the lowest affinity[48,49]. In order to open the Ca^{2+} channel, four $InsP_3$ molecules need to bind to ITPR[50]. Moreover, Ca^{2+} ions directly modulate the open probability of the channel[51,52]. ITPR1 displays what is called a "bell shape" open probability curve, in other words, at lower concentrations of Ca^{2+} the ITPR1 releases Ca^{2+}, while higher Ca^{2+} concentrations inhibit the channel[53,54]. For ITPR3, the open probability of the channel increases with increased Ca^{2+} concentration[52,55], and the ITPR2 dependence on Ca^{2+} concentration remains controversial. While single-channel studies show that ITPR2 displays the same configuration as observed for ITPR3, studies with whole cells exhibit similarity with ITPR1[51,56,57], suggesting an effect of the modulatory proteins on the ITPRs channel activity.

ITPRs are widely expressed, sometimes with the prevalence of a single ITPR isoform in a specific tissue. For example, in the central nervous the main ITPR isoform is ITPR1, regulating neurite formation among other functions[58]. ITPR2 is the isoform mainly expressed in cardiomyocytes, participating in heart rate and in the action potential duration[59]. In pancreatic tissue, ITPR2 and ITPR3 are involved in the exocytosis of zymogen granules[60].

In the liver, hepatocytes express ITPR1 and ITPR2[6], whereas all three isoforms are expressed in cholangiocytes[12]. Below, we discuss separately about the ITPR isoforms in hepatic cells, focusing on hepatocytes and cholangiocytes, while indicating their main function and expression pattern in normal condition and in liver disease.

ITPR1: Metabolism and electrolyte secretion

ITPR1 is expressed in both hepatocytes and cholangiocytes, corresponding to approximately 20% of the total ITPRs present in these cells. It is localized along the endoplasmic reticulum, throughout the cytoplasm and near the nucleus[6,61-63].

In normal liver tissue, ITPR1 regulates metabolism in hepatocytes[63-65]. After exposure to glucagon, mouse hepatocytes display an increase in ITPR1 phosphorylation by the activity of protein kinase A (PKA), raising intracellular Ca^{2+} concentration that leads to glucose secretion[64]. More evidence of the ITPR1 function in liver metabolism was shown in obese (ob/ob) and high fat diet (HFD) mouse models. Ob/ob mice and mice maintained on a high-fat diet (HFD) overexpress ITPR1, increasing the amount of these Ca^{2+} channels in close proximity to the mitochondria[65]. In accordance with the increase in ITPR expression, cytoplasmic and

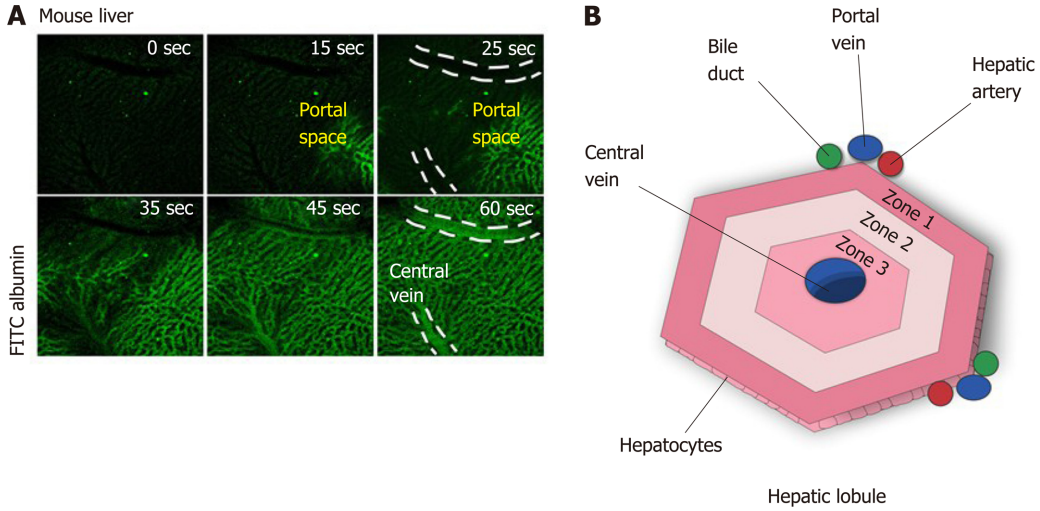

Figure 2 The microenvironment in the hepatic lobules. A: Perfusion with fluorescein isothiocyanate albumin shows that the blood flow arrives in the liver by portal vein, passes throughout the sinusoidal space, and drains into the central vein; B: Due to this blood flux, different zones of oxygenation are observed: zone 1, closer to portal vein, is the most highly oxygenated and zone 3 is the least oxygenated. zone 2 is intermediary. The direction of bile flux is opposite to that of blood flow. The bile acids excreted by the hepatocytes go to the bile duct through the biliary canaliculous.

mitochondrial Ca^{2+} concentration is increased in obese mice, causing mitochondrial dysfunction and impairment of metabolic homeostasis[65]. Conversely, the reduction of ITPR1 expression in the mouse liver, by short hairpin RNA technique, improved glucose tolerance and mitochondrial metabolism[65]. These results were validated in ITPR1 liver-specific knockout mice (ITPR1 LSKO). ITPR1 LSKO mice are leaner and display less hepatic steatosis after HFD, and also have reduced levels of triglycerides and lipogenic gene expression. These metabolic alterations are in accordance with the lower mitochondrial Ca^{2+} signal observed in isolated hepatocytes from ITPR1 LSKO mice[63]. Translational studies corroborate these findings by showing that liver specimens from non-alcoholic steatohepatitis (NASH) donors display increased hepatic ITPR1 expression which is concentrated closer to mitochondria. Based on these observations, it has been suggested that ITPR1 plays a role in steatosis in human fatty liver diseases[63].

Another function of ITPR1 in hepatocytes is related to the liver regeneration. Knocking down ITPR1 in rat with small interfering RNA (siRNA), attenuates Ca^{2+} signaling, and results in an impairment of hepatocytes proliferation after partial hepatectomy, measured by proliferating cell nuclear antigen staining positive cells. Consequently, the liver growth is diminished at the early phase (up to 48 h) of liver regeneration[66]. The involvement of ITPR1 in the beginning of the liver regeneration process is supported by the normal expression of this isoform immediately after the partial hepatectomy, followed by a downregulation of ITPR1 afterwards[67].

In cholangiocytes, ITPR1, together with the ITPR2, are responsible for releasing bicarbonate after the activation of type 3 muscarine receptor by acetylcholine. These findings were observed by using intrahepatic bile duct units isolated from rat liver tissue, previously transfected with ITPR1 and ITPR2 siRNA, and then by measuring the luminal pH after acetylcholine exposition. It was shown that the bicarbonate secretion was reduced in ITPR1 and ITPR2 knockdown cells[61]. Moreover, in cholestasis, which is a disorder that causes bile accumulation, the expression of ITPR1 is decreased, similarly to what occur to the other ITPR isoforms[12]. These observations suggest that the downregulation of ITPRs is an early event in the pathogenesis of cholestasis. As a consequence of the decrease of ITPR1 expression in a rat model of bile duct ligation, the Ca^{2+} signal is reduced and the biliary bicarbonate secretion is impaired in isolated cholangiocytes[12]. Together, these findings show that ITPR1 isoform plays a crucial role in hepatocyte metabolism and proliferation, as well as in cholangiocyte secretory activity, which are essential functions for normal liver.

ITPR2: Bile acid /electrolyte secretion and liver regeneration

ITPR2 is considered the principal intracellular Ca^{2+} release channel expressed in human and rodent hepatocytes[6,68]. This isoform is mostly concentrated in the canalicular membrane (apical region) of hepatocytes[62,69], and due to its localization and high affinity for $InsP_3$[48,49], ITPR2 plays an essential role in bile formation[6,69]. ITPR2 modulates the multidrug resistance associated protein 2 (Mrp2), which is

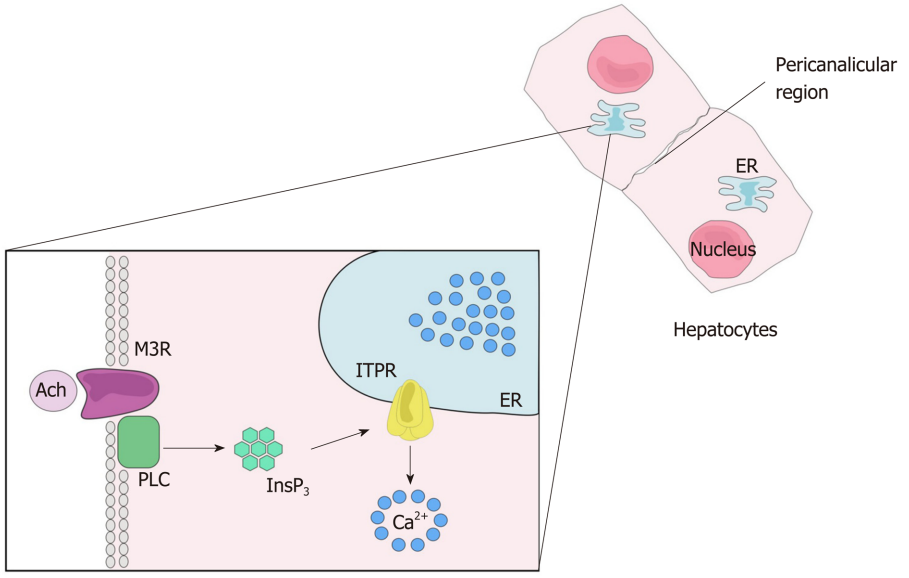

Figure 3 Calcium signaling. After the ligation of an agonist to its receptor, here represent by the ligation of acetylcholine to muscarinic acetylcholine receptor, phospholipase C is activated and produces 1,4,5 inositol triphosphate. The inositol 1,4,5-trisphosphate binds its receptor, inositol 1,4,5-trisphosphate receptor, that is expressed mainly along the endoplasmic reticulum, leading to Ca^{2+} release into the cytosol. Ach: Acetylcholine; M3R: Muscarinic acetylcholine receptor; PLC: Phospholipase C; $InsP_3$: Inositol 1,4,5-trisphosphate; ITPR: Inositol 1,4,5-trisphosphate receptor; ER: Endoplasmic reticulum.

responsible for organic anion secretion into bile, such as bilirubin, glutathione S-conjugates, and oxidized glutathione. Impairment of intracellular Ca^{2+} signal inhibits the insertion of the Mrp2 into the apical plasma membrane in hepatocytes and reduces organic ion secretion. Similarly, hepatocytes isolated from ITPR2 knockout mice also presented decreased intracellular Ca^{2+} signaling, as well as impaired organic ion secretion[69].

Another bile salt transporter regulated by ITPR2 activity is the bile salt export pump (Bsep), an important protein normally positioned along the canalicular membrane of the hepatocyte. In a three-dimensional culture system of rat hepatocytes, siRNA against ITPR2 significantly reduced bile salt secretion, correlating with the downregulation and mislocalization of Bsep. Reduced bile secretion was also observed when the pericanalicular localization of ITPR2 was disrupted by methyl-β-cyclodextrin to disturb lipid rafts[62]. Confirming the importance of ITPR2 to the correct bile salt transporter localization and secretory activity, immunohistochemistry analysis of hepatocytes from lipopolysaccharides (LPS) and estrogen cholestasis rat models showed a reduction of ITPR2 expression level and its diffuse distribution, different from its normal localization to the apical membrane[62]. Conversely, fasting causes a physiological upregulation of ITPR2 expression level[70]. It was shown that overnight fasting raises the mRNA and protein levels of ITPR2 in rat hepatocytes. It happens by the activation of cAMP signaling caused by a fast-dependent increase of serum glucagon levels[70].

The correct expression level of ITPR2 is also important for hepatocyte proliferation. Downregulation of ITPR2 was observed in obese mice[71], a condition that compromises liver regeneration[72]. ITPR2 downregulation was also observed in human liver specimens of patients diagnosed with steatosis and NAFLD, common liver diseases associated with obesity[13]. Recently, the connection between lower expression of ITPR2 and impairment of liver regeneration in some liver diseases was clarified[13]. In both human biopsies of steatosis and NAFLD, as well as in a high fructose diet induced rat model of NAFLD, the transcriptional factor c-Jun activates a pro-inflammatory environment that negatively regulates ITPR2 expression in hepatocytes[13]. As consequence of downregulation of ITPR2, a delay of liver regeneration was observed. Similarly, ITPR2 knockout mice subjected to partial hepatectomy showed more liver damage and decreased proliferation of hepatocytes[13]. This was a consequence of decreased nuclear Ca^{2+} signaling, a fundamental event for cell proliferation[10,66]. ITPR2-knockout cells markedly reduced nucleoplasmic Ca^{2+} and proliferation rates compared to WT cells[13].

In cholangiocytes, ITPR2 represents about 10% of total ITPR, and is distributed diffusely throughout the endoplasmic reticulum membrane in the cytosol[12].

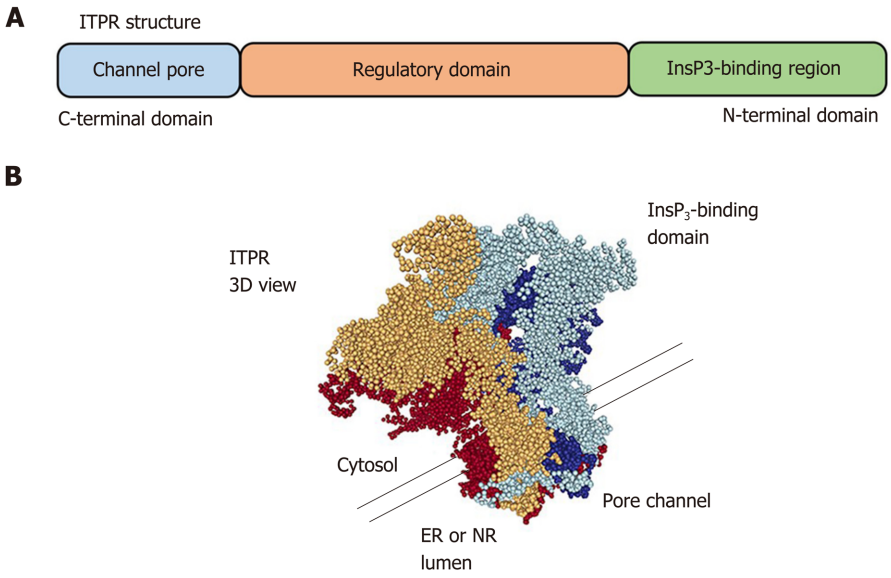

Figure 4 Inositol 1,4,5-trisphosphate receptor structure. A: Linear structure of inositol 1,4,5-trisphosphate receptor (ITPR). The inositol 1,4,5-trisphosphate ($InsP_3$)-binding domain is located on the N-terminal region and the pore channel is on the C-terminal region. The receptor spans organelle membrane six times; B: Tridimensional view of ITPR showing that the receptor is formed by a 4 single chain. It is necessary that four $InsP_3$ molecules bind to the receptor to lead the calcium releases by a pore of the channel. The tridimensional structure was adapted from Molecular Modeling Database (National Center for Biotechnology Information). ER: Endoplasmic reticulum; ITPR: Inositol 1,4,5-trisphosphate receptor; NR: Nucleoplasmic reticulum.

Functional studies showed that ITPR2 participates in the bicarbonate secretion by cholangiocytes. As discussed above, ITPR1 and ITPR2 knockdown cholangiocytes show a decrease in Ca^{2+} signal, and a reduction in Ca^{2+}-dependent bicarbonate secretion when stimulated by acetylcholine[61]. Similar observations have been made in some cholestatic human diseases. The expression of ITPR2 is dramatically reduced in cholangiocytes from samples of patients with bile duct obstruction and primary biliary cirrhosis[12]. In summary, the ITPR2 displays an essential function in the liver, regulating bile formation and bicarbonate secretion, as well as regenerating hepatocytes.

ITPR3: Cell proliferation and electrolyte secretion

In normal conditions, hepatocytes express ITPR1 and ITPR2 isoforms, but not the ITPR3[6]. However, ITPR3 is present in several hepatocellular carcinoma (HCC) cell lines[73,74], as well as in NASH-related HCC[75]. The mechanism of the "de novo" ITPR3 expression in hepatocytes in the context of HCC has been partially described and involves epigenetic modification[74], which represents changes in the genome structure that do not alter the nucleotide sequence. Examples include DNA methylation and histone modification[76]. Recently, bioinformatics analysis showed that the ITPR3 promoter region has a large number of CpG islands[74] that can be methylated by DNA methyltransferases, resulting in suppression of the gene[76,77]. Due to high level of DNA methylation at the ITPR3 promoter region, ITPR3 expression is repressed in hepatocytes under normal conditions. However, the referred methylation level is decreased in patients with HCC, allowing the expression of ITPR3 to be increased under hepatocellular disease conditions[74]. The expression of ITPR3 drives cell proliferation besides preventing the apoptotic cascade activation[74], events closely related to tumor development. Together, these findings put the ITPR3 Ca^{2+} channel as an essential factor that contributes to the pathogenesis of HCC.

Contrary to the normal hepatocytes, cholangiocytes constitutively express all three isoforms of ITPR[7], with the ITPR3 being the most widely expressed, constituting approximately 80% of ITPRs in this cell type. ITPR3 mainly localizes to the apical region of the cholangiocytes in rodents and humans[7]. This apical localization of ITPR3 in cholangiocytes is important for its physiological function of secreting bicarbonate[78]. It was shown that downregulation of ITPR3 selectively disturbs the cAMP-induced bicarbonate secretion[61]. Different from ITPR1 and ITPR2, in which the bicarbonate secretion is dependent on activation of muscarinic acetylcholine receptors, ITPR3 leads to bicarbonate secretion by a cAMP-dependent cascade, wherein activation of secretin receptor indirectly stimulates $InsP_3$ production and Ca^{2+}

release via ITPR3[61].

As described above to the other ITPR isoforms, the ITPR3 expression is progressively decreased in bile duct ligation cholestasis rat model. Downregulation of ITPR3 was also observed after acute cholestasis, such as the endotoxin mouse model, as well as in chronic cholestatic disease in human, *e.g.*, bile duct obstruction, biliary atresia, primary biliary cirrhosis, sclerosing cholangitis, and autoimmune cholestatic[12].

Several intracellular mechanisms have already been elucidated as being responsible for the loss of ITPR3 in cholangiocytes under pathological conditions. It was demonstrated for instance that LPS inoculation activates Toll like receptor 4 in cholangiocytes and, consequently, the transcription factor NF-κB. NF-κB then associates to the ITPR3 promoter region, inhibiting its expression in cholangiocytes. This mechanism is responsible for the loss of ITPR3 in patients affected by cholestasis due to sepsis or severe alcoholic hepatitis[79]. In cholangiopathies under oxidative stress conditions, including sclerosing cholangitis, primary biliary cholangitis, primary biliary obstruction and biliary atresia, the nuclear erythroid 2-like transcription factor 2 (Nrf2) is activated, acting negatively on ITPR3 expression[80]. Finally, the ITPR3 expression is also negatively regulated by the microRNA miR-506 in patients with primary biliary cholangitis[81].

Conversely to the downregulation of ITPR3 in cholangiopathies and cholestasis, this Ca^{2+} channel becomes over-expressed in cholangiocarcinoma[82]. ITPR3 accumulates in ER-mitochondrial junctions in cholangiocarcinoma cell lines, increasing mitochondrial Ca^{2+} signaling. Moreover, ITPR3 increases nuclear Ca^{2+} signaling in cholangiocarcinoma, which contributes to cell proliferation, migration, and survival[82].

Together, these findings show that ITPR3 is absent in healthy hepatocytes but is expressed in HCC and indicates that it may be a target to understand liver cancer and its clinical implications. On the other hand, in cholangiocytes, ITPR3 is crucial to bile formation and the decrease in its expression causes cholestasis, observed in many liver diseases, while it is over-expressed in cholangiocarcinoma, contributing to malignant features, such as cell proliferation, migration and survival.

CONCLUSION

In this review, we described several evidences of the role of the Ca^{2+} signaling, and consequently the activity of ITPRs, in normal liver functions. Mislocalization and/or change in expression level of these Ca^{2+} channels have been directly related to some liver disease (summarized in Figure 5). The alterations in ITPR expression and localization point these Ca^{2+} channels as a valuable biomarker for prediction and prognosis of hepatic disease. In addition to diagnosis for liver diseases, ITPR would be a rational target for these pathological conditions. Epigenetic modification, pro-inflammatory transcription factors and miRNA have already been associated to the modulation of ITPR expression in pathological conditions. However, this field remains to be better explored to elucidate the upstream cascade that drives ITPR expression alterations. Better understanding of this pathway could open the perspective of developing pharmacological strategies for liver diseases, specifically targeting each ITPR isoforms.

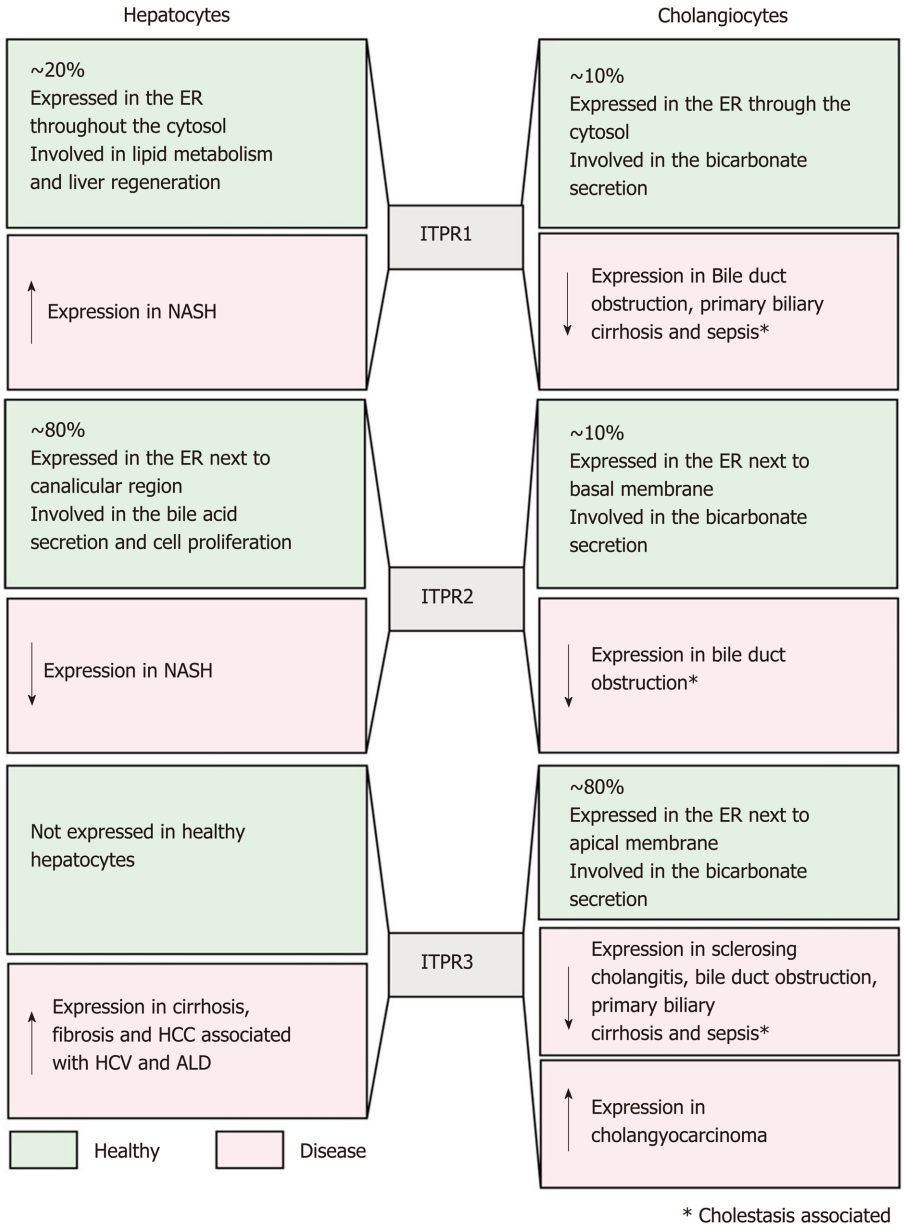

Figure 5 Inositol 1,4,5-trisphosphate receptors in the liver: Expression and functions. This figure summarizes, in green, Inositol 1,4,5-trisphosphate receptor (ITPR) isoform expression in hepatocytes and cholangiocytes under physiological condition, and in red the expression level and function of each ITPR isoform in liver diseases. ITPR1: ITPR isoform 1; ITPR2: ITPR isoform 2; ITPR3: ITPR isoform 3; ER: Endoplasmic reticulum; NAFLD: Non-alcoholic fatty liver disease; HCC: Hepatocellular carcinoma.

ACKNOWLEDGEMENTS

We thank Dr Christopher Kushmerick (Universidade Federal de Minas Gerais), Mr Sriram Amirneni (University of Pittsburgh) and Dr Michael Nathanson (Yale University) for generously providing many useful suggestions and comments on the manuscript. Fellowship and scholarships are acknowledged from Conselho Nacional de Desenvolvimento Científico e Tecnológico and Coordenação de Aperfeiçoamento de Pessoal.

REFERENCES

1 **Han HS**, Kang G, Kim JS, Choi BH, Koo SH. Regulation of glucose metabolism from a liver-centric perspective. *Exp Mol Med* 2016; **48**: e218 [PMID: 26964834 DOI: 10.1038/emm.2015.122]
2 **Robinson MW**, Harmon C, O'Farrelly C. Liver immunology and its role in inflammation and homeostasis. *Cell Mol Immunol* 2016; **13**: 267-276 [PMID: 27063467 DOI: 10.1038/cmi.2016.3]
3 **Bechmann LP**, Hannivoort RA, Gerken G, Hotamisligil GS, Trauner M, Canbay A. The interaction of

hepatic lipid and glucose metabolism in liver diseases. *J Hepatol* 2012; **56**: 952-964 [PMID: 22173168 DOI: 10.1016/j.jhep.2011.08.025]
4 **Chiang JYL**, Ferrell JM. Bile Acid Metabolism in Liver Pathobiology. *Gene Expr* 2018; **18**: 71-87 [PMID: 29325602 DOI: 10.3727/105221618X15156018385515]
5 **Bhatia SN**, Underhill GH, Zaret KS, Fox IJ. Cell and tissue engineering for liver disease. *Sci Transl Med* 2014; **6**: 245sr2 [PMID: 25031271 DOI: 10.1126/scitranslmed.3005975]
6 **Hirata K**, Pusl T, O'Neill AF, Dranoff JA, Nathanson MH. The type II inositol 1,4,5-trisphosphate receptor can trigger Ca2+ waves in rat hepatocytes. *Gastroenterology* 2002; **122**: 1088-1100 [PMID: 11910359 DOI: 10.1053/gast.2002.32363]
7 **Hirata K**, Dufour JF, Shibao K, Knickelbein R, O'Neill AF, Bode HP, Cassio D, St-Pierre MV, Larusso NF, Leite MF, Nathanson MH. Regulation of Ca(2+) signaling in rat bile duct epithelia by inositol 1,4,5-trisphosphate receptor isoforms. *Hepatology* 2002; **36**: 284-296 [PMID: 12143036 DOI: 10.1053/jhep.2002.34432]
8 **Pantazaka E**, Taylor CW. Differential distribution, clustering, and lateral diffusion of subtypes of the inositol 1,4,5-trisphosphate receptor. *J Biol Chem* 2011; **286**: 23378-23387 [PMID: 21550988 DOI: 10.1074/jbc.M111.236372]
9 **Tu H**, Wang Z, Nosyreva E, De Smedt H, Bezprozvanny I. Functional characterization of mammalian inositol 1,4,5-trisphosphate receptor isoforms. *Biophys J* 2005; **88**: 1046-1055 [PMID: 15533917 DOI: 10.1529/biophysj.104.049593]
10 **Echevarría W**, Leite MF, Guerra MT, Zipfel WR, Nathanson MH. Regulation of calcium signals in the nucleus by a nucleoplasmic reticulum. *Nat Cell Biol* 2003; **5**: 440-446 [PMID: 12717445 DOI: 10.1038/ncb980]
11 **Streb H**, Irvine RF, Berridge MJ, Schulz I. Release of Ca2+ from a nonmitochondrial intracellular store in pancreatic acinar cells by inositol-1,4,5-trisphosphate. *Nature* 1983; **306**: 67-69 [PMID: 6605482 DOI: 10.1038/306067a0]
12 **Shibao K**, Hirata K, Robert ME, Nathanson MH. Loss of inositol 1,4,5-trisphosphate receptors from bile duct epithelia is a common event in cholestasis. *Gastroenterology* 2003; **125**: 1175-1187 [PMID: 14517800 DOI: 10.1016/S0016-5085(03)01201-0]
13 **Khamphaya T**, Chukijrungroat N, Saengsirisuwan V, Mitchell-Richards KA, Robert ME, Mennone A, Ananthanarayanan M, Nathanson MH, Weerachayaphorn J. Nonalcoholic fatty liver disease impairs expression of the type II inositol 1,4,5-trisphosphate receptor. *Hepatology* 2018; **67**: 560-574 [PMID: 29023819 DOI: 10.1002/hep.29588]
14 **Desmet VJ**. Ductal plates in hepatic ductular reactions. Hypothesis and implications. II. Ontogenic liver growth in childhood. *Virchows Arch* 2011; **458**: 261-270 [PMID: 21298286 DOI: 10.1007/s00428-011-1049-2]
15 **Huppert SS**, Iwafuchi-Doi M. Molecular regulation of mammalian hepatic architecture. *Curr Top Dev Biol* 2019; **132**: 91-136 [PMID: 30797519 DOI: 10.1016/bs.ctdb.2018.12.003]
16 **Dodds WJ**, Erickson SJ, Taylor AJ, Lawson TL, Stewart ET. Caudate lobe of the liver: anatomy, embryology, and pathology. *AJR Am J Roentgenol* 1990; **154**: 87-93 [PMID: 2104732 DOI: 10.2214/ajr.154.1.2104732]
17 **Sagoo MG**, Aland RC, Gosden E. Morphology and morphometry of the caudate lobe of the liver in two populations. *Anat Sci Int* 2018; **93**: 48-57 [PMID: 27586453 DOI: 10.1007/s12565-016-0365-7]
18 **Saxena R**, Theise ND, Crawford JM. Microanatomy of the human liver-exploring the hidden interfaces. *Hepatology* 1999; **30**: 1339-1346 [PMID: 10573509 DOI: 10.1002/hep.510300607]
19 **Wisse E**, Braet F, Luo D, De Zanger R, Jans D, Crabbé E, Vermoesen A. Structure and function of sinusoidal lining cells in the liver. *Toxicol Pathol* 1996; **24**: 100-111 [PMID: 8839287 DOI: 10.1177/019262339602400114]
20 **Maher JJ**. Cell-specific expression of hepatocyte growth factor in liver. Upregulation in sinusoidal endothelial cells after carbon tetrachloride. *J Clin Invest* 1993; **91**: 2244-2252 [PMID: 7683700 DOI: 10.1172/JCI116451]
21 **Crawford JM**. Development of the intrahepatic biliary tree. *Semin Liver Dis* 2002; **22**: 213-226 [PMID: 12360416 DOI: 10.1055/s-2002-34508]
22 **Strazzabosco M**, Fabris L. Functional anatomy of normal bile ducts. *Anat Rec (Hoboken)* 2008; **291**: 653-660 [PMID: 18484611 DOI: 10.1002/ar.20664]
23 **Krishna M**. Microscopic anatomy of the liver. *Clin Liver Dis (Hoboken)* 2013; **2**: S4-S7 [PMID: 30992875 DOI: 10.1002/cld.147]
24 **Torre C**, Perret C, Colnot S. Transcription dynamics in a physiological process: β-catenin signaling directs liver metabolic zonation. *Int J Biochem Cell Biol* 2011; **43**: 271-278 [PMID: 19914393 DOI: 10.1016/j.biocel.2009.11.004]
25 **Kietzmann T**. Metabolic zonation of the liver: The oxygen gradient revisited. *Redox Biol* 2017; **11**: 622-630 [PMID: 28126520 DOI: 10.1016/j.redox.2017.01.012]
26 **Halpern KB**, Shenhav R, Matcovitch-Natan O, Toth B, Lemze D, Golan M, Massasa EE, Baydatch S, Landen S, Moor AE, Brandis A, Giladi A, Avihail AS, David E, Amit I, Itzkovitz S. Single-cell spatial reconstruction reveals global division of labour in the mammalian liver. *Nature* 2017; **542**: 352-356 [PMID: 28166538 DOI: 10.1038/nature21065]
27 **Hata S**, Namae M, Nishina H. Liver development and regeneration: from laboratory study to clinical therapy. *Dev Growth Differ* 2007; **49**: 163-170 [PMID: 17335437 DOI: 10.1111/j.1440-169X.2007.00910.x]
28 **Gilgenkrantz H**, Collin de l'Hortet A. Understanding Liver Regeneration: From Mechanisms to Regenerative Medicine. *Am J Pathol* 2018; **188**: 1316-1327 [PMID: 29673755 DOI: 10.1016/j.ajpath.2018.03.008]
29 **Rodrigues MA**, Gomes DA, Leite MF, Grant W, Zhang L, Lam W, Cheng YC, Bennett AM, Nathanson MH. Nucleoplasmic calcium is required for cell proliferation. *J Biol Chem* 2007; **282**: 17061-17068 [PMID: 17420246 DOI: 10.1074/jbc.M700490200]
30 **Andrade V**, Guerra M, Jardim C, Melo F, Silva W, Ortega JM, Robert M, Nathanson MH, Leite F. Nucleoplasmic calcium regulates cell proliferation through legumain. *J Hepatol* 2011; **55**: 626-635 [PMID: 21237226 DOI: 10.1016/j.jhep.2010.12.022]
31 **Guimarães E**, Machado R, Fonseca MC, França A, Carvalho C, Araújo E Silva AC, Almeida B, Cassini P, Hissa B, Drumond L, Gonçalves C, Fernandes G, De Brot M, Moraes M, Barcelos L, Ortega JM, Oliveira A, Leite MF. Inositol 1, 4, 5-trisphosphate-dependent nuclear calcium signals regulate angiogenesis and cell motility in triple negative breast cancer. *PLoS One* 2017; **12**: e0175041 [PMID:

28376104 DOI: 10.1371/journal.pone.0175041]
32 **Resende RR**, Andrade LM, Oliveira AG, Guimarães ES, Guatimosim S, Leite MF. Nucleoplasmic calcium signaling and cell proliferation: calcium signaling in the nucleus. *Cell Commun Signal* 2013; **11**: 14 [PMID: 23433362 DOI: 10.1186/1478-811X-11-14]
33 **Berridge MJ**, Bootman MD, Roderick HL. Calcium signalling: dynamics, homeostasis and remodelling. *Nat Rev Mol Cell Biol* 2003; **4**: 517-529 [PMID: 12838335 DOI: 10.1038/nrm1155]
34 **Oliveira AG**, Guimarães ES, Andrade LM, Menezes GB, Fatima Leite M. Decoding calcium signaling across the nucleus. *Physiology (Bethesda)* 2014; **29**: 361-368 [PMID: 25180265 DOI: 10.1152/physiol.00056.2013]
35 **Irvine RF**, Lloyd-Burton SM, Yu JC, Letcher AJ, Schell MJ. The regulation and function of inositol 1,4,5-trisphosphate 3-kinases. *Adv Enzyme Regul* 2006; **46**: 314-323 [PMID: 16857241 DOI: 10.1016/j.advenzreg.2006.01.009]
36 **Connolly TM**, Bansal VS, Bross TE, Irvine RF, Majerus PW. The metabolism of tris- and tetraphosphates of inositol by 5-phosphomonoesterase and 3-kinase enzymes. *J Biol Chem* 1987; **262**: 2146-2149 [PMID: 3029066]
37 **Blaustein MP**, Lederer WJ. Sodium/calcium exchange: its physiological implications. *Physiol Rev* 1999; **79**: 763-854 [PMID: 10390518 DOI: 10.1152/physrev.1999.79.3.763]
38 **Perocchi F**, Gohil VM, Girgis HS, Bao XR, McCombs JE, Palmer AE, Mootha VK. MICU1 encodes a mitochondrial EF hand protein required for Ca^{2+}. *Nature* 2010; **467**: 291-296 [PMID: 20693986 DOI: 10.1038/nature09358]
39 **Jiang QX**, Thrower EC, Chester DW, Ehrlich BE, Sigworth FJ. Three-dimensional structure of the type 1 inositol 1,4,5-trisphosphate receptor at 24 A resolution. *EMBO J* 2002; **21**: 3575-3581 [PMID: 12110570 DOI: 10.1093/emboj/cdf380]
40 **Shah SZA**, Zhao D, Khan SH, Yang L. Regulatory Mechanisms of Endoplasmic Reticulum Resident IP3 Receptors. *J Mol Neurosci* 2015; **56**: 938-948 [PMID: 25859934 DOI: 10.1007/s12031-015-0551-4]
41 **Foskett JK**, White C, Cheung KH, Mak DO. Inositol trisphosphate receptor Ca2+ release channels. *Physiol Rev* 2007; **87**: 593-658 [PMID: 17429043 DOI: 10.1152/physrev.00035.2006]
42 **Baker MR**, Fan G, Serysheva II. Structure of IP_3R channel: high-resolution insights from cryo-EM. *Curr Opin Struct Biol* 2017; **46**: 38-47 [PMID: 28618351 DOI: 10.1016/j.sbi.2017.05.014]
43 **Yang J**, Vais H, Gu W, Foskett JK. Biphasic regulation of InsP3 receptor gating by dual Ca2+ release channel BH3-like domains mediates Bcl-xL control of cell viability. *Proc Natl Acad Sci USA* 2016; **113**: E1953-E1962 [PMID: 26976600 DOI: 10.1073/pnas.1517935113]
44 **Choe CU**, Ehrlich BE. The inositol 1,4,5-trisphosphate receptor (IP3R) and its regulators: sometimes good and sometimes bad teamwork. *Sci STKE* 2006; **2006**: re15 [PMID: 17132820 DOI: 10.1126/stke.3632006re15]
45 **Wang L**, Wagner LE 2nd, Alzayady KJ, Yule DI. Region-specific proteolysis differentially regulates type 1 inositol 1,4,5-trisphosphate receptor activity. *J Biol Chem* 2017; **292**: 11714-11726 [PMID: 28526746 DOI: 10.1074/jbc.M117.789917]
46 **Khan MT**, Wagner L 2nd, Yule DI, Bhanumathy C, Joseph SK. Akt kinase phosphorylation of inositol 1,4,5-trisphosphate receptors. *J Biol Chem* 2006; **281**: 3731-3737 [PMID: 16332683 DOI: 10.1074/jbc.M509262200]
47 **Mikoshiba K**. IP3 receptor/Ca2+ channel: from discovery to new signaling concepts. *J Neurochem* 2007; **102**: 1426-1446 [PMID: 17697045 DOI: 10.1111/j.1471-4159.2007.04825.x]
48 **Iwai M**, Michikawa T, Bosanac I, Ikura M, Mikoshiba K. Molecular basis of the isoform-specific ligand-binding affinity of inositol 1,4,5-trisphosphate receptors. *J Biol Chem* 2007; **282**: 12755-12764 [PMID: 17327232 DOI: 10.1074/jbc.M609833200]
49 **Newton CL**, Mignery GA, Südhof TC. Co-expression in vertebrate tissues and cell lines of multiple inositol 1,4,5-trisphosphate (InsP3) receptors with distinct affinities for InsP3. *J Biol Chem* 1994; **269**: 28613-28619 [PMID: 7961809]
50 **Alzayady KJ**, Wang L, Chandrasekhar R, Wagner LE 2nd, Van Petegem F, Yule DI. Defining the stoichiometry of inositol 1,4,5-trisphosphate binding required to initiate Ca2+ release. *Sci Signal* 2016; **9**: ra35 [PMID: 27048566 DOI: 10.1126/scisignal.aad6281]
51 **Ramos-Franco J**, Fill M, Mignery GA. Isoform-specific function of single inositol 1,4,5-trisphosphate receptor channels. *Biophys J* 1998; **75**: 834-839 [PMID: 9675184 DOI: 10.1016/S0006-3495(98)77572-1]
52 **Hagar RE**, Burgstahler AD, Nathanson MH, Ehrlich BE. Type III InsP3 receptor channel stays open in the presence of increased calcium. *Nature* 1998; **396**: 81-84 [PMID: 9817204 DOI: 10.1038/23954]
53 **Finch EA**, Turner TJ, Goldin SM. Calcium as a coagonist of inositol 1,4,5-trisphosphate-induced calcium release. *Science* 1991; **252**: 443-446 [PMID: 2017683 DOI: 10.1126/science.2017683]
54 **De Young GW**, Keizer J. A single-pool inositol 1,4,5-trisphosphate-receptor-based model for agonist-stimulated oscillations in Ca^{2+} concentration. *Proc Natl Acad Sci USA* 1992; **89**: 9895-9899 [PMID: 1329108 DOI: 10.1073/pnas.89.20.9895]
55 **Hagar RE**, Ehrlich BE. Regulation of the type III InsP(3) receptor by InsP(3) and ATP. *Biophys J* 2000; **79**: 271-278 [PMID: 10866953 DOI: 10.1016/S0006-3495(00)76289-8]
56 **Michikawa T**, Hirota J, Kawano S, Hiraoka M, Yamada M, Furuichi T, Mikoshiba K. Calmodulin mediates calcium-dependent inactivation of the cerebellar type 1 inositol 1,4,5-trisphosphate receptor. *Neuron* 1999; **23**: 799-808 [PMID: 10482245 DOI: 10.1016/S0896-6273(01)80037-4]
57 **Miyakawa T**, Maeda A, Yamazawa T, Hirose K, Kurosaki T, Iino M. Encoding of Ca2+ signals by differential expression of IP3 receptor subtypes. *EMBO J* 1999; **18**: 1303-1308 [PMID: 10064596 DOI: 10.1093/emboj/18.5.1303]
58 **Fiedler MJ**, Nathanson MH. The type I inositol 1,4,5-trisphosphate receptor interacts with protein 4.1N to mediate neurite formation through intracellular Ca waves. *Neurosignals* 2011; **19**: 75-85 [PMID: 21389686 DOI: 10.1159/000324507]
59 **Guatimosim S**, Amaya MJ, Guerra MT, Aguiar CJ, Goes AM, Gómez-Viquez NL, Rodrigues MA, Gomes DA, Martins-Cruz J, Lederer WJ, Leite MF. Nuclear Ca^{2+} regulates cardiomyocyte function. *Cell Calcium* 2008; **44**: 230-242 [PMID: 18201761 DOI: 10.1016/j.ceca.2007.11.016]
60 **Futatsugi A**, Nakamura T, Yamada MK, Ebisui E, Nakamura K, Uchida K, Kitaguchi T, Takahashi-Iwanaga H, Noda T, Aruga J, Mikoshiba K. IP3 receptor types 2 and 3 mediate exocrine secretion underlying energy metabolism. *Science* 2005; **309**: 2232-2234 [PMID: 16195467 DOI: 10.1126/science.1114110]
61 **Minagawa N**, Nagata J, Shibao K, Masyuk AI, Gomes DA, Rodrigues MA, Lesage G, Akiba Y, Kaunitz JD, Ehrlich BE, Larusso NF, Nathanson MH. Cyclic AMP regulates bicarbonate secretion in

cholangiocytes through release of ATP into bile. *Gastroenterology* 2007; **133**: 1592-1602 [PMID: 17916355 DOI: 10.1053/j.gastro.2007.08.020]
62 **Kruglov EA**, Gautam S, Guerra MT, Nathanson MH. Type 2 inositol 1,4,5-trisphosphate receptor modulates bile salt export pump activity in rat hepatocytes. *Hepatology* 2011; **54**: 1790-1799 [PMID: 21748767 DOI: 10.1002/hep.24548]
63 **Feriod CN**, Oliveira AG, Guerra MT, Nguyen L, Richards KM, Jurczak MJ, Ruan HB, Camporez JP, Yang X, Shulman GI, Bennett AM, Nathanson MH, Ehrlich BE. Hepatic Inositol 1,4,5 Trisphosphate Receptor Type 1 Mediates Fatty Liver. *Hepatol Commun* 2017; **1**: 23-35 [PMID: 28966992 DOI: 10.1002/hep4.1012]
64 **Wang Y**, Li G, Goode J, Paz JC, Ouyang K, Screaton R, Fischer WH, Chen J, Tabas I, Montminy M. Inositol-1,4,5-trisphosphate receptor regulates hepatic gluconeogenesis in fasting and diabetes. *Nature* 2012; **485**: 128-132 [PMID: 22495310 DOI: 10.1038/nature10988]
65 **Arruda AP**, Pers BM, Parlakgül G, Güney E, Inouye K, Hotamisligil GS. Chronic enrichment of hepatic endoplasmic reticulum-mitochondria contact leads to mitochondrial dysfunction in obesity. *Nat Med* 2014; **20**: 1427-1435 [PMID: 25419710 DOI: 10.1038/nm.3735]
66 **Oliveira AG**, Andrade VA, Guimarães ES, Florentino RM, Sousa PA, Marques PE, Melo FM, Ortega MJ, Menezes GB, Leite MF. Calcium signalling from the type I inositol 1,4,5-trisphosphate receptor is required at early phase of liver regeneration. *Liver Int* 2015; **35**: 1162-1171 [PMID: 24814243 DOI: 10.1111/liv.12587]
67 **Nicou A**, Serrière V, Hilly M, Prigent S, Combettes L, Guillon G, Tordjmann T. Remodelling of calcium signalling during liver regeneration in the rat. *J Hepatol* 2007; **46**: 247-256 [PMID: 17125880 DOI: 10.1016/j.jhep.2006.08.014]
68 **Nagata J**, Guerra MT, Shugrue CA, Gomes DA, Nagata N, Nathanson MH. Lipid rafts establish calcium waves in hepatocytes. *Gastroenterology* 2007; **133**: 256-267 [PMID: 17631147 DOI: 10.1053/j.gastro.2007.03.115]
69 **Cruz LN**, Guerra MT, Kruglov E, Mennone A, Garcia CR, Chen J, Nathanson MH. Regulation of multidrug resistance-associated protein 2 by calcium signaling in mouse liver. *Hepatology* 2010; **52**: 327-337 [PMID: 20578149 DOI: 10.1002/hep.23625]
70 **Kruglov E**, Ananthanarayanan M, Sousa P, Weerachayaphorn J, Guerra MT, Nathanson MH. Type 2 inositol trisphosphate receptor gene expression in hepatocytes is regulated by cyclic AMP. *Biochem Biophys Res Commun* 2017; **486**: 659-664 [PMID: 28327356 DOI: 10.1016/j.bbrc.2017.03.086]
71 **Feriod CN**, Nguyen L, Jurczak MJ, Kruglov EA, Nathanson MH, Shulman GI, Bennett AM, Ehrlich BE. Inositol 1,4,5-trisphosphate receptor type II (InsP3R-II) is reduced in obese mice, but metabolic homeostasis is preserved in mice lacking InsP3R-II. *Am J Physiol Endocrinol Metab* 2014; **307**: E1057-E1064 [PMID: 25315698 DOI: 10.1152/ajpendo.00236.2014]
72 **Kele PG**, van der Jagt EJ, Gouw AS, Lisman T, Porte RJ, de Boer MT. The impact of hepatic steatosis on liver regeneration after partial hepatectomy. *Liver Int* 2013; **33**: 469-475 [PMID: 23311417 DOI: 10.1111/liv.12089]
73 **Leite MF**, Thrower EC, Echevarria W, Koulen P, Hirata K, Bennett AM, Ehrlich BE, Nathanson MH. Nuclear and cytosolic calcium are regulated independently. *Proc Natl Acad Sci U S A* 2003; **100**: 2975-2980 [PMID: 12606721 DOI: 10.1073/pnas.0536590100]
74 **Guerra MT**, Florentino RM, Franca A, Lima Filho AC, Dos Santos ML, Fonseca RC, Lemos FO, Fonseca MC, Kruglov E, Mennone A, Njei B, Gibson J, Guan F, Cheng YC, Ananthanarayanam M, Gu J, Jiang J, Zhao H, Lima CX, Vidigal PT, Oliveira AG, Nathanson MH, Leite MF. Expression of the type 3 $InsP_3$ receptor is a final common event in the development of hepatocellular carcinoma. *Gut* 2019; **68**: 1676-1687 [PMID: 31315892 DOI: 10.1136/gutjnl-2018-317811]
75 **Liang JQ**, Teoh N, Xu L, Pok S, Li X, Chu ESH, Chiu J, Dong L, Arfianti E, Haigh WG, Yeh MM, Ioannou GN, Sung JJY, Farrell G, Yu J. Dietary cholesterol promotes steatohepatitis related hepatocellular carcinoma through dysregulated metabolism and calcium signaling. *Nat Commun* 2018; **9**: 4490 [PMID: 30367044 DOI: 10.1038/s41467-018-06931-6]
76 **Portela A**, Esteller M. Epigenetic modifications and human disease. *Nat Biotechnol* 2010; **28**: 1057-1068 [PMID: 20944598 DOI: 10.1038/nbt.1685]
77 **Jones PA**, Takai D. The role of DNA methylation in mammalian epigenetics. *Science* 2001; **293**: 1068-1070 [PMID: 11498573 DOI: 10.1126/science.1063852]
78 **Rodrigues MA**, Gomes DA, Nathanson MH. Calcium Signaling in Cholangiocytes: Methods, Mechanisms, and Effects. *Int J Mol Sci* 2018; **19** [PMID: 30563259 DOI: 10.3390/ijms19123913]
79 **Franca A**, Carlos Melo Lima Filho A, Guerra MT, Weerachayaphorn J, Loiola Dos Santos M, Njei B, Robert M, Xavier Lima C, Vieira Teixeira Vidigal P, Banales JM, Ananthanarayanam M, Leite MF, Nathanson MH. Effects of Endotoxin on Type 3 Inositol 1,4,5-Trisphosphate Receptor in Human Cholangiocytes. *Hepatology* 2019; **69**: 817-830 [PMID: 30141207 DOI: 10.1002/hep.30228]
80 **Weerachayaphorn J**, Amaya MJ, Spirli C, Chansela P, Mitchell-Richards KA, Ananthanarayanan M, Nathanson MH. Nuclear Factor, Erythroid 2-Like 2 Regulates Expression of Type 3 Inositol 1,4,5-Trisphosphate Receptor and Calcium Signaling in Cholangiocytes. *Gastroenterology* 2015; **149**: 211-222.e10 [PMID: 25796361 DOI: 10.1053/j.gastro.2015.03.014]
81 **Ananthanarayanan M**, Banales JM, Guerra MT, Spirli C, Munoz-Garrido P, Mitchell-Richards K, Tafur D, Saez E, Nathanson MH. Post-translational regulation of the type III inositol 1,4,5-trisphosphate receptor by miRNA-506. *J Biol Chem* 2015; **290**: 184-196 [PMID: 25378392 DOI: 10.1074/jbc.M114.587030]
82 **Ueasilamongkol P**, Khamphaya T, Guerra MT, Rodrigues MA, Gomes DA, Kong Y, Wei W, Jain D, Trampert DC, Ananthanarayanan M, Banales JM, Roberts LR, Farshidfar F, Nathanson MH, Weerachayaphorn J. Type 3 Inositol 1,4,5-Trisphosphate Receptor Is Increased and Enhances Malignant Properties in Cholangiocarcinoma. *Hepatology* 2019 [PMID: 31251815 DOI: 10.1002/hep.30839]

World Journal of Gastroenterology

Submit a Manuscript: https://www.f6publishing.com

World J Gastroenterol 2019 November 28; 25(44): 6495-6507

DOI: 10.3748/wjg.v25.i44.6495

ISSN 1007-9327 (print) ISSN 2219-2840 (online)

ORIGINAL ARTICLE

Basic Study

Reduced microRNA 375 in colorectal cancer upregulates metadherin-mediated signaling

Seol-Hee Han, Ji-Su Mo, Won-Cheol Park, Soo-Cheon Chae

ORCID number: Seol-Hee Han (0000-0002-8960-0779); Ji-Su Mo (0000-0002-3150-9665); Won-Cheol Park (0000-0002-2389-5738); Soo Cheon Chae (0000-0002-5427-714X).

Author contributions: Chae SC conceived and designed the experiments; Han SH and Mo JS performed the experiments; Han SH and Chae SC analyzed the data; Park WC and Chae SC contributed reagents/materials/analysis tools, and drafted the manuscript.

Supported by a grant from the National Research Foundation of Korea, No. 2017R1A2B4004801.

Institutional review board statement: The study was reviewed and approved by the Review Board of Wonkwang University, South Korea (WKIRB-201710-BR-012).

Conflict-of-interest statement: The authors declare that they have no conflicts of interest.

Data sharing statement: No additional data are available.

ARRIVE guidelines statement: This study was prepared according to the ARRIVE guidelines.

Seol-Hee Han, Ji-Su Mo, Soo-Cheon Chae, Department of Pathology, School of Medicine, Wonkwang University, Iksan, Chonbuk 54538, South Korea

Ji-Su Mo, Won-Cheol Park, Soo-Cheon Chae, Digestive Disease Research Institute, Wonkwang University, Iksan, Chonbuk 54538, South Korea

Corresponding author: Soo-Cheon Chae, PhD, Professor of Medicine, Department of Pathology, School of Medicine, Wonkwang University, Iksan, Chonbuk 54538, South Korea.
chaesc@wku.ac.kr
Telephone: +82-63-8506793
Fax: +82-63-8506760

Abstract

BACKGROUND

The human microRNA 375 (*MIR375*) is significantly downregulated in human colorectal cancer (CRC) and we have previously shown that *MIR375* is a CRC-associated miRNA. The metadherin (*MTDH*) is a candidate target gene of *MIR375*.

AIM

To investigate the interaction and function between *MIR375* and *MTDH* in human CRC.

METHODS

A luciferase reporter system was used to confirm the effect of *MIR375* on *MTDH* expression. The expression levels of *MIR375* and the target genes were evaluated by quantitative RT-PCR (qRT-PCR), western blotting, or immunohistochemistry.

RESULTS

MTDH expression was found to be upregulated in human CRC tissues compared to that in healthy controls. We show that *MIR375* regulates the expression of many genes involved in the MTDH-mediated signal transduction pathways [BRAF-MAPK and phosphatidylinositol-4,5-biphosphate-3-kinase catalytic subunit alpha (PIK3CA)-AKT] in CRC cells. Upregulated MTDH expression levels were found to inhibit NF-κB inhibitor alpha, which further upregulated NFKB1 and RELA expression in CRC cells.

CONCLUSION

Our findings suggest that suppressing *MIR375* expression in CRC regulates cell proliferation and angiogenesis by increasing MTDH expression. Thus, *MIR375* may be of therapeutic value in treating human CRC.

Manuscript source: Invited Manuscript

Received: October 10, 2019
Peer-review started: October 10, 2019
First decision: November 10, 2019
Revised: November 20, 2019
Accepted: November 23, 2019
Article in press: November 23, 2019
Published online: November 28, 2019

P-Reviewer: Donato R, Tarnawski AS, Yu B
S-Editor: Wang J
L-Editor: A
E-Editor: Qi LL

Key words: MicroRNA 375; Metadherin; Mitogen-activated protein kinase; Angiogenesis; Cell proliferation; Colorectal cancer

Core tip: The microRNA 375 (*MIR375*) is significantly downregulated in human colorectal cancer (CRC) tissues. In this study, we investigated that metadherin (*MTDH*) is a direct target gene of *MIR375* and that MTDH expression levels were upregulated in CRC tissues. Upregulated MTDH expression levels were found to inhibit NF-κB inhibitor alpha expression, which further upregulated NFKB1 and RELA expression in CRC cells. *MIR375* also regulate MTDH-mediated BRAF-MAPK and PIK3CA-AKT signal pathways in CRC cells. Consequently, *MIR375* regulates cell proliferation, cell migration, and angiogenesis by suppressing MTDH expression in CRC progression.

Citation: Han SH, Mo JS, Park WC, Chae SC. Reduced microRNA 375 in colorectal cancer upregulates metadherin-mediated signaling. *World J Gastroenterol* 2019; 25(44): 6495-6507
URL: https://www.wjgnet.com/1007-9327/full/v25/i44/6495.htm
DOI: https://dx.doi.org/10.3748/wjg.v25.i44.6495

INTRODUCTION

Colorectal cancer (CRC) is a common malignant tumor and is the third leading cause of cancer-related mortality worldwide[1,2]. The cause of CRC is multifactorial, which includes genetic variation as well as epigenetic factors[3]. Overall survival of patients with CRC has not much improved relative to significant advances in the management of CRC[4]. Thus, it is most importance to understand the molecular mechanisms underlying CRC tumorigenesis and recognize the fundamental genes responsible for such fatal cancer.

MicroRNAs (miRNAs) are endogenously expressed, small noncoding RNAs that bind at the 3′ untranslated region (3′-UTR) of their target mRNAs and promote mRNA degradation or inhibit translation[5]. miRNAs act as tumor suppressors or oncogenes by targeting the genes involved in cell proliferation, cell survival, apoptosis, and metastasis[6-8].

In humans, microRNA 375 (*MIR375*) is located on chromosomal band 2q35. *MIR375* has been shown to have dual functions: As a tumor suppressor[9,10] and as an oncogene[11,12]. The dual characteristic of *MIR375* depends on the target mRNA. In our previous study, we detected *MIR375* in CRC[13] and dextran sulphate sodium (DSS)-induced mice colitis[14] via miRNA expression profiling of CRC tissues versus healthy colorectal tissues and DSS-induced colitis versus healthy colons, respectively. We found that *MIR375* was significantly downregulated in both CRC and DSS-induced colitis tissue samples[13,14]. Additionally, we have shown that downregulation of *MIR375* modulates epidermal growth factor receptor (EGFR) signaling pathways in human CRC cells and tissues by upregulating connective tissue growth factor (CTGF) expression[15].

Metadherin (*MTDH*, also known as *AEG1*, *LYRIC*, or *LYRIC/3D3*) is located on chromosome 8q22.1 and encodes for a 64 kDa protein. It was first detected as an upregulated transcript in primary human fetal astrocytes infected with human immunodeficiency virus 1 (HIV-1)[16]. Brown and Ruoslahti have shown that metadherin mediates tumor cell localization at the metastatic sites[17]. Several studies have shown the role of *MTDH* as an oncogene in different types of human malignant tumors[18] and revealed various functions such as increased tumor growth, invasion and metastasis, angiogenesis, and chemoresistance[19]. Furthermore, our previous research has shown that *MTDH* is one of the putative target genes of *MIR375*[15].

In this study, we show that *MTDH* is a target gene of *MIR375* in CRC and analyze its functions in CRC tissues and cell lines. Additionally, we reveal that *MIR375* regulates cell proliferation and migration in CRC progression by suppressing MTDH-mediated signaling pathways.

MATERIALS AND METHODS

Patients and tissue samples

The tissue samples used in this study were provided by Biobank of Wonkwang University Hospital, a member of National Biobank of Korea. On approval from the institutional review board and obtaining informed consent (WKIRB-201710-BR-012) from the patients, we collected 19 CRC tissue samples from 16 patients with colon cancer (10 males and 6 females) and 3 patients with rectal cancer (2 males and 1 female). Mean age of the patients with colon cancer and rectal cancer was 68.4 years and 67.0 years, respectively. Ten colon cancer tissue samples and matching healthy colon tissue samples (7 males and 3 females) were investigated to confirm the endogenous expression of *MIR375*. Additionally, 12 colon cancer tissue samples with matching healthy colon tissue samples and 3 rectal cancer tissue samples with matching healthy rectal tissue samples were assessed for MTDH expression levels. Four colon cancer tissue samples and matching healthy colon tissue samples (3 males and 1 female) were examined for immunohistochemistry analysis.

Cells culture and reagents

Human CRC cell lines; Caco2, HT29, LoVo, HCT116, and SW48 were obtained from Korea Cell Line Bank (KCLB, Seoul, South Korea) or American Type Culture Collection (ATCC, Manassas, VA, United States). SW48, HT29, Lovo, and HCT116 cells were cultured in RPMI 1640 (HyClone, Logan, UT, United States) supplemented with 10% FBS while Caco2 cells were cultured in α-MEM (HyClone, Logan, UT, United States) supplemented with 20% FBS in a humidified atmosphere containing 5% CO_2 at 37 °C.

MTDH antibody and all secondary antibodies were purchased from Thermo Fisher Scientific (Waltham, MA, United States). NF-κB inhibitor alpha (NFKBIA/IκBα), nuclear factor κ B subunit 1 (NFκB1/p50), RELA (NFkB3/p65), protein kinase B (AKT), and glyceraldehyde-3-phosphate dehydrogenase (GAPDH) antibodies were obtained from Santa Cruz Biotechnology, Inc. (Dallas, Texas, United States). RAS, BRAF, p44/42 mitogen-activated protein kinase (MAPK) (Erk1/2), phospho-MAPK, phosphatidylinositol-4,5-biphosphate-3-kinase catalytic subunit alpha (PIK3CA), phospho-AKT, and GAPDH antibodies were purchased from Cell Signaling Technology (Danvers, MA, United States). β catenin (CTNNB1) antibody was purchased from Abcam (Cambridge, United Kingdom). Vascular endothelial growth factor A (VEGFA) antibody was purchased from Novus Biologicals (Centennial, CO, United States). Ez-cytox was obtained from DoGenBio (Seoul, South Korea) and dual luciferase reporter assay system was obtained from Promega (Madison, WI, United States). TRIzol and siPORT NeoFx transfection reagents were purchased from Ambion, Inc. (Waltham, MA, United States). Lipofectamine 2000 reagent was purchased from Invitrogen (Waltham, MA, United States) while Viromer blue transfection agent was purchased from Lipocalyx (Weinbergweg, Halle, Germany). RIPA buffer was obtained from Elpis biotech (Daejeon, South Korea) and DAB substrate kit was purchased from Pierce Biotechnology (Waltham, MA, United States).

RNA extraction and quantitative real-time polymerase chain reaction

RNA extraction and quantitative real-time polymerase chain reaction (qRT-PCR) were performed according to our previously established protocol[13-15]. Total RNA was isolated using TRIzol reagent. After digesting with DNase and performing a sample clean-up, RNA samples were quantified, aliquoted, and stored at -80 °C. qRT-PCR was performed on total RNA samples that were isolated from tissue samples or cultured cells to synthesize cDNA using StepOne Real-time PCR system (Applied Biosystems, Foster City, CA, United States).

Differential miRNA expression patterns were validated by TaqMan qRT-PCR assay (Applied Biosystems, Foster City, CA, United States). qRT-PCR was performed using SYBR Green dye (ELPIS Biotech, Daejeon, Korea) to assess mRNA expression. *RNU48* (for TaqMan qRT-PCR) or 5.8S (for SYBR qRT-PCR), and GAPDH served as endogenous controls for qRT-PCR of miRNA and mRNA, respectively. Each sample was analyzed in triplicates by qRT-PCR. Primers for qRT-PCR and TaqMan analysis are listed in Supplementary Table 1.

Transfection of oligonucleotides

Endogenous *MIR375* mimic [hsa-miR-375, Pre-miR™ miRNA precursor (AM17100)], *MTDH* small interfering RNA (siRNA), and each of the negative controls were synthesized commercially (Ambion, Austin, TX, United States) and transfected at 50 nM. Transfection was performed according to our previously published protocols[13-15].

Luciferase reporter assay

Wild-type (WT) or mutant type (MT) fragments of the 3'-UTR of *MTDH* containing the predicted binding site for *MIR375* were amplified using PCR. The primer set used for the experiment is shown in Supplementary Table 1. Plasmid constructions and analysis of the luciferase assay were executed following our previously published protocols[13-15].

Protein extraction and Western blot analysis

Protein extraction and western blot analysis were performed according to our earlier established methods[13-15]. Briefly, membranes were incubated overnight at 4 °C with primary antibodies to MTDH (1:250), NFKBIA (1:100), NFKB1 (1:50), RELA (1:100), KRAS (1:1000), BRAF (1:500), MAPK (1:1000), p-MAPK (1:500), CTNNB1 (1:2500), PIK3CA (1:1000), AKT (1:100), p-AKT (1:500), and VEGFA (1:500). Subsequently, the membranes were incubated with secondary antibodies (1:1000).

Cell proliferation assay

For cell proliferation assay, cells (2×10^4 cells/well) were transfected with *MIR375* mimic, negative control siRNA, or *MTDH* siRNA (*siMTDH*) in 96-well plates. Cell growth was measured at 72 h after transfection using Ez-Cytox cell viability assay kit following manufacturer's instructions. After incubating for 2 h, absorbance values were measured at 450 nm using SpectraMax (Molecular Devices, CA, United States). Percentage of viable cells was calculated by comparing to the number of viable cells in the untreated controls. Experiments were performed in triplicates. Cell proliferation assay was performed following our previously published protocols[15,20].

Immunohistochemistry

Immunohistochemistry assay was performed according to our previously established protocols[14,15]. The tissue slides were blocked with 3% BSA for 2 h at room temperature followed by overnight incubation at 4 °C with primary antibodies against MTDH (1:50) and RELA (1:50). The following day, the slides were incubated with SignalStain® Boost IHC detection reagent (Cell Signaling Technology; Danvers, MA, United States) for 2 h at room temperature. After washing, chromogenic substrate (Thermo Fisher Scientific; Waltham, MA, United States) was applied to visualize the staining of the target proteins. Following counterstaining with hematoxylin, the sections were dehydrated and mounted using a coverslip.

Statistical analysis

Sample size was estimated using the G*power software (Version 3.1., Heinrich Heine University, Duesseldorf, Germany). Each experiment was repeated at least three times and consistent results were obtained. Data are expressed as mean ± standard deviation (SD). The differences between the groups were evaluated using GraphPad Prism 5.0 statistical software (GraphPad Software Inc., San Diego, CA, United States) or Student's *t*-test. Differences with *P* value less than 0.05 were considered as statistically significant.

RESULTS

Validation of MIR375 expression level in CRC tissues

Previously, we have shown *MIR375* as a colon cancer-associated miRNA using miRNA microarray analysis of colon tumor tissues and matched healthy colon tissues[13]. Additionally, we have shown that *MIR375* expression is downregulated in human CRC tissues. To confirm the result, we compared *MIR375* expression in 10 human CRC tissues and matched healthy colon tissues by qRT-PCR. We found that *MIR375* expression levels were significantly reduced in CRC tissues ($P < 0.01$; Supplementary Figure 1A).

Endogenous expression levels of MIR375 in CRC cell lines

To determine the endogenous expression levels of *MIR375* in different cell lines, we performed qRT-PCR on the total RNA isolated from various cell lines including Caco2, SW480, HT29, HCT116, LoVo, and SW48 cells. As shown in Figure S1B, *MIR375* expression level was highest in HT29 cells while it was lower in HCT116 and Caco2 cells (Supplementary Figure 1B).

MTDH is a direct target of MIR375

To determine the direct interaction between *MTDH* 3'-UTR and *MIR375*, we cloned the WT *MTDH* 3'-UTR region, the putative target sequence of *MIR375*, in a luciferase reporter vector (Figure 1A). We observed that luciferase activity was reduced by approximately 24% when cells were co-transfected with *pre-MIR375* ($P < 0.01$, Figure

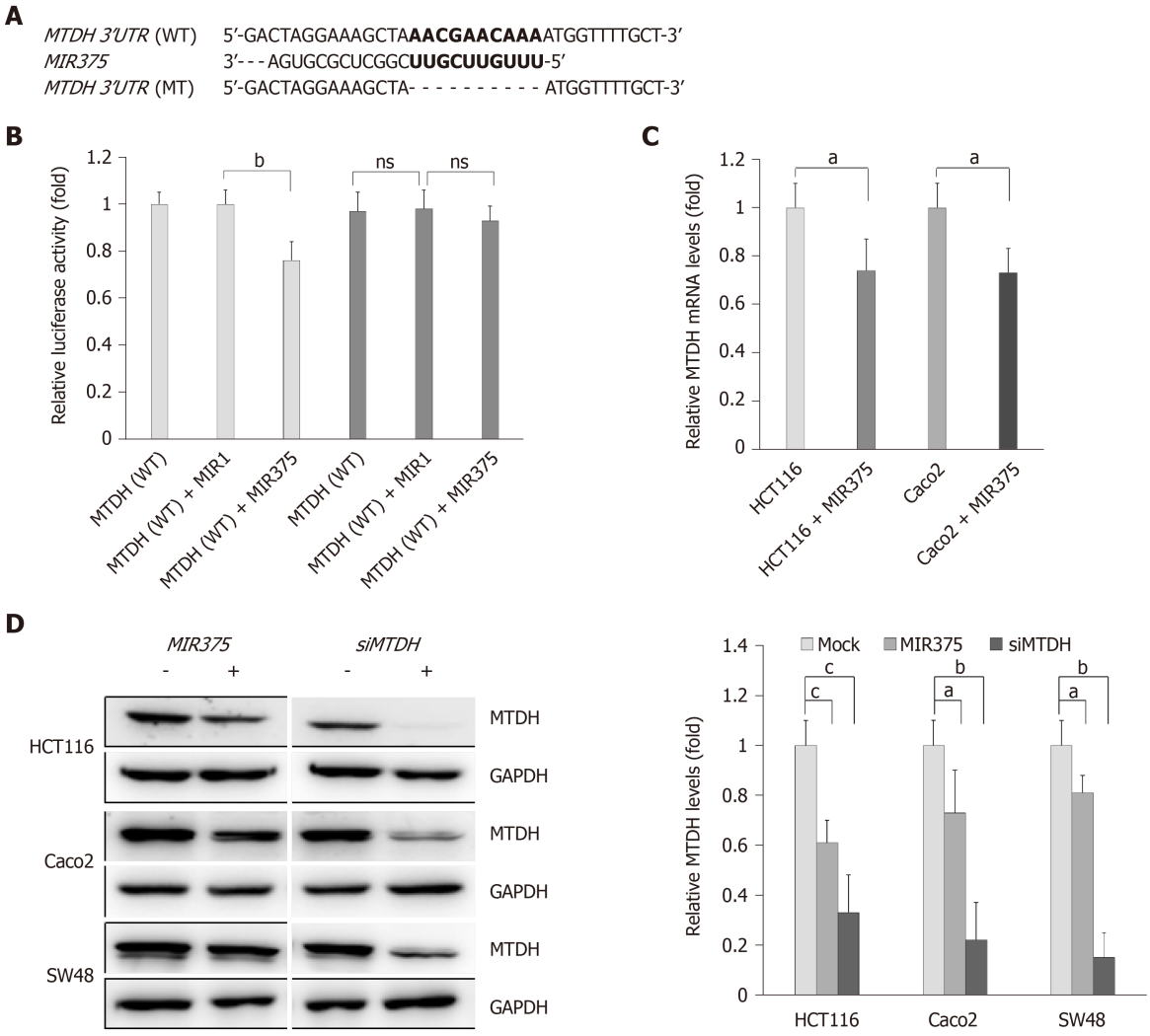

Figure 1 Metadherin is a direct target of *microRNA 375*. A: Sequence alignment of the wild type (WT) and mutated type (MT) microRNA 375 (*MIR375)* target site in the 3'-UTR of metadherin (*MTDH)*; B: A luciferase reporter plasmid containing WT or MT *MTDH* 3'-UTR was co-transfected in HCT116 and Caco2 cells with *pre-MIR1* as a negative control or *pre-MIR375*. Results are shown as relative firefly luciferase activity which is standardized to *Renilla* luciferase activity. Three independent experiments were conducted with duplicates; C: qRT-PCR analysis of *MTDH* mRNA expression in HCT116 and Caco2 cells. The data are presented as the fold change in *MIR375* mimic transfected cells relative to non-transfected cells. Experiment was performed in duplicate and repeated 5 times; D: Cellular MTDH levels in *MIR375* mimic-transfected and *siMTDH*-transfected HCT116, Caco2, and SW48 cells. Three independent experiments were conducted with duplicates. *P* values were calculated using Student's *t*-test ($^{a}P < 0.05$, $^{b}P < 0.01$, $^{c}P < 0.001$). *MTDH:* Metadherin; *MIR375:* MicroRNA 375; ns: Not significant.

1B). As a control experiment, we cloned mutated *MTDH* 3'-UTR sequence which lacked ten of the total complementary bases (Figure 1A). As expected, repression of the luciferase activity was revoked when the interaction between *MIR375* and its target 3'-UTR was disrupted (Figure 1B). Additionally, another control experiment was performed where *pre-MIR1* (instead of *pre-MIR375*) was co-transfected with WT and mutated *MTDH* 3'-UTR constructs. We found that transfection with *pre-MIR1* did not affect the luciferase activity of either of the constructs (Figure 1B).

MIR375 regulate MTDH expression in CRC cells

To validate the obtained data, we investigated whether *MIR375* regulates *MTDH* mRNA levels in HCT116 and Caco2 cells. We found that *MTDH* mRNA expression levels were lower in HCT116 as well as Caco2 cells on transfection with *MIR375* mimic compared with that in non-transfected control cells ($P < 0.05$; Figure 1C). Additionally, we investigated MTDH expression levels in *MIR375* mimic or *siMTDH*-transfected HCT116, Caco2, and SW48 cells and found that cellular MTDH expression was significantly reduced in *MIR375*-overexpressing HCT116, Caco2, and SW48 cells. Furthermore, MTDH was significantly downregulated by *siMTDH* transfection (Figure 1D).

MIR375 regulates MTDH-mediated BRAF-MAPK signaling pathways

To determine the functional interaction between *MIR375* and its target gene *MTDH*,

we analyzed the expression levels of KRAS, BRAF, MAPK, pMAPK, and CTNNB1 in HCT116 and Caco2 cells on *MIR375* mimic transfection. Earlier study has shown that HCT116 cells express WT *BRAF* and mutated *KRAS* while Caco2 cells express only WT *KRAS* and WT *BRAF*[21]. Although KRAS expression level was unaltered on *MIR375* transfection, BRAF, MAPK, pMAPK, and CTNNB1 expression levels were significantly downregulated in HCT116 (Figure 2A) and Caco2 (Figure 2B) cells. We observed a similar expression trend in CRC cells on silencing *MTDH* with *siMTDH* (Figure 2A and B). These results suggested that *MIR375* regulates the MTDH-mediated BRAF-MAPK signal pathway in CRC cells.

MIR375 inhibits CRC cells viability by inhibiting MTDH expression

We investigated the biological functions of *MIR375* in CRC cells. MTT assay showed that cell viability was steadily reduced on *MIR375* transfection in the CRC cell lines HCT116 ($P < 0.01$), Caco2 ($P < 0.05$), and SW48 ($P < 0.05$; Figure 2C) cells. Further, we found a similar trend on *siMTDH* transfection in HCT116 ($P < 0.01$), Caco2 ($P < 0.001$), and SW48 cells ($P < 0.05$; Figure 2C). These results suggested that *MIR375* downregulates CRC cell proliferation by inhibiting MTDH expression. The rate of inhibition was lower in SW48 cells compared with that in HCT116 and Caco2 cells. This might be due to relatively high endogenous expression of *MIR375* in SW48 cells than that observed in HCT116 and Caco2 cells (Supplementary Figure 1B).

MIR375 regulates MTDH-mediated PIK3CA-AKT signaling pathways

We investigated the functional correlation between *MIR375* and MTDH expression in HCT116 and Caco2 cells. HCT116 cells are mutated for PIK3CA whereas Caco2 cells express wild type PIK3CA. We found that PIK3CA, AKT, pAKT, and VEGFA expression levels were downregulated on *MIR375* mimic transfection in HCT116 as well as Caco2 cells (Figure 3A and 3B). Similar results were obtained on silencing *MTDH* in HCT116 and Caco2 cells (Figure 3C and 3D). Thus, the results suggested that *MIR375* regulates MTDH-mediated PIK3CA-AKT signaling pathway by inhibiting MTDH expression levels in CRC cells.

MIR375 regulates MTDH-mediated NFKB1 signaling pathways

Furthermore, we investigated another MTDH-mediated signaling pathway in CRC cells. To determine the role of *MIR375* or MTDH-mediated pathways in NFKB1 signaling, we quantified the expression of relevant proteins in HCT116 and Caco2 cells on *MIR375* mimic or *siMTDH* transfection. NFKB1 and RELA expression levels were found to be significantly downregulated in both the cell lines (HCT116 and Caco2 cells) on *MIR375* transfection while NFKBIA expression levels were found to be upregulated (Figure 4A and B). We observed similar results on silencing *MTDH* using *siMTDH* in CRC cells (Figure 4C and D). Overall, the results evidently suggested that NFKBIA expression was upregulated on inhibiting MTDH in *MIR375*-overexpressing CRC cells which further leads to downregulation of NFKB1 and RELA expression in CRC cells. These results showed that *MIR375* regulates MTDH-mediated NFKB1 signaling pathway.

MTDH expression levels in human CRC tissues

Based on the findings of this study, we evaluated MTDH expression in 15 human CRC tissues and matching healthy colon tissues. Western blot analysis showed that MTDH expression levels were upregulated (12 out of 15 samples) in CRC tissue samples compared with that in healthy colon tissues ($P < 0.05$, Figure 5A). Further, we investigated NFKB1 and RELA expression levels in five CRC tissues and four CRC tissue samples, respectively. NFKB1 expression level was significantly upregulated in all CRC tissues while RELA expression level was predominantly upregulated in three (75%) CRC tissues (Figure 5B).

Consistent with the results obtained, we investigated MTDH and RELA expression in four human CRC tissues and matching healthy colon tissues using immunohistochemical analysis. MTDH and RELA expression levels were significantly upregulated in CRC tissues (Figure 5C).

DISCUSSION

Many miRNAs have been detected as associated biomarkers and therapeutic targets in CRC. Several studies have shown that targeting specific miRNAs effectively inhibits cell proliferation and angiogenesis in CRC[22-24]. Thus, a better identification of CRC-associated miRNAs may contribute to the development of efficient miRNA-based therapy for CRC. In our previous study, we used miRNA expression profiling and showed *MIR375* to be associated with human CRC tissue[13] as well as DSS-

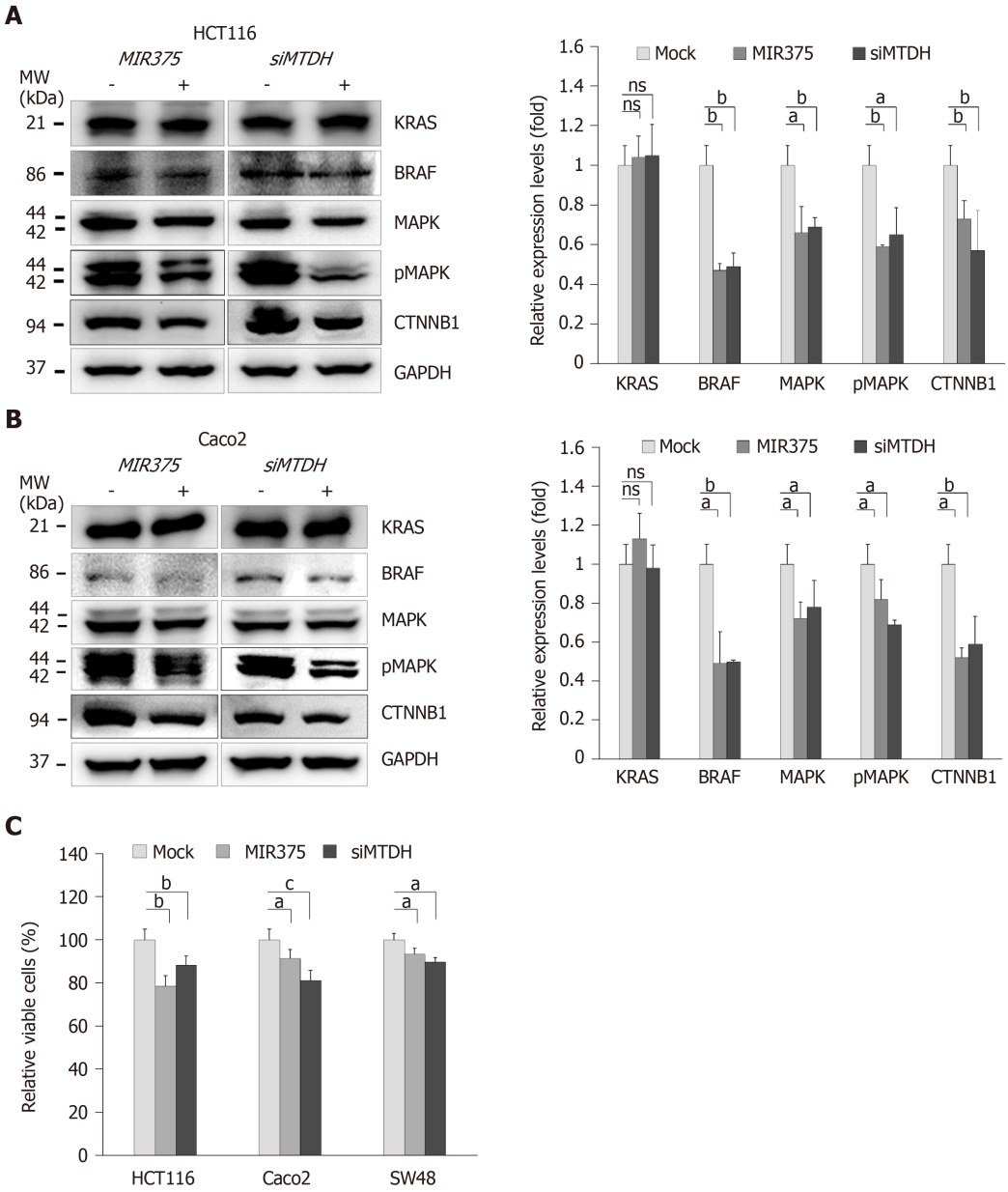

Figure 2 ***MicroRNA 375*** **regulates metadherin-mediated BRAF-MAPK signaling in colorectal cancer cell lines.** A: Western blot analysis of KRAS, BRAF, mitogen-activated protein kinase 3/1 (MAPK3/1), pMAPK3/1 and β catenin (CTNNB1) expression levels in colorectal cancer (CRC) cells. Except for KRAS; BRAF, MAPK3/1, pMAPK3/1 and CTNNB1 expression levels were downregulated on microRNA 375 (*MIR375)* mimic and *siMTDH* transfection in HCT116 cells; B: Western blot analysis of KRAS, BRAF, MAPK3/1, pMAPK3/1 and CTNNB1 expression levels in CRC cells. Except for KRAS; BRAF, MAPK3/1, pMAPK3/1 and CTNNB1 expression levels were downregulated on *MIR375* mimic and *siMTDH* transfection in Caco2 cells. Five independent experiments were performed with duplicates; C: Effects of *MIR375* and *siMTDH* on cell viability in HCT116, Caco2, and SW480 cells. Cell viability was determined by MTT assay. Three independent experiments were performed with duplicates and *P* values were calculated using Student's *t*-test ($^{a}P < 0.05$, $^{b}P < 0.01$, $^{c}P < 0.001$). ns: Not significant; *MTDH:* Metadherin; CTNNB1: β catenin; MAPK3/1: Mitogen-activated protein kinase 3/1; *MIR375:* microRNA 375; CRC: Colorectal cancer.

induced mice colitis[14] by comparing the expression pattern in CRC tissues versus matching healthy colorectal tissues and DSS-induced mice colitis versus healthy mice colons, respectively. Hyper-methylation of MIR375 has been demonstrated in CRC cell lines including HCT116 and SW480. Down regulation of MIR375 in HCT116 and SW480 cells compere to HT29 cells is due to hyper-methylation of MIR375 in HCT116 and SW480 cells[25]. In the present study, we confirmed the findings in a larger sample size and showed that *MIR375* expression was downregulated in human CRC tissues compared with that in matching healthy colon tissues (Supplementary Figure 1A). The results of the current study are consistent with the earlier research work by Dai *et al*[26]. In addition to that in our study, *MIR375* downregulation has been observed in several other types of cancer such as hepatocellular carcinoma[27], gastric cancer[28], and glioma[29]. However, some reports have revealed that *MIR375* is upregulated in tumors of prostate cancer[12] and breast cancer[30]. Primarily, miRNA expression levels were believed to be cell type-specific in many cancer tissues[31].

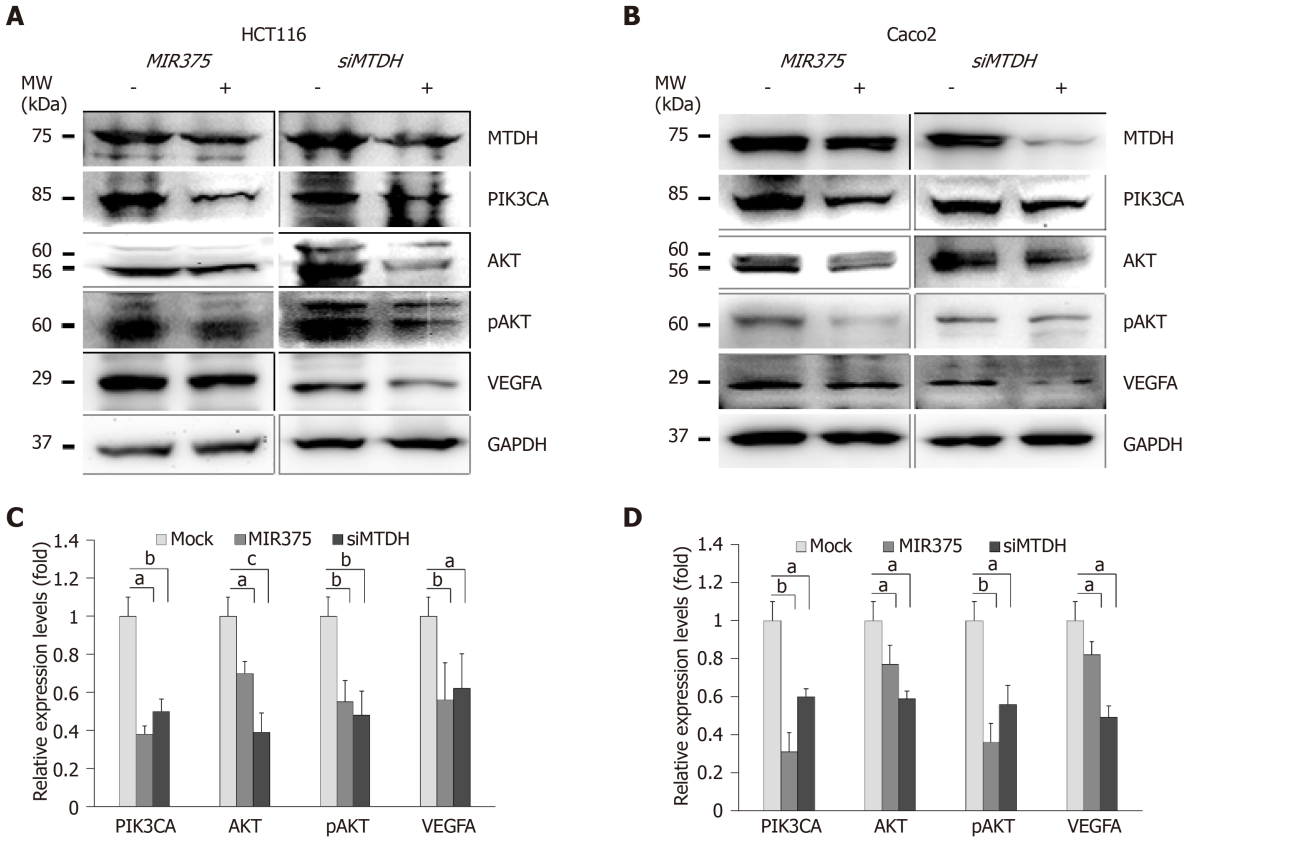

Figure 3 ***MicroRNA 375*** **regulates metadherin-mediated phosphatidylinositol-4,5-biphosphate-3-kinase catalytic subunit alpha-protein kinase B signaling in colorectal cancer cell lines.** A: Western blot analysis of phosphatidylinositol-4,5-biphosphate-3-kinase catalytic subunit alpha (PIK3CA), protein kinase B (AKT), pAKT, and vascular endothelial growth factor A (VEGFA) expression levels in colorectal cancer (CRC) cells; B: Western blot analysis of PIK3CA, AKT, pAKT, and VEGFA expression levels in CRC cells; C: PIK3CA, AKT, pAKT, and VEGFA expression levels were downregulated on microRNA 375 (*MIR375)* mimic and *siMTDH* transfection in HCT116 cells; D: PIK3CA, AKT, pAKT, and VEGFA expression levels were downregulated on *MIR375* mimic and *siMTDH* transfection in Caco2 cells. Five independent experiments were performed with duplicates and *P* values were calculated using Student's *t*-test ($^aP < 0.05$, $^bP < 0.01$, $^cP < 0.001$). *MTDH:* Metadherin; PIK3CA: Phosphatidylinositol-4,5-biphosphate-3-kinase catalytic subunit alpha; AKT: Protein kinase B; VEGFA: Vascular endothelial growth factor A; *MIR375:* microRNA 375; CRC: Colorectal cancer.

In our previous study, we found that *MIR375* regulates the CTGF-mediated EGFR-PIK3CA-AKT signaling pathway by directly downregulating CTGF expression in CRC cells. However, CTGF is not involved in EGFR-KRAS-BRAF-ERK1/2 signaling[15]. Although KRAS expression was unaffected by *MIR375* overexpression, BRAF-ERK1/2 signaling was regulated on *MIR375* overexpression in CRC cells[15]. These results guided us to investigate a novel *MIR375* target gene that mediates the BRAF-ERK1/2 signaling pathway in CRC cells. In this study, we found that *MTDH* is a direct target gene of *MIR375* in CRC cells (Figure 1). Further, we confirmed that *MIR375* regulates the MTDH-mediated BRAF-ERK1/2 (MAPK3/1) signaling pathway (Figure 2A and 2B), which controls proliferation in CRC cells (Figure 2C). It is well known that MTDH contributes to the carcinogenic process of different tissues and organs by regulating multiple signaling pathways such as PI3K/AKT, NF-kB, and MAPK, which subsequently promotes tumorigenesis and metastasis[32,33].

MTDH promotes an invasive phenotype and angiogenesis via the PIK3CA-AKT signaling pathway. In addition, *PIK3CA* has been proven as a direct target of *MIR375* in CRC cells[34]. MTDH expression is upregulated in many types of cancers, and is crucial in oncogenic transformation and angiogenesis[35-37]. The potential role of MTDH in angiogenesis has been correlated with VEGFA expression *via* the PIK3CA-AKT pathway in head and neck squamous cells[38]. Thus, PIK3CA-AKT-VEGFA signaling is affected on *MIR375* overexpression or on *VEGFA* silencing (*siVEGFA*). We showed that PIK3CA-AKT-VEGFA signaling is downregulated on *MIR375* overexpression and *siVEGFA* treatment in CRC cells (Figure 3). Our previous study using xenograft mouse model showed that the expression level of the angiogenic marker, CD31 was significantly decreased in xenograft tumors on *MIR375* overexpression[15]. Consequently, these results suggest that *MIR375* regulates angiogenesis *via* the MTDH-mediated PIK3CA-AKT-VEGFA signaling pathway in CRC progression.

Furthermore, MTDH has been shown to regulate the anchorage independent

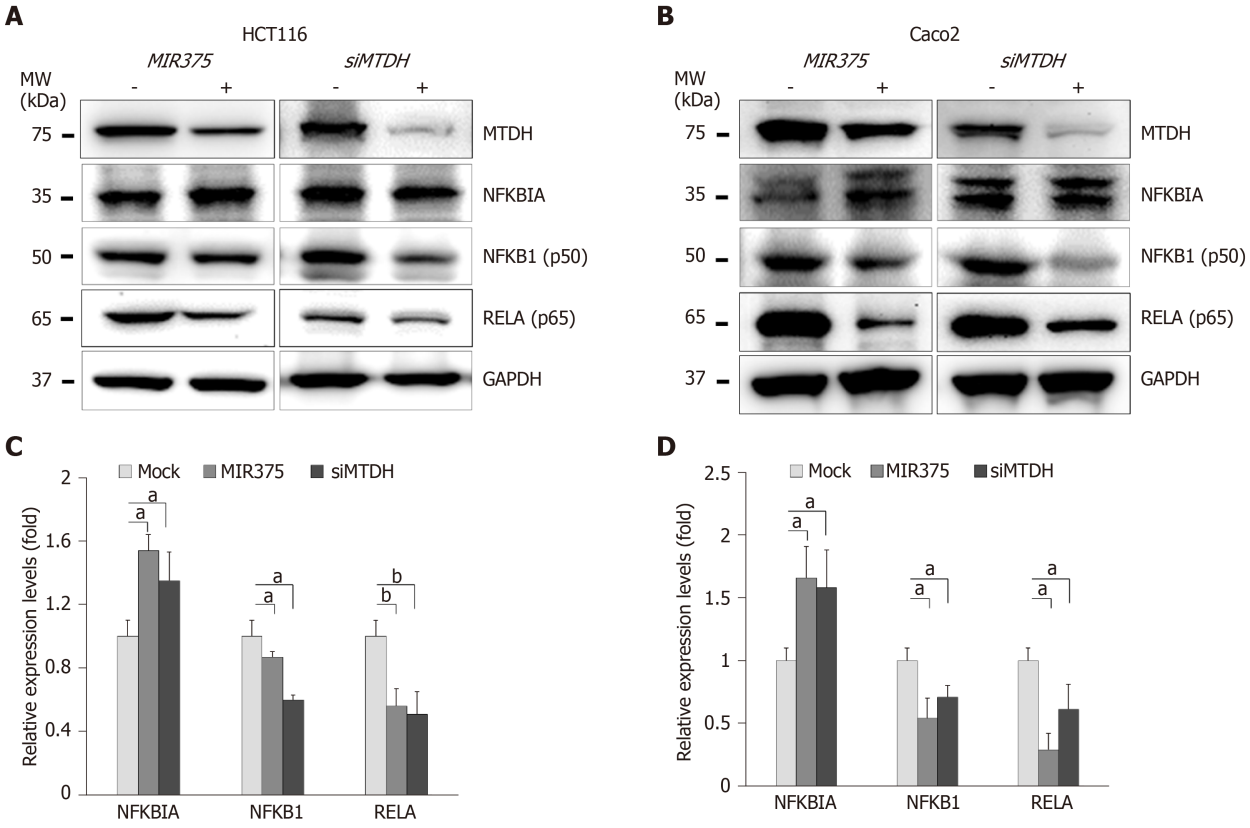

Figure 4 ***MicroRNA 375*** **regulates metadherin-mediated NFKB1 signaling in colorectal cancer cell lines.** Western blot analysis of NF-κB inhibitor alpha (NFKBIA), NFKB1 (p50), and RELA (p65) expression levels in colorectal cancer (CRC) cells. A: NFKBIA expression levels were upregulated on microRNA 375 (*MIR375)* mimic and *siMTDH* transfection in HCT116 cells; B: NFKBIA expression levels were upregulated on *MIR375* mimic and *siMTDH* transfection in Caco2 cells; C: NFKB1 and RELA levels were downregulated on *MIR375* mimic and *siMTDH* transfection in HCT116 cells; D: NFKB1 and RELA levels were downregulated on *MIR375* mimic and *siMTDH* transfection in Caco2 cells. Four independent experiments were performed with duplicates and *P* values were calculated using Student's *t*-test ($^{a}P < 0.05$, $^{b}P < 0.01$). *MTDH:* Metadherin; *MIR375:* MicroRNA 375; NFKBIA: NF-κB inhibitor alpha; CRC: Colorectal cancer.

growth and invasion of HeLa cells via activation of the NF-κB pathway[35]. MTDH has also been shown to be upregulated during CRC development and liver metastasis through the NF-κB signaling pathway[39]. Similarly, in malignant glioma cells, MTDH has been found to mediate invasion and migration through activation of the NF-κB signaling pathway[40]. In this study, we showed that *MIR375* regulates MTDH-mediated NFKB1 and RELA signaling by inhibiting NFKBIA expression in CRC cells (Figure 4).

In this study, *MIR375* expression levels were downregulated in CRC tissues (Supplementary Figure 1A). Inversely, MTDH, NFKB1, and RELA expression levels were predominantly upregulated in CRC tumor tissues compared to their expression levels in matched healthy colon tissues (Figure 5A). Additionally, immunohistochemistry staining of the CRC tissues showed that MTDH and RELA expression were upregulated in CRC tumor tissues. Overall, these results suggested that MTDH expression levels were negatively correlated with *MIR375* expression in CRC tissues.

In summary, our study found that *MIR375* expression is suppressed in tissues of patients with CRC and that *MTDH* is a direct target of *MIR375*. Furthermore, MTDH expression was upregulated in the tumors of CRC tissues on inhibiting *MIR375* expression. Overall, our results suggest that *MIR375* regulates MTDH-mediated signaling pathways such as MTDH-BRAF-MAPK, MTDH-PIK3CA-AKT, and MTDH-NFKBIA-NFKB1/RELA in CRC progression. Although we did not show MIR375-mediated VEGFA-VEGFR signaling in this study, our previous and present studies suggest that the generated VEGFA by MIR375-mediated PIK3CA-AKT or MTDH-PIK3CA-AKT signaling might effect to endothelial cell's angiogenesis. Subsequently, *MIR375* regulates cell proliferation, cell migration, and angiogenesis in CRC progression (Figure 6). Thus, we propose *MIR375* to be a promising therapeutic target in inhibiting CRC tumorigenesis. However, this needs to be further investigated.

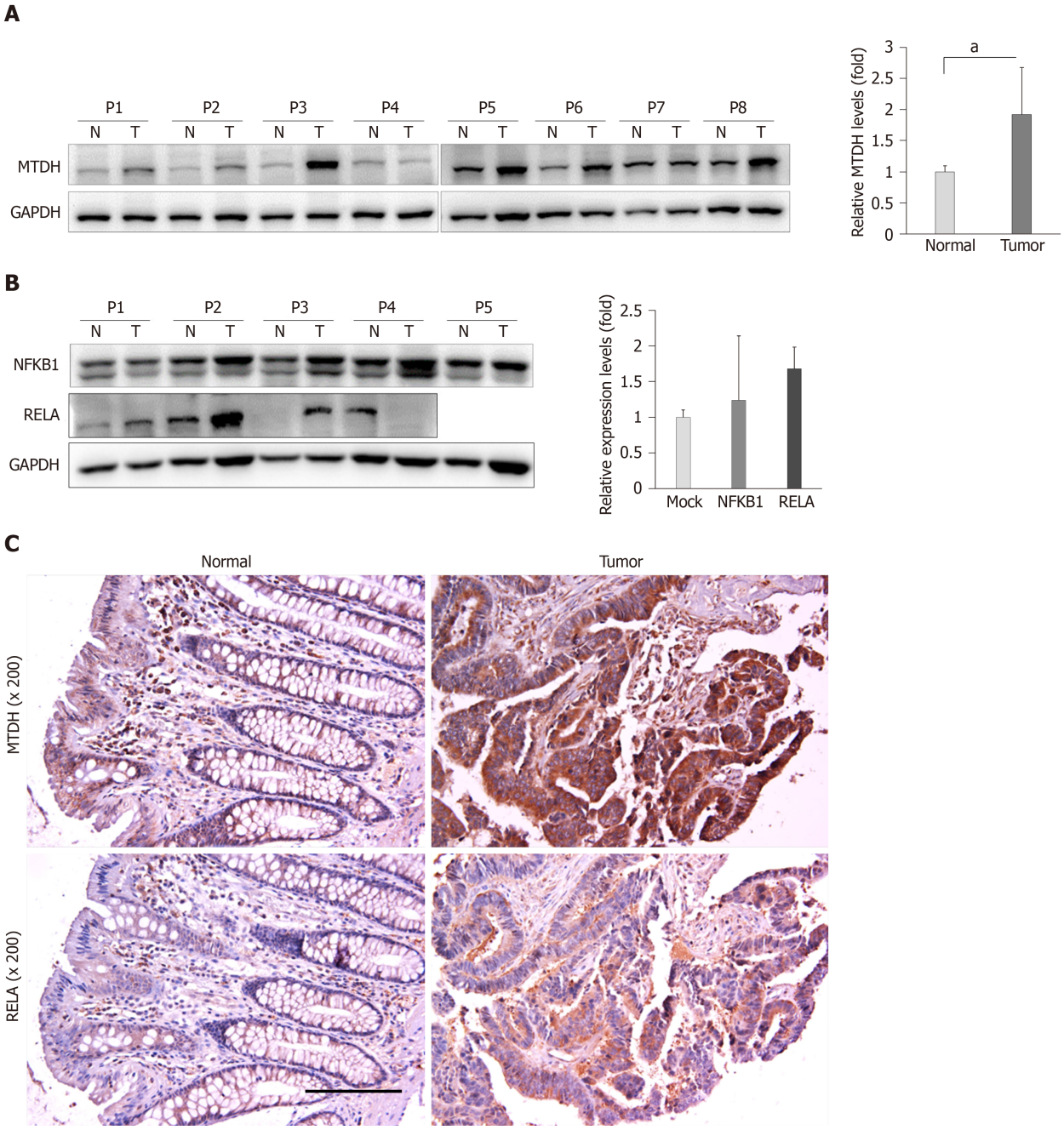

Figure 5 Endogenous metadherin expression in colorectal cancer tissues. A: metadherin (MTDH) expression levels were investigated in 15 colorectal cancer (CRC) tissue samples and matching healthy colorectal tissue samples. Results are shown for 8 colon cancer tissues in pairs. P1 to P8 indicate patients with colon cancer. Data are presented as fold change in the expression in tumor tissues relative to expression in matching healthy colon tissues. *P* values were calculated using Student's *t*-test ($^{a}P < 0.05$); B: Relative endogenous NFKB1 ($n = 5$) and RELA ($n = 4$) expression levels in colon cancer tissue samples and matching healthy colon tissue samples. Data are presented as fold change in the expression in tumor tissues relative to expression in matching healthy colon tissues; C: Immunostaining of MTDH in human CRC and adjacent healthy colorectal samples (200 × magnification). Experiments were independently performed three times in duplicates. *MTDH:* Metadherin.

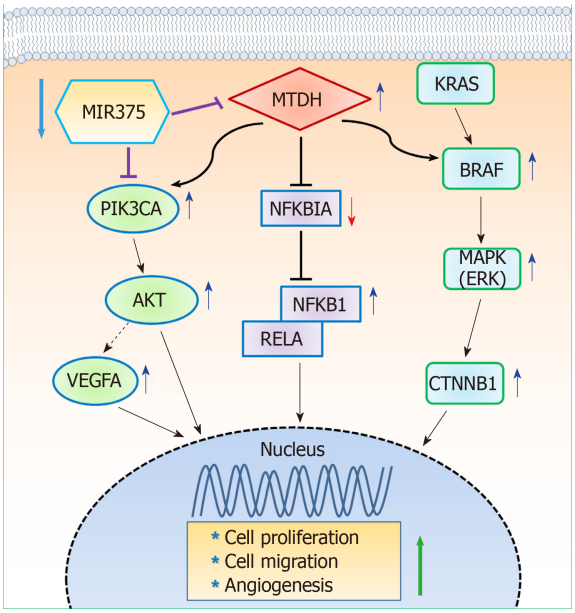

Figure 6 Diagrammatic representations of putative mechanisms of *microRNA 375* in regulating metadherin-induced cell proliferation, cell migration, and angiogenesis in human colorectal cancer. Decreased microRNA 375 (*MIR375)* expression in colorectal cancer (CRC) cells leads to upregulation of cellular metadherin (MTDH) levels. Subsequently, upregulated expression of MTDH promotes inhibition of NFKBIA and thus, NFKB1 and RELA expression is upregulated in CRC tissues and CRC cells. Upregulated MTDH expression level stimulates the BRAF-MAPK and PIK3CA-AKT signaling pathway. However, KRAS expression is unaltered by upregulation of MTDH. Consequently, downregulated *MIR375* expression levels in CRC leads to upregulation of cell proliferation, cell migration, and angiogenesis. This simple hypothetical mechanism of *MIR375*-mediated upregulation of angiogenesis is based on the results of previous studies and our current study. *MTDH:* Metadherin; *MIR375:* MicroRNA 375; CRC: Colorectal cancer.

ARTICLE HIGHLIGHTS

Research background

Colorectal cancer (CRC) is the third most prevalent type of cancer worldwide. The cause of CRC is multifactorial including genetic variation and epigenetic and environmental factors. However, the precise molecular mechanism underlying the development and progression of CRC remains largely unknown. We previously found that microRNA 375 (*MIR375*) is significantly downregulated in CRC, and identified metadherin (*MTDH*) as a candidate target gene of *MIR375*.

Research motivation

MIR375 and their target *MTDH* will provide a new therapeutic information for human CRC.

Research objectives

To study the interaction and signaling between *MIR375* and *MTDH* in human CRC pathogenesis.

Research methods

We constructed luciferase reporter plasmids to confirm the effect of *MIR375* on *MTDH* gene expression. The expression levels of the *MIR375* and *MTDH* were measured by qRT-PCR, Western blot, or immunohistochemistry. The effects of *MIR375* on cell growth and angiogenesis were conducted by functional experiments in CRC cells. Assays were performed to explore functional correlation between *MTDH* and *MIR375* in human CRC cells and tissues.

Research results

In the present study, we found that the expression levels of MTDH were significantly downregulated in CRC cells by *MIR375* mimic or *siMTDH* transfection. MTDH expression was upregulated in human CRC tissues in comparing to match normal colon tissues. Upregulated MTDH expression levels were found to inhibit NF-κB inhibitor alpha (NFKBIA) expression, which further upregulated NFKB1 and RELA expression. We found that *MIR375* regulate the expression levels of molecules in MTDH-mediated BRAF-MAPK and PIK3CA-AKT signal pathways in CRC cells.

Research conclusions

MIR375 regulates cell proliferation and angiogenesis by regulation of MTDH-mediated signaling pathways such as MTDH-BRAF-MAPK, MTDH-PIK3CA-AKT, and MTDH-NFKBIA-NFKB1/RELA in CRC progression.

Research perspectives

This study provides insight into the role of *MIR375* in CRC pathogenesis by targeting MTDH. *MIR375* might be a new therapeutic target for CRC.

ACKNOWLEDGEMENTS

Biospecimens used in this study were provided by Biobank of Wonkwang University Hospital, a member of the National Biobank of Korea which is supported by Ministry of Health and Welfare.

REFERENCES

1 **Greenlee RT**, Hill-Harmon MB, Murray T, Thun M. Cancer statistics, 2001. *CA Cancer J Clin* 2001; **51**: 15-36 [PMID: 11577478 DOI: 10.3322/canjclin.51.1.15]
2 **Parkin DM**, Bray F, Ferlay J, Pisani P. Global cancer statistics, 2002. *CA Cancer J Clin* 2005; **55**: 74-108 [PMID: 15761078 DOI: 10.3322/canjclin.55.2.74]
3 **Fearon ER**. Molecular genetics of colorectal cancer. *Annu Rev Pathol* 2011; **6**: 479-507 [PMID: 21090969 DOI: 10.1146/annurev-pathol-011110-130235]
4 **Markowitz SD**, Bertagnolli MM. Molecular origins of cancer: Molecular basis of colorectal cancer. *N Engl J Med* 2009; **361**: 2449-2460 [PMID: 20018966 DOI: 10.1056/NEJMra0804588]
5 **Bartel DP**. MicroRNAs: genomics, biogenesis, mechanism, and function. *Cell* 2004; **116**: 281-297 [PMID: 14744438 DOI: 10.1016/s0092-8674(04)00045-5]
6 **Brennecke J**, Hipfner DR, Stark A, Russell RB, Cohen SM. bantam encodes a developmentally regulated microRNA that controls cell proliferation and regulates the proapoptotic gene hid in Drosophila. *Cell* 2003; **113**: 25-36 [PMID: 12679032 DOI: 10.1016/s0092-8674(03)00231-9]
7 **Ma L**, Teruya-Feldstein J, Weinberg RA. Tumour invasion and metastasis initiated by microRNA-10b in breast cancer. *Nature* 2007; **449**: 682-688 [PMID: 17898713 DOI: 10.1038/nature06174]
8 **Su H**, Yang JR, Xu T, Huang J, Xu L, Yuan Y, Zhuang SM. MicroRNA-101, down-regulated in hepatocellular carcinoma, promotes apoptosis and suppresses tumorigenicity. *Cancer Res* 2009; **69**: 1135-1142 [PMID: 19155302 DOI: 10.1158/0008-5472.CAN-08-2886]
9 **Jung HM**, Patel RS, Phillips BL, Wang H, Cohen DM, Reinhold WC, Chang LJ, Yang LJ, Chan EK. Tumor suppressor miR-375 regulates MYC expression via repression of CIP2A coding sequence through multiple miRNA-mRNA interactions. *Mol Biol Cell* 2013; **24**: 1638-1648, S1-S7 [PMID: 23552692 DOI: 10.1091/mbc.E12-12-0891]
10 **Wang F**, Li Y, Zhou J, Xu J, Peng C, Ye F, Shen Y, Lu W, Wan X, Xie X. *miR-375 is down-regulated in squamous cervical cancer and inhibits cell migration and invasion via targeting transcription factor SP1. Am J Pathol* 2011; 2580-2588 [PMID: 21945323 DOI: 10.1016/j.ajpath.2011.07.037]
11 **Giricz O**, Reynolds PA, Ramnauth A, Liu C, Wang T, Stead L, Childs G, Rohan T, Shapiro N, Fineberg S, Kenny PA, Loudig O. Hsa-miR-375 is differentially expressed during breast lobular neoplasia and promotes loss of mammary acinar polarity. *J Pathol* 2012; **226**: 108-119 [PMID: 21953071 DOI: 10.1002/path.2978]
12 **Szczyrba J**, Nolte E, Wach S, Kremmer E, Stöhr R, Hartmann A, Wieland W, Wullich B, Grässer FA. Downregulation of Sec23A protein by miRNA-375 in prostate carcinoma. *Mol Cancer Res* 2011; **9**: 791-800 [PMID: 21593139 DOI: 10.1158/1541-7786.MCR-10-0573]
13 **Mo JS**, Alam KJ, Kang IH, Park WC, Seo GS, Choi SC, Kim HS, Moon HB, Yun KJ, Chae SC. MicroRNA 196B regulates FAS-mediated apoptosis in colorectal cancer cells. *Oncotarget* 2015; **6**: 2843-2855 [PMID: 25605245 DOI: 10.18632/oncotarget.3066]
14 **Mo JS**, Alam KJ, Kim HS, Lee YM, Yun KJ, Chae SC. MicroRNA 429 Regulates Mucin Gene Expression and Secretion in Murine Model of Colitis. *J Crohns Colitis* 2016; **10**: 837-849 [PMID: 26818658 DOI: 10.1093/ecco-jcc/jjw033]
15 **Alam KJ**, Mo JS, Han SH, Park WC, Kim HS, Yun KJ, Chae SC. MicroRNA 375 regulates proliferation and migration of colon cancer cells by suppressing the CTGF-EGFR signaling pathway. *Int J Cancer* 2017; **141**: 1614-1629 [PMID: 28670764 DOI: 10.1002/ijc.30861]
16 **Su ZZ**, Kang DC, Chen Y, Pekarskaya O, Chao W, Volsky DJ, Fisher PB. Identification and cloning of human astrocyte genes displaying elevated expression after infection with HIV-1 or exposure to HIV-1 envelope glycoprotein by rapid subtraction hybridization, RaSH. *Oncogene* 2002; **21**: 3592-3602 [PMID: 12032861 DOI: 10.1038/sj.onc.1205445]
17 **Brown DM**, Ruoslahti E. Metadherin, a cell surface protein in breast tumors that mediates lung metastasis. *Cancer Cell* 2004; **5**: 365-374 [PMID: 15093543 DOI: 10.1016/S1535-6108(04)00079-0]
18 **Ying Z**, Li J, Li M. Astrocyte elevated gene 1: biological functions and molecular mechanism in cancer and beyond. *Cell Biosci* 2011; **1**: 36 [PMID: 22060137 DOI: 10.1186/2045-3701-1-36]
19 **Emdad L**, Sarkar D, Su ZZ, Randolph A, Boukerche H, Valerie K, Fisher PB. Activation of the nuclear factor kappaB pathway by astrocyte elevated gene-1: implications for tumor progression and metastasis. *Cancer Res* 2006; **66**: 1509-1516 [PMID: 16452207 DOI: 10.1158/0008-5472.CAN-05-3029]
20 **Mo JS**, Han SH, Yun KJ, Chae SC. MicroRNA 429 regulates the expression of CHMP5 in the inflammatory colitis and colorectal cancer cells. *Inflamm Res* 2018; **67**: 985-996 [PMID: 30334065 DOI: 10.1007/s00011-018-1194-z]
21 **Ahmed D**, Eide PW, Eilertsen IA, Danielsen SA, Eknæs M, Hektoen M, Lind GE, Lothe RA. Epigenetic and genetic features of 24 colon cancer cell lines. *Oncogenesis* 2013; **2**: e71 [PMID: 24042735 DOI: 10.1038/oncsis.2013.35]
22 **Li Y**, Lauriola M, Kim D, Francesconi M, D'Uva G, Shibata D, Malafa MP, Yeatman TJ, Coppola D, Solmi R, Cheng JQ. Adenomatous polyposis coli (APC) regulates miR17-92 cluster through β-catenin pathway in colorectal cancer. *Oncogene* 2016; **35**: 4558-4568 [PMID: 26804172 DOI: 10.1038/onc.2015.522]
23 **Ji S**, Ye G, Zhang J, Wang L, Wang T, Wang Z, Zhang T, Wang G, Guo Z, Luo Y, Cai J, Yang JY. miR-574-5p negatively regulates Qki6/7 to impact β-catenin/Wnt signalling and the development of colorectal cancer. *Gut* 2013; **62**: 716-726 [PMID: 22490519 DOI: 10.1136/gutjnl-2011-301083]

24 **Liang L**, Gao C, Li Y, Sun M, Xu J, Li H, Jia L, Zhao Y. miR-125a-3p/FUT5-FUT6 axis mediates colorectal cancer cell proliferation, migration, invasion and pathological angiogenesis via PI3K-Akt pathway. *Cell Death Dis* 2017; **8**: e2968 [PMID: 28771224 DOI: 10.1038/cddis.2017.352]

25 **Christensen LL**, Holm A, Rantala J, Kallioniemi O, Rasmussen MH, Ostenfeld MS, Dagnaes-Hansen F, Øster B, Schepeler T, Tobiasen H, Thorsen K, Sieber OM, Gibbs P, Lamy P, Hansen TF, Jakobsen A, Riising EM, Helin K, Lubinski J, Hagemann-Madsen R, Laurberg S, Ørntoft TF, Andersen CL. Functional screening identifies miRNAs influencing apoptosis and proliferation in colorectal cancer. *PLoS One* 2014; **9**: e96767 [PMID: 24892549 DOI: 10.1371/journal.pone.0096767]

26 **Dai X**, Chiang Y, Wang Z, Song Y, Lu C, Gao P, Xu H. Expression levels of microRNA-375 in colorectal carcinoma. *Mol Med Rep* 2012; **5**: 1299-1304 [PMID: 22377847 DOI: 10.3892/mmr.2012.815]

27 **He XX**, Chang Y, Meng FY, Wang MY, Xie QH, Tang F, Li PY, Song YH, Lin JS. MicroRNA-375 targets AEG-1 in hepatocellular carcinoma and suppresses liver cancer cell growth in vitro and in vivo. *Oncogene* 2012; **31**: 3357-3369 [PMID: 22056881 DOI: 10.1038/onc.2011.500]

28 **Ding L**, Xu Y, Zhang W, Deng Y, Si M, Du Y, Yao H, Liu X, Ke Y, Si J, Zhou T. MiR-375 frequently downregulated in gastric cancer inhibits cell proliferation by targeting JAK2. *Cell Res* 2010; **20**: 784-793 [PMID: 20548334 DOI: 10.1038/cr.2010.79]

29 **Chang C**, Shi H, Wang C, Wang J, Geng N, Jiang X, Wang X. Correlation of microRNA-375 downregulation with unfavorable clinical outcome of patients with glioma. *Neurosci Lett* 2012; **531**: 204-208 [PMID: 23103713 DOI: 10.1016/j.neulet.2012.10.021]

30 **de Souza Rocha Simonini P**, Breiling A, Gupta N, Malekpour M, Youns M, Omranipour R, Malekpour F, Volinia S, Croce CM, Najmabadi H, Diederichs S, Sahin O, Mayer D, Lyko F, Hoheisel JD, Riazalhosseini Y. Epigenetically deregulated microRNA-375 is involved in a positive feedback loop with estrogen receptor alpha in breast cancer cells. *Cancer Res* 2010; **70**: 9175-9184 [PMID: 20978187 DOI: 10.1158/0008-5472.CAN-10-1318]

31 **Volinia S**, Calin GA, Liu CG, Ambs S, Cimmino A, Petrocca F, Visone R, Iorio M, Roldo C, Ferracin M, Prueitt RL, Yanaihara N, Lanza G, Scarpa A, Vecchione A, Negrini M, Harris CC, Croce CM. A microRNA expression signature of human solid tumors defines cancer gene targets. *Proc Natl Acad Sci USA* 2006; **103**: 2257-2261 [PMID: 16461460 DOI: 10.1073/pnas.0510565103]

32 **Emdad L**, Das SK, Dasgupta S, Hu B, Sarkar D, Fisher PB. AEG-1/MTDH/LYRIC: signaling pathways, downstream genes, interacting proteins, and regulation of tumor angiogenesis. *Adv Cancer Res* 2013; **120**: 75-111 [PMID: 23889988 DOI: 10.1016/B978-0-12-401676-7.00003-6]

33 **Huang Y**, Li LP. Progress of cancer research on astrocyte elevated gene-1/Metadherin (Review). *Oncol Lett* 2014; **8**: 493-501 [PMID: 25009642 DOI: 10.3892/ol.2014.2231]

34 **Wang Y**, Tang Q, Li M, Jiang S, Wang X. MicroRNA-375 inhibits colorectal cancer growth by targeting PIK3CA. *Biochem Biophys Res Commun* 2014; **444**: 199-204 [PMID: 24440701 DOI: 10.1016/j.bbrc.2014.01.028]

35 **Emdad L**, Lee SG, Su ZZ, Jeon HY, Boukerche H, Sarkar D, Fisher PB. Astrocyte elevated gene-1 (AEG-1) functions as an oncogene and regulates angiogenesis. *Proc Natl Acad Sci USA* 2009; **106**: 21300-21305 [PMID: 19940250 DOI: 10.1073/pnas.0910936106]

36 **Li C**, Li R, Song H, Wang D, Feng T, Yu X, Zhao Y, Liu J, Yu X, Wang Y, Geng J. Significance of AEG-1 expression in correlation with VEGF, microvessel density and clinicopathological characteristics in triple-negative breast cancer. *J Surg Oncol* 2011; **103**: 184-192 [PMID: 21259255 DOI: 10.1002/jso.21788]

37 **Long M**, Dong K, Gao P, Wang X, Liu L, Yang S, Lin F, Wei J, Zhang H. Overexpression of astrocyte-elevated gene-1 is associated with cervical carcinoma progression and angiogenesis. *Oncol Rep* 2013; **30**: 1414-1422 [PMID: 23835593 DOI: 10.3892/or.2013.2598]

38 **Zhu GC**, Yu CY, She L, Tan HL, Li G, Ren SL, Su ZW, Wei M, Huang DH, Tian YQ, Su RN, Liu Y, Zhang X. Metadherin regulation of vascular endothelial growth factor expression is dependent upon the PI3K/Akt pathway in squamous cell carcinoma of the head and neck. *Medicine (Baltimore)* 2015; **94**: e502 [PMID: 25674742 DOI: 10.1097/MD.0000000000000502]

39 **Gnosa S**, Shen YM, Wang CJ, Zhang H, Stratmann J, Arbman G, Sun XF. Expression of AEG-1 mRNA and protein in colorectal cancer patients and colon cancer cell lines. *J Transl Med* 2012; **10**: 109 [PMID: 22643064 DOI: 10.1186/1479-5876-10-109]

40 **Sarkar D**, Park ES, Emdad L, Lee SG, Su ZZ, Fisher PB. Molecular basis of nuclear factor-kappaB activation by astrocyte elevated gene-1. *Cancer Res* 2008; **68**: 1478-1484 [PMID: 18316612 DOI: 10.1158/0008-5472.CAN-07-6164]

World Journal of Gastroenterology

Submit a Manuscript: https://www.f6publishing.com

World J Gastroenterol 2019 November 28; 25(44): 6508-6526

DOI: 10.3748/wjg.v25.i44.6508

ISSN 1007-9327 (print) ISSN 2219-2840 (online)

ORIGINAL ARTICLE

Basic Study

Long noncoding RNA NALT1-induced gastric cancer invasion and metastasis *via* NOTCH signaling pathway

Hai-Yan Piao, Shuai Guo, Yue Wang, Jun Zhang

ORCID number: Hai-Yan Piao (0000-0002-3039-5758); Shuai Guo (0000-0002-7418-6915); Yue Wang (0000-0003-4536-9904); Jun Zhang (0000-0003-1739-6462).

Author contributions: Zhang J designed the research; Piao HY performed the majority of experiments, analyzed the data, and drafted the manuscript; Guo S conducted the molecular biology assays and assisted in writing the manuscript; Wang Y collected and analyzed the data.

Supported by Liaoning S&T Project, No. 20180550971 and No. 20170520447; and CSCO-MERCK SERNO oncology research fund, No. Y-MX2016-031.

Institutional review board statement: The study was reviewed and approved by the Faculty of Science Ethics Committee at Liaoning Cancer Hospital & Institute (Cancer Hospital of China Medical University) (20150308-2).

Informed consent statement: All study participants provided informed written consent prior to their treatments and study enrollment.

Conflict-of-interest statement: The authors declare that there are no conflicts of interest related to this study.

Data sharing statement: No additional data are available.

ARRIVE guidelines statement: The authors have read the ARRIVE guidelines, and the manuscript

Hai-Yan Piao, Medical Oncology Department of Gastrointestinal Cancer, Liaoning Province Cancer Hospital & Institute (Cancer Hospital of China Medical University), Shenyang 110042, Liaoning Province, China

Shuai Guo, Yue Wang, Jun Zhang, Gastric Cancer Department, Liaoning Province Cancer Hospital & Institute (Cancer Hospital of China Medical University), Shenyang 110042, Liaoning Province, China

Corresponding author: Jun Zhang, MD, Doctor, Gastric Cancer Department, LiaoNing Cancer Hospital & Institute (Cancer Hospital of China Medical University) No. 44 Xiaoheyan Road, Dadong District, Shenyang 110042, Liaoning Province, China.
zhangjun@cancerhosp-ln-cmu.com
Telephone: +86-24-31916823
Fax: +86-24-2431-5679

Abstract

BACKGROUND

Long noncoding RNAs (lncRNAs) are aberrant and play critical roles in gastric cancer (GC) progression and metastasis. Searching for coexpressed lncRNA clusters or representative biomarkers related to malignant phenotypes of GC may help to elucidate the mechanism of tumor development and predict the prognosis of GC.

AIM

To investigate the prognostic value of NOTCH1 associated with lncRNA in T cell acute lymphoblastic leukemia 1 (NALT1) in GC and the mechanism of its involvement in GC invasion and metastasis.

METHODS

RNA sequencing and corresponding clinical data were downloaded from The Cancer Genome Atlas database. The significance module was studied by weighted gene coexpression network analysis. A total of 336 clinical samples were included in the study. Gene silencing, reverse transcription polymerase chain reaction, western blotting, scrape motility assay, and Transwell migration assay were used to assess the function of hub-lncRNAs.

RESULTS

At the transcriptome level, 3339 differentially expressed lncRNAs were obtained. weighted gene coexpression network analysis was used to obtain 15 lncRNA clusters and observe their coexpression. Pearson's correlation showed that blue

module was correlated with tumor grade and survival. NALT1 was the hub-lncRNA of blue module and was an independent risk factor for GC prognosis. NALT1 was overexpressed in GC and its expression was closely related to invasion and metastasis. The mechanism may involve NALT1 regulation of NOTCH1, which is associated with lncRNA in T cell acute lymphoblastic leukemia, through *cis* regulation, thereby affecting the expression of the NOTCH signaling pathway.

CONCLUSION

NALT1 is overexpressed and promotes invasion and metastasis of GC. The mechanism may be related to regulation of NOTCH1 by NALT1 and its effect on NOTCH signaling pathway expression.

Key words: Gastric cancer; Weighted gene coexpression network analysis; NALT1; NOTCH1; Cancer survival

Core tip: Analysis of the Cancer Genome Atlas and clinical data revealed that the long noncoding RNA (lncRNA) NOTCH1 associated with lncRNA in T cell acute lymphoblastic leukemia 1 (NALT1) was associated with poor prognosis of gastric cancer (GC). We investigated the possible mechanism of this association. We downloaded the Cancer Genome Atlas-Stomach Adenocarcinoma RNA-seq data and identified the differentially expressed lncRNAs. Weighted gene coexpression network analysis was used to clarify the connection between modules and clinical information. We then chose lncRNA NALT1 as the hub-lncRNA of blue-module. NALT1 was overexpressed in GC and promoted invasion and metastasis of GC. The over-expression of NALT1 was linked to poor prognosis in GC. The mechanism may be related to the regulation of NOTCH1 by NALT1 and its effect on the expression of NOTCH signaling pathway.

Citation: Piao HY, Guo S, Wang Y, Zhang J. Long noncoding RNA NALT1-induced gastric cancer invasion and metastasis *via* NOTCH signaling pathway. *World J Gastroenterol* 2019; 25(44): 6508-6526
URL: https://www.wjgnet.com/1007-9327/full/v25/i44/6508.htm
DOI: https://dx.doi.org/10.3748/wjg.v25.i44.6508

Manuscript source: Unsolicited manuscript

Received: August 30, 2019
Peer-review started: August 30, 2019
First decision: October 14, 2019
Revised: October 30, 2019
Accepted: November 13, 2019
Article in press: November 13, 2019
Published online: November 28, 2019

P-Reviewer: Chuang SM
S-Editor: Wang J
L-Editor: Filipodia
E-Editor: Ma YJ

INTRODUCTION

Gastric cancer (GC) is one of the most common digestive system malignant tumors and poses a serious threat to human health[1]. Long-term survival of GC is still poor due to the high recurrence and distal metastasis rates, despite advances in diagnosis and treatment[2]. Therefore, it is necessary to explore new biomarkers and clarify relevant molecular mechanisms for the formulation of GC treatment strategies. With the completion of Human Genome Project and the parallel development of next-generation sequencing, human transcriptome analysis has revealed that > 98% of the transcriptional output encodes noncoding RNAs (ncRNAs), which have little or even no protein-coding capability[3]. Long noncoding RNAs (lncRNAs), with a length not less than 200 nucleotides, are dominant in the ncRNA family[4]. Accumulated studies have indicated that dysregulation of lncRNAs plays a crucial role in regulation of oncogenes or tumor suppressor genes[5]. LncRNAs are involved in cellular biological processes at multiple levels, including epigenetics, transcription, and post-transcriptional regulation[6]. Therefore, it is believed that the complex regulatory network between mRNA and lncRNAs may mediate the malignant phenotype of GC. For example, lncRNA GClnc1 acts as a "scaffold" to recruit the WDR5 and KAT2A complex and thus induces tumorigenesis, metastasis, and poor prognosis in GC[7]. HOXC-AS3 activated by abnormal histone modification may play an important role in regulation of GC cell proliferation and migration[8].

As a large multiplatform database of molecular maps and clinicopathological annotated data, The Cancer Genome Atlas (TCGA) facilitates the analysis of molecules associated with various clinicopathological parameters of cancer[9]. Using weighted gene coexpression network analysis (WGCNA), coexpression modules or

networks of genes can be established to explore the correlation between different gene clusters and clinicopathological parameters[10]. In this investigation, lncRNAs with abnormal expression in GC were searched using transcriptome data of GC in TCGA database [TCGA-stomach adenocarcinoma (STAD)]. WGCNA was used to construct coexpression networks of differentially expressed lncRNAs (DELs) and to analyze the correlation between lncRNA clusters and clinicopathological parameters. In addition, it was revealed that lncRNA NOTCH1 associated with lncRNA in T cell acute lymphoblastic leukemia 1 (NALT1) was the hub-RNA of blue cluster and overexpressed in both GC tissues and cells. Mechanistic analyses revealed that NALT1 was involved in invasion and metastasis of GC, which was through the NOTCH signaling pathway. We studied the role of NALT1 in GC prognosis because the blue module was closely related to tumor differentiation and survival.

MATERIALS AND METHODS

Data download and DELs analysis

The RNA sequencing dataset and corresponding clinical records of GC were downloaded from TCGA (TCGA-STAD, https://portal.gdc.cancer.gov/). The RNA expression profile raw data were download by RTCGA Toolbox package in R platform. There were 406 samples, with 375 GC tissues and 31 normal tissues. Clinical data of 375 tumor tissue specimens were complete. Package edgeR was used to identify DELs. $P < 0.05$ and $|\log_2 FC| \geq 1$ were set as the cutoff criteria.

Construction of WGCNA

WGCNA package was used to construct a coexpression network of DELs[11]. The power function, which was dependent on soft-thresholding β, was used to create the weighted adjacency matrix. We transformed the adjacency matrix to topological overlap matrix (TOM). We performed average linkage hierarchical clustering based on per TOM dissimilarity measurement. The minimum size of the gene group for the genes dendrogram was 30, was the deep split, and 0.15 was the cutoff for module dendrogram and merged modules. Pearson's correlation was used to search for biologically meaningful clusters and to evaluate the correlation between clusters and clinicopathological parameters. Age, tumor stage, grade, and overall survival (OS) were recorded. The module with the highest correlation was selected as the meaningful research cluster. Cytoscape 3.6.1 software (http://www.cytoscape.org/) was used to construct the network[12]. Molecular Complex Detection (MCODE) was used to filter the network module.

Patients and ethics statement

The study was approved by the Ethics Committee, Liaoning Cancer Hospital & Institute. The patients gave signed informed consent before surgery. There were 336 patients who underwent D2 lymph node dissected gastrectomy at Liaoning Cancer Hospital between January 2011 and March 2014, including 236 (70.2%) men and 100 (29.8%) women, with a mean age of 57 years. Patients treated with preoperative chemotherapy or radiotherapy were excluded. Adenosquamous carcinoma or neuroendocrine carcinoma patients were excluded. Tumor staging was based on the 8th edition of the tumor node metastasis (TNM) staging manual (American Joint Committee on Cancer/Union for International Cancer Control, 2017).

Patients with stage IIA and worse were routinely treated with postoperative adjuvant chemotherapy. Table 1 describes the clinicopathological parameters involved in the analysis. Follow-up was conducted every 3-6 mo within 5 years after the operation, including physical examination, pulmonary, abdominal, and pelvic computed tomography, blood count, endoscopic examination, and liver function examination. OS was the time between surgery and final follow-up or death. Disease-free survival (DFS) was the time between the date of resection and first diagnosis of recurrence. The final investigation date was 1 March 2019.

Cell culture

Human normal gastric epithelial cell line GES-1 and human gastric cancer cell lines SGC-7901 and BGC-823 were obtained from China Medical University (Shenyang, China). Cells were cultured in RPMI 1640 medium supplemented with 10% fetal bovine serum (Invitrogen, Carlsbad, CA, United States), 100 U/mL penicillin, and 100 μg/mL streptomycin (Invitrogen) at 37 °C under 5% CO_2 and 1% O_2. All experiments were repeated three times independently.

Real-time reverse transcription polymerase chain reaction

Total RNA was isolated from cells and tissues with TRIzol cell separation reagent

Table 1 Patients characteristics and univariate analysis, *n* = 336

Characteristics	*n* (%)	DFS			OS		
		Mo	*P* value	F	Mo	*P* value	F
Age, median, yr			0.280	1.172		0.641	0.218
≥ 60	178	37.73			44.80		
< 60	158	40.77			45.95		
Gender			0.085	2.982		0.216	1.537
Male	236 (70.2)	37.59			44.35		
Female	100 (29.8)	42.86			47.68		
Bormann type			0.000	55.616		0.000	49.755
I	25	64.00			64.00		
II	147	45.92			51.50		
III	159	29.62			37.20		
IV	5	19.60			29.80		
Tumor size			0.000	26.829		0.000	20.674
≥ 5 cm	142	30.99			38.99		
< 5 cm	194	45.13			49.99		
Location			0.142	3.899		0.325	2.247
Up	75	34.15			41.80		
Middle	90	42.04			47.60		
Low	171	39.84			45.70		
Tumor histological morphology			0.788	0.476		0.870	0.277
Adenocarcinoma	260	39.30			45.33		
Mixed carcinoma	75	38.35			45.13		
Absolute signet ring cell carcinoma	1	35.00			45.00		
Lauren type			0.298	2.420		0.309	2.349
Intestinal	156	38.79			44.88		
Mixed carcinoma	75	35.15			41.99		
Diffuse	105	42.57			48.42		
Tumor differentiation			0.000	20.700		0.000	17.649
Moderate and high	167	45.38			50.41		
Poor	169	33.01			40.33		
Vessel invasion			0.000	19.213		0.000	15.243
Yes	98	29.85			37.40		
No	238	42.99			48.61		
Perineural invasion			0.000	17.809		0.000	16.686
Yes	84	28.45			36.83		
No	252	42.73			48.17		
T category			0.000	105.672		0.000	91.002
T1	60	65.95			65.98		
T2	22	58.82			61.32		
T3	12	60.25			62.00		
T4	242	29.68			37.94		
N category			0.000	232.168		0.000	217.417
N0	139	62.74			63.47		
N1	58	36.12			48.07		
N2	65	23.88			33.55		
N3	74	10.66			18.16		
TNM stage			0.000	218.328		0.000	204.741
I	69	64.52			64.55		
II	81	63.59			66.40		
III	14	19.26			29.27		
IV	2	5.00			8.50		
NALT1			0.000	20.645		0.000	18.035

Weak-expression	159	45.24	50.30
Over-expression	177	33.69	40.88

DFS: Disease-free survival; OS: Overall survival.

(Invitrogen). Promega cDNA core kit (Madison, WI, United States) was used to generate cDNA from 500 ng total RNA. SYBR Master Mix (Takara Bio, Kusatsu, Japan) was used to perform real-time reverse transcription polymerase chain reaction (RT-PCR) (LightCycler 480; Roche AG, Basel, Switzerland). Each sample was analyzed three times. U6 was the loading control. Fold changes in mRNA expression in different cells were determined by $2^{-\Delta\Delta CT}$ normalization. Each sample was analyzed in triplicate. The sequence information is listed in Supplementary table 1.

Western blotting

Sodium dodecyl sulfate polyacrylamide gel electrophoresis (10%-15%) and polyvinylidene difluoride membranes were used to separate and transfer protein (20 μg) from cells. TBS-Tween buffer (20 mmol/L Tris–HCl, 5% nonfat milk, 150 mmol/L NaCl, and 0.05% Tween-20, pH 7.5) was used to block membranes for 1 h at 21 °C after blotting. The membranes were incubated with primary antibodies overnight at 4 °C (NOTCH1, SNAI1, 1: 200, Boster Biological Technology; SLUG, MMP9, 1:150, Boster Biological Technology; and β-actin, 1: 4000, Santa Cruz Biotechnology, Santa Cruz, CA, United States). Finally, membranes were incubated with secondary antibody (1: 5000, Santa Cruz Biotechnology). β-Actin acted as a control. The gray value of proteins was measured by ImageJ (NIH, Bethesda, MD, United States). Averages of three independent data were presented as the final results.

Lentiviral vector system, plasmids, and cell transfection

Lentiviruses carrying siRNA sequences targeting human NALT1 were obtained from GeneChem (Shanghai, China). Full-length human NOTCH1 cDNA was subcloned into the pcDNA 3.1 vector. Lipofectamine 2000 Reagent (Invitrogen) was used to transfect the GC cells.

Scrape motility and Transwell invasion assays

Scrape motility assay was used to evaluate cell migration. GC cells were plated into culture inserts (Ibidi, Regensburg, Germany). After 24 h incubation, we removed the inserts. An inverted microscope (XDS-100; Shanghai Caikon Optical Instrument, Shanghai, China) was used to capture the wound monolayers images at 0 and 24 h post-wounding.

Transwell assay was performed to determine cell invasion. Transwell upper chambers coated with gelatin were used to plate GC cells. The lower chambers were coated with 600 μL fetal bovine serum (30%, Costar, Lowell, MA, United States). Methanol, hematoxylin, and eosin were used to fix and stain cells after incubation for 24 h (Sigma–Aldrich, St. Louis, MO, United States). We removed the upper chambers; the cells on the surface of the lower chambers were migrated cells that were counted and captured by microscopy at 100 × magnification in five fields. The average cell number per field represented the migrated cells.

Statistical analysis

Statistical analysis was performed using SPSS version 23.0 (IBM, Armonk, NY, United States). All data are presented as mean ± standard deviation. Data were compared by Student's t test when homogeneity of variance was satisfied between groups; otherwise, the Wilcoxon-signed rank test was used. Multiple groups were compared using one-way analysis of variance. χ^2 test or Fisher's exact test reflected the correlation between clinicopathological parameters and biomarkers. Kaplan-Meier survival curves were generated from the survival data. Univariate survival analysis was performed by log-rank test. Cox proportional hazard model was used to evaluate the clinical significance of the biomarkers. $P < 0.05$ was considered to be statistically significant.

RESULTS

DELs in GC

TCGA-STAD RNA sequence dataset included 375 GC samples and 31 para-carcinoma tissues. EdgeR was applied to identify the DELs (fold change ≥ 2, $P < 0.05$). A total of 4264 DELs were screened from the expression profile data, which included 14449

lncRNAs. Among them, 3339 were upregulated DELs (uDELs) and 925 were downregulated DELs (dDELs) (Figure 1A). All these were further investigated by WGCNA. The volcano showed the top 25 uDELs and dDELs (Figure 1B).

WCGNA and hub-lncRNA identification

WGCNA was performed to identify the functional RNA cluster of GC patients. The scale-free network was constructed based on 4264 DELs with a soft threshold $\beta = 2$ (Figure 2A). A total of 15 RNA clusters were obtained that contained 36–729 DELs (Figure 2B). Correlation analysis showed that the blue module had the most significant correlation with clinical features. It was significantly correlated with grade ($r = 0.25$, $P = 4 \times 10^{-7}$; Figure 2C) and prognosis ($r = 0.17$, $P = 6 \times 10^{-4}$; Figure 2C). TOM plot was generated from the TOM plot function to verify module correlation (Figure 2D). Eigengenes were treated as representative profiles to quantify module similarity correlation. The dendrogram and heatmap showed the correlation and eigengene adjacency between modules, respectively (Figure 2E).

The gene significance in the blue module was imported into Cytoscape software to construct a WGCN. MCODE was applied to filter the network module and select hub-lncRNAs. Weight > 0.4 and MCODE score > 8 combined were selected as significant. NALT1 had the highest score for follow-up (Figure 2F).

Clinical significance of NALT1

RT-PCR was used to detect expression of NALT1 in 35 paired samples (GC *vs* adjacent noncancerous samples). It was obvious that NALT1 was overexpressed in GC samples (Figure 3A). As predicted by bioinformatics, expression of NALT1 was closely related to tumor differentiation in 336 GC specimens (Figure 3B).

To explore further the relationship between NALT1 and clinicopathological parameters, we grouped them according to the expression level of NALT1. The median value of NALT1 expression was set as the cutoff value in 336 samples. One hundred and seventy-seven (52.7%) samples were assigned to the overexpressed group and 159 (47.3%) to the weak expression group. Table 2 summarizes the correlation between clinicopathological parameters and NALT1 expression levels. Not surprisingly, expression of NALT1 was closely related to tumor differentiation ($P = 0.000$, $\chi^2 = 247.392$) and TNM stage ($P = 0.001$, $\chi^2 = 17.625$).

Of the 336 patients, 319 had complete follow-up data, and 196 (58.3%) died before the end of follow-up. DFS was 5-91 mo, with a median of 33 mo, and OS was 7-91 mo, with a median of 45.5 mo. Patients with overexpression of NALT1 showed poorer DFS (45.24 *vs* 33.69 mo, $P < 0.01$) and OS (50.30 *vs* 40.88 mo, $P < 0.01$) (Table 1, Figure 3C, 3D). Multiple factor analysis included the clinicopathological parameters with $P < 0.05$ in univariate analysis. A backward stepwise method was applied in the Cox proportional hazards model. TNM stage and expression of NALT1 served as independent prognostic factors for prediction of DFS [TNM: $P < 0.01$, hazard ratio (HR) = 125.49, 95% confidence interval (CI): 42.47–370.76; NALT1: $P = 0.02$, HR = 0.71, 95%CI: 0.53-0.96; Table 3) and OS (TNM: $P < 0.01$, HR = 87.98, 95%CI: 37.29-207.38; NALT1: $P = 0.02$, HR = 0.71, 95%CI: 0.52-0.95; Table 3).

NALT1 was overexpressed and associated with invasion and metastasis of GC

Similar to overexpression in GC tissues, NALT1 was also overexpressed in GC (SGC-7901 and BGC-823) cells (Figure 4A). To evaluate the biology of NALT1 in GC, NALT1 siRNAs were transfected into GC cell lines. Two siRNAs targeting NALT1 were detected (si-NALT1#1, si-NALT1#2), among which si-NALT1#1 was the most effective siRNA to remove NALT1 expression and was selected for subsequent research (Figure 4B). Scrape and Transwell assays were performed to evaluate the effect of NALT1 on cell invasion and metastasis. Decrease of NALT1 expression significantly decreased cell migration (Figure 4C and D).

NALT1 and NOTCH1 affect invasion and metastasis synergistically

Bioinformatics analysis showed that NALT1 was 10 kb upstream of NOTCH1 (Figure 5A, http://asia.ensembl.org). Expression of NOTCH1 in GC was verified by western blotting and RT-PCR. It showed that compared with control GES-1 cells, NOTCH1 was overexpressed in BGC-823 and SGC-7901 cells at mRNA and protein levels (Figure 5B, 5C). With the downregulation of NALT1 expression, expression of NOTCH1 also decreased. Moreover, both the mRNA (Figure 5D) and protein (Figure 5E) levels of NOTCH1 were all significantly decreased. NALT1 may regulate NOTCH1 at the transcriptional level. As mentioned above, we found that downregulating expression of NALT1 significantly inhibited the invasiveness of GC cells, but this decrease was partially abolished by overexpression of NOTCH1 (Figure 5F and G). With the increase in NOTCH1 expression, the invasion and metastasis of cells were enhanced: the number (Figure 5F) and migratory distance (Figure 5G) of

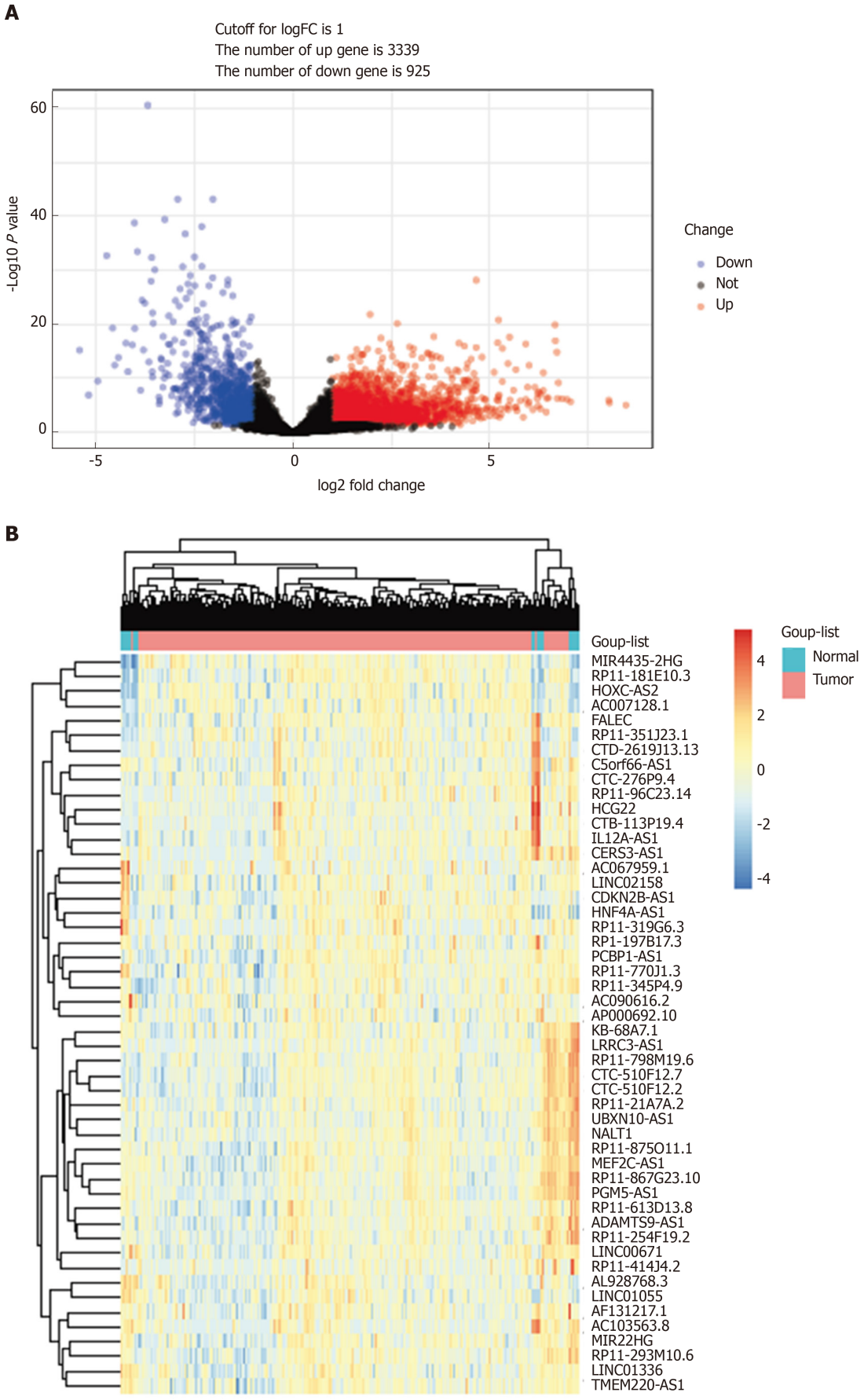

Figure 1 DELs in gastric cancer. A: Volcano plots of the expression levels of DELs screened by limma; B: Heatmaps of the expression levels of top 50 DELs. DELs: Differentially expressed lncRNAs; lncRNAs: Long noncoding RNAs.

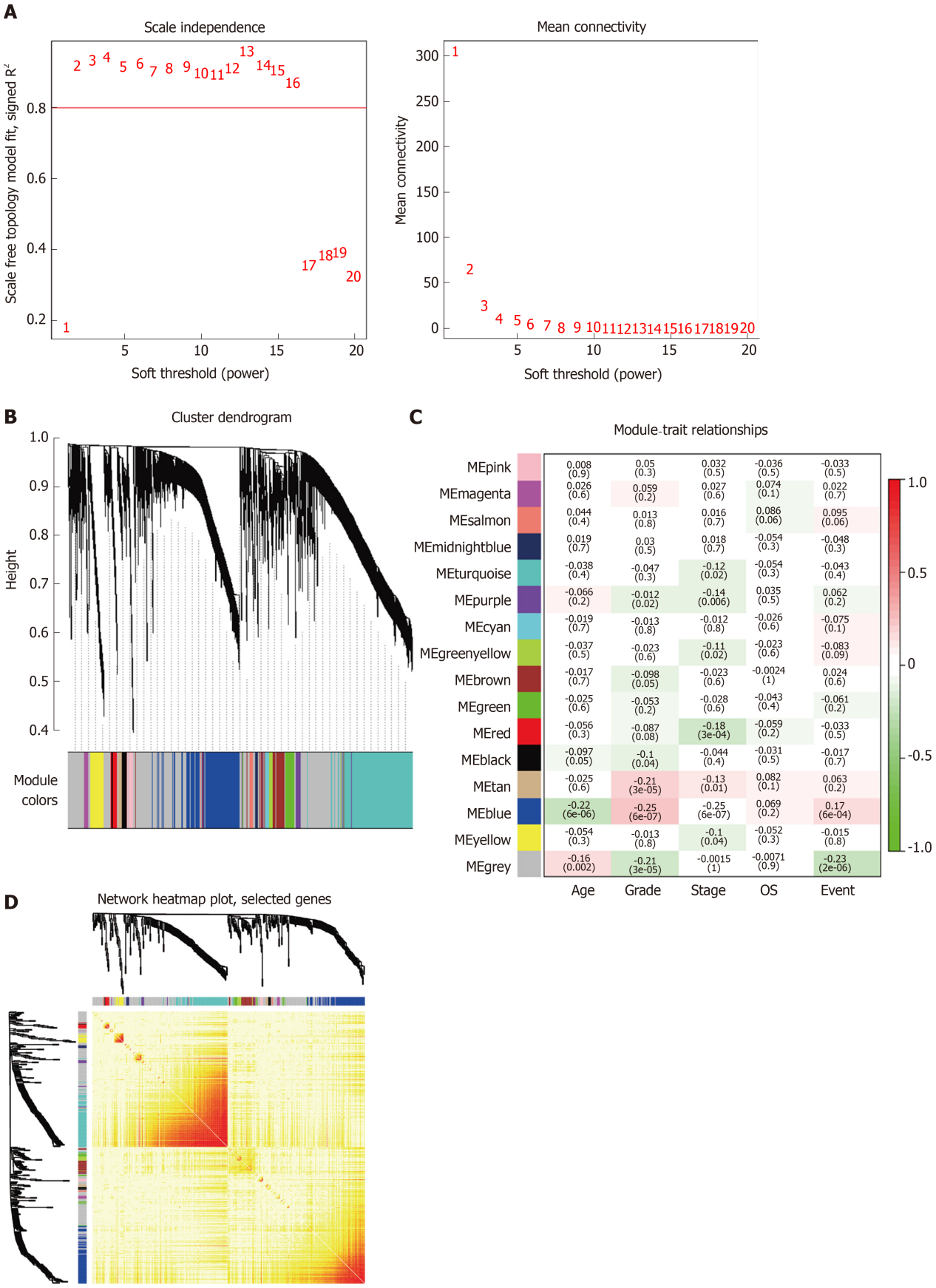
A
Scale independence
Scale free topology model fit, signed R²
Soft threshold (power)
Mean connectivity
Mean connectivity
Soft threshold (power)
B
Cluster dendrogram
Height
Module colors
C
Module-trait relationships
MEpink
MEmagenta
MEsalmon
MEmidnightblue
MEturquoise
MEpurple
MEcyan
MEgreenyellow
MEbrown
MEgreen
MEred
MEblack
MEtan
MEblue
MEyellow
MEgrey
Age
Grade
Stage
OS
Event
D
Network heatmap plot, selected genes

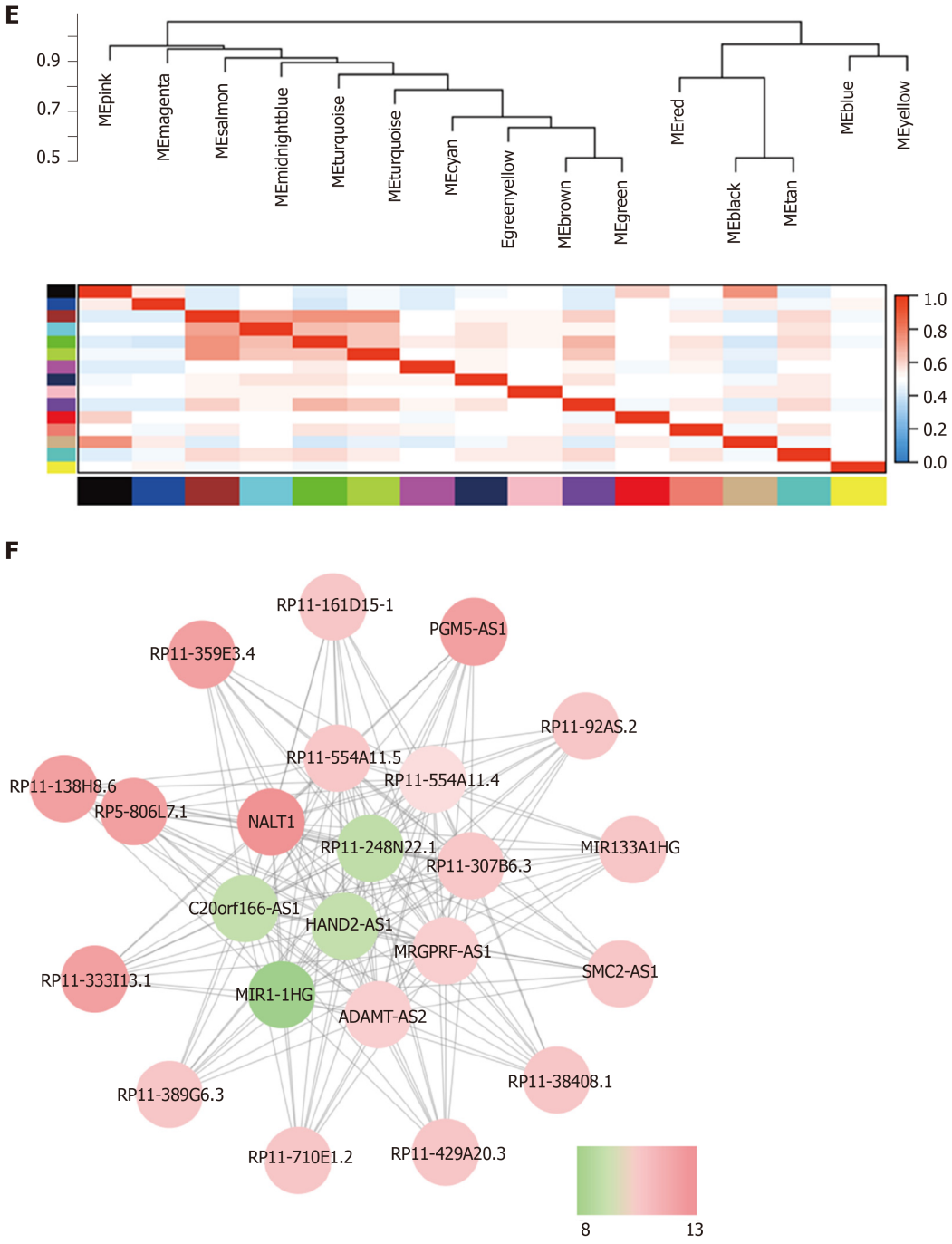

Figure 2 Weighted gene coexpression network analysis identify function module. A: The soft-thresholding powers (β) of scale-free fit index and mean connectivity; B: Cluster dendrogram obtained by hierarchical clustering of adjacency-based dissimilarity; C: Heatmap of the correlation between module and gastric cancer clinical traits; D: Topological overlap matrix plot; E: Hierarchical clustering and heatmap of eigengene adjacency. The color bars on left and below indicate the module of each row or column; F: Weighted coexpression network for blue-module lncRNAs (Node colors are according to the molecular complex detection score). LncRNAs: Long noncoding RNAs.

the cells increased significantly.

We studied the effect of NALT1 on NOTCH pathway components. We evaluated the expression levels of NOTCH intracellular cytoplasmic domain (NICD), HES1, and HES5 (downstream target genes of notch signaling pathway) in the cells treated with NALT1 siRNA. With knockdown of NALT1, expression of these proteins was decreased. However, the downregulation could partially be reversed by overexpression of NOTCH1 (Figure 6).

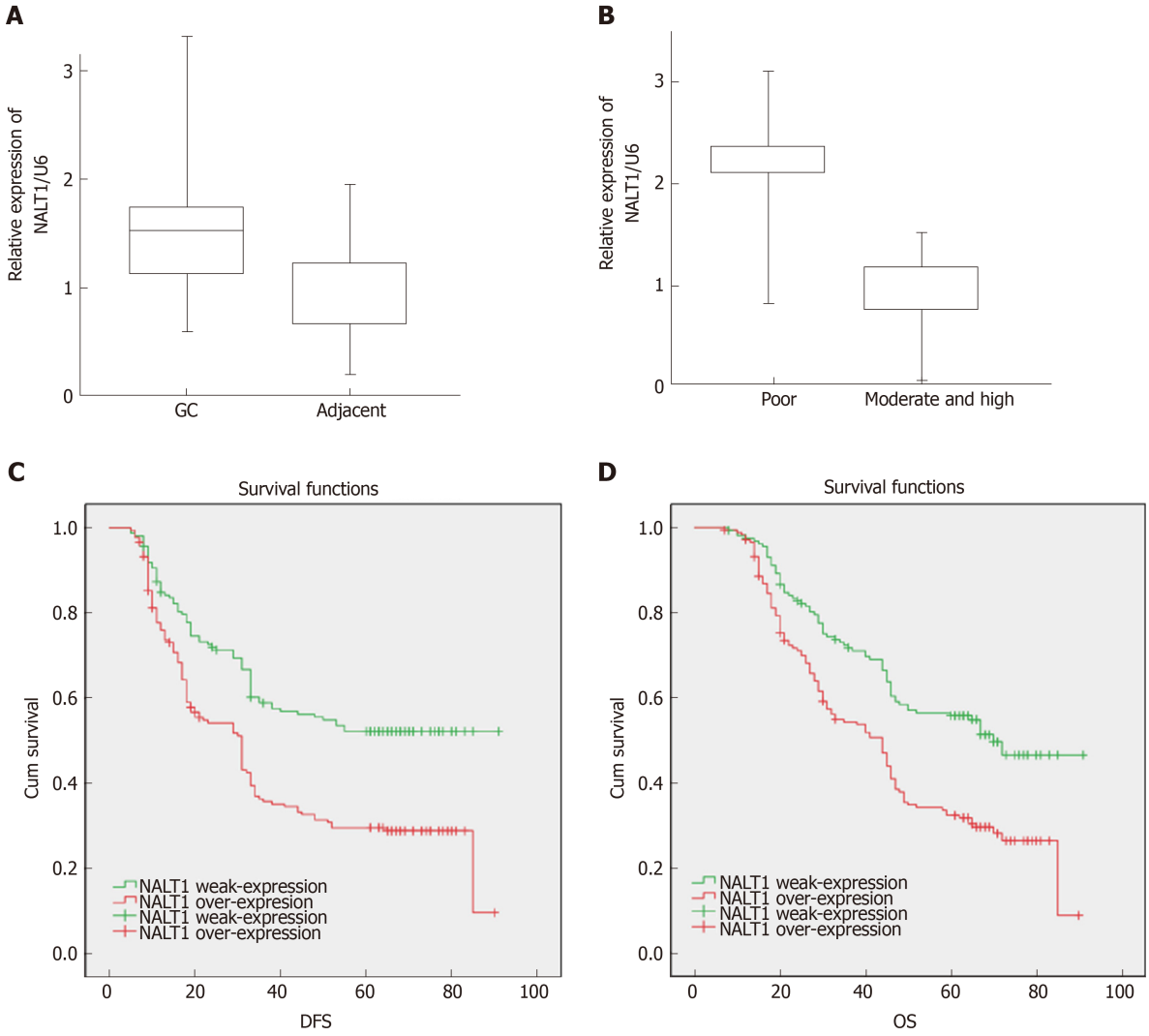

Figure 3 The expression of NALT1 in GC tissue and its effect on survival. A: NALT1 expression in GC tissue compare to paired adjacent tissue in 35 patients; B: The relationship between NALT1 expression and tumor differentiation; C: Kaplan–Meier analysis of the correlation between NALT1 expression levels and DFS in 336 GC patients; D: Kaplan–Meier analysis of the correlation between NALT1 expression levels and OS in 336 GC patients. NALT1: NOTCH1 associated with lncRNA in T cell acute lymphoblastic leukemia 1; GC: Gastric cancer; DFS: Disease-free survival; OS: Overall survival.

DISCUSSION

With the development of next-generation sequencing technology and molecular biology, thousands of genes have been proved to play an important role in the development of malignant tumors[13,14]. Moreover, the significance of ncRNA in gene expression regulation is being recognized[15,16]. LncRNAs can regulate gene expression at multiple levels: transcription and post-transcriptional processing as well as chromatin modification[17]. Correspondingly, lncRNAs can also bind various molecules (DNA, RNA, and protein) to perform biological functions. Therefore, it is of utmost importance to search for lncRNA that is closely related to the occurrence and development of GC and explore its functions and mechanisms. In this study, we downloaded transcriptome and clinical data from TCGA-STAD and attempted to explore GC-related lncRNAs through bioinformatics analysis. WGCNA is a scale-free network algorithm that is widely used in big data mining and analysis[11]. WGCNA can be used to study the differential coexpression between GC and normal tissue samples as a systematic biological method to explain the relationship between clinical characteristics and RNAs[10]. Different from other clustering algorithms, which use geometric distance between data for clustering, WGCNA clustering criteria focus on biological significance. These clustering modules are based on differences between RNA expression profiles and hub RNAs, which lead to changes in expression of cell signaling pathways[18]. Thus, the problem can be simplified to an equation between modular hub RNAs and clinical features to reveal the main causes of GC progression.

We found that the blue module was closely related to GC grade and survival

Table 2 NALT1 expressions and clinicopathologic parameters

Characteristics	NALT1			
	Low	High	*P* value	χ^2
	159 (47.3)	177 (52.7)		
Age			0.444	0.680
≥ 60	88 (49.4)	90 (50.6)		
< 60	71 (44.9)	87 (55.1)		
Gender			0.551	0.410
Male	109 (46.2)	127 (53.8)		
Female	50 (50.0)	50 (50.0)		
Tumor size			0.659	0.236
≥ 5 cm	65 (45.8)	77 (54.2)		
< 5 cm	94 (48.5)	100 (51.5)		
Location			0.589	1.058
Up	32 (42.7)	43 (57.3)		
Middle	42 (46.7)	48 (53.3)		
Low	85 (49.7)	86 (50.3)		
Bormann type			0.208	4.549
I	13 (52.0)	12 (48.0)		
II	77(52.4)	70 (47.6)		
III	68 (42.8)	91 (57.2)		
V	1 (20.0)	4 (80.0)		
Tumor histological morphology			0.569	1.126
Adenocarcinoma	123 (47.3)	137 (52.7)		
Absolute signet ring cell carcinoma	35 (46.7)	40 (53.3)		
Mixed carcinoma	1 (100)	0 (0)		
Lauren type			0.190	3.326
Intestinal	71 (45.5)	85 (54.5)		
Mixed carcinoma	31 (41.3)	44 (58.7)		
Diffuse	57 (54.3)	48 (45.7)		
Tumor differentiation			0.000	247.392
Moderate and high	151 (90.4)	16 (9.6)		
Poor	8 (4.7)	161 (95.3)		
Vessel invasion			0.471	0.658
Yes	43 (43.9)	55 (56.1)		
No	116 (48.7)	122 (51.3)		
Perineural invasion			0.706	0.195
Yes	38 (45.2)	46 (54.8)		
No	121 (48.0)	131 (52.0)		
T category			0.035	8.619
T1	37 (61.7)	23 (38.3)		
T2	10 (45.5)	12 (54.5)		
T3	8 (66.7)	4 (33.3)		
T4	104 (43.0)	138 (57.0)		
N category			0.000	20.693
N0	86 (61.9)	53 (38.1)		
N1	22 (37.9)	36 (62.1)		
N2	26 (40.0)	39 (60.0)		
N3	25 (33.8)	49 (66.2)		
TNM stage			0.001	17.625
I	41 (59.4)	28 (40.6)		
II	49 (60.5)	32 (39.5)		
III	68 (37.0)	116 (63.0)		
IV	1 (50.0)	1 (50.0)		

NALT1: NOTCH1 associated with lncRNA in T cell acute lymphoblastic leukemia 1; TNM: Tumor node metastasis.

through differential expression analysis and WGCNA. NALT1 is the hub-RNA of the blue module. NALT1, also named LINC01573, was first found in 2015 and contributes to the proliferation of T cell acute lymphoblastic leukemia[19]. However, its biological role in solid tumors has not been reported. In this study, we found that NALT1 was overexpressed in GC tissues and cells and was involved in tumor invasion and metastasis. Unfortunately, NALT1 overexpression is strongly associated with poor prognosis of GC. To explore further the role of NLAT1 in GC malignant phenotype, we studied its localization in the genome. As a neighbor, the well-known NOTCH1 is located 400 bp downstream of NALT1. Flank 10 k theory suggests that lncRNA can *cis* regulate adjacent genes within the range of 10000 bp on the chromosome location[20,21]. Therefore, we supposed that the influence of NALT1 on GC invasion and metastasis was realized by NOTCH1. The NOTCH signaling pathway regulates cell proliferation and differentiation in various gastrointestinal tissues, including the stomach[22]. The interaction between receptor and ligand initiates NOTCH signaling pathway, which activates NICD, thereby promoting transcription of downstream genes of the NOTCH pathway. The NOTCH family consists of four receptors and five ligands (Jagged-1, Jagged-2, Delta-like-1, Delta-like-3, and Delta-like-4). Mediated by NOTCH1 and NOTCH2 receptors, NOTCH is involved in the proliferation of gastric stem cells[23]. In addition, Xiao *et al*[24] proposed that inhibiting the activity of NOTCH signaling pathway could fully inhibit the invasion, metastasis, and proliferation of GC.

Unsurprisingly, NOTCH1 was also highly expressed in GC tissues and cells in the present study. Expression of NOTCH1 was decreased at mRNA and protein levels with knockdown of NALT1. This indicates that NALT1 regulates NOTCH1 expression at the transcriptional level, which is consistent with our hypothesis. In subsequent experiments, we found that downregulation of NALT1 inhibited the invasion and metastasis of GC, which could be partially restored by upregulation of NOTCH1. Subsequently, we detected the biomarkers (NICD, HES1, and HES5) of the NOTCH signaling pathway. Similarly, inhibited expression of NALT1 can downregulate the corresponding biomarkers. The upregulated NOTCH1 can partially abolished this effect. This further proved that the biological role of NALT1 in GC is achieved by NOTCH1 and NOTCH signaling pathway.

RNA sequencing and clinical data of TCGA-STAD patients were studied by WGCNA and other methods. NALT1 is one of the hub RNAs, which is closely related to poor prognosis of GC. Moreover, NALT1 is closely related to GC invasion and metastasis, which is achieved through the NOTCH signaling pathway.

Although we speculated about the important role of NALT1 in GC by bioinformatics analysis and verified it by molecular biological methods, there were some limitations to this study. First, the study lacked experimental evidence for a direct mechanism. Second, the expression and function of NALT1 in GC need to be verified by *in vivo* experiments.

Table 3 Multivariate analysis of significant prognostic factor for survival in gastric cancer patients

Variables	DFS			OS		
	P value	HR	95%CI	*P* value	HR	95%CI
Bormann	0.44	1.11	0.86-1.43	0.53	1.09	0.84-1.41
Tumor size	0.54	0.91	0.68-1.23	0.72	0.95	0.70-1.27
Tumor differentiation	0.81	0.91	0.43-1.98	0.74	0.88	0.41-1.88
Vessel invasion	0.45	1.34	0.63-2.85	0.50	1.30	0.61-2.80
Perineural invasion	0.18	0.82	0.60-1.10	0.25	0.84	0.62-1.14
TNM stage	0.00	125.49	42.47-370.76	0.00	87.98	37.29-207.38
NALT1 expression	0.02	0.71	0.53-0.96	0.02	0.71	0.52-0.95

HR: Hazard ratio; 95%CI: 95% confidence interval.

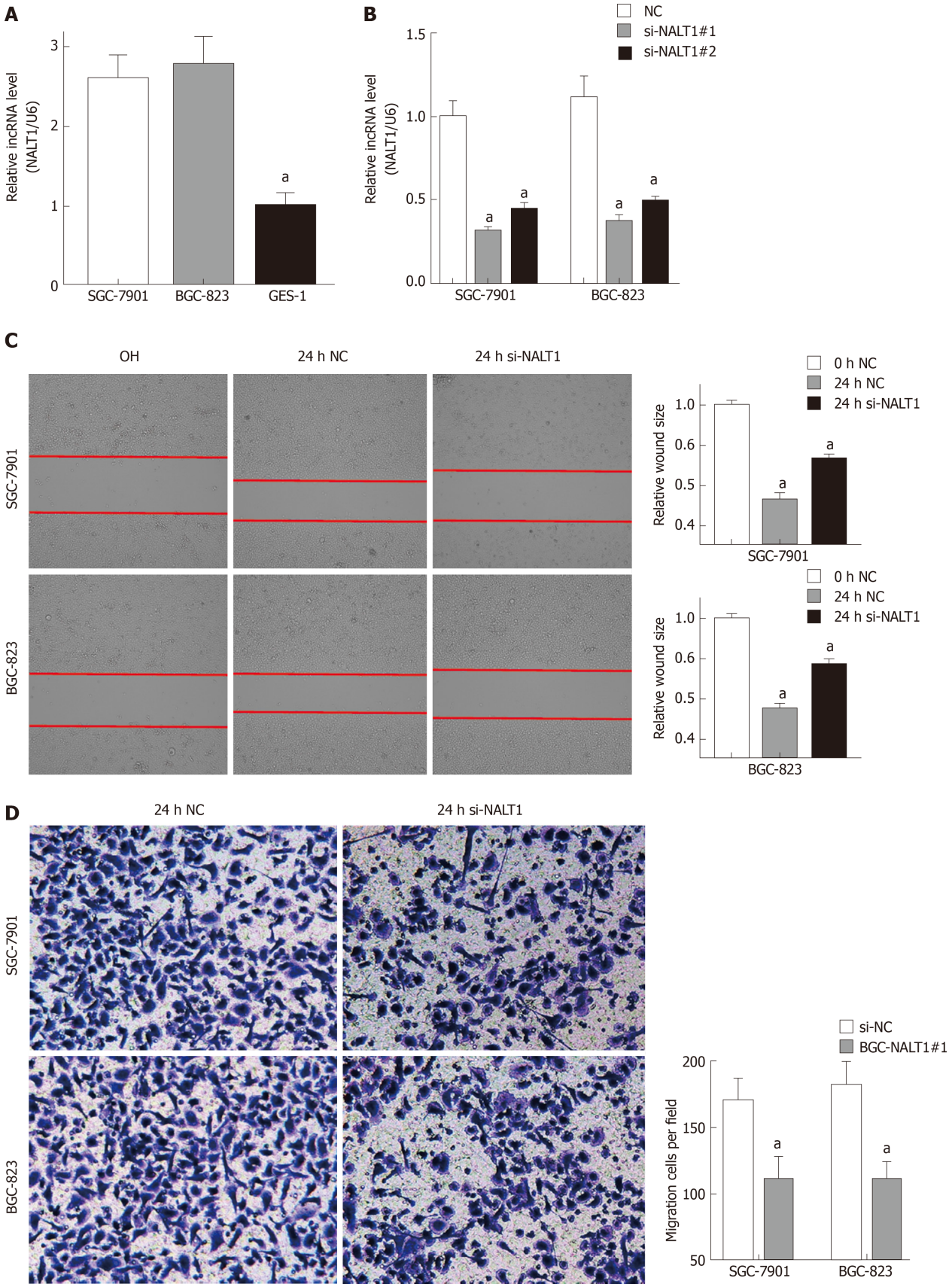

Figure 4 NALT1 induced GC invasion and metastasis. A: NALT1 expression in GC cells compare to GES-1 cells; B: The expression of NALT1 in GC cells before and after transfection si-NALT1 sequence; C: Scrape motility assays were monitored for 24 h in NALT1-knockdown GC cells; D: Transwell assays were used to evaluate the role of NALT1 in invasion in NALT1-knockdown. U6 was used as a loading control in RT-PCR; In all figures, 100 × magnification was used, $n = 3$, $^{a}P < 0.05$. NALT1: NOTCH1 associated with lncRNA in T cell acute lymphoblastic leukemia 1; GC: Gastric cancer; GES-1: Human normal gastric epithelial cell line.

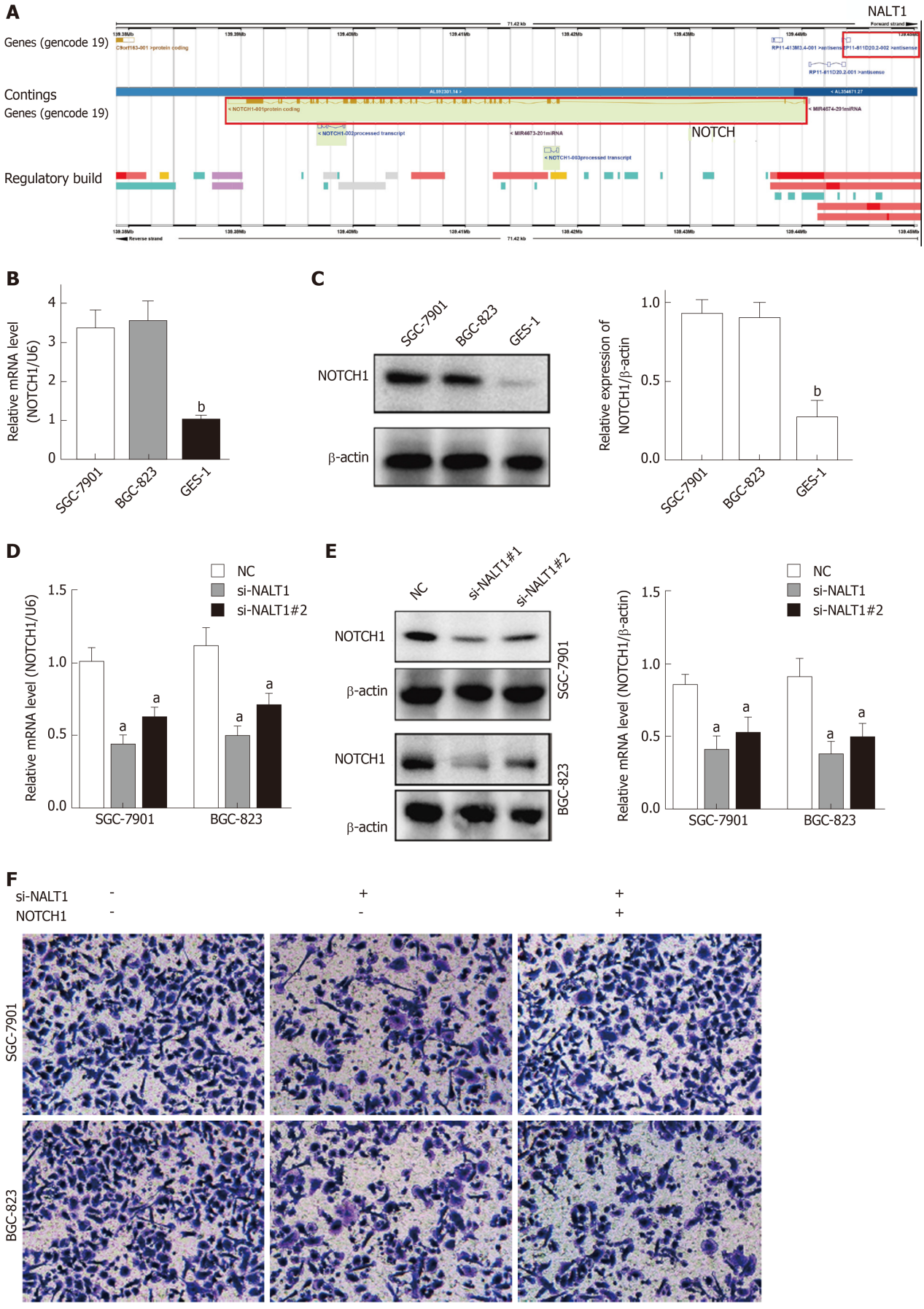
A
NALT1
Genes (gencode 19)
Contings
Genes (gencode 19)
Regulatory build
NOTCH
B
Relative mRNA level (NOTCH1/U6)
SGC-7901
BGC-823
GES-1
C
NOTCH1
β-actin
Relative expression of NOTCH1/β-actin
D
NC
si-NALT1
si-NALT1#2
Relative mRNA level (NOTCH1/U6)
E
Relative mRNA level (NOTCH1/β-actin)
F
si-NALT1
NOTCH1
SGC-7901
BGC-823

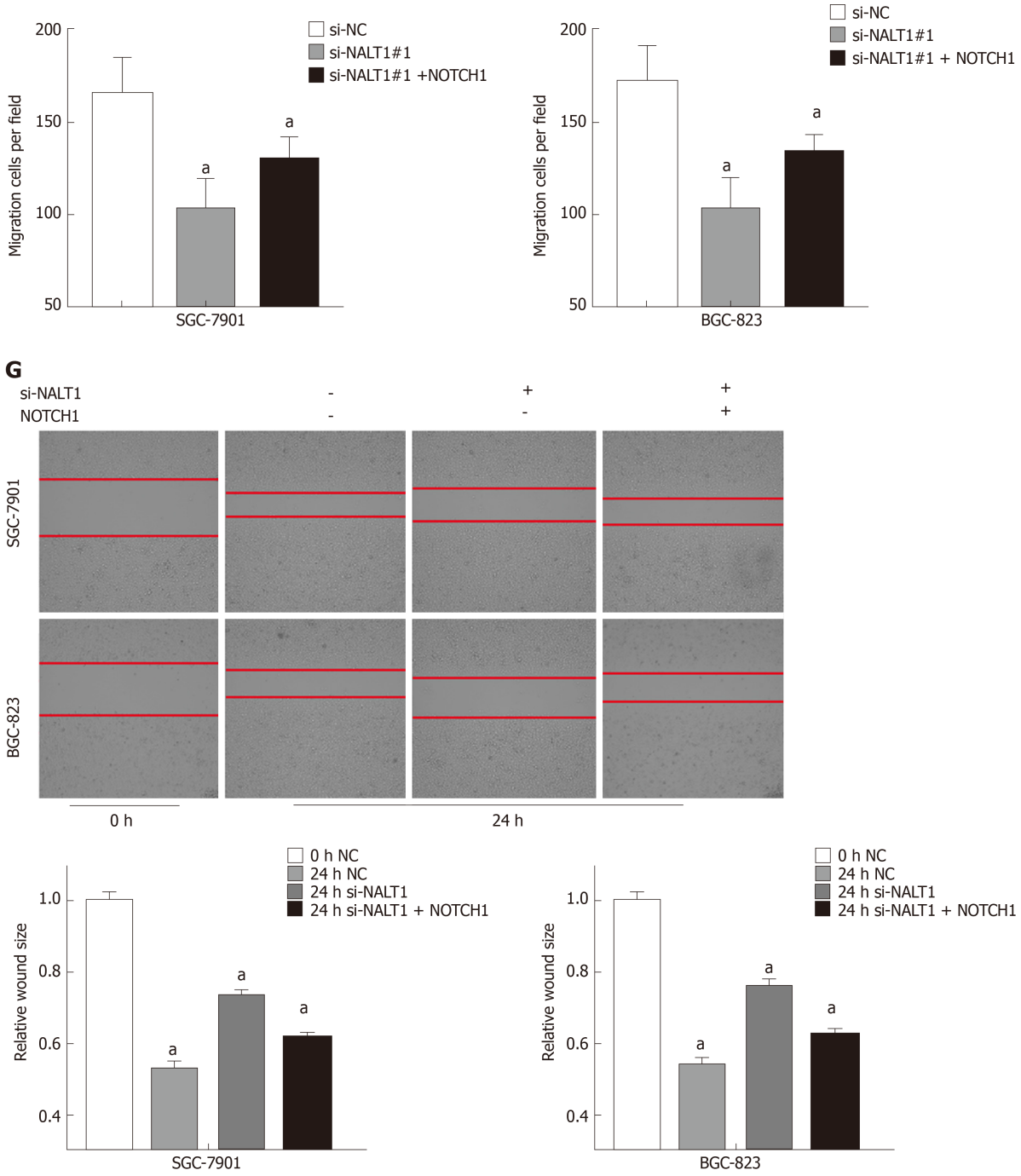

Figure 5 NALT1 influence NOTCH1 expression. A: Schematic figure of NALT1 and NOTCH1 in chromosome 9. They were highlight with red box; B: NOTCH1 was overexpression in GC cells by RT-PCR; C: NOTCH1 was overexpression in GC cells by western-blot; D: The expression of NOTCH1 mRNA was effected by NALT1; E: The expression of protein was effected by NALT1; F: Transwell assay was used to evaluate the association of NALT1 and NOTCH1 in invasion in NALT1-knockdown and NALT1-knockdown + NOTCH1-overexpression GC cells; G: Scrape motility assays were monitored for 24 h in NALT1-knockdown and NALT1-knockdown + NOTCH1-overexpression GC cells. U6 and β-actin were used as loading control in RT-PCR and western-blot, respectively. In all figures, 100 × magnification was used. $n = 3$, $^{a}P < 0.05$, $^{b}P < 0.01$. NALT1: NOTCH1 associated with lncRNA in T cell acute lymphoblastic leukemia 1; GC: Gastric cancer.

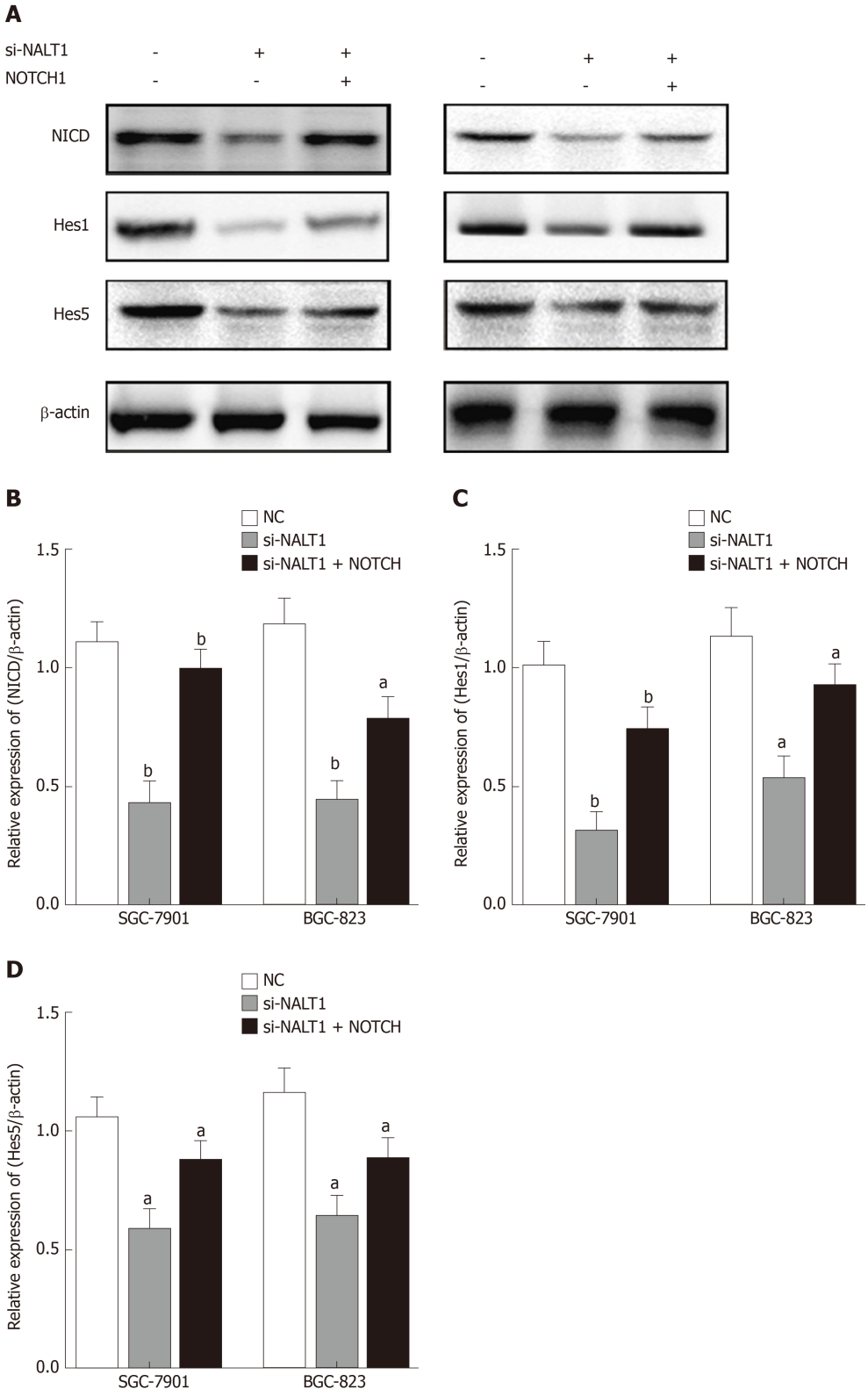

Figure 6 Decreased NALT1 suppressed the NOTCH signaling pathway. A: Western blot was used to detect whether the loss of NALT1 led to the abnormal expression of NOTCH signaling pathway. NICD, Hes1, and Hes5 were selected; B: The relative expression of NICD; C: The relative expression of Hes1; D: The relative expression of Hes5. β-actin was used as a loading control; $n = 3$, $^{a}P < 0.05$, $^{b}P < 0.01$. NALT1: NOTCH1 associated with lncRNA in T cell acute lymphoblastic leukemia 1.

ARTICLE HIGHLIGHTS

Research background

Gastric cancer (GC) is the most common and aggressive tumor of the digestive system and poses a serious threat to human health. Long noncoding RNAs (lncRNAs) are aberrant and play critical

roles in GC. Since genes do not work alone, our aim was to elucidate the potential relationship between mRNA and noncoding RNA in this study.

Research motivation
Searching for coexpressed lncRNA clusters may help to elucidate the mechanism of tumor development and predict the prognosis of GC.

Research objectives
To explore the prognostic value of NOTCH1 associated with lncRNA in T cell acute lymphoblastic leukemia 1 (NALT1) in GC and the mechanism of its involvement in gastric cancer invasion and metastasis.

Research methods
Based on the TCGA database, we obtained differentially expressed lncRNAs. The significance module was studied by weighted gene coexpression network analysis. The function of NALT1 was assessed by reverse transcription polymerase chain reaction, western blotting, scrape motility assay, and Transwell migration assay.

Research results
Fifteen coexpression modules were constructed based on 3339 differentially expressed lncRNAs and weighted gene coexpression network analysis. The blue module was correlated with tumor grade and survival, and the hub-lncRNA of blue NALT1 was an independent risk factor for GC prognosis. Through *cis* regulation, NALT1 affected the expression of the NOTCH signaling pathway and was related to GC invasion and metastasis.

Research conclusions
NALT1 was overexpressed in GC and was an independent risk factor for GC prognosis. It affected invasion and metastasis of GC by regulating NOTCH1 and NOTCH signaling pathway.

Research perspectives
In future studies, we will verify the results of this study through *in vivo* experiments. The specific binding sites of NALT1 and NOTCH1 will be studied by chromatin immunoprecipitation and pull-down assays.

REFERENCES

1 **Siegel RL**, Miller KD, Jemal A. Cancer statistics, 2019. *CA Cancer J Clin* 2019; **69**: 7-34 [PMID: 30620402 DOI: 10.3322/caac.21551]

2 **Al-Batran SE**, Homann N, Pauligk C, Goetze TO, Meiler J, Kasper S, Kopp HG, Mayer F, Haag GM, Luley K, Lindig U, Schmiegel W, Pohl M, Stoehlmacher J, Folprecht G, Probst S, Prasnikar N, Fischbach W, Mahlberg R, Trojan J, Koenigsmann M, Martens UM, Thuss-Patience P, Egger M, Block A, Heinemann V, Illerhaus G, Moehler M, Schenk M, Kullmann F, Behringer DM, Heike M, Pink D, Teschendorf C, Löhr C, Bernhard H, Schuch G, Rethwisch V, von Weikersthal LF, Hartmann JT, Kneba M, Daum S, Schulmann K, Weniger J, Belle S, Gaiser T, Oduncu FS, Güntner M, Hozaeel W, Reichart A, Jäger E, Kraus T, Mönig S, Bechstein WO, Schuler M, Schmalenberg H, Hofheinz RD; FLOT4-AIO Investigators. Perioperative chemotherapy with fluorouracil plus leucovorin, oxaliplatin, and docetaxel versus fluorouracil or capecitabine plus cisplatin and epirubicin for locally advanced, resectable gastric or gastro-oesophageal junction adenocarcinoma (FLOT4): a randomised, phase 2/3 trial. *Lancet* 2019; **393**: 1948-1957 [PMID: 30982686 DOI: 10.1016/S0140-6736(18)32557-1]

3 **Liyanage KIP**, Ganegoda GU. Therapeutic Approaches and Role of ncRNAs in Cardiovascular Disorders and Insulin Resistance. *Biomed Res Int* 2017; **2017**: 4078346 [PMID: 29057258 DOI: 10.1155/2017/4078346]

4 **Lin C**, Yang L. Long Noncoding RNA in Cancer: Wiring Signaling Circuitry. *Trends Cell Biol* 2018; **28**: 287-301 [PMID: 29274663 DOI: 10.1016/j.tcb.2017.11.008]

5 **Schmitt AM**, Chang HY. Long Noncoding RNAs in Cancer Pathways. *Cancer Cell* 2016; **29**: 452-463 [PMID: 27070700 DOI: 10.1016/j.ccell.2016.03.010]

6 **Bartonicek N**, Maag JL, Dinger ME. Long noncoding RNAs in cancer: mechanisms of action and technological advancements. *Mol Cancer* 2016; **15**: 43 [PMID: 27233618 DOI: 10.1186/s12943-016-0530-6]

7 **Sun TT**, He J, Liang Q, Ren LL, Yan TT, Yu TC, Tang JY, Bao YJ, Hu Y, Lin Y, Sun D, Chen YX, Hong J, Chen H, Zou W, Fang JY. LncRNA GClnc1 Promotes Gastric Carcinogenesis and May Act as a Modular Scaffold of WDR5 and KAT2A Complexes to Specify the Histone Modification Pattern. *Cancer Discov* 2016; **6**: 784-801 [PMID: 27147598 DOI: 10.1158/2159-8290.CD-15-0921]

8 **Zhang E**, He X, Zhang C, Su J, Lu X, Si X, Chen J, Yin D, Han L, De W. A novel long noncoding RNA HOXC-AS3 mediates tumorigenesis of gastric cancer by binding to YBX1. *Genome Biol* 2018; **19**: 154 [PMID: 30286788 DOI: 10.1186/s13059-018-1523-0]

9 **Liu J**, Lichtenberg T, Hoadley KA, Poisson LM, Lazar AJ, Cherniack AD, Kovatich AJ, Benz CC, Levine DA, Lee AV, Omberg L, Wolf DM, Shriver CD, Thorsson V; Cancer Genome Atlas Research Network, Hu H. An Integrated TCGA Pan-Cancer Clinical Data Resource to Drive High-Quality Survival Outcome Analytics. *Cell* 2018; **173**: 400-416.e11 [PMID: 29625055 DOI: 10.1016/j.cell.2018.02.052]

10 **Zhang J**, Wu Y, Jin HY, Guo S, Dong Z, Zheng ZC, Wang Y, Zhao Y. Prognostic value of sorting nexin 10 weak expression in stomach adenocarcinoma revealed by weighted gene co-expression network analysis. *World J Gastroenterol* 2018; **24**: 4906-4919 [PMID: 30487700 DOI: 10.3748/wjg.v24.i43.4906]

11 **Langfelder P**, Horvath S. WGCNA: an R package for weighted correlation network analysis. *BMC Bioinformatics* 2008; **9**: 559 [PMID: 19114008 DOI: 10.1186/1471-2105-9-559]

12 **Shannon P**, Markiel A, Ozier O, Baliga NS, Wang JT, Ramage D, Amin N, Schwikowski B, Ideker T.

Cytoscape: a software environment for integrated models of biomolecular interaction networks. *Genome Res* 2003; **13**: 2498-2504 [PMID: 14597658 DOI: 10.1101/gr.1239303]

13 **Aravanis AM**, Lee M, Klausner RD. Next-Generation Sequencing of Circulating Tumor DNA for Early Cancer Detection. *Cell* 2017; **168**: 571-574 [PMID: 28187279 DOI: 10.1016/j.cell.2017.01.030]

14 **McDaniel AS**, Stall JN, Hovelson DH, Cani AK, Liu CJ, Tomlins SA, Cho KR. Next-Generation Sequencing of Tubal Intraepithelial Carcinomas. *JAMA Oncol* 2015; **1**: 1128-1132 [PMID: 26181193 DOI: 10.1001/jamaoncol.2015.1618]

15 **Anastasiadou E**, Jacob LS, Slack FJ. Non-coding RNA networks in cancer. *Nat Rev Cancer* 2018; **18**: 5-18 [PMID: 29170536 DOI: 10.1038/nrc.2017.99]

16 **Karreth FA**, Pandolfi PP. ceRNA cross-talk in cancer: when ce-bling rivalries go awry. *Cancer Discov* 2013; **3**: 1113-1121 [PMID: 24072616 DOI: 10.1158/2159-8290.CD-13-0202]

17 **Sun Q**, Hao Q, Prasanth KV. Nuclear Long Noncoding RNAs: Key Regulators of Gene Expression. *Trends Genet* 2018; **34**: 142-157 [PMID: 29249332 DOI: 10.1016/j.tig.2017.11.005]

18 **Botía JA**, Vandrovcova J, Forabosco P, Guelfi S, D'Sa K; United Kingdom Brain Expression Consortium, Hardy J, Lewis CM, Ryten M, Weale ME. An additional k-means clustering step improves the biological features of WGCNA gene co-expression networks. *BMC Syst Biol* 2017; **11**: 47 [PMID: 28403906 DOI: 10.1186/s12918-017-0420-6]

19 **Wang Y**, Wu P, Lin R, Rong L, Xue Y, Fang Y. LncRNA NALT interaction with NOTCH1 promoted cell proliferation in pediatric T cell acute lymphoblastic leukemia. *Sci Rep* 2015; **5**: 13749 [PMID: 26330272 DOI: 10.1038/srep13749]

20 **Kopp F**, Mendell JT. Functional Classification and Experimental Dissection of Long Noncoding RNAs. *Cell* 2018; **172**: 393-407 [PMID: 29373828 DOI: 10.1016/j.cell.2018.01.011]

21 **Wang KC**, Chang HY. Molecular mechanisms of long noncoding RNAs. *Mol Cell* 2011; **43**: 904-914 [PMID: 21925379 DOI: 10.1016/j.molcel.2011.08.018]

22 **Demitrack ES**, Samuelson LC. Notch as a Driver of Gastric Epithelial Cell Proliferation. *Cell Mol Gastroenterol Hepatol* 2017; **3**: 323-330 [PMID: 28462374 DOI: 10.1016/j.jcmgh.2017.01.012]

23 **Demitrack ES**, Gifford GB, Keeley TM, Horita N, Todisco A, Turgeon DK, Siebel CW, Samuelson LC. NOTCH1 and NOTCH2 regulate epithelial cell proliferation in mouse and human gastric corpus. *Am J Physiol Gastrointest Liver Physiol* 2017; **312**: G133-G144 [PMID: 27932500 DOI: 10.1152/ajpgi.00325.2016]

24 **Xiao HJ**, Ji Q, Yang L, Li RT, Zhang C, Hou JM. In vivo and in vitro effects of microRNA-124 on human gastric cancer by targeting JAG1 through the Notch signaling pathway. *J Cell Biochem* 2018; **119**: 2520-2534 [PMID: 28941308 DOI: 10.1002/jcb.26413]

World Journal of Gastroenterology

Submit a Manuscript: https://www.f6publishing.com

World J Gastroenterol 2019 November 28; 25(44): 6527-6540

DOI: 10.3748/wjg.v25.i44.6527

ISSN 1007-9327 (print) ISSN 2219-2840 (online)

ORIGINAL ARTICLE

Basic Study

Gasdermin D-mediated hepatocyte pyroptosis expands inflammatory responses that aggravate acute liver failure by upregulating monocyte chemotactic protein 1/CC chemokine receptor-2 to recruit macrophages

Hong Li, Xue-Ke Zhao, Yi-Ju Cheng, Quan Zhang, Jun Wu, Shuang Lu, Wei Zhang, Yang Liu, Ming-Yu Zhou, Ya Wang, Jing Yang, Ming-Liang Cheng

ORCID number: Hong Li (0000-0003-0601-3198); Xue-Ke Zhao (0000-0002-3032-4933); Yi-Ju Cheng (0000-0001-9215-7520); Quan Zhang (0000-0001-8353-9957); Jun Wu (0000-0002-6450-3956); Shuang Lu (0000-0001-9662-6216); Wei Zhang (0000-0001-6215-7706); Yang Liu (0000-0002-1140-2588); Ming-Yu Zhou (0000-0002-51305950); Ya Wang (0000-0002-8789-2085); Jing Yang (0000-0002-1780-289X); Ming-Liang Cheng (0000-0002-2525-3595).

Author contributions: Cheng ML and Wu J designed the research; Li H, Zhao XK and Wang Y performed the experiments shown in Figures 1-5; Cheng YJ, Zhang Q, Lu S and Zhang W analyzed the data; Li H wrote the paper; Yang J, Liu Y and Zhou MY provided technical assistance and contributed to the preparation of the figures; Li H, Zhao XK and Cheng YJ contributed equally to this work. All authors reviewed the results and approved the final version of the manuscript.

Supported by the National Natural Science Foundation of China, No. 81570543 and No. 81560104.

Institutional review board statement: This study was approved by the Ethics Committee of the Affiliated Hospital of Guizhou Medical University.

Institutional animal care and use

Hong Li, Xue-Ke Zhao, Yi-Ju Cheng, Quan Zhang, Jun Wu, Shuang Lu, Yang Liu, Ming-Yu Zhou, Ya Wang, Jing Yang, Ming-Liang Cheng, Department of Infectious Diseases, Affiliated Hospital of Guizhou Medical University, Guiyang 550004, Guizhou Province, China

Wei Zhang, Comprehensive Liver Cancer Center of the Fifth Medical Center of PLA General Hospital, Beijing 100039, China

Corresponding author: Ming-Liang Cheng, BSc, Chief Physician, Professor, Department of Infectious Diseases, Affiliated Hospital of Guizhou Medical University, No. 28, Guiyi Road, Guiyang 550004, Guizhou Province, China. mlcheng@yeah.net
Telephone: +86-851-86773914
Fax: +86-851-86741623

Abstract

BACKGROUND

Massive hepatocyte death is the core event in acute liver failure (ALF). Gasdermin D (GSDMD)-mediated pyroptosis is a type of highly inflammatory cell death. However, the role of hepatocyte pyroptosis and its mechanisms of expanding inflammatory responses in ALF are unclear.

AIM

To investigate the role and mechanisms of GSDMD-mediated hepatocyte pyroptosis through *in vitro* and *in vivo* experiments.

METHODS

The expression of pyroptosis pathway-associated proteins in liver tissues from ALF patients and a hepatocyte injury model was examined by Western blot. GSDMD short hairpin RNA (shRNA) was used to investigate the effects of downregulation of GSDMD on monocyte chemotactic protein 1 (MCP1) and its receptor CC chemokine receptor-2 (CCR2) *in vitro*. For *in vivo* experiments, we used GSDMD knockout mice to investigate the role and mechanism of GSDMD in a D-galactose/lipopolysaccharide (D-Galn/LPS)-induced ALF mouse model.

RESULTS

The levels of pyroptosis pathway-associated proteins in liver tissue from ALF

committee statement: This study was approved by the Institutional Animal Care and Use Committee of Guizhou Medical University.

Conflict-of-interest statement: The authors declare that there is no conflict of interest related to this study.

Data sharing statement: No additional data are available.

ARRIVE guidelines statement: The authors have read the ARRIVE guidelines and prepared the manuscript accordingly.

Manuscript source: Unsolicited manuscript

Received: September 18, 2019
Peer-review started: September 18, 2019
First decision: October 14, 2019
Revised: October 31, 2019
Accepted: November 13, 2019
Article in press: November 13, 2019
Published online: November 28, 2019

P-Reviewer: Enosawa S, Inoue K, Wongkajornsilp A
S-Editor: Tang JZ
L-Editor: Wang TQ
E-Editor: Zhang YL

patients and a hepatocyte injury model increased significantly. The level of GSDMD-N protein increased most obviously ($P < 0.001$). *In vitro*, downregulation of GSDMD by shRNA decreased the cell inhibition rate and the levels of MCP1/CCR2 proteins ($P < 0.01$). *In vivo*, GSDMD knockout dramatically eliminated inflammatory damage in the liver and improved the survival of D-Galn/LPS-induced ALF mice ($P < 0.001$). Unlike the mechanism of immune cell pyroptosis that involves releasing interleukin (IL)-1β and IL-18, GSDMD-mediated hepatocyte pyroptosis recruited macrophages *via* MCP1/CCR2 to aggravate hepatocyte death. However, this pathological process was inhibited after knocking down GSDMD.

CONCLUSION

GSDMD-mediated hepatocyte pyroptosis plays an important role in the pathogenesis of ALF, recruiting macrophages to release inflammatory mediators by upregulating MCP1/CCR2 and leading to expansion of the inflammatory responses. GSDMD knockout can reduce hepatocyte death and inflammatory responses, thus alleviating ALF.

Key words: Gasdermin D; Hepatocyte; Pyroptosis; Acute liver failure; Monocyte chemotactic protein 1/CC chemokine receptor-2

Core tip: The expression of gasdermin D N terminal domain was significantly increased in the liver during human acute liver failure (ALF), in a D-galactose/lipopolysaccharide (D-Galn/LPS)-induced ALF mouse model and in D-Galn/LPS-treated AML12 hepatocytes. GSDMD-mediated hepatocyte pyroptosis expanded the inflammatory response by upregulating monocyte chemotactic protein 1 and its receptor CC chemokine receptor-2 to recruit macrophages. GSDMD knockout could significantly alleviate ALF in the mouse model. Finding effective intervention targets or drugs inhibiting GSDMD may provide a possible treatment approach to improve the outcomes of ALF.

Citation: Li H, Zhao XK, Cheng YJ, Zhang Q, Wu J, Lu S, Zhang W, Liu Y, Zhou MY, Wang Y, Yang J, Cheng ML. Gasdermin D-mediated hepatocyte pyroptosis expands inflammatory responses that aggravate acute liver failure by upregulating monocyte chemotactic protein 1/CC chemokine receptor-2 to recruit macrophages. *World J Gastroenterol* 2019; 25(44): 6527-6540
URL: https://www.wjgnet.com/1007-9327/full/v25/i44/6527.htm
DOI: https://dx.doi.org/10.3748/wjg.v25.i44.6527

INTRODUCTION

Multiple factors such as drugs, alcohol, and hepadnaviruses can lead to large-scale hepatocyte death in a short period of time, which may progress into acute liver failure (ALF) with a mortality rate of up to 80%[1]. The only known therapy, liver transplantation, often cannot be performed in a timely fashion due to the shortage of donors. As of now, there is no effective intervention target or specific drug therapy available for ALF[2].

Massive hepatocyte death is the core event of ALF. The manner of death and number of dead hepatocytes determine the intensity of the expanding inflammatory responses[3]. Necrosis has classically been considered to be the major mechanism of hepatocyte death during the pathogenesis of ALF. However, knockout of the receptor-interacting protein serine-threonine kinases-3 gene or the mixed lineage kinase domain-like pseudokinase gene in mice did not significantly improve the survival rate of mice subjected to ALF[4].

Pyroptosis is a novel programmed cell death mechanism that can induce strong inflammatory reactions and mainly only occurs in immune cells such as phagocytic cells, macrophages, and monocytes[5]. Endogenous and exogenous danger signals can activate caspase 1 or caspases 4 and 5 (human)/caspase 11 (mouse), which cleave

gasdermin D (GSDMD) to produce its active N-terminal region [cleaved N-terminal fragment of GSDMD (GSDMD-N)] and an inactive C-terminal fragment. GSDMD-N inserts into the cell membrane and forms a large number of sieve-like pores with a diameter of approximately 10-20 nm through the membrane, resulting in cell death and releasing inflammatory factors such as interleukin (IL)-1β and IL-18[6-8]. Pyroptosis plays an important role in the process of defending against pathogenic microbial infections by the body, but excessive uncontrolled pyroptosis can lead to severe tissue damage[9]. Studies in recent years have found that there is a pyroptosis mechanism in parenchymal cells such as myocardial cells, renal tubular cells, and neuronal cells[10]. However, the mechanisms of hepatocyte pyroptosis in ALF are unclear.

The triggering and progression of ALF are closely related to uncontrolled inflammatory responses[11]. Monocyte chemotactic proteins 1, 2, and 3 (MCP1, MCP2, and MCP3) are expressed in many cell lineages. By binding to their common receptor CC chemokine receptor-2 (CCR2), MCPs play a role in amplifying inflammatory responses that aggravate tissue injury by strongly recruiting the directional migration of immune cells[12]. Studies have found that among these, only MCP1 is expressed in hepatocytes and released to extracellular sites in response to hepatocyte injury. MCP1 thus plays a role as an important inflammatory response amplifier in ALF[13,14]. However, the functions of MCP1 in hepatocyte pyroptosis have not been fully elucidated.

Our study showed that the expression of GSDMD-N was upregulated significantly in D-galactose/lipopolysaccharide (D-Galn/LPS)-treated AML12 hepatocytes as well as in liver tissue from ALF patients and a D-Galn/LPS-induced mouse ALF model. Reduction of hepatocyte pyroptosis by knockdown of GSDMD significantly inhibited MCP1/CCR2 expression, reduced liver injury, and increased the survival rate of mice. Our results suggested that finding effective intervention targets or drugs to inhibit GSDMD may be a potential approach to the effective treatment of ALF.

MATERIALS AND METHODS

Human serum and liver samples

According to the "Guidelines for Acute Liver Failure" recommended by the European Association for the Study of the Liver in 2017[1], ALF is defined as the occurrence of jaundice and encephalopathy and an international normalized ratio (INR) > 1.5 within fewer than 26 wk after onset. Peripheral serum samples from 30 ALF patients and 30 healthy people were collected from the Affiliated Hospital of Guizhou Medical University. There were seven diseased liver tissue specimens from ALF patients (caused by hepatitis B virus infection) and six healthy liver specimens (from deceased organ donors who died from intracranial bleeding or head injury and were free from chronic diseases) available for study.

Acute liver failure mouse model

Wild-type (WT) male C57BL/6 mice aged 6-8 wk were purchased from the Experimental Animal Center of the Third Military Medical University (Chongqing). Male GSDMD gene knockout (GSDMD-/-) mice (C57BL/6J strain) aged 6–8 wk were a generous gift from Shao Feng's Laboratory, Beijing Institute of Life Sciences, China. All animals received humane care according to established standards and were maintained in an air-conditioned animal room at 25 °C with free access to water and food. The wild-type mice and GSDMD-/- mice were randomly divided into a normal control group (n = 5) and a D-Galn/LPS group (n = 15). Mice in the D-Galn/LPS group were intraperitoneally injected with D-Galn 300 mg/kg + LPS 10 μg/kg once[15,16], while mice in the normal control group were intraperitoneally injected with an equal amount of phosphate buffer saline (PBS). After 6 h, all mice were sacrificed. Blood was collected from the eyeball vein and centrifuged at 3000 rpm/min for 15 min, and the serum was separated and stored at -80 °C. Liver tissues were harvested by portal vein perfusion. Some of the specimens were fixed using paraformaldehyde for 48 h, and then pathological examination was performed. The remaining tissues were quickly placed at -80 °C.

Culture and treatment of hepatocytes

The mouse liver cell line AML12 was purchased from Shanghai Institute of Cell Biology, Chinese Academy of Sciences, and was cultured in DMEM-F12 culture medium containing 10% foetal bovine serum, 1% insulin-transferrin-selenium, and 40 ng/mL dexamethasone (Gibco, United States). The cells were cultured in an incubator containing 5% CO_2 at a constant temperature of 37 °C. The cells were treated with D-Galn (15 mmol/L)/LPS (100 μg/mL) for 0, 6, 12, and 24 h to establish hepatocyte

injury models at dynamic time periods.

GSDMD RNA interference and transfection in AML12

GSDMD short hairpin RNA (shRNA) and negative control (control shRNA) vectors were purchased from Sangon Biotech and were transfected into the AML12 cells following the manufacturer's instructions with Lipofectamine 3000 (Invitrogen, United States). The culture medium was replaced with fresh complete medium after 6 h for continuous culture in an incubator containing 5% CO_2 at the constant temperature of 37 °C for 48 h. Further experiments were performed if the transfection rate was greater than 50%.

Biochemical and coagulation function analysis

Alanine aminotransferase (ALT) and blood ammonia in human and mouse serum samples and the supernatant of cell culture medium were detected using an automatic biochemical analyser (Siemens Advia 1650; Siemens, Bensheim, Germany). The INR of prothrombin was tested using a SysmexCA-7000 coagulation detector.

Western blot analysis

Antibodies against the following proteins were used for Western blot analysis: caspase 1 and caspase 4 (human), caspase 11 (mouse), GSDMD, MCP1, CCR2 (1:1000, Abcam), and glyceraldehyde-3-phosphate dehydrogenase (GAPDH; 1:10000, Abcam). The secondary antibody was horseradish peroxidase-conjugated IgG (1:8000, Abcam). For the blots, 30–50 μg of total protein was added into each well and the proteins were separated by electrophoresis on a 10% sodium dodecylsulphate polyacrylamide gel electrophoresis precast gel (Invitrogen, CA, United States). The proteins were then transferred to polyvinylidene fluoride membranes (Millipore, Bedford, MA, United States). The protein bands were developed with an enhanced luminescent developer (Millipore) and photographed using a Chemi Doc MP System (Bio-Rad, Hercules, United States). The grey value was measured using ImageJ software.

Cell counting kit-8 assay

A total of 2×10^4 AML12 cells were seeded in 96-well plates and cultured for 24 h. Then, they were treated for 0, 6, 12, and 24 h, followed by incubation with 10 μL of cell counting kit-8 assay solution in each well for 2 h. The absorbance was measured with a microplate reader at 450 nm. According to the instructions of the kit, cell inhibition rate was calculated as [(control - experimental)/(control - blank)] × 100%.

Cellular immunofluorescence

Cells were fixed with 4% paraformaldehyde and cellular immunofluorescence was performed according to previously described protocols. The cells were incubated with an anti-GSDMD antibody (1:200) at 4 °C overnight. Then, the cells were incubated with an Alexa Fluor 488 fluorescence labelled goat anti-rabbit IgG secondary antibody (1:1000) for 2 h, followed by nuclear staining with 4',6-diamidino-2-phenylindole (DAPI). The cells were visually observed and photographed using an Olympus FV1000 (Olympus, Tokyo, Japan).

Detection of inflammatory cytokines

Inflammatory cytokines, including IL-1β, IL-18, tumor necrosis factor-alpha (TNFα), and IFN-γ, in human serum samples were detected with the Bioplex multi-cytokine assay kit according to the kit instructions using a BD FACS CantoII flow cytometer (BD Biosciences, NJ, United States). Calculations were conducted using LEGENDplex8.0 software. MCP1, IL-1β, IL-18, TNFα, and IFN-γ in mouse serum were detected based on the kit instructions provided for the enzyme-linked immunosorbent assay (ELISA) kits (Cusabio Biotech Co., Ltd., China).

Haematoxylin and eosin staining and immunohistochemical staining

Haematoxylin and eosin (H and E) staining was performed based on the routine procedure. Pathological changes of the liver were observed with an A12.1503 microscope [Opto-Edu (Beijing) Co., Ltd., Beijing, China]. The degree of inflammation of the liver in mice was evaluated independently by three senior physicians at the Department of Pathology based on the Ishaki score system.

For immunohistochemical staining, F4/80 rat anti-mouse monoclonal antibody (Abcam, diluted to 10 μg/mL) was incubated with the tissue at 4 °C overnight. On the next day, the tissue was incubated with a biotinylated goat anti-rat IgG (1:2000, Abcam) at room temperature for 30 min, then diaminobenzidine staining was performed. Photographs were taken with an Olympus BX41 microscope. The percentage of the average optical density area of five random fields (200×) was calculated using Image J.

Statistical analysis

Data were analysed using Student's *t*-test (Sigma Plot, SPSS Inc., IL, United States) for differences between two groups and are expressed as the mean ± square error. For comparisons between multiple groups, three-way analysis of variance was performed, followed by *t*-tests with Bonferroni correction using SAS 9.3 (SAS Institute Inc., Cary, NC, United States). In addition, a log-rank test was used for survival analysis. All experiments were repeated at least three times. Differences were considered statistically significant at $P < 0.05$ ($^{a}P < 0.05$, $^{b}P < 0.01$, and $^{e}P < 0.001$).

RESULTS

Pyroptosis-associated inflammatory cytokines and proteins increase in human ALF

To investigate whether pyroptosis is involved in the pathogenesis of ALF, we first collected serum samples from 30 ALF patients and 30 normal controls. Serum ALT, TBIL, blood ammonia, and the INR of prothrombin were significantly higher in samples from patients with ALF compared to the control samples (Figure 1A). Pyroptosis-associated inflammatory cytokines, including IL-1β, IL-18, TNFα, and IFN-γ, increased in the ALF cases (Figure 1B). Pyroptosis-associated protein expression in liver tissues from patients with ALF and normal controls were then detected by Western blot. The expression levels of caspase 1/4, full-length GSDMD (GSDMD-FL), and GSDMD-N in liver tissues increased in ALF cases compared to the controls (Figure 1C), and the expression of GSDMD-N increased significantly. These data suggest that pyroptosis is involved in the pathogenesis of ALF.

Pyroptosis-associated proteins increase in a D-Galn/LPS-induced hepatocyte injury model

Hepatocyte death is the core event of ALF, and in order to investigate whether there is GSDMD-mediated pyroptosis when hepatocyte injury occurs, the liver cell line AML12 was used to establish a dynamic time-axis model of hepatocyte injury at 0, 6, 12, and 24 h using D-Galn/LPS. With the prolongation of the intervention, the cell inhibition rate increased gradually, and ALT content in the supernatant increased as well (Figure 2A and B). It was observed under a confocal fluorescence microscope that GSDMD protein was only slightly expressed in normal AML12 cells. However, the expression of GSDMD protein increased in the hepatocyte cytoplasm over time after the intervention. After 24 h of intervention, the GSDMD protein gradually accumulated on the medial side of the hepatocyte membrane, which is in line with the previous observations that cleaved GSDMD-N segments were displaced from the cytoplasm to the cell membrane and then inserted into the medial membrane to form membrane pores, thus leading to cell death (Figure 2C).

Protein expression levels of caspase 1/11, GSDMD-FL, and GSDMD-N were found to increase over time by Western blot (Figure 2D). However, the downstream inflammatory cytokines IL-1β and IL-18 were not detected in the supernatant, but MCP1 content increased with the prolongation of intervention time (Figure 2E). These results suggested that pyroptosis is an important form of death in this D-Galn/LPS-induced *in vitro* hepatocyte injury model. However, hepatocyte pyroptosis may mediate and expand the inflammatory responses by mechanisms different from the mechanisms used for pyroptosis in immune cells.

GSDMD knockdown by shRNA decreases the expression of MCP1 and CCR2 in a D-Galn/LPS-induced AML12 hepatocyte injury model

It has been confirmed in previous studies that the MCP1/CCR2 signalling pathway has the effect of strongly triggering neutrophil aggregation to mediate immune injury of the liver and is thus involved in the pathogenesis of ALF. The above study results showed that D-Galn/LPS-induced hepatocyte pyroptosis did not release IL-1β and IL-18, but the levels of MCP1 increased significantly in the cell supernatant. To further observe whether the pyroptosis executing protein GSDMD has regulatory effects on MCP1/CCR2, Lipofectamine 3000 was used to transfect shRNA to knock down GSDMD expression in AML12 hepatocytes (Figure 3A). Our results revealed that downregulation of GSDMD expression significantly reduced the protein expression levels of MCP1 and CCR2 in the D-Galn/LPS-induced hepatocyte injury model (Figure 3B). Moreover, the cell inhibition rate decreased (Figure 3C), and the ALT and MCP1 contents in the cell supernatant were also reduced (Figure 3D).

GSDMD knockout dramatically eliminates inflammatory damage in the liver and improves the survival of D-Galn/LPS-induced ALF mice

In the D-Galn/LPS-induced ALF model in mice, the WT + D-Galn/LPS group started

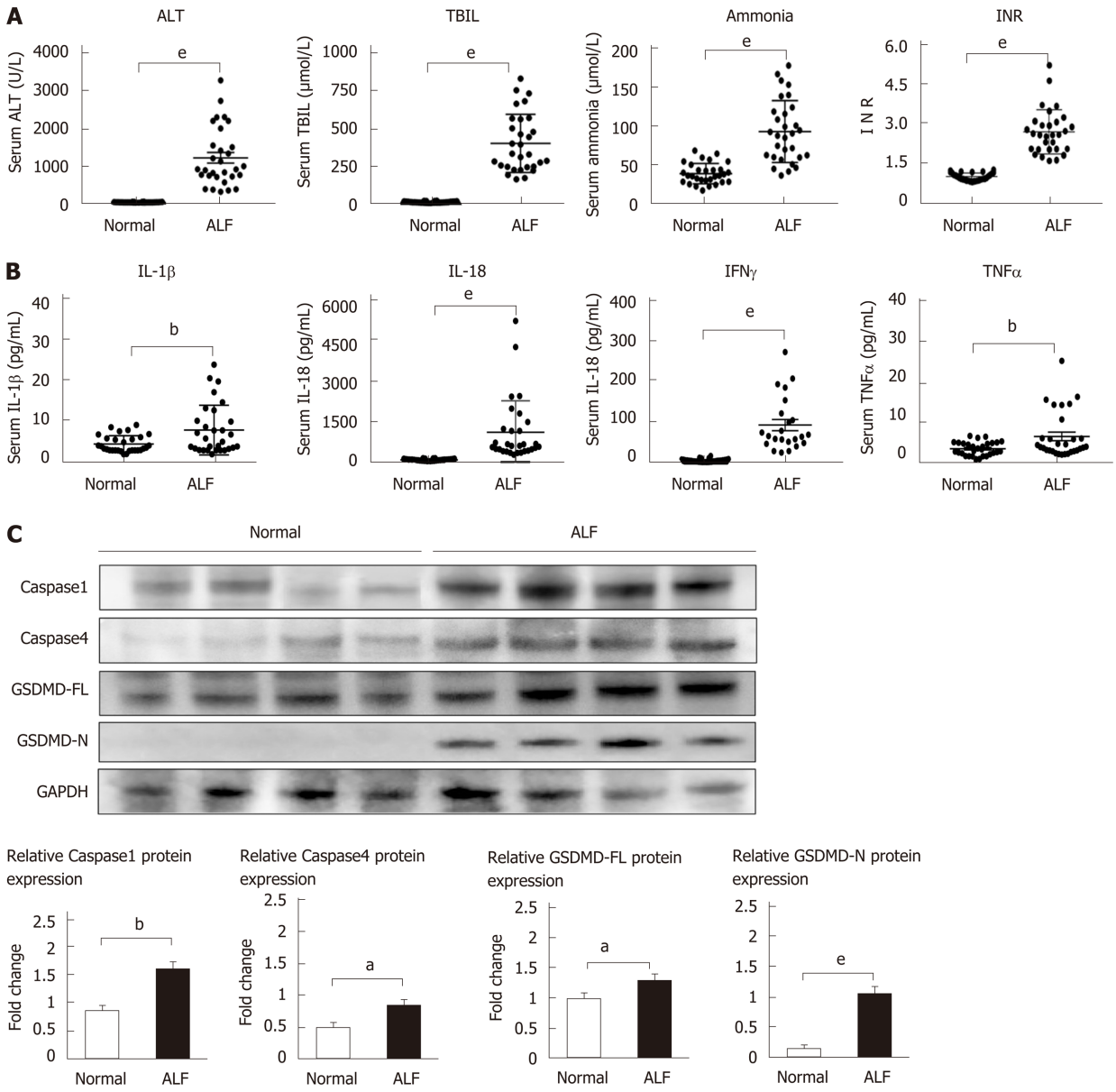

Figure 1 The levels of pyroptosis-associated inflammatory cytokines and proteins increase in human acute liver failure. A: Serum levels of alanine aminotransferase, total bilirubin, ammonia, and international normalized ratio; B: Serum levels of inflammatory cytokines interleukin (IL)-1β, IL-18, tumor necrosis factor-alpha, and interferon-γ detected by flow cytometry; C: Expression levels of caspase 1, caspase 4, full-length gasdermin D, and cleaved N-terminal fragment of gasdermin D in liver tissues from acute liver failure cases and controls detected using Western blot with GAPDH as the internal reference. Data are presented as the mean ± square error. $^{a}P < 0.05$, $^{b}P < 0.01$, and $^{e}P < 0.001$. ALT: Alanine aminotransferase; TBIL: Total bilirubin; INR: International normalized ratio; IL-1β: Interleukin-1β; IL-18: Interleukin-18; TNFα: Tumor necrosis factor-alpha; IFN-γ: Interferon-γ; GSDMD-FL: Full-length gasdermin D; GSDMD-N: Cleaved N-terminal fragment of gasdermin D; ALF: Acute liver failure.

to die at approximately 6 h, and only 1 out of the 15 mice survived to 24 h. In the GSDMD-/- + D-Galn/LPS group, the 24-h survival rate improved tremendously with only 3 out of the 15 mice dying (Figure 4A). Anatomy analysis showed that the liver surface was smooth and fine, the colour was dark pink, the edge was sharp, and the texture was medium for mice in the WT + PBS and GSDMD-/- + PBS groups. For mice in the WT + D-Galn/LPS group, the liver was significantly congested and swollen, the liver volume was enlarged with a dark brown colour, and the membrane was tight. For mice in the GSDMD-/- + D-Galn/LPS group, the liver was slightly congested and swollen (Figure 4B). Compared to the WT + PBS group, ALT, INR, and blood ammonia increased significantly for mice in the WT + D-Galn/LPS group, but the above indicators decreased significantly for mice in the GSDMD-/- + D-Galn/LPS group compared to mice in the WT + D-Galn/LPS group (Figure 4C). H and E staining of the pathological sections of the liver (Figure 4D) showed that the hepatocyte cytoplasm was evenly stained red, the size of the nucleus was normal, the

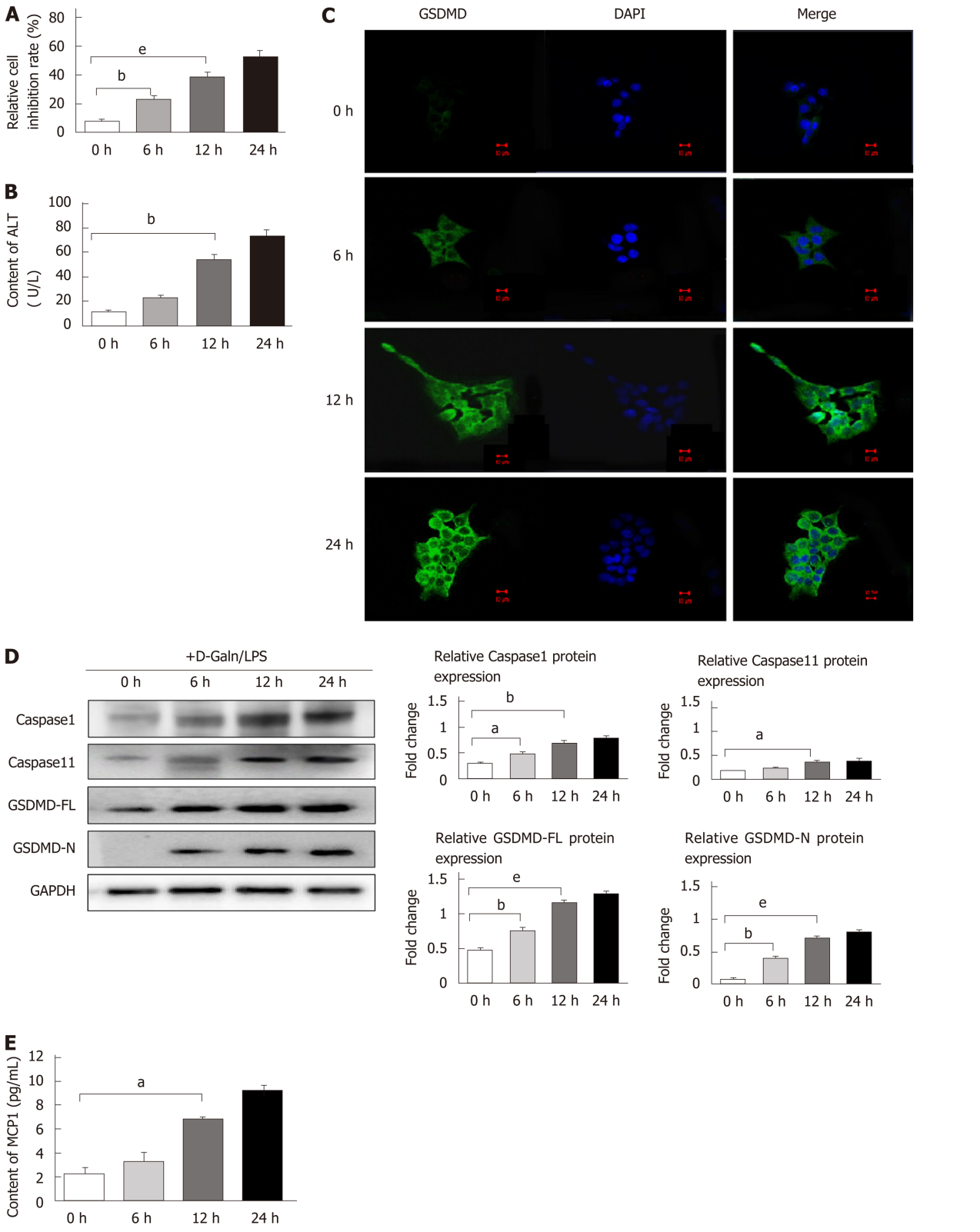

Figure 2 Expression of pyroptosis pathway-associated proteins increases in a D-galactose/lipopolysaccharide-induced AML12 hepatocyte injury model. Intervention was performed using D-Galn (15 mmol/L) + LPS (100 μg/mL) for 0, 6, 12, and 24 h. A: Changes in the cell inhibition rate at 0, 6, 12, and 24 h evaluated by CCK8; B: Content of ALT in the supernatant; C: Expression of gasdermin D (GSDMD) protein detected under a confocal fluorescence microscope. Scale bars = 10 μm; D: Caspase 1/11, GSDMD-FL, and GSDMD-N protein expression evaluated by Western blot with GAPDH as the internal reference; E: Content of MCP1 in the cell culture supernatant. Data are presented as the mean ± square error. $^{a}P < 0.05$, $^{b}P < 0.01$, and $^{e}P < 0.001$. ALT: Alanine aminotransferase; D-Galn/LPS: D-galactose/lipopolysaccharide; GSDMD-FL: Full-length GSDMD; GSDMD-N: Cleaved N-terminal fragment of GSDMD; MCP1: Monocyte chemotactic protein 1; DAPI: 4',6-diamidino-2-phenylindole.

hepatic sinus was clear, and the hepatic cords were neatly organized for the mice in

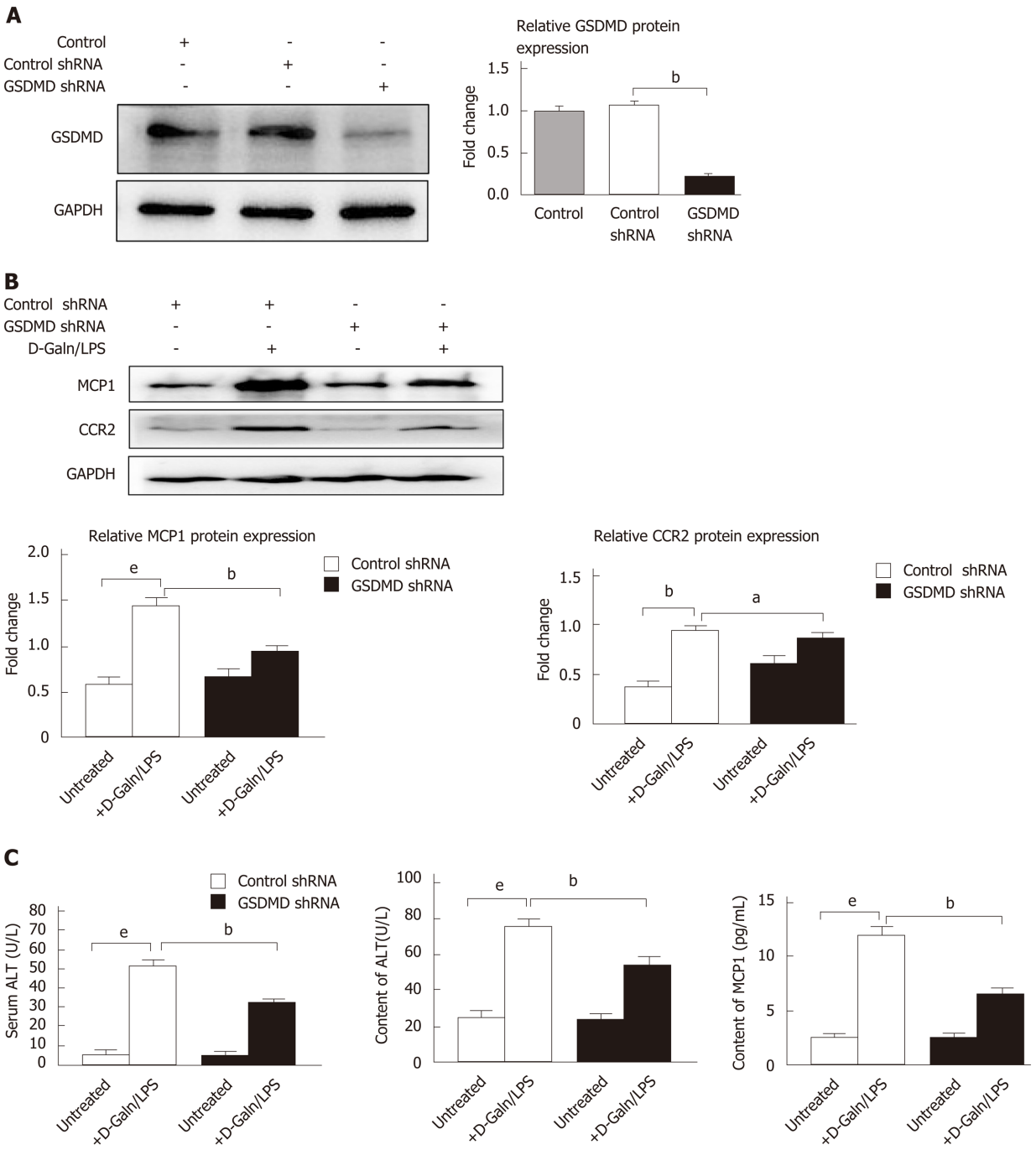

Figure 3 Gasdermin D knockdown by shRNA decreases the expression of monocyte chemotactic protein 1 and CC chemokine receptor-2 in a D-galactose/lipopolysaccharide-induced AML12 hepatocyte injury model. Control shRNA and gasdermin D (GSDMD) shRNA were transfected into AML12 using Lipofectamine 3000, and the intervention was performed using D-galactose (15 mmol/L)/lipopolysaccharide (100 μg/L) for 24 h. A: Expression changes of GSDMD protein evaluated by Western blot; B: Protein expression levels of monocyte chemotactic protein 1 (MCP1) and CC chemokine receptor-2 evaluated by Western blot; C: Cell inhibition rate evaluated by CCK8 assay; D: Contents of alanine aminotransferase and MCP1 in the cell supernatant. Data are presented as the mean ± square error. $^{a}P < 0.05$, $^{b}P < 0.01$, and $^{e}P < 0.001$. D-Galn/LPS: D-galactose/lipopolysaccharide; GSDMD: Gasdermin D; ALT: Alanine aminotransferase; MCP1: Monocyte chemotactic protein 1; CCR2: CC chemokine receptor-2.

the WT + PBS group and the GSDMD-/- + PBS group. For mice in the WT + D-Galn/LPS group, the hepatocytes suffered from massive necrosis, the structure of the hepatic lobule collapsed, a large number of red blood cells were deposited in the hepatic sinus, and there was extensive inflammatory cell infiltration into the portal area and the surrounding area. For GSDMD-/- mice, H and E staining of the liver showed that the hepatocytes were swollen and degenerated, there was focal necrosis, the liver lobular structure existed, and the inflammatory cell infiltration was reduced significantly. The Ishak score showed that the degree of inflammation in the GSDMD-/- + D-Galn/LPS group was reduced significantly compared to the WT + D-

Galn/LPS group (Figure 4E).

GSDMD knockout significantly decreases the expression of MCP1/CCR2 and macrophage infiltration in D-Galn/LPS-induced ALF mice

The expression of GSDMD-N in the liver of the WT + D-Galn/LPS group mice increased significantly compared to that in the WT + PBS group mice. The protein expression of MCP1/CCR2 in the GSDMD-/- + D-Galn/LPS group decreased compared to that in the WT + D-Galn/LPS group (Figure 5A). Immunohistochemistry of the liver showed that macrophage-specific F4/80 protein expression in the GSDMD-/- + D-Galn/LPS group was reduced significantly compared to that in the WT + D-Galn/LPS group (Figure 5B). Serum MCP1, IL-1β, IL-18, TNFα, and IFN-γ were decreased in the GSDMD-/- + D-Galn/LPS group compared to the WT + D-Galn/LPS group (Figure 5C).

DISCUSSION

The aetiology of ALF varies and the pathogenesis is thus slightly different in different geographic regions, but massive hepatocyte death and the secondary severe inflammatory responses are the same and are more important than the initial trigger[17,18].

GSDMD is a key substrate protein for pyroptosis, which rapidly leads to cell death and attracts a large number of immune cells. Therefore, GSDMD is known to be one of the important switches for inflammatory responses[19]. The role and mechanism of GSDMD-mediated hepatocyte pyroptosis in the pathogenesis of ALF remain unclear.

First, we clarified that the protein expression levels of caspase 1/4, GSDMD-FL, and GSDMD-N increased in the liver and the levels of IL1β, IL-18, TNFα, and INFγ in the serum were elevated in human cases of ALF compared with controls. Second, we established 0, 6, 12, and 24 h dynamic hepatocyte injury models in AML12 cells by treatment with D-Galn/LPS. We found that along with the gradual increase in the cell inhibition rate, the protein expression levels of caspase 1/11, GSDMD-FL, and the cleaved N-terminal fragment increased with the prolongation of the intervention time. However, knocking down GSDMD by shRNA obviously decreased the cell inhibition rate in the D-Galn/LPS AML12 hepatocyte injury model. Third, in *in vivo* experiments, compared to the WT + D-Galn/LPS group, serum ALT, ammonia, and inflammatory factors including IL1β, IL-18, TNFα, and INFγ were decreased significantly in the GSDMD-/- + D-Galn/LPS group and the INR was shortened. Furthermore, H and E staining of histopathological sections of the liver showed that hepatocyte death was reduced significantly, the hepatic inflammatory response was alleviated significantly, and the survival rate improved dramatically. These results showed that GSDMD-mediated hepatocyte pyroptosis plays a key role in both human ALF and the D-Galn/LPS induced mouse ALF model.

Pyroptosis promotes and expands inflammatory responses by releasing inflammatory factors IL-1β and IL-18, but we did not detect IL-1β and IL-18 in the culture supernatant of the D-Galn/LPS induced AML12 hepatocyte injury model by ELISA, which is consistent with the experimental results of Kofahi *et al* who used HCV infection to induce Huh-7.5 human hepatocyte pyroptosis *in vitro*[20]. In addition, Geng *et al*[21] also reported that the process of hepatocyte pyroptosis cannot be inhibited by the interfering heat shock-induced ALF model in rats by using the IL-1 receptor antagonist anakinra, suggesting that the mechanisms of hepatocyte pyroptosis in inducing inflammatory responses are different from those of immune cell pyroptosis.

In this study, we found that the content of MCP1 in the supernatant was increased in the AML12 hepatocyte injury model. Downregulation of GSDMD by shRNA can significantly reduce the protein expression levels of MCP1/CCR2 and the amount of MCP1 released to the supernatant.

The previous experiments showed that the hepatic inflammatory response was alleviated and the survival rate improved significantly in the GSDMD-/- + D-Galn/LPS group mice. Downregulation of GSDMD inhibited MCP1/CCR2 *in vitro*, thus it is important to explore whether GSDMD-mediated hepatocyte pyroptosis expands inflammatory responses by upregulating MCP1/CCR2 to recruit macrophages in ALF mice. We found that the expression levels of MCP1, CCR2, and F4/80 in the liver of the WT + D-Galn/LPS group mice were increased, and compared to the WT + D-Galn/LPS group, the expression levels of MCP1, CCR2, and F4/80 in the liver were decreased significantly in the GSDMD-/-+D-Galn/LPS mice. Our study has provided new evidence for the role and mechanisms of hepatocyte pyroptosis in ALF.

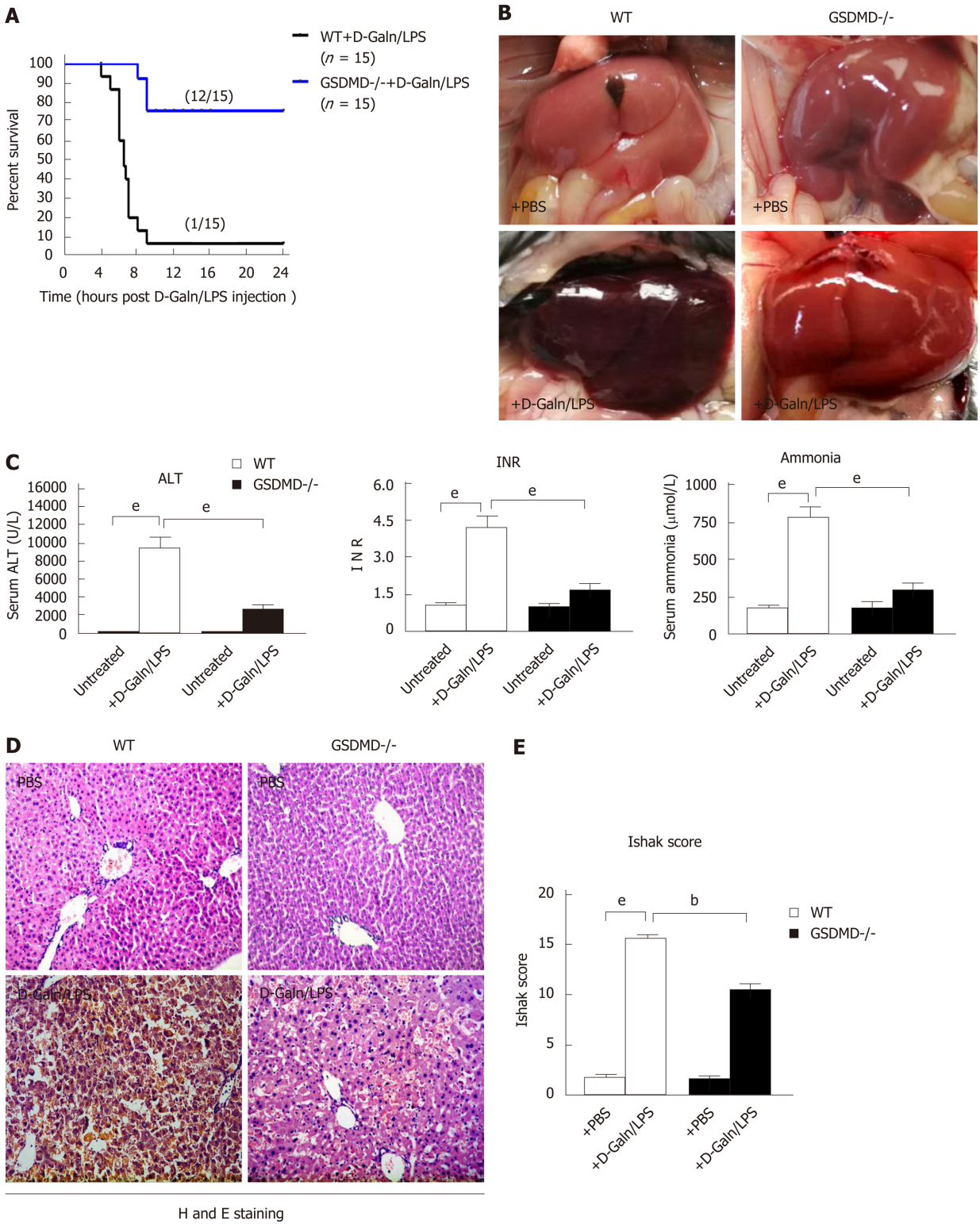

Figure 4 Gasdermin D knockout dramatically eliminates inflammatory damage in the liver and improves survival in D-galactose/lipopolysaccharide-induced acute liver failure mice. A: Survival curve; B: Changes in liver tissue appearance; C: Alanine aminotransferase, international normalized ratio, and blood ammonia in mice; D: Pathological examination of the liver by haematoxylin and eosin staining. Scale bars = 100 μm; E: Ishak score of the liver tissue pathology. Data are presented as the mean ± square error. $^{a}P < 0.05$, $^{b}P < 0.01$, and $^{e}P < 0.001$. WT: Wild type; GSDMD-/-: Gasdermin D genetic knockout; D-Galn/LPS: D-galactose/lipopolysaccharide; PBS: Phosphate buffer saline; ALT: Alanine aminotransferase; INR: International normalized ratio; H and E: Haematoxylin and eosin.

Our study demonstrated that GSDMD-mediated pyroptosis played an important role in the pathogenesis of human ALF and D-Galn/LPS-induced hepatocyte injury *in vitro* as well as in mouse ALF *in vivo*. Unlike the mechanism of immune cell pyroptosis expanding inflammatory responses by releasing IL1β and IL-18, hepatocyte pyroptosis recruited immune cells to infiltrate the liver by upregulating

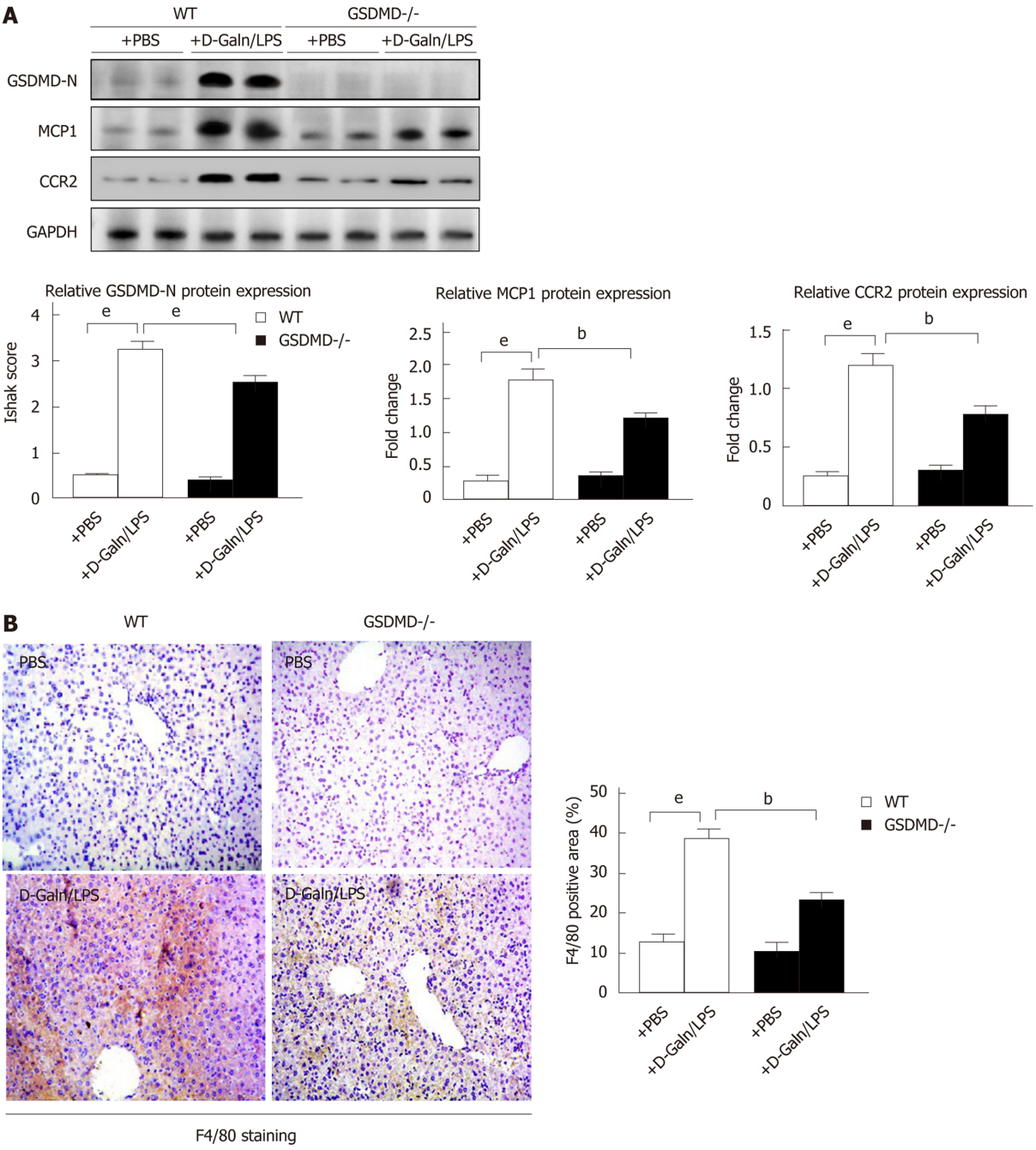
A
WT
GSDMD-/-
+PBS
+D-Galn/LPS
+PBS
+D-Galn/LPS
GSDMD-N
MCP1
CCR2
GAPDH
Relative GSDMD-N protein expression
Ishak score
WT
GSDMD-/-
Relative MCP1 protein expression
Fold change
Relative CCR2 protein expression
Fold change
B
WT
GSDMD-/-
PBS
PBS
D-Galn/LPS
D-Galn/LPS
F4/80 staining
F4/80 positive area (%)
WT
GSDMD-/-

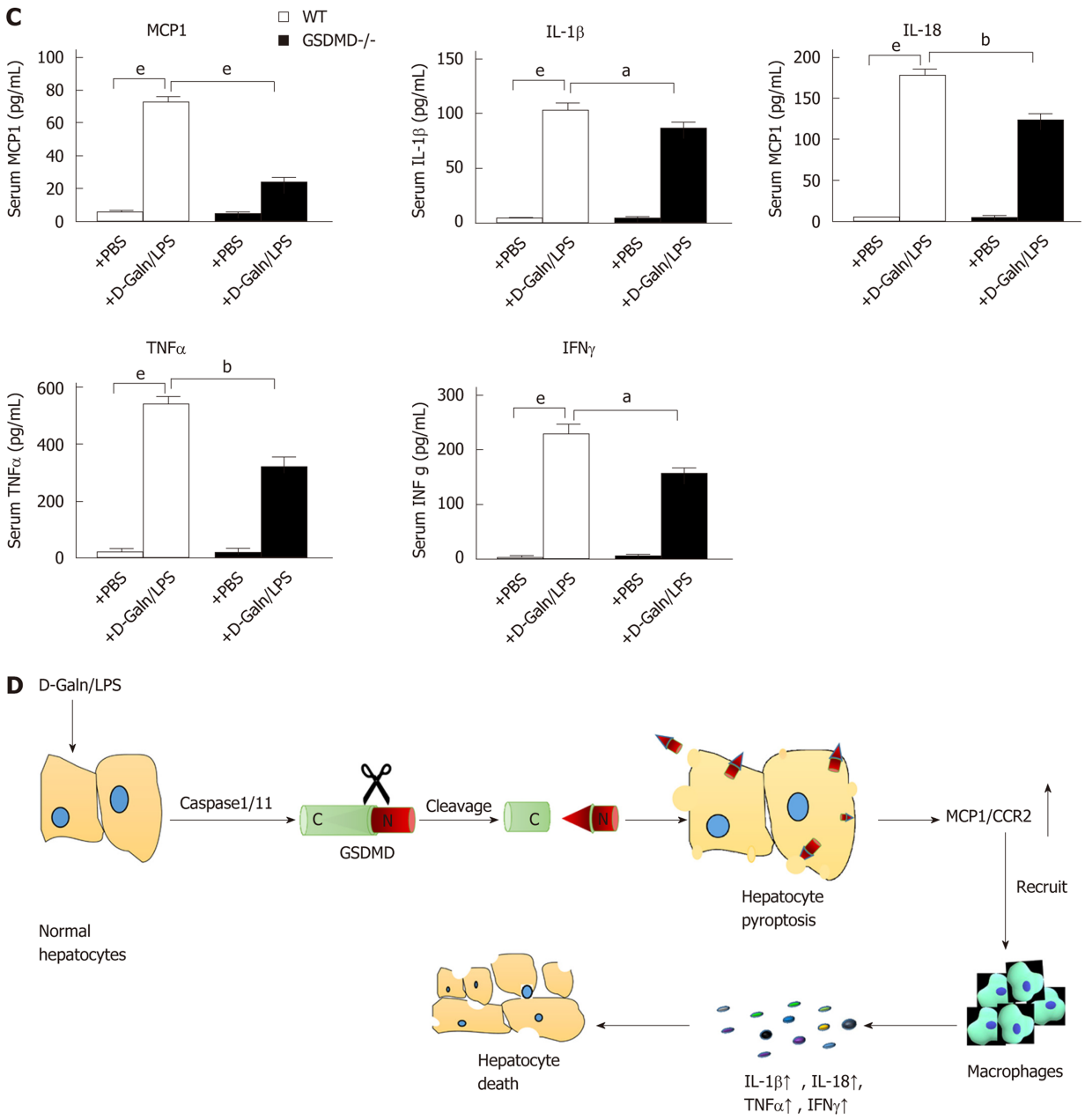

Figure 5 Gasdermin D knockout significantly decreases the expression of monocyte chemotactic protein 1/ CC chemokine receptor-2 and macrophage infiltration in D-galactose/lipopolysaccharide-induced acute liver failure mice. A: Protein expression levels of cleaved N-terminal fragment of gasdermin D, monocyte chemotactic protein 1 (MCP1), and CC chemokine receptor-2 in the liver evaluated by Western blot; B: Immunohistochemical staining for macrophage-specific F4/80 in the liver. Scale bars = 100 μm; C: Detection of serum MCP1, interleukin (IL)-1β, IL-18, tumor necrosis factor-alpha, and interferon-γ by enzyme-linked immunosorbent assay; D: The diagram showing the mechanism of hepatocyte pyroptosis for expanding the inflammatory responses; Data are presented as the mean ± square error. $^{a}P < 0.05$, $^{b}P < 0.01$, and $^{e}P < 0.001$. WT: Wild type; GSDMD-/-: GSDMD genetic knockout; D-Galn/LPS: D-galactose/lipopolysaccharide; PBS: Phosphate buffer saline; GSDMD-N: Cleaved N-terminal fragment of GSDMD; MCP1: Monocyte chemotactic protein 1; CCR2: CC chemokine receptor-2; IL-1β: Interleukin-1β; IL-18: Interleukin-18; TNFα: Tumor necrosis factor-alpha; IFNγ: Interferon-γ.

MCP1/CCR2, further expanding the cascading inflammatory responses. Inhibition or knockdown of GSDMD can reduce hepatocyte pyroptosis by downregulating MCP1/CCR2, which alleviates the inflammatory cytokine storm, thus improving ALF. Developing drugs that have the effects of targeted inhibition of GSDMD is thus a potential new therapeutic approach to develop ALF therapies. However, the present study has its shortcomings. In the present study, we did not use adenovirus to promote GSDMD gene or protein expression, and thus observing the effects of overexpression of GSDMD on hepatocyte pyroptosis will be the focus of our future work.

ARTICLE HIGHLIGHTS

Research background

Acute liver failure (ALF) seriously endangers human life due to its high mortality. There is currently no specific treatment method or drugs available for treating ALF. Pyroptosis is a highly inflammatory type of programmed cell death. Gasdermin D (GSDMD), as the final executor of pyroptosis, is also known as one of the important control switches in inflammatory responses. However, the actual effects of GSDMD in hepatocyte pyroptosis and ALF are still unclear.

Research motivation

Our findings may provide a research basis for developing inhibitors or drugs with targeted inhibition or knockdown of GSDMD for the treatment of ALF.

Research objectives

To detect GSDMD expression in liver tissues from humans and mice with ALF and in injured hepatocytes and to investigate the possible molecular mechanism of GSDMD-mediated hepatocyte pyroptosis for expanding inflammatory responses.

Research methods

The expression levels of pyroptosis pathway proteins in liver tissues from humans with ALF, the injured AML12 cell line, and liver tissues from Galn/LPS-induced ALF mouse models were detected by using Western blot. In further study of the molecular mechanism, downregulation of GSDMD by shRNA was induced *in vitro*, and GSDMD knockout mice were used in a Galn/LPS-induced ALF model.

Research results

The expression of the cleaved N-terminal fragment of GSDMD protein (GSDMD-N) was increased significantly in liver tissues from humans and mice with ALF and in an *in vitro* injured AML12 hepatocyte cell line. The mechanism of inflammation induced by hepatocyte pyroptosis was different from the release of interleukin (IL)-1β and IL-18 by immune cell pyroptosis. Hepatocyte pyroptosis promoted and expanded inflammatory responses by upregulating monocyte chemotactic protein 1 (MCP1)/CC chemokine receptor-2 (CCR2). GSDMD knockout can significantly alleviate D-galactose/lipopolysaccharide (D-Galn/LPS)-induced ALF in mice, reduce serum inflammatory cytokines, and improve the survival rate of the ALF mice. Its effects were associated with a decrease in the expression of the MCP1/CCR2 proteins and a reduction of MCP1 release. However, the effects of downregulating GSDMD in ALF patients are still unclear and should be confirmed in clinical studies.

Research conclusions

GSDMD-mediated hepatocyte pyroptosis plays a key role in ALF, both in humans and D-Galn/LPS-induced ALF mice. GSDMD upregulates MCP1/CCR2 to release inflammatory cytokines, which leads to deterioration of the condition in ALF. Inhibition or knockdown of GSDMD can significantly reduce the levels of inflammatory cytokines and alleviate liver injury in ALF.

Research perspectives

The present study clarified the role of hepatocyte pyroptosis in ALF as well as its mechanism of inducing and expanding inflammatory responses by upregulating MCP1/CCR2. This study also demonstrated that targeted GSDMD inhibitors or effective intervention drugs may be a treatment approach to the prevention and treatment of ALF.

REFERENCES

1 **Flamm SL**, Yang YX, Singh S, Falck-Ytter YT; AGA Institute Clinical Guidelines Committee. American Gastroenterological Association Institute Guidelines for the Diagnosis and Management of Acute Liver Failure. *Gastroenterology* 2017; **152**: 644-647 [PMID: 28056348 DOI: 10.1053/j.gastro.2016.12.026]

2 **Bernal W**, Auzinger G, Dhawan A, Wendon J. Acute liver failure. *Lancet* 2010; **376**: 190-201 [PMID: 20638564 DOI: 10.1016/S0140-6736(10)60274-7]

3 **van Paassen J**, Bauer MP, Arbous MS, Visser LG, Schmidt-Chanasit J, Schilling S, Ölschläger S, Rieger T, Emmerich P, Schmetz C, van de Berkmortel F, van Hoek B, van Burgel ND, Osterhaus AD, Vossen AC, Günther S, van Dissel JT. Acute liver failure, multiorgan failure, cerebral oedema, and activation of proangiogenic and antiangiogenic factors in a case of Marburg haemorrhagic fever. *Lancet Infect Dis* 2012; **12**: 635-642 [PMID: 22394985 DOI: 10.1016/S1473-3099(12)70018-X]

4 **Dara L**, Johnson H, Suda J, Win S, Gaarde W, Han D, Kaplowitz N. Receptor interacting protein kinase 1 mediates murine acetaminophen toxicity independent of the necrosome and not through necroptosis. *Hepatology* 2015; **62**: 1847-1857 [PMID: 26077809 DOI: 10.1002/hep.27939]

5 **Bergsbaken T**, Fink SL, Cookson BT. Pyroptosis: host cell death and inflammation. *Nat Rev Microbiol* 2009; **7**: 99-109 [PMID: 19148178 DOI: 10.1038/nrmicro2070]

6 **Kuang S**, Zheng J, Yang H, Li S, Duan S, Shen Y, Ji C, Gan J, Xu XW, Li J. Structure insight of GSDMD reveals the basis of GSDMD autoinhibition in cell pyroptosis. *Proc Natl Acad Sci USA* 2017; **114**: 10642-10647 [PMID: 28928145 DOI: 10.1073/pnas.1708194114]

7 **Ding J**, Wang K, Liu W, She Y, Sun Q, Shi J, Sun H, Wang DC, Shao F. Pore-forming activity and structural autoinhibition of the gasdermin family. *Nature* 2016; **535**: 111-116 [PMID: 27281216 DOI: 10.1038/nature18590]

8 **He WT**, Wan H, Hu L, Chen P, Wang X, Huang Z, Yang ZH, Zhong CQ, Han J. Gasdermin D is an executor of pyroptosis and required for interleukin-1β secretion. *Cell Res* 2015; **25**: 1285-1298 [PMID: 26611636 DOI: 10.1038/cr.2015.139]

9 **Burzynski LC**, Clarke MCH. Death Is Coming and the Clot Thickens, as Pyroptosis Feeds the Fire. *Immunity* 2019; **50**: 1339-1341 [PMID: 31216455 DOI: 10.1016/j.immuni.2019.05.015]

10 **Green DR**. The Coming Decade of Cell Death Research: Five Riddles. *Cell* 2019; **177**: 1094-1107 [PMID: 31100266 DOI: 10.1016/j.cell.2019.04.024]

11 **Stravitz RT**, Lee WM. Acute liver failure. *Lancet* 2019; **394**: 869-881 [PMID: 31498101 DOI: 10.1016/S0140-6736(19)31894-X]

12 **Tsuneyama K**, Harada K, Yasoshima M, Hiramatsu K, Mackay CR, Mackay IR, Gershwin ME, Nakanuma Y. Monocyte chemotactic protein-1, -2, and -3 are distinctively expressed in portal tracts and granulomata in primary biliary cirrhosis: implications for pathogenesis. *J Pathol* 2001; **193**: 102-109 [PMID: 11169522 DOI: 10.1002/1096-9896(2000)9999:9999<::AID-PATH725>3.0.CO;2-P]

13 **Weisberg SP**, Hunter D, Huber R, Lemieux J, Slaymaker S, Vaddi K, Charo I, Leibel RL, Ferrante AW. CCR2 modulates inflammatory and metabolic effects of high-fat feeding. *J Clin Invest* 2006; **116**: 115-124 [PMID: 16341265 DOI: 10.1172/JCI24335]

14 **Ruze A**, Chen BD, Liu F, Chen XC, Gai MT, Li XM, Ma YT, Du XJ, Yang YN, Gao XM. Macrophage migration inhibitory factor plays an essential role in ischemic preconditioning-mediated cardioprotection. *Clin Sci (Lond)* 2019; **133**: 665-680 [PMID: 30804219 DOI: 10.1042/CS20181013]

15 **Mignon A**, Rouquet N, Fabre M, Martin S, Pagès JC, Dhainaut JF, Kahn A, Briand P, Joulin V. LPS challenge in D-galactosamine-sensitized mice accounts for caspase-dependent fulminant hepatitis, not for septic shock. *Am J Respir Crit Care Med* 1999; **159**: 1308-1315 [PMID: 10194182 DOI: 10.1164/ajrccm.159.4.9712012]

16 **Wang H**, Chen L, Zhang X, Xu L, Xie B, Shi H, Duan Z, Zhang H, Ren F. Kaempferol protects mice from d-GalN/LPS-induced acute liver failure by regulating the ER stress-Grp78-CHOP signaling pathway. *Biomed Pharmacother* 2019; **111**: 468-475 [PMID: 30594786 DOI: 10.1016/j.biopha.2018.12.105]

17 **Miyake Y**, Iwasaki Y, Terada R, Takaguchi K, Sakaguchi K, Shiratori Y. Systemic inflammatory response syndrome strongly affects the prognosis of patients with fulminant hepatitis B. *J Gastroenterol* 2007; **42**: 485-492 [PMID: 17671764 DOI: 10.1007/s00535-007-2029-9]

18 **Stravitz RT**, Kramer DJ. Management of acute liver failure. *Nat Rev Gastroenterol Hepatol* 2009; **6**: 542-553 [PMID: 19652652 DOI: 10.1038/nrgastro.2009.127]

19 **Man SM**, Kanneganti TD. Gasdermin D: the long-awaited executioner of pyroptosis. *Cell Res* 2015; **25**: 1183-1184 [PMID: 26482951 DOI: 10.1038/cr.2015.124]

20 **Kofahi HM**, Taylor NG, Hirasawa K, Grant MD, Russell RS. Hepatitis C Virus Infection of Cultured Human Hepatoma Cells Causes Apoptosis and Pyroptosis in Both Infected and Bystander Cells. *Sci Rep* 2016; **6**: 37433 [PMID: 27974850 DOI: 10.1038/srep37433]

21 **Geng Y**, Ma Q, Liu YN, Peng N, Yuan FF, Li XG, Li M, Wu YS, Li BL, Song WB, Zhu W, Xu WW, Fan J, Su L. Heatstroke induces liver injury via IL-1β and HMGB1-induced pyroptosis. *J Hepatol* 2015; **63**: 622-633 [PMID: 25931416 DOI: 10.1016/j.jhep.2015.04.010]

World Journal of Gastroenterology

Submit a Manuscript: https://www.f6publishing.com

World J Gastroenterol 2019 November 28; 25(44): 6541-6550

DOI: 10.3748/wjg.v25.i44.6541

ISSN 1007-9327 (print) ISSN 2219-2840 (online)

ORIGINAL ARTICLE

Retrospective Study

Cystic duct cancer: Should it be deemed as a type of gallbladder cancer?

Tu-Nan Yu, Ying-Ying Mao, Fang-Qiang Wei, Hui Liu

ORCID number: Tu-Nan Yu (0000-0003-0866-3178); Ying-Ying Mao (0000-0003-3644-9160); Fang-Qiang Wei (0000-0003-0871-2275); Hui Liu (0000-0002-5531-3640).

Author contributions: Mao YY, Wei FQ and Liu H designed the research; Yu TN, Mao YY, Wei FQ and Liu H performed the research; Yu TN and Liu H analyzed the data; Yu TN, Mao YY, Wei FQ and Liu H wrote the paper.

Supported by Zhejiang Provincial Natural Science Foundation of China, No. LQ17H030003.

Institutional review board statement: The data in this study was obtained from the SEER database and the National Cancer Institute had given us permission to access data for researching (Reference number: 10536-Nov2017). Given that SEER data is de-identified and ethics approval is waived, this study was exempted from Institutional Research Board review.

Informed consent statement: Patients were not required to give informed consent to the study because the analysis used anonymous clinical data that are publicly available from the SEER database.

Conflict-of-interest statement: All authors declare no conflicts of interest related to this article.

Data sharing statement: No additional data are available.

Tu-Nan Yu, Department of General Surgery, Sir Run Run Shaw Hospital, School of Medicine, Zhejiang University, Hangzhou 310016, Zhejiang Province, China

Ying-Ying Mao, Department of Epidemiology and Biostatistics, Zhejiang Chinese Medical University, Hangzhou 310053, Zhejiang Province, China

Fang-Qiang Wei, Department of Hepatobiliary and Pancreatic Surgery, Zhejiang Provincial People's Hospital, Hangzhou Medical College, Hangzhou 310014, Zhejiang Province, China

Hui Liu, Zhejiang Provincial Key Laboratory of Laparoscopic Technology, Sir Run Run Shaw Hospital, School of Medicine, Zhejiang University, Hangzhou 310016, Zhejiang Province, China

Corresponding author: Hui Liu, PhD, Research Assistant Professor, Zhejiang Provincial Key Laboratory of Laparoscopic Technology, Sir Run Run Shaw Hospital, School of Medicine, Zhejiang University, Hangzhou 310016, Zhejiang Province, China. lhui2010@zju.edu.cn
Telephone: +86-571-86006653
Fax: +86-571-86006653

Abstract

BACKGROUND

According to the latest American Joint Committee on Cancer and Union for International Cancer Control manuals, cystic duct cancer (CC) is categorized as a type of gallbladder cancer (GC), which has the worst prognosis among all types of biliary cancers. We hypothesized that this categorization could be verified by using taxonomic methods.

AIM

To investigate the categorization of CC based on population-level data.

METHODS

Cases of biliary cancers were identified from the Surveillance, Epidemiology, and End Results 18 registries database. Together with routinely used statistical methods, three taxonomic methods, including Fisher's discriminant, binary logistics and artificial neuron network (ANN) models, were used to clarify the categorizing problem of CC.

RESULTS

The T staging system of perihilar cholangiocarcinoma [a type of extrahepatic cholangiocarcinoma (EC)] better discriminated CC prognosis than that of GC. After adjusting other covariates, the hazard ratio of CC tended to be closer to that

Manuscript source: Unsolicited manuscript

Received: August 16, 2019
Peer-review started: August 16, 2019
First decision: October 14, 2019
Revised: October 24, 2019
Accepted: November 13, 2019
Article in press: November 13, 2019
Published online: November 28, 2019

P-Reviewer: Michalinos A
S-Editor: Wang J
L-Editor: Wang TQ
E-Editor: Zhang YL

of EC, although not reaching statistical significance. To differentiate EC from GC, three taxonomic models were built and all showed good accuracies. The ANN model had an area under the receiver operating characteristic curve of 0.902. Using the three models, the majority (75.0%-77.8%) of CC cases were categorized as EC.

CONCLUSION
Our study suggested that CC should be categorized as a type of EC, not GC. Aggressive surgical attitude might be considered in CC cases, to see whether long-term prognosis could be immensely improved like the situation in EC.

Key words: Cystic duct cancer; Gallbladder cancer; Extrahepatic cholangiocarcinoma; Surgical management; Taxonomy; Categorization

Core tip: In the latest American Joint Committee on Cancer and Union for International Cancer Control manuals, cystic duct cancer (CC) is categorized as a type of gallbladder cancer, yet not verified by direct epidemiological evidence in previous studies. Our study used taxonomic methods to analyze population-based big data, including Fisher's discriminant, binary logistics and artificial neuron network models. By using these three models, our study proved that CC is better to be deemed and treated as a kind of extrahepatic cholangiocarcinoma.

Citation: Yu TN, Mao YY, Wei FQ, Liu H. Cystic duct cancer: Should it be deemed as a type of gallbladder cancer? *World J Gastroenterol* 2019; 25(44): 6541-6550
URL: https://www.wjgnet.com/1007-9327/full/v25/i44/6541.htm
DOI: https://dx.doi.org/10.3748/wjg.v25.i44.6541

INTRODUCTION

Cystic duct cancer (CC) is a rare type of biliary cancer which arises in the conjunction between the gallbladder and the extraheptic bile duct[1]. By Farrar[2] in 1951, CC was defined based on the following three criteria: "(1) The growth must be restricted to the cystic duct; (2) There must be no neoplastic process in the gallbladder, hepatic or common bile ducts; and (3) A histological examination of the growth must confirm the presence of carcinoma cells". Unlike other biliary neoplasms, the incidence of CC is extremely low (0.03%-0.05%[3]), and previous studies on this disease were focusing on single cases[4-7] or very small-volume series (less than 10 cases)[8,9]. As a consequence, the clinical characteristics of CC remain largely unknown. According to the 8th American Joint Committee on Cancer (AJCC)[10] and 9th Union for International Cancer Control (UICC)[11] manuals, CC is categorized as a type of gallbladder cancer (GC), which has the worst prognosis among all types of biliary tumor[12,13]. However, this categorization lacks verification by direct epidemiological evidence until now.

In the field of botany, a well-known statistical tool is the Fisher's linear discriminant analysis, which was invented by Sir Ronald Aylmer Fisher[14] and initially used to make optimum categorization for three types of iris flowers, namely, Setosa, Versicolour and Virginica. In the current study, besides routinely used statistical tools, we applied to use this taxonomic method together with binary logistics and artificial neuron network (ANN) models, to clarify the categorizing problem of CC. To our knowledge, this is the first study attempting to re-categorize CC using population based data.

MATERIALS AND METHODS

Extraction of data

Eligible cases of CC, GC and extrahepatic cholangiocarcinoma (EC) diagnosed between 2006 and 2015 were obtained from the Surveillance, Epidemiology, and End Results (SEER) 18 registries database (last submission in November, 2017). CC or GC cases were retrieved with their terms in "CS schema v0204+"; while EC cases were

retrieved with a combined term of "BileductsPerihilar" and "BileductsDistal". All cases reviewed had their pathologies microscopically confirmed, their ages known, and their biological behavior classified as malignant.

For each case, ten variables were evaluated as follows: Sex, age at diagnosis, year of diagnosis, marital status at diagnosis, race recode, SEER historical stage A, tumor size, Rx Summ-Surg Prim Site (1998+), CHDSA region and histology recode-broad grouping.

For marital status, the values of single, separated, divorced, widowed and unmarried or domestic partner were defined as "unmarried". For Rx Summ-Surg Prim Site (1998+)[15], which means surgical procedure, a value of 0 was defined as "no operation"; values from 10 to 30, and of 50 were defined as "biopsy/ partial resection"; a value of 40 was defined as "total resection"; and a value of 60 was defined as "radical resection". For histology recode, a value of 8140-8389 was defined as "adenocarcinoma", while other values were defined as "others".

Statistical analysis

Routine statistical methods: The Pearson's χ^2 test or Fisher's exact test was used for categorical data to compare the distributions of variables between CC, GC and EC. The Mann-Whitney U test was used for continuous variables. The 1, 3 and 5-year overall survival (OS) and cancer specific survival (CSS) rates were calculated by the method of life table. CC cases were divided into T1-2 group and T3-4 group by the current T staging system for GC or EC, respectively (Supplementary table 1), and the prognosis of different groups was compared by the log-rank test. The COX proportional model was utilized to analyze the whole population of CC, GC and EC, and identify the independent prognostic factors for OS and CSS.

Methods to categorize CC: Three steps were required to categorize CC. First, three models were built. All cases of GC and EC were randomly partitioned, and then divided into either a training (70%) or testing group (30%). Three models were constructed to differentiate between GC and EC. In Fisher's linear discriminant model, the importance of variables was evaluated by the absolute values of their coefficients in a structure matrix. In binary logistic model, multivariate analysis was performed, and *P*-value was calculated for each variable. In ANN model, a multilayer perceptron neural network was utilized, and normalized importance was calculated for each variable.

In the next step, the models were evaluated. Accuracies were calculated for the training, testing and whole groups, respectively, and good models generally had these three values very close. The power of a model was also evaluated by the area under the receiver operating characteristic curve (AUROC). Generally, AUROC indicated a model of "good" accuracy at a value between 0.75 and 1.00, of "fair" accuracy at a value between 0.60 and 0.75, and of "poor" accuracy at a value under 0.60.

Finally, CC cases were categorized. Each case of CC would be categorized as GC or EC using the three models. Overall agreement of results of the three models was evaluated by an online Kappa test calculator[16] as well as the McNemar's test.

Between 2006 and 2015, the SEER database recognized a total of 71 cases of CC. However, a certain proportion of cases had missing values and could not be utilized for analysis for all aims. Regarding the analysis of 1, 3 and 5-year survival and T stage, the included cases should have valid data for the variables of "CS extension", "Survival months" and "Vital status recode" (for OS, or "SEER cause-specific classification" for CSS). Consequently, 65 CC cases were analyzed for OS and 56 were analyzed for CSS. In other analyses (comparison of clinical characteristics between different diseases, COX analysis, building models and categorization of CC), all cases involved should have valid data for 10 variables from sex to histology, and cases with missing data could not be produced. Consequently, a total of 36 CC cases were analyzed for the aim of categorization, together with 4878 GC cases and 3295 EC cases. $P < 0.05$ was considered statistically significant, and the IBM SPSS version 22.0 software (SPSS Inc., Chicago, IL, United States) was utilized for all analyses.

RESULTS

Comparison of clinical characteristics

Table 1 shows the comparison of the clinical characteristics between CC, GC and EC. Five variables were found to be statistically different between CC and GC, including sex, tumor size, SEER historical stage, surgical procedure and histology ($P < 0.05$). However, only one variable (surgical procedure) was found to be different between CC and EC ($P < 0.05$).

Table 1 Comparison of clinical characteristics between cystic duct cancer, gallbladder cancer and extrahepatic cholangiocarcinoma, *n* (%)

Variable	No. (%) of patients			*P* value	
	GC (*n* = 4878)	EC (*n* = 3295)	CC (*n* = 36)	CC *vs* GC	CC *vs* EC
Sex				< 0.001[a]	0.067
Male	1528 (31.3)	1880 (57.1)	26 (72.2)		
Female	3350 (68.7)	1415 (42.9)	10 (27.8)		
Age at diagnosis (median)	71	69	66.5	0.059	0.161
Year of diagnosis				0.487	0.492
2006 to 2010	2041 (41.8)	1377 (41.8)	13 (36.1)		
2011 to 2015	2837 (58.2)	1918 (58.2)	23 (63.9)		
Marital status				0.269	0.948
Not married	2348 (48.1)	1264 (38.4)	14 (38.9)		
Married	2530 (51.9)	2031 (61.6)	22 (61.1)		
Race				0.703	0.330
White	3604 (73.9)	2529 (76.8)	25 (69.4)		
Black	683 (14.0)	246 (7.5)	5 (13.9)		
Others	591 (12.1)	520 (15.8)	6 (16.7)		
Tumor size (median)	33	25	25.5	0.005[a]	0.195
SEER historical stage				< 0.001[a]	0.326
Localized	1934 (39.6)	522 (15.8)	3 (8.3)		
Regional	1150 (23.6)	2098 (63.7)	27 (75.0)		
Distant	1794 (36.8)	675 (20.5)	6 (16.7)		
Surgical procedure				< 0.001[a]	0.047[a]
No operation	1014 (20.8)	1468 (44.6)	8 (22.2)		
Biopsy/partial resection	833 (17.1)	535 (16.2)	10 (27.8)		
Total resection	2490 (51.0)	417 (12.7)	6 (16.7)		
Radical resection	541 (11.1)	875 (26.6)	12 (33.3)		
Region				0.928	0.865
Alaska	10 (0.2)	6 (0.2)	0 (0.0)		
East	1705 (35.0)	1104 (33.5)	14 (38.9)		
Northern plains	441 (9.0)	301 (9.1)	5 (13.9)		
Pacific coast	1858 (51.1)	1346 (41.9)	16 (44.4)		
Southwest	149 (4.1)	86 (3.4)	1 (2.8)		
Histology				0.042[a]	0.725
Adenocarcinoma	4152 (85.1)	3086(93.7)	35 (97.2)		
Others	726 (14.9)	209 (6.3)	1 (2.8)		

CC: Cystic duct cancer; GC: Gallbladder cancer; EC: Extrahepatic cholangiocarcinoma; SEER: Surveillance, Epidemiology, and End Results.
[a]$P < 0.05$.

Staging CC cases with the system of GC or EC

The 1, 3 and 5-year survival rates of CC were 50%, 27% and 12% for OS, and 51%, 30% and 20% for CSS, respectively. The median survival time was 13.0 months for both OS and CSS.

All CC cases were divided into T1-2 and T3-4 groups according to the T staging system of GC or EC (Figure 1). Based on the GC system, the prognosis was similar between the T1-2 and T3-4 groups ($P = 0.961$ for OS, and 0.568 for CSS). Comparatively, the EC system (perihilar cholangiocarcinoma) showed statistically different prognoses between the T1-2 and T3-4 groups ($P < 0.05$ for both OS and CSS). Therefore, the T staging system of EC better discriminated CC prognosis than that of GC.

COX analysis

In COX analysis for the whole population of biliary cancer cases, nine variables were found as independent prognostic factors for OS and CSS, including sex, age at

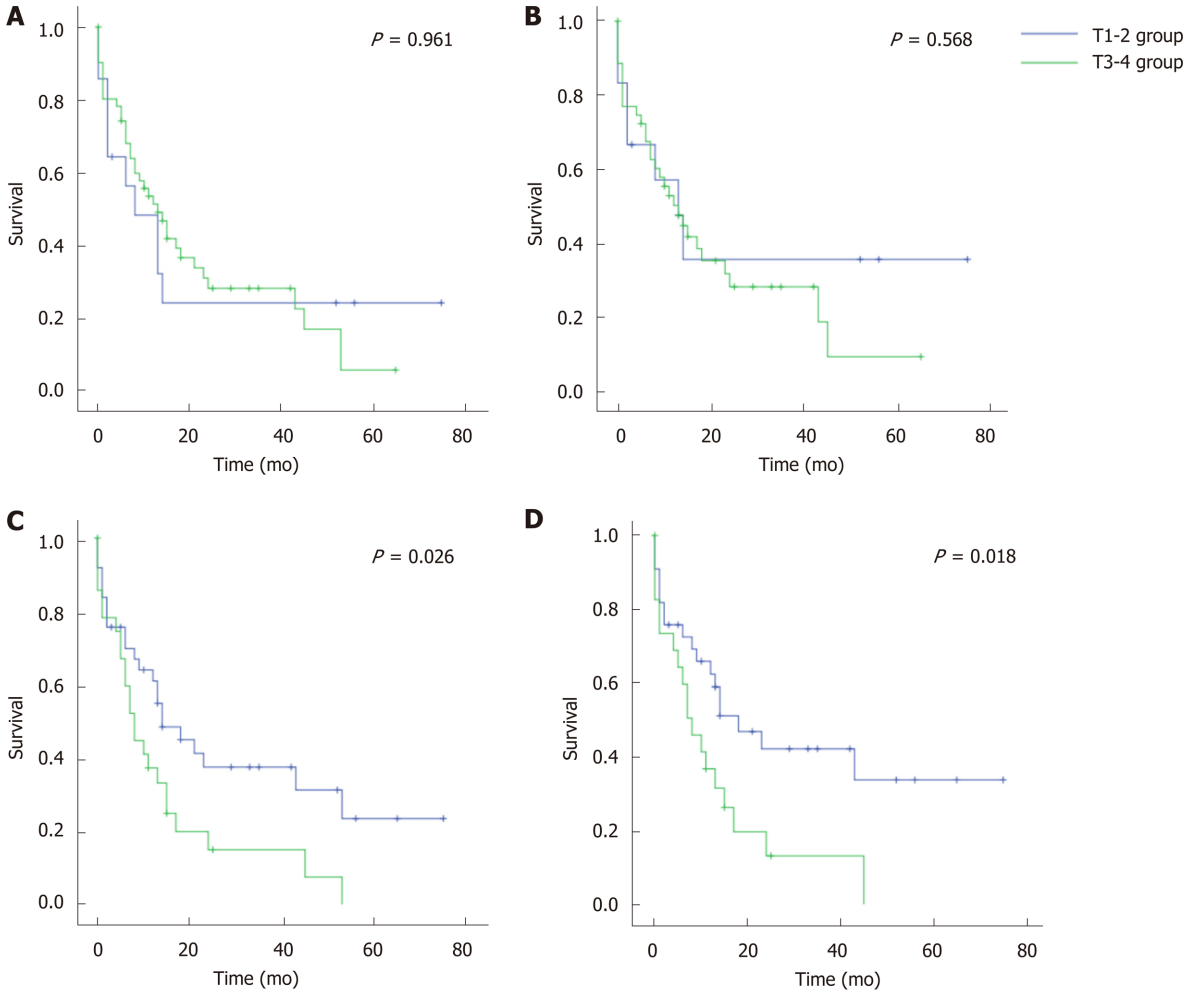

Figure 1 Survival curves of cystic duct cancer based on T staging system of gallbladder cancer or extrahepatic cholangiocarcinoma. A: Overall survival (OS) based on the gallbladder cancer (GC) system; B: Cancer specific survival (CSS) based on the GC system; C: OS based on the extrahepatic cholangiocarcinoma (EC) system; D: CSS based on the EC system. Blue line: T1-2 group; green line: T3-4 group. OS: Overall survival; GC: Gallbladder cancer; EC: Extrahepatic cholangiocarcinoma; CSS: Cancer specific survival.

diagnosis, year of diagnosis, marital status, SEER historical stage, tumor size, surgical procedure, histology and disease (Table 2, $P < 0.05$). By using CC as the reference (1.000), the hazard ratio (HR) for OS was 1.238 [95% confidence interval (CI): 0.813 to 1.884, $P = 0.320$] for EC but 1.494 (95%CI: 0.980 to 2.279, $P = 0.062$) for GC. Regarding CSS, the HR was 1.124 (95%CI: 0.706 to 1.789, $P = 0.623$) for EC but 1.348 (95%CI: 0.845 to 2.151, $P = 0.210$) for GC. Compared with GC, the HR of EC tended to be closer to that of CC, although not reaching statistical significance ($P > 0.05$).

Taxonomic methods to categorize CC

Three models were constructed to differentiate GC from EC (Table 3). In the Fisher's linear discriminant model, the most important three variables (highest absolute values) were sex (0.479), SEER historical stage (0.665) and surgical procedure (-0.238). In the binary logistic model, six variables had statistical significance ($P < 0.05$), including sex, age at diagnosis, tumor size, SEER historical stage, surgical procedure and histology. In the ANN model, the variables with the highest value of normalized importance were tumor size (71.8%), SEER historical stage (80.4%) and surgical procedure (100.0%).

The accuracies of the Fisher's linear discriminant, binary logistic and ANN models were 69.9%, 73.0% and 82.1%, respectively. And for each model, the accuracies in the training, testing and whole populations were close. The AUROCs of the aforementioned three models were 0.781 (95%CI: 0.771-0.791), 0.785 (95%CI: 0.775-0.795) and 0.902 (95%CI: 0.895-0.908), all of which suggested "good" accuracies (Figure 2). The ANN model had the best categorizing power.

Based on the ANN model, the majority (77.8%, 28/36) of CC cases were categorized as EC, the percentage of which was similar to those obtained based on the Fisher's

Table 2 The COX multivariate analysis for cystic duct cancer, gallbladder cancer, and extrahepatic cholangiocarcinoma

Variable	OS			CSS		
	HR	95%CI	*P* value	HR	95%CI	*P* value
Sex						
Male	Ref			Ref		
Female	0.886	0.838 to 0.938	< 0.001[a]	0.895	0.838 to 0.957	0.001[a]
Age at diagnosis	1.025	1.022 to 1.027	< 0.001[a]	1.022	1.019 to 1.025	< 0.001[a]
Year of diagnosis						
2006 to 2009	Ref			Ref		
2010 to 2013	0.938	0.889 to 0.990	0.019[a]	0.927	0.870 to 0.987	0.018[a]
Marital status						
Married	Ref			Ref		
Unmarried	0.839	0.794 to 0.887	< 0.001[a]	0.855	0.801 to 0.912	< 0.001[a]
Race			0.110			0.258
White	Ref			Ref		
Black	0.929	0.857 to 1.007	0.074	0.941	0.856 to 1.033	0.200
Other	1.042	0.956 to 1.135	0.347	1.048	0.948 to 1.158	0.359
Tumor size	1.002	1.001 to 1.002	< 0.001[a]	1.003	1.002 to 1.004	< 0.001[a]
SEER historical stage			< 0.001[a]			< 0.001[a]
Distant	Ref			Ref		
Regional	0.342	0.316 to 0.370	< 0.001[a]	0.277	0.252 to 0.306	< 0.001[a]
Localized	0.642	0.599 to 0.668	< 0.001[a]	0.613	0.566 to 0.664	< 0.001[a]
Surgical procedure			< 0.001[a]			< 0.001[a]
No operation	Ref			Ref		
Partial resection	0.412	0.378 to 0.449	< 0.001[a]	0.395	0.356 to 0.438	< 0.001[a]
Total resection	0.403	0.373 to 0.435	< 0.001[a]	0.383	0.350 to 0.419	< 0.001[a]
Radical resection	0.359	0.330 to 0.391	< 0.001[a]	0.352	0.318 to 0.388	< 0.001[a]
Region			0.934			0.883
Alaska	Ref			Ref		
East	1.081	0.623 to 1.878	0.781	1.055	0.593 to 1.878	0.855
Northern Plains	1.127	0.646 to 1.967	0.673	1.116	0.623 to 2.001	0.711
Pacific coast	1.088	0.628 to 1.885	0.764	1.052	0.593 to 1.867	0.863
Southwest	1.090	0.619 to 1.920	0.766	1.06	0.584 to 1.926	0.847
Histology						
Adenocarcinoma	Ref			Ref		
Others	1.186	1.094 to 1.285	< 0.001[a]	1.215	1.107 to 1.334	< 0.001[a]
Disease			< 0.001[a]			< 0.001[a]
CC	Ref			Ref		
GC	1.494	0.980 to 2.279	0.062	1.348	0.845 to 2.151	0.210
EC	1.238	0.813 to 1.884	0.320	1.124	0.706 to 1.789	0.623

OS: Overall survival; CCS: Cancer-specific survival; HR: Hazard ratio; CC: Cystic duct cancer; GC: Gallbladder cancer; EC: Extrahepatic cholangiocarcinoma; SEER: Surveillance, Epidemiology, and End Results, CI: Confidence interval.
[a]$P < 0.05$.

(77.8%) and binary logistic (75.0%) models (Table 3). The three categorizing results had an overall agreement of 85.19%, and Mcnemer tests between each two models showed no statistical differences ($P = 1.000$).

DISCUSSION

CC was categorized as a type of GC in the latest AJCC[10] and UICC[11] manuals. However, our study argued with their practice, mainly based on two statistical

Table 3 Three models to differentiate between gallbladder cancer and extrahepatic cholangiocarcinoma, and categorize cystic duct cancer cases

	Fisher's linear discriminant	Binary logistic	ANN
	Coefficient in structure matrix	*P* value	Normalized importance (%)
Variable			
Sex	0.479[b]	< 0.001[a]	26.1
Age at diagnosis	-0.091	< 0.001[a]	44.1
Year of diagnosis	0.018	0.508	12.4
Martial status	0.164	0.088	7.1
Race	-0.011	0.426	22
Tumor size	-0.215	< 0.001[a]	71.8[c]
SEER historical stage	0.665[b]	< 0.001[a]	80.4[c]
Surgical procedure	-0.238[b]	< 0.001[a]	100.0[c]
Region	0.011	0.315	25.9
Histology	0.221	< 0.001[a]	26.6
Model performance			
Accuracy (%)			
Training sample (n = 5743)	70.1	72.7	82.2
Testing sample (n = 2430)	69.3	73.6	81.9
Whole (n = 8173)	69.9	73.0	82.1
AUROC (95% CI)	0.781 (0.771-0.791)	0.785 (0.775-0.795)	0.902 (0.895-0.908)
Categorization in CC cases			
Categorized as GC (%)	8 (22.2)	9 (25.0)	8 (22.2)
Categorized as EC (%)	28 (77.8)	27 (75.0)	28 (77.8)

[a]$P < 0.05$;
[b]Top 3 variables with the highest absolute values in the Fisher's linear discriminant model;
[c]The most important three variables in the artificial neuron network mode. ANN: Artificial neuron network; SEER: Surveillance, Epidemiology, and End Results; AUROC: Area under the receiver operating characteristic curve; CI: Confidence interval; CC: Cystic duct cancer; GC: Gallbladder cancer; EC: Extrahepatic cholangiocarcinoma.

findings: (1) Compared with the staging system of GC, the T staging system of perihilar cholangiocarcinoma (a type of EC) better discriminated the prognosis of CC. Unlike the staging system of lymphatic or distant metastasis (N or M), the T staging system was obviously different in EC and GC. That is, a lesion of GC would be staged as T3-4 when it involved the serosa of the biliary wall, while a lesion of EC would not be staged as T3-4 only when it invaded the portal vein, artery, or the second-order biliary system[10,11]. In this study, when the GC staging system was used, no prognostic differences were observed between the T1-2 and T3-4 groups. However, the difference was of statistical significance when the EC system was used ($P < 0.05$); and (2) The majority of CC cases (75.0%-77.8%) were categorized as EC by using the three taxonomic models. The three models used, including the Fisher's discriminant, binary logistics and ANN models, were constructed based on big data of over 8000 biliary cancer cases. Based on the AUROC, all models had "good" categorizing power, and the ANN model even had a value of over 0.90.

To our knowledge, this study provided the first population-level evidence for the categorizing problem of CC. In the 6th AJCC manual, CC was included in the EC chapter, but was classified as a type of GC since the 7th edition[17]. This practice was agreed by a recent single-center study by Nakanishi *et al*[18]. However, in that study, the definition of CC seemed to be not strict, because the incidence of CC was too high and even exceeded that of GC (47 *vs* 43) during the follow-up period. Besides, a large proportion of cases were at very advanced stage (with invasion to the duodenum, artery or portal vein), possibly attributed to the fact that some GC cases were misjudged as CC due to difficulty in detecting primary lesions.

Interestingly, in previous publications, there were also some clues to suggest the difference between CC and ordinary GC. In the study of Nishio[19], "GC cases" with common bile duct invasion (most of which were CC) had a favorable 5-year survival rate of over 20%, which was much better than the commonly expected prognosis in T3 stage GC cases. In the study of Ozden[20], "GC cases" with their lesion centers located in the cystic ducts (actually CC) had some unique clinical features, including their

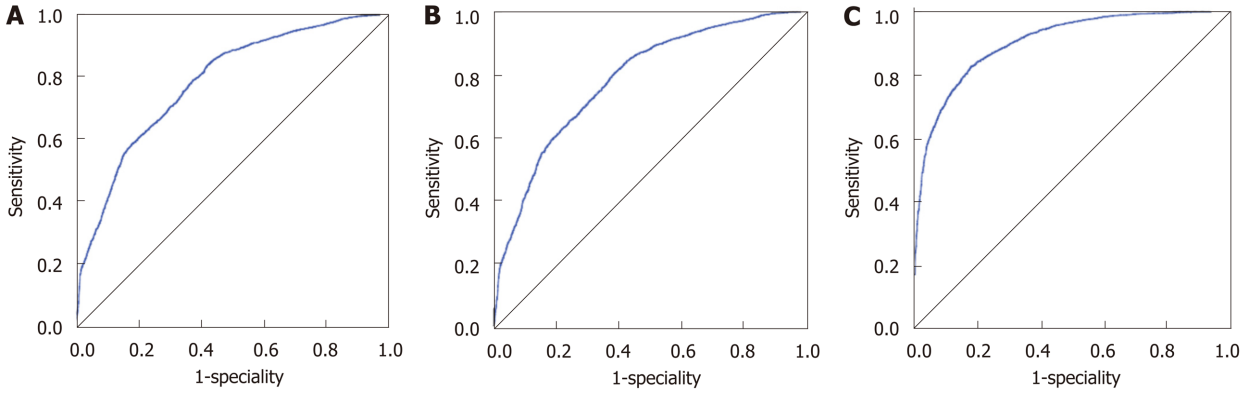

Figure 2 Receiver operating characteristic curves to discriminate between gallbladder cancer and extrahepatic cholangiocarcinoma. A: Fisher's linear discriminant model; B: Binary logistic model; C: ANN model.

approximately equal proportion of sex, advanced T stage, and a lower than expected frequency of lymph node metastasis, which more resembled EC.

However, the surgical attitude for EC and GC was different in clinical practice. EC (especially for perihiliar cholangiocarcinoma) was considered as being worthy of extensive resection even at the expense of increased complication rates (biliary fistula, *etc*.), since a successful R0 resection could drastically improve long-term prognosis[21], and transplantation could be considered in well-selected patients[22]. Comparatively, in advanced GC cases, aggressive surgical resection did not show concrete survival benefits, including combined common bile duct resection[23] and extended regional lymphadenectomy[24]. According to a recent United States population-level study[25], extended resection alone in GC provided a worse prognosis than simple removal of the gallbladder plus adjuvant chemotherapy. The similarity between CC and EC suggested the rationality that CC should not be treated like GC. In other words, extended surgical resection could be attempted in CC even at advanced stage, to see whether this treatment could immensely improve the prognosis like the situation in EC.

There are several limitations to this study. First, the variable of lymphatic status was not analyzed. In the SEER database, most of biliary cases had their lymphatic status unknown, and few cases had their harvested lymph nodes more than three, which was the minimum number to accurately evaluate lymphatic metastasis[26]. Therefore, although the pattern of lymphatic metastasis was different among CC, GC and EC[20,27,28], inclusion of this variable had modest value to increase performance of models. Second, whole genome sequencing also could help to clarify the categorization of CC. However, due to the extreme rarity of CC specimens, this molecular evidence is currently not available.

CONCLUSION

In conclusion, our study argued with categorization of CC in the current AJCC and UICC manuals, and suggested that CC should be categorized as a type of EC. Extended surgical resection might be considered in CC cases, to see whether long-term prognosis could be immensely improved like the situation in EC.

ARTICLE HIGHLIGHTS

Research background

According to the current guidelines, cystic duct cancer (CC) is categorized as a type of gallbladder cancer (GC), which has the worst prognosis among all types of biliary cancers.

Research motivation

In previous studies, no direct epidemiological evidence verified that CC was more similar to GC, rather than extrahepatic cholangiocarcinoma (EC).

Research objectives

This study aimed to investigate the categorization of CC based on population-level data.

Research methods

We used three taxonomic methods for analysis, including Fisher's discriminant, binary logistics and artificial neuron network models.

Research results

The T staging system of perihilar cholangiocarcinoma (a type of EC) better discriminated CC prognosis than that of GC. By using the three taxonomic models, the majority (75.0%-77.8%) of CC cases were categorized as EC.

Research conclusions

Our study suggested that CC should be categorized as a type of EC, not GC.

Research perspectives

Aggressive surgical attitude might be considered in CC cases, to see whether long-term prognosis could be immensely improved like the situation in EC. Future studies with larger sample size are needed.

REFERENCES

1 **Stewart HL**, Lieber MM, Morgan DR. Carcinoma of extrahepatic bile ducts. *Arch Surg* 1940; **41**: 662-713 [DOI: 10.1001/archsurg.1940.01210030096008]
2 **FARRAR DA**. Carcinoma of the cystic duct. *Br J Surg* 1951; **39**: 183-185 [PMID: 14886607 DOI: 10.1002/bjs.18003915414]
3 **Phillips SJ**, Estrin J. Primary adenocarcinoma in a cystic duct stump. Report of a case and review of the literature. *Arch Surg* 1969; **98**: 225-227 [PMID: 5765677 DOI: 10.1001/archsurg.1969.01340080117026]
4 **Eum JS**, Kim GH, Park CH, Kang DH, Song GA. A remnant cystic duct cancer presenting as a duodenal submucosal tumor. *Gastrointest Endosc* 2008; **67**: 975-6; discussion 976 [PMID: 18291386 DOI: 10.1016/j.gie.2007.11.010]
5 **Maeda T**, Natsume S, Kato T, Hiramatsu K, Aoba T, Matsubara H. Early cystic duct cancer with widely spreading carcinoma in situ in the gallbladder: A case report. *Jjba* 2015; **29**: 261-265 [DOI: 10.11210/tando.29.261]
6 **Komori S**, Tsuchiya J, Kumazawa I, Kawagoe H, Nishio K, Misao Y. Preoperative diagnosis of an asymptomatic cancer restricted to the cystic duct. *Int J Surg Case Rep* 2014; **5**: 354-357 [PMID: 24858978 DOI: 10.1016/j.ijscr.2014.04.022]
7 **Bains L**, Kaur D, Kakar AK, Batish A, Rao S. Primary carcinoma of the cystic duct: a case report and review of classifications. *World J Surg Oncol* 2017; **15**: 30 [PMID: 28103928 DOI: 10.1186/s12957-016-1073-4]
8 **Chan KM**, Yeh TS, Tseng JH, Liu NJ, Jan YY, Chen MF. Clinicopathological analysis of cystic duct carcinoma. *Hepatogastroenterology* 2005; **52**: 691-694 [PMID: 15966184]
9 **Kubota K**, Kakuta Y, Inayama Y, Yoneda M, Abe Y, Inamori M, Kirikoshi H, Saito S, Nakajima A, Sugimori K, Matuo K, Kazunaga T, Shimada H. Clinicopathologic study of resected cases of primary carcinoma of the cystic duct. *Hepatogastroenterology* 2008; **55**: 1174-1178 [PMID: 18795652]
10 **Amin MB**, Edge SB, Greene FL, Byrd DR, Brookland RK, Washington MK, Gershenwald JE, Compton CC, Hess KR, Sullivan DC, Jessup JM, Brierley JD, Gaspar LE, Schilsky RL, Balch CM, Winchester DP, Asare EA, Madera M, Gress DM, Meyer LR. AJCC Cancer Staging Manual. 8th ed. Springer International Publishing. 2018; 303
11 **O'Sullivan B**, Brierley JD, D'Cruz AK, Fey MF, Pollock R, Vermorken JB, Shao HH. UICC Manual of Clinical Oncology. 9th ed. Wiley-Blackwell. 2015; 267
12 **Yamaguchi K**, Nishihara K, Tsuneyoshi M. Carcinoma of the cystic duct. *J Surg Oncol* 1991; **48**: 282-286 [PMID: 1745055 DOI: 10.1002/jso.2930480413]
13 **Chijiiwa K**, Torisu M. Primary carcinoma of the cystic duct. *J Clin Gastroenterol* 1993; **16**: 309-313 [PMID: 8331264 DOI: 10.1097/00004836-199306000-00008]
14 **Fisher RA**. THE USE OF MULTIPLE MEASUREMENTS IN TAXONOMIC PROBLEMS. *Annals of Human Genetics* 1936; **7**: 179-188 [DOI: 10.1111/j.1469-1809.1936.tb02137.x]
15 SEER Program Coding and Staging Manual 2016. Available from: https://seer.cancer.gov/manuals/2016/AppendixC/Surgery_Codes_Other_Sites_2016.pdf
16 Online Kappa Calculator. Available from: http://justusrandolph.net/kappa/
17 Collaborative Stage Data Set (Cystic Duct C240). Available from: http://web2.facs.org/cstage0205/cystic-duct/CysticDuctschema.html
18 **Nakanishi Y**, Tsuchikawa T, Okamura K, Nakamura T, Noji T, Asano T, Tanaka K, Shichinohe T, Mitsuhashi T, Hirano S. Clinicopathological features and prognosis of advanced biliary carcinoma centered in the cystic duct. *HPB (Oxford)* 2018; **20**: 28-33 [PMID: 28890312 DOI: 10.1016/j.hpb.2017.08.014]
19 **Nishio H**, Ebata T, Yokoyama Y, Igami T, Sugawara G, Nagino M. Gallbladder cancer involving the extrahepatic bile duct is worthy of resection. *Ann Surg* 2011; **253**: 953-960 [PMID: 21490453 DOI: 10.1097/SLA.0b013e318216f5f3]
20 **Ozden I**, Kamiya J, Nagino M, Uesaka K, Oda K, Sano T, Kamiya S, Nimura Y. Cystic duct carcinoma: a proposal for a new "working definition". *Langenbecks Arch Surg* 2003; **387**: 337-342 [PMID: 12536328 DOI: 10.1007/s00423-002-0333-7]
21 **Ribero D**, Amisano M, Lo Tesoriere R, Rosso S, Ferrero A, Capussotti L. Additional resection of an intraoperative margin-positive proximal bile duct improves survival in patients with hilar cholangiocarcinoma. *Ann Surg* 2011; **254**: 776-81; discussion 781-3 [PMID: 22042470 DOI: 10.1097/SLA.0b013e3182368f85]
22 **Ethun CG**, Lopez-Aguiar AG, Anderson DJ, Adams AB, Fields RC, Doyle MB, Chapman WC, Krasnick BA, Weber SM, Mezrich JD, Salem A, Pawlik TM, Poultsides G, Tran TB, Idrees K, Isom CA, Martin RCG, Scoggins CR, Shen P, Mogal HD, Schmidt C, Beal E, Hatzaras I, Shenoy R, Cardona K, Maithel SK. Transplantation Versus Resection for Hilar Cholangiocarcinoma: An Argument for Shifting Treatment Paradigms for Resectable Disease. *Ann Surg* 2018; **267**: 797-805 [PMID: 29064885 DOI:

10.1097/SLA.0000000000002574]
23 **Lim JH**, Chong JU, Kim SH, Park SW, Choi JS, Lee WJ, Kim KS. Role of common bile duct resection in T2 and T3 gallbladder cancer patients. *Ann Hepatobiliary Pancreat Surg* 2018; **22**: 42-51 [PMID: 29536055 DOI: 10.14701/ahbps.2018.22.1.42]
24 **Niu GC**, Shen CM, Cui W, Li Q. Surgical treatment of advanced gallbladder cancer. *Am J Clin Oncol* 2015; **38**: 5-10 [PMID: 25616200 DOI: 10.1097/COC.0b013e318287bb48]
25 **Kasumova GG**, Tabatabaie O, Najarian RM, Callery MP, Ng SC, Bullock AJ, Fisher RA, Tseng JF. Surgical Management of Gallbladder Cancer: Simple Versus Extended Cholecystectomy and the Role of Adjuvant Therapy. *Ann Surg* 2017; **266**: 625-631 [PMID: 28692469 DOI: 10.1097/SLA.0000000000002385]
26 **Jensen EH**, Abraham A, Jarosek S, Habermann EB, Al-Refaie WB, Vickers SA, Virnig BA, Tuttle TM. Lymph node evaluation is associated with improved survival after surgery for early stage gallbladder cancer. *Surgery* 2009; **146**: 706-711; discussion 711-713 [PMID: 19789030 DOI: 10.1016/j.surg.2009.06.056]
27 **Kayahara M**, Nagakawa T, Ueno K, Ohta T, Takeda T, Miyazaki I. Lymphatic flow in carcinoma of the distal bile duct based on a clinicopathologic study. *Cancer* 1993; **72**: 2112-2117 [PMID: 8374870 DOI: 10.1002/1097-0142(19931001)72:7<2112::AID-CNCR2820720709>3.0.CO;2-X]
28 **Tsukada K**, Kurosaki I, Uchida K, Shirai Y, Oohashi Y, Yokoyama N, Watanabe H, Hatakeyama K. Lymph node spread from carcinoma of the gallbladder. *Cancer* 1997; **80**: 661-667 [PMID: 9264348 DOI: 10.1002/(SICI)1097-0142(19970815)80:4<661:AID-CNCR3>3.0.CO;2-Q]

World Journal of Gastroenterology

Submit a Manuscript: https://www.f6publishing.com

World J Gastroenterol 2019 November 28; 25(44): 6551-6560

DOI: 10.3748/wjg.v25.i44.6551

ISSN 1007-9327 (print) ISSN 2219-2840 (online)

ORIGINAL ARTICLE

Observational Study

Real life efficacy and safety of direct-acting antiviral therapy for treatment of patients infected with hepatitis C virus genotypes 1, 2 and 3 in northwest China

Ying Yang, Feng-Ping Wu, Wen-Jun Wang, Juan-Juan Shi, Ya-Ping Li, Xin Zhang, Shuang-Suo Dang

ORCID number: Ying Yang (0000-0002-8718-0993); Feng-Ping Wu (0000-0002-4572-3873); Wen-Jun Wang (0000-0001-9861-1763); Juan-Juan Shi (0000-0002-5626-9821); Ya-Ping Li (0000-0002-0900-5559); Xin Zhang (0000-0002-5966-0471); Shuang-Suo Dang (0000-0003-0918-9535).

Author contributions: Yang Y, Wu FP, Shi JJ, Li YP and Zhang X collected the data; Yang Y analyzed the data and wrote the paper; Dang SS and Wang WJ reviewed the manuscript; all authors read and approved the manuscript.

Institutional review board statement: This study was approved by the Institutional Review Board of Xi'an Jiaotong University.

Informed consent statement: All study participants, or their legal guardian, provided written informed consent prior to study enrollment.

Conflict-of-interest statement: The authors do not have any conflict of interest to disclose.

Data sharing statement: No additional data are available.

STROBE statement: The authors have read the STROBE Statement-checklist of items and the manuscript was prepared and revised accordingly.

Ying Yang, Feng-Ping Wu, Wen-Jun Wang, Juan-Juan Shi, Ya-Ping Li, Xin Zhang, Shuang-Suo Dang, Department of Infectious Diseases, the Second Affiliated Hospital of Xi'an Jiaotong University, Xi'an 710004, Shaanxi Province, China

Corresponding author: Shuang-Suo Dang, MD, PhD, Academic Fellow, Academic Research, Doctor, Professor, Department of Infectious Diseases, the Second Affiliated Hospital of Xi'an Jiaotong University, 157 Xiwu Road, Xincheng District, Xi'an 710004, Shaanxi Province, China. dangshuangsuo123@xjtu.edu.cn
Telephone: +86-29-87679688

Abstract

BACKGROUND

Regimens involving direct-acting antiviral agents (DAAs) are recommended for the treatment of infection with hepatitis C virus (HCV) genotypes 1, 2 and 3. But real-world data is still not enough, especially in Asia.

AIM

To investigate the efficacy and safety of DAA-based regimens in a real-life setting in China.

METHODS

This study included 366 patients infected with HCV genotypes 1, 2 and 3, with or without cirrhosis, who were observed between May 2015 and December 2018. They were treated with ledipasvir and sofosbuvir (SOF) (genotype 1) with or without ribavirin (RBV), SOF and RBV (genotype 2), or SOF and daclatasvir (genotype 3), with or without RBV, for 12 or more wk. The participants' sustained virological responses (SVR) at post-treatment week 12 (SVR12) was the primary endpoint. The occurrence of adverse events and drug-drug interactions were recorded.

RESULTS

In the 366 patients, genotype 1 (59.0%) was the most common genotype, followed by genotypes 2 (34.4%) and 3 (6.6%). Liver cirrhosis was diagnosed in 154 (42.1%) patients. Fifty (13.7%) patients were treatment-experienced. Intention-to-treat analysis revealed that SVR12 was 86.3% (316/366). For modified intention-to-treat analysis, SVR12 was achieved in 96.6% of overall patients (316/327), 96.3% in patients with genotype 1, 97.5% in those with genotype 2, and 95.0% in those with genotype 3. Most of the treatment failures were due to lack of follow-up (3

Manuscript source: Unsolicited manuscript

Received: September 6, 2019
Peer-review started: September 6, 2019
First decision: October 14, 2019
Revised: November 8, 2019
Accepted: November 13, 2019
Article in press: November 13, 2019
Published online: November 28, 2019

P-Reviewer: Johansen S, Kanda T, Koshy A, Rukavina M
S-Editor: Tang JZ
L-Editor: Wang TQ
E-Editor: Zhang YL

cases had non-responses, 1 had virological breakthrough, 11 relapsed and 36 did not participate in the follow-up). There was no significant difference in SVR between different genotypes and liver statuses ($P < 0.05$). Patients with lower alanine aminotransferase levels at baseline who achieved an end of treatment response were more likely to achieve SVR12 ($P < 0.05$). High SVR was observed regardless of age, gender, liver status, alpha-fetoprotein, HCV RNA levels or history of antiviral therapy ($P > 0.05$ for all). The cumulative hepatocellular carcinoma occurrence and recurrence rate after using the DAAs was 0.9%. Most of the adverse events were mild. We found two cases of special adverse events. One case involved facial and bilateral lower extremity edema, and the other case showed an interesting change in lipid levels while on medication. No severe adverse events were noted.

CONCLUSION
The DAA-based regimens tested in this study have excellent effectiveness and safety in all patients infected with HCV genotypes 1, 2 and 3, including those with cirrhosis.

Key words: Hepatitis C virus; Direct-acting antiviral agents; Efficacy; Safety; Drug-drug interactions; Real-life experience

Core tip: Direct-acting antiviral agent (DAA)-based regimens are currently the preferred treatment for hepatitis C. However, there is not enough data reporting the results of real-world research, especially in countries such as China where DAAs have only been approved for using in recent years. We found that there was no significant difference in sustained virological responses (SVR) between patients with different genotypes and liver statuses. Patients with lower alanine aminotransferase levels at baseline who achieved end of treatment response were more likely to achieve SVR at post-treatment week 12. Also, we found two cases of special adverse events. One case involved facial and bilateral lower extremity edema, which was due to drug-drug interactions, and the other case showed an interesting change in lipid levels while the patient was on medication.

Citation: Yang Y, Wu FP, Wang WJ, Shi JJ, Li YP, Zhang X, Dang SS. Real life efficacy and safety of direct-acting antiviral therapy for treatment of patients infected with hepatitis C virus genotypes 1, 2 and 3 in northwest China. *World J Gastroenterol* 2019; 25(44): 6551-6560
URL: https://www.wjgnet.com/1007-9327/full/v25/i44/6551.htm
DOI: https://dx.doi.org/10.3748/wjg.v25.i44.6551

INTRODUCTION

Hepatitis C virus (HCV) has infected approximately 3% of the world's population[1-3], and 70% to 80% of patients have chronic hepatitis. The leading cause of liver cirrhosis and hepatocellular carcinoma (HCC) is hepatitis. No effective vaccine to prevent hepatitis C is currently available[4-6]. Thus, the treatment of hepatitis C is particularly important. There are several HCV genotypes, including 1a, 1b, 1c, 2a, 2b, 2c, 3a, 3b, 4, 5 and 6, which correspond to the number of HCV gene sequences, of which genotypes 1, 2 and 3 are the most common types[7-10]. Clinical care has advanced for patients with HCV-related liver disease in recent years. But, in some countries, such as China, the standard care has been a combination therapy using pegylated interferon and ribavirin (RBV). However, this treatment has shown a low rate of effectiveness. Due to severe adverse reactions and harsh indications, many patients cannot tolerate this treatment. Since the advent of direct-acting antiviral drugs (DAAs) in 2011, the landscape of HCV treatment has changed remarkably. These oral combinations make it possible to achieve exceptional cure rates with better tolerability, minimal side effects and a shorter duration of treatment.

Among the NS5B polymerase nucleoside inhibitors, sofosbuvir (SOF) is a potent

pan-genotypic inhibitor. Many clinical trials based on SOF have shown high rates of sustained virological response (SVR). A phase 3, randomized, open-label study involving patients infected with HCV genotype 1 with or without cirrhosis achieved SVR rates between 94% and 99% with SOF and ledipasvir[11]. Among patients infected with HCV genotype 2, the VALENCE trial reported that therapy with SOF-RBV for 12 wk resulted in a high rate of SVR (93%)[12]. One year later, another phase III trial, ASTRAL-3, reported a higher rate of SVR (99%) using a regimen of SOF-velpatasvir (VEL)[13]. In patients infected with genotype 3, the ALLY-3 trial showed that patients treated with a regimen of daclatasvir and SOF achieved SVR rates of 63% and 96%, with and without cirrhosis, respectively[14].

Although high rates of SVR have been shown, results derived from controlled settings may not be representative to the real world. Also, data gathered from different races is insufficient. Therefore, evaluations of drugs in real-world settings are critical, especially in patients such as those from northwest China, where clinical trial data is limited.

MATERIALS AND METHODS

Our study was a single center, prospective, observational study. Prospective patients were identified by a search of the clinical records at the Department of Infectious Diseases of the Second Affiliated Hospital of Xi'an Jiaotong University, in order to evaluate the treatment outcomes in a real-world cohort of patients infected with HCV genotypes 1, 2 and 3 who were evaluated between May 2015 and December 2018.

Patients and treatment

All the patients who had been diagnosed as having a chronic HCV infection (positive anti-HCV antibodyfor greater thansix months with detectable HCV RNA), with or without cirrhosis, including those who were treatment naïve or had previously been exposed to interferon or direct-acting antiviral therapy, were included in our study. Patients who had co-infections with hepatitis B virus (HBV) were also included. Patients meeting the following criteria were excluded: Human immunodeficiency virus co-infection, pregnant and lactating female patients, male patients with fertility willingness, patients under the age of 18, those with chronic kidney disease, and those with advanced liver disease (Child-Pugh C). All the patients clearly understood the potential benefits and risks and were willing to receive antiviral treatment. All the patients voluntarily joined this study after giving informed consent.

The treatment regimens used are in accordance with the European Association of Study of the Liver guidelines (2015) and are summarized in Table 1. Before the treatment, the patients were informed about the potential drug-drug interactions (DDIs) and were advised to consult pharmacists before starting any new treatment.

Measurements

Each patient's detailed medical history was recorded. Clinical examinations were performed on all patients. Baseline laboratory values were collected in all patients within 3 mo before starting treatment. The following data were recorded at the time of enrollment: Age, gender, fibrosis stage, history of treatment, anti-HCV antibody (ELISCAN HCV; RFCL Limited, Dehradun, India), genotype (Abbott Molecular Inc., Des Plaines, IL, United States), and any comorbidities, such as diabetes, HBV co-infection, hypertension and fatty liver disease. The baseline clinical chemistry results are shown in Table 2. HCV RNA was analyzed using COBAS TaqMan HCV Test 2.0 (Roche Diagnostics Corporation, Indianapolis, IN, United States). FibroScan transabdominal ultrasound and abdominal computerized tomography were also performed on the patients. Liver stiffness value > 12.5 kPa (FibroScan®, Echosens, France), clinical manifestations such as esophageal varices and ascites or distinct sonographic signs of portal hypertension indicated cirrhosis.

This study was approved by the Institutional Review Board of Xi'an Jiaotong University.

Efficacy assessment

HCV RNA was monitored at 4 wk [rapid virological response (RVR)], the end of therapy [end of treatment response (ETR)] and 12 wk after the treatment (SVR12). Viral relapse was defined as detectable HCV RNA after treatment. Non-response was defined as failure to achieve a 1 log 10 reduction in HCV RNA after 12 wk of treatment. Viral breakthrough was defined as detectable HCV RNA after a period of initial response while still on therapy.

Safety assessments

Table 1 Regimens of direct-acting antivirals for treatment of hepatitis C virus infection

Patients		Genotype 1	Genotype 2	Genotype 3
Chronic hepatitis	Treatment naïve	SOF + LDV for 12 wk	SOF + RBV for 12 wk	SOF + DCV for 12 wk
	Treatment experienced		SOF + RBV for 16-20 wk	SOF + DCV + RBV for 12 wk or 24 wk without RBV
Cirrhosis, compensated or decompensated		SOF + LDV + RBV for 12 wk or 24 wk without RBV	SOF + RBV for 16-20 wk	SOF + DCV + RBV for 24 wk

A fixed dose combination of sofosbuvir (SOF) and ledipasvir was administered once per day. One tablet each of SOF and daclatasvir should be taken daily. Ribavirin was 1000 or 1200 mg/d in patients < 75 kg or ≥ 75 kg, respectively. SOF: Sofosbuvir (400 mg); LDV: Ledipasvir (90 mg); DCV: Daclatasvir (60 mg); RBV: Ribavirin (200 mg).

All the patients were assessed for adverse reactions, including severe fatigue, depression, insomnia, skin reactions, and dyspnea. Adverse hematological reactions included neutropenia and anemia. If hypocytosis occurred, routine bloodwork would be examined more frequently. When hemoglobin was < 100 g/L or ≥ 85 g/L with no significant cardiovascular disease, the following steps were taken: During the subsequent 4 wk of treatment, if hemoglobin decreased by ≥ 20 g/L, RBV was reduced to 600 mg/d (200 mg in the morning and 400 mg at night), and if hemoglobin decreased to 85 g/L or remained below 120 g/L after 4 wk of RBV reduction, RBV was discontinued.

Statistical analysis

The statistical methods of this study were reviewed by Lei-Lei Pei from Institute of Public Health Xi'an Jiaotong University.

For continuous variables, the outcome is expressed as the mean ± standard deviation or as median and range. It was compared using the Kruskal-Wallis *H* test or the Mann-Whitney *U* test. For categorical data, the outcome is presented as percentage, and the differences were tested using the χ^2 test. Logistic regression was used to analyze which variables had a statistical impact on SVR. SVR12 was evaluated by an intention-to-treat (ITT) analysis, which was based on the initial treatment assignment, including all patients who received at least one dose of the medicine. SVR12 was also analyzed by a modified ITT (mITT) analysis. The significance level was set at $P < 2009;0.05$. All analyses were performed using SPSS 25.0 software.

RESULTS

Characteristics of patients

Between May 2015 and December 2018, a total of 498 patients were diagnosed with HCV infection, and 366 of them commenced treatment with DAAs (Figure 1). There were 216 patients with genotype 1 (1a, 10.2%; 1b, 68.5%; subtype not specified, 21.3%), 108 with genotype 2 (2a, 68.3%; 2b, 5.6%; subtype not specified, 26.2%) and 24 with genotype 3 (3a, 25.0%; 3b, 12.5%; subtype not specified, 62.5%). Of the patients, 12 (3.3%) were found to have controlled co-existing HCC. Table 2 shows the baseline characteristics of the patients. The mean age of the patients was 52.2 ± 12.0 years, and 192 (47.5%) were male. Fifty (13.7%) patients had been treated with interferon (IFN) or DAAs before. Some of the patients (154, 42.1%) had cirrhosis. Most of the cirrhotic patients (123, 79.9%) had a Child-Pugh score of A, while the rest of them had a Child-Pugh score of B. A total of 25 (6.8%) of the patients had HBV co-infection, 17 (4.6%) had diabetes mellitus, 24 (6.6) had hypertension, and 52 (14.2%) had fatty liver disease.

The baseline clinical, biochemical, hematological and virologic characteristics of the patients based on the severity of their liver disease are shown in Table 3. Patients with cirrhosis (including compensated and decompensated cirrhosis) were older. They had higher levels of total bilirubin, alanine transaminase (ALT), aspartate aminotransferase (AST), alpha-fetoprotein (AFP), liver stiffness measurement (LSM) score, fibrosis 4 score, and AST-to-platelet ratio index (APRI). Patients with cirrhosis had lower levels of albumin, hemoglobin, platelets, and HCV RNA compared to patients without ($P < 0.05$ for all).

Efficacy of treatment

In our study, RVR was achieved in 321 (87.7%) of 366 patients, and ETR was achieved in 338 (98.5%) of 343 patients. ITT analysis showed that 316 (86.3%) patients reached

Table 2 Baseline characteristics of hepatitis C virus patients based on genotype

	Total (*n* = 366)	Genotype 1 (*n* = 216)	Genotype 2 (*n* = 126)	Genotype 3 (*n* = 24)
Age (yr)	52.2 ± 12.0	51.7 ± 12.8	53.6 ± 10.0	49.8 ± 14.1
Gender (males, %)	174 (47.5)	101 (46.8)	62 (49.2)	11 (45.8)
TBIL (μmol/L)	19.63 ± 10.60	19.62 ± 10.77	19.52 ± 10.72	20.07 ± 8.47
ALT (U/L)	53.48 ± 45.18	56.95 ± 47.79	51.55 ± 40.35	54.33 ± 36.91
AST (U/L)	51.89 ± 39.12	50.79 ± 41.96	48.9 ± 33.74	53.5 ± 33.31
Albumin (g/L)	36.6 ± 8.6	38.9 ± 8.6	41.2 ± 8.5	36.6 ± 8.6
TCHO (mmol/L)	3.85 ± 0.60	3.81 ± 0.58	3.85 ± 0.66	4.14 ± 0.41
Hemoglobin (mg/dL)	120.3 ± 23.6	120.4 ± 23.3	121.2 ± 23.2	114.8 ± 27.9
Platelets (10^9/L)	147.7 ± 75.8	144.5 ± 74.8	155.7 ± 77.8	134.3 ± 73.6
AFP (ng/mL)	4.69 ± 5.79	5.01 ± 7.33	4.30 ± 2.02	3.81 ± 2.27
Treatment experienced, *n* (%)	50 (13.7)	26 (12.0)	20 (15.9)	4 (16.7)
Cirrhosis, *n* (%)	154 (42.1)	96 (43.5)	46 (36.5)	12 (50)
HBV/HCV co-infection, *n* (%)	25 (6.8)	12 (5.6)	9 (7.1)	4 (16.7)
Diabetes mellitus, *n* (%)	17 (4.6)	12 (5.6)	4 (3.2)	1 (4.2)
Hypertension, *n* (%)	24 (6.6)	16 (7.4)	8 (6.3)	0 (0)
Fatty liver disease, *n* (%)	52 (14.2)	31 (14.4)	16 (12.7)	5 (20.8)

TBil: Total bilirubin; ALT: Alanine aminotransferase; AST: Aspartate aminotransferase; TCHO: Total cholesterol; AFP: Alpha fetoprotein; HCV: Hepatitis C virus; HBV: Hepatitis B virus.

SVR12, accounting for 182 (84.3%) of 216 patients with genotype 1, 115 (91.3%) of 126 with genotype 2, and 19 (79.2%) of 24 with genotype 3 (P = 0.375). SVR (mITT analysis) was 96.3% in patients with genotype 1, 97.5% in those with genotype 2, and 95.0% in those with genotype 3. No statistically significant difference in SVR was found among patients with different genotypes (P = 0.759). In patients without cirrhosis (96.2%), SVR12 rates were similar to those of patients with cirrhosis (97.2%, P = 0.971). Of all the patients, a total of 51 (13.6%) failed to achieve SVR, most of which (n = 36) were due to loss to follow-up. In addition, 3 patients had non-responses, 1 had a viral breakthrough, and 11 relapsed. Patients with genotype 3 had more treatment failures (non-response in 1, and 1 had a relapse). After treatment, the patients' liver stiffness as determined by Fibroscan decreased by 0.64 ± 1.1, and patients with cirrhosis had an even more decrease (P = 0.023).

In the correlation analysis between the baseline characteristics and SVR (Table 4), we found that patients with lower ALT levels (P = 0.034) were more likely to achieve SVR12. However, there were no significant difference in age, gender, bilirubin, AST, albumin, cholesterol, hemoglobin, platelets, AFP, liver status, or HCV RNA levels (P > 0.05 for all). Additionally, patients who achieved ETR were more likely to achieve SVR12.

Safety and tolerability

A total of 114 (31.1%) patients reported that they had at least one adverse event, but no serious adverse reactions (SARs) occurred. Most of the adverse events were mild or moderate, such as fatigue (66, 18.0%), rash (25, 6.8%), anemia (16, 4.4%), and myocardial enzymes abnormality (7, 1.9%), which were mainly due to the use of RBV. The patients with cirrhosis tended to have more adverse reactions (P = 0.027). Twelve wk after the end of treatment, one patient had developed HCC, and two others had a recurrence of HCC. The cumulative HCC occurrence and recurrence rate after DAA treatment was 0.9%. The patient with newly discovered HCC also had cirrhosis and experienced treatment failure. These two cases of recurrence were in patients with cirrhosis and SVR.

We found two cases of special adverse events. In one case, a patient had had benign prostatic hyperplasia in addition to hepatitis C. His HCV viral load was 5.8 log IU/mL, and his genotype was 3b. After 24 h of co-administration with tamsulosin hydrochloride, edema occurred in his face and the patient also had bilateral lower extremity edema. The edema disappeared after he discontinued tamsulosin hydrochloride. We checked medicine specifications of tamsulosin hydrochloride and the DAA regimens but none of them mentioned edema in adverse reactions. So, we believed that his edema was due to DDIs between tamsulosin hydrochloride and DAAs. In the other case, we observed an interesting change in the serum lipids. A

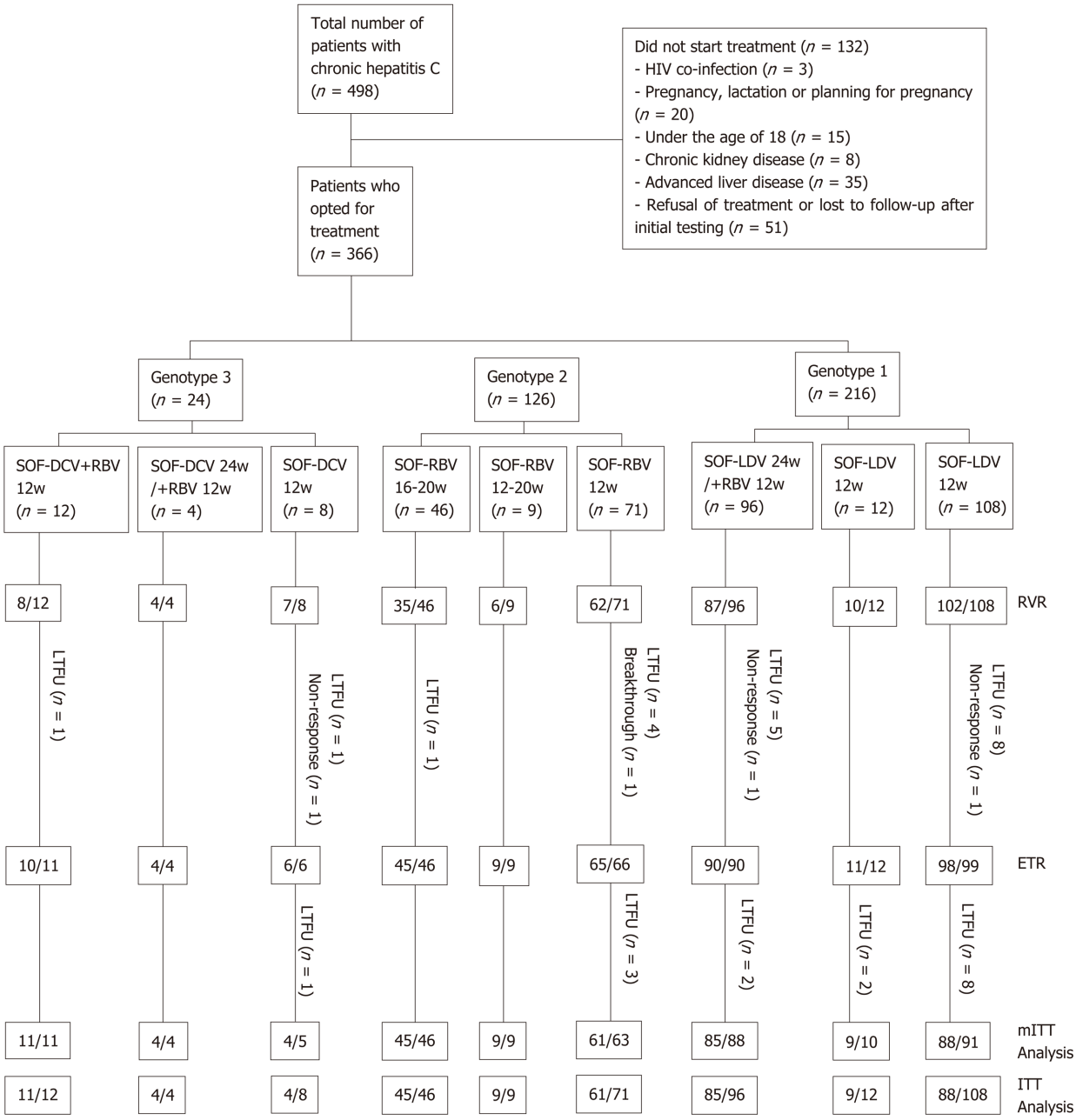

Figure 1 Treatment of chronic hepatitis C virus patients with direct-acting antiviral agents. RVR: Rapid virological response; ETR: End of treatment response; SVR12: Sustained virological response at post-treatment week 12; ITT: Intention-to-treat; mITT: Modified ITT; SOF: Sofosbuvir; LDV: Ledipasvir; RBV: Ribavirin; DCV: Daclatasvir; mITT: Modified intention-to-treat; LTFU: Lost to follow-up; HIV: Human immunodeficiency virus.

middle-aged man on stable methadone maintenance therapy took VEL/SOF for antiviral therapy. Before the new treatment started, his total cholesterol and triglyceride levels were basically normal. After starting antiviral treatment, his triglyceride level rose rapidly, and peaked 8 wk later. His cholesterol increased slowly and then decreased slowly. But 24 h after withdrawing from VEL/SOF, his triglyceride and total cholesterol levels were basically normal. There was no severe adverse reaction during his antiviral therapy. The viral load was still negative at the end of the treatment.

DISCUSSION

Chronic HCV infection is a global health problem. It can be associated with many several hepatic and extrahepatic disorders. Of patients with chronic infection, many develop cirrhosis and HCC. Before 2011, the standard antiviral therapy was pegylated interferon-alpha and RBV for 24–48 wk[15,16]. After a few years, unremitting research

Table 3 Baseline characteristics of hepatitis C virus patients based on severity of liver disease

	Non-cirrhosis (*n* = 212)	Cirrhosis (compensated and decompensated) (*n* = 154)	*P* value
Age (yr)	48.5 ± 12.6	57.3 ± 8.9	< 0.001
Gender (males, %)	115 (54.2)	77 (50.0)	0.423
TBil (μmol/L)	15.04 ± 8.78	25.95 ± 9.59	< 0.001
ALT (U/L)	41.74 ± 43.00	64.88 ± 44.81	0.029
AST (U/L)	31.47 ± 26.67	68.12 ± 43.44	0.034
Albumin (g/L)	44.5 ± 4.5	33.0 ± 8.6	< 0.001
TCHO (mmol/L)	3.86 ± 0.55	3.82 ± 0.66	0.349
Hemoglobin (mg/dL)	135.3 ± 10.6	99.5 ± 20.4	0.002
Platelets (10^9/L)	195.3 ± 59.8	86.1 ± 32.2	< 0.001
AFP (ng/mL)	4.04 ± 1.79	5.58 ± 8.61	0.045
Log10 HCV RNA (IU/mL)	6.6 ± 0.8	6.3 ± 1.3	0.040
LSM (kPa)	5.71 ± 1.7	10.26 ± 5.1	< 0.001
Fibrosis 4 score	1.43 ± 1.0	7.49 ± 6.0	< 0.001
APRI	1.06 ± 0.9	2.3 ± 1.5	< 0.001

TBil: Total bilirubin; ALT: Alanine aminotransferase; AST: Aspartate aminotransferase; TCHO: Total cholesterol; AFP: Alpha fetoprotein; LSM: Liver stiffness measurement; APRI: AST-to-platelet ratio index.

has led to the discovery of several DAAs that target several molecular targets. DAA-based regimens can greatly increase the efficacy and shorten the duration of HCV therapy. Since about 2015, DAAs have had access to the Chinese market, and Chinese patients with hepatitis C have been treated with legal DAA regimens. Since this is such a short amount of time, the real-world data on the use of DAA drugs in China has not been sufficient.

Our study is a large, prospective, real-world study evaluating the efficacy and safety of DAA-based regimens in patients infected with genotype 1, 2, and 3 observed from 2015 to 2018. In this study, a total of 498 patients were diagnosed with HCV infections, but only 366 (73.5%) of them received treatments. Most of the patients had genotypes 1 and 2, which basically reflects the prevalence of genotypes among HCV sufferers in China[17]. We noticed that in our study, patients with genotype 3 were younger than patients with genotypes 1 and 2, and patients with genotype 3 had a higher proportion of HBV/HCV co-infections, though this difference was not statistically significant. We discovered that genotype 3 was highly prevalent among intravenous drug users, who were younger and more likely to be associated with other blood-borne diseases. Also, we found that the patients with cirrhosis were older. Those patients had higher levels of total bilirubin, ALT, AST and AFP, LSM scores, fibrosis 4 scores and APRIs. They also had lower levels of albumin, hemoglobin, platelets and HCV RNA compared to the patients without cirrhosis, which is consistent with our clinical experiences.

Overall, the patients in our study achieved high rates of SVR12 (96.6%) on the mITT analysis, which are roughly identical to those observed in the phase III trials. The SVR rates were consistently high in all patients regardless of the regimens used. No statistically significant difference in SVR was found among patients with different genotypes and with different liver statuses. In addition, patients with cirrhosis (97.2%) responded similarly to those without cirrhosis (96.2%) 12 wk after the end of the treatment. Analysis of the changes of liver stiffness before and after treatment showed that the decrease of liver stiffness was significantly correlated with liver status. In patients with cirrhosis, LSM decreased even more compared to patients with chronic infections. However, it should be noted that we divided our patients into cirrhotic (compensated cirrhosis and decompensated cirrhosis) and non-cirrhotic groups (chronic hepatitis and liver fibrosis), then we made the comparison, which may lead to bias.

Interestingly, by analyzing the treatment failures, we found that the patients with genotype 3 were more likely to relapse. Although the total number is small (24 patients), the proportion of patients experiencing a relapse or no response was much higher than that of patients with the other genotypes. Other researchers have also found that genotype 3 patients had poorer clinical outcomes than patients with the other genotypes[18]. In our study, 12 patients had controlled co-existing HCC at baseline. After DAA antiviral therapy, one patient developed HCC, and two had HCC recurrence. The incidence of HCC was lower than that in the untreated patients[19-21].

Table 4 Baseline data for patients with and without sustained virological responses (by modified intention-to-treat analysis)

	Non-SVR12 (*n* = 11)	SVR12 (*n* = 315)	*P* value
Age (yr)	54.1 ± 13.5	51.8 ±11.9	0.098
Gender (males, %)	4 (36.4)	162 (51.4)3	0.080
TBil (μmol/L)	20.16 ± 10.13	19.58 ± 10.69	0.184
ALT (U/L)	62.45 ± 53.85	52.28 ± 46.14	0.034
AST (U/L)	42.73 ± 30.30	47.29 ± 39.74	0.516
Albumin (g/L)	37.7 ± 10.0	39.6 ± 8.6	0.214
TCHO (mmol/L)	3.93 ± 0.59	3.85 ± 0.60	0.879
Hemoglobin (mg/dL)	119.1 ± 15.0	119.5 ± 23.8	0.497
Platelets (10^9/L)	165.6 ± 68.4	144.9 ± 76.0	0.167
AFP (ng/mL)	5.03 ± 4.49	4.77 ± 6.15	0.407
Log10 HCV RNA (IU/mL)	6.5 ± 0.6	6.5 ± 1.0	0.450
Cirrhosis, *n* (%)	5 (45.5)	138 (43.8)	0.621
Treatment experienced, *n* (%)	1 (9.1)	49 (15.6)	0.052

TBil: Total bilirubin; ALT: Alanine aminotransferase; AST: Aspartate aminotransferase; TCHO: Total cholesterol; AFP: Alpha fetoprotein; HCV: Hepatitis C virus; SVR12: Sustained virological response at post-treatment week 12.

The patient with newly discovered HCC had cirrhosis and experienced treatment failure. These two cases of recurrence both had cirrhosis and SVR. These findings indicate that patients with cirrhosis and experience treatment failure are more likely to develop HCC. This is the same result as those obtained in other studies[22-24]. Therefore, when patients also have cirrhosis, especially those patients with treatment failure, we should pay more attention to their tumor markers and conduct regular imageological liver examinations.

Also, we found that the level of ALT at baseline was the only characteristic associated with SVR. Patients who had lower levels of ALT at baseline and achieved ETR were more likely to achieve SVR, which is consistent with other research[25]. We also found that SVR rates were independent of either liver status or baseline HCV viral load. Furthermore, whether patients had received antiviral therapy before had no influence on SVR. Hence, based on these findings, and regardless of liver status, HCV viral load and prior treatment experience, the appropriate DAA-based regimens and an adequate course of treatment can achieve satisfactory curative effects.

The safety of our study was quite satisfactory. Although 31.1% of patients experienced one or more adverse events, no SARs were observed. Also, most of the adverse events were mild or moderate, of which fatigue was the most common adverse event. Patients with liver cirrhosis or who were given RBV in their regimens should receive more attention because they are more likely to have adverse reactions. In our study, patients with complications such as hypertension were told to try to avoid taking drugs that have potential DDIs with DAAs. However, we observed two cases of special adverse events. One was facial and bilateral lower extremity edema, which was due to DDIs and the other was an interesting change in lipid levels while on DAA medication. No similar cases have been reported yet. These adverse events indicate that even now, real-world data on the use of DAA drugs is still needed and meaningful.

This study had a few limitations. It was a single center study and the number of genotype 3 patients was quite small. Some patients used Indian generics for antiviral therapy. The drug availabilities may also lead to bias. However, our study provided data from the real-life experience of using DAAs in northwest China, and confirmed their efficacy and safety, thus providing physicians with the data needed for potential positive treatment outcomes. The long-term efficacy and safety of DAAs need to be studied, but the short-term results are encouraging.

ARTICLE HIGHLIGHTS

Research background

Regimens involving direct-acting antiviral agents (DAAs) are recommended for the treatment of infection with hepatitis C virus (HCV) genotypes 1, 2 and 3. But real-world data is still not

enough, especially in Asia.

Research motivation
Although high rates of sustained virological responses (SVR) have been shown in trials, results derived from controlled settings may not be representative to the real world. Drugs may have many unexpected adverse events in clinical applications. Also, data gathered from different races is insufficient. Therefore, evaluations of drugs in real-world settings are critical, especially in patients such as those from northwest China, where clinical trial data is limited.

Research objectives
Our study aimed to investigate the efficacy and safety of DAA-based regimens in a Chinese real-life setting in China and find out whether there are any differences in different genotypes and liver statuses.

Research methods
This study included 366 patients infected with HCV genotypes 1, 2 and 3, with or without cirrhosis, who were observed between May 2015 and December 2018. They were treated with ledipasvir and sofosbuvir (SOF) (genotype 1) with or without ribavirin (RBV), SOF and RBV (genotype 2), or SOF and daclatasvir (genotype 3), with or without RBV, for 12 or more wk. The participants' SVR at post-treatment week 12 (SVR12) was the primary endpoint. The occurrence of adverse events and drug-drug interactions were recorded.

Research results
In the 366 patients, genotype 1 (59.0%) was the most common genotype, followed by genotypes 2 (34.4%) and 3 (6.6%). Liver cirrhosis was diagnosed in 154 (42.1%) patients. Fifty (13.7%) patients were treatment-experienced. Intention-to-treat analysis revealed that SVR12 was 86.3% (316/366). For modified intention-to-treat analysis, SVR12 was achieved in 96.6% of overall patients (316/327), 96.3% in patients with genotype 1, 97.5% in those with genotype 2, and 95.0% in those with genotype 3. Most of the treatment failures were due to lack of follow-up (3 cases had non-responses, 1 had virological breakthrough, 11 relapsed and 36 did not participate in the follow-up). There was no significant difference in SVR between different genotypes and liver statuses ($P < 0.05$). Patients with lower alanine aminotransferase levels at baseline who achieved an end of treatment response were more likely to achieve SVR12 ($P < 0.05$). High SVR was observed regardless of age, gender, liver status, alpha-fetoprotein, HCV RNA levels or history of antiviral therapy ($P > 0.05$ for all). The cumulative hepatocellular carcinoma occurrence and recurrence rate after using the DAAs was 0.9%. Most of the adverse events were mild. We found two cases of special adverse events. One case involved facial and bilateral lower extremity edema, and the other case showed an interesting change in lipid levels while on medication. No severe adverse events were noted.

Research conclusions
The DAA-based regimens tested in this study have excellent effectiveness and safety in all patients infected with HCV genotypes 1, 2 and 3, including those with cirrhosis. In clinical applications, there are indeed unexpected adverse events.

Research perspectives
The antiviral effect of DAAs is quite satisfying. However, in the clinic, many adverse events may occur due to combination with other medications and individual variation. Strict monitoring is required for clinical use of DAAs. Besides, the long-term efficacy and safety of DAAs need to be studied.

REFERENCES

1 **Spearman CW**, Dusheiko GM, Hellard M, Sonderup M. Hepatitis C. *Lancet* 2019; **394**: 1451-1466 [PMID: 31631857 DOI: 10.1016/S0140-6736(19)32320-7]
2 **Stepanova M**, Younossi ZM. Economic Burden of Hepatitis C Infection. *Clin Liver Dis* 2017; **21**: 579-594 [PMID: 28689595 DOI: 10.1016/j.cld.2017.03.012]
3 **Younossi ZM**. Hepatitis C Infection: A Systemic Disease. *Clin Liver Dis* 2017; **21**: 449-453 [PMID: 28689584 DOI: 10.1016/j.cld.2017.03.001]
4 **Ghasemi F**, Rostami S, Meshkat Z. Progress in the development of vaccines for hepatitis C virus infection. *World J Gastroenterol* 2015; **21**: 11984-12002 [PMID: 26576087 DOI: 10.3748/wjg.v21.i42.11984]
5 **Hesamizadeh K**, Sharafi H, Rezaee-Zavareh MS, Behnava B, Alavian SM. Next Steps Toward Eradication of Hepatitis C in the Era of Direct Acting Antivirals. *Hepat Mon* 2016; **16**: e37089 [PMID: 27275164 DOI: 10.5812/hepatmon.37089]
6 **Bukh J**. The history of hepatitis C virus (HCV): Basic research reveals unique features in phylogeny, evolution and the viral life cycle with new perspectives for epidemic control. *J Hepatol* 2016; **65**: S2-S21 [PMID: 27641985 DOI: 10.1016/j.jhep.2016.07.035]
7 **Petruzziello A**, Marigliano S, Loquercio G, Cozzolino A, Cacciapuoti C. Global epidemiology of hepatitis C virus infection: An up-date of the distribution and circulation of hepatitis C virus genotypes. *World J Gastroenterol* 2016; **22**: 7824-7840 [PMID: 27678366 DOI: 10.3748/wjg.v22.i34.7824]
8 **D'Ambrosio R**, Degasperi E, Colombo M, Aghemo A. Direct-acting antivirals: the endgame for hepatitis C? *Curr Opin Virol* 2017; **24**: 31-37 [PMID: 28419938 DOI: 10.1016/j.coviro.2017.03.017]
9 **Manns MP**, Buti M, Gane E, Pawlotsky JM, Razavi H, Terrault N, Younossi Z. Hepatitis C virus infection. *Nat Rev Dis Primers* 2017; **3**: 17006 [PMID: 28252637 DOI: 10.1038/nrdp.2017.6]

10 **Polaris Observatory HCV Collaborators**. Global prevalence and genotype distribution of hepatitis C virus infection in 2015: a modelling study. *Lancet Gastroenterol Hepatol* 2017; **2**: 161-176 [PMID: 28404132 DOI: 10.1016/S2468-1253(16)30181-9]

11 **Afdhal N**, Reddy KR, Nelson DR, Lawitz E, Gordon SC, Schiff E, Nahass R, Ghalib R, Gitlin N, Herring R, Lalezari J, Younes ZH, Pockros PJ, Di Bisceglie AM, Arora S, Subramanian GM, Zhu Y, Dvory-Sobol H, Yang JC, Pang PS, Symonds WT, McHutchison JG, Muir AJ, Sulkowski M, Kwo P; ION-2 Investigators. Ledipasvir and sofosbuvir for previously treated HCV genotype 1 infection. *N Engl J Med* 2014; **370**: 1483-1493 [PMID: 24725238 DOI: 10.1056/NEJMoa1316366]

12 **Zeuzem S**, Dusheiko GM, Salupere R, Mangia A, Flisiak R, Hyland RH, Illeperuma A, Svarovskaia E, Brainard DM, Symonds WT, Subramanian GM, McHutchison JG, Weiland O, Reesink HW, Ferenci P, Hézode C, Esteban R; VALENCE Investigators. Sofosbuvir and ribavirin in HCV genotypes 2 and 3. *N Engl J Med* 2014; **370**: 1993-2001 [PMID: 24795201 DOI: 10.1056/NEJMoa1316145]

13 **Foster GR**, Afdhal N, Roberts SK, Bräu N, Gane EJ, Pianko S, Lawitz E, Thompson A, Shiffman ML, Cooper C, Towner WJ, Conway B, Ruane P, Bourlière M, Asselah T, Berg T, Zeuzem S, Rosenberg W, Agarwal K, Stedman CA, Mo H, Dvory-Sobol H, Han L, Wang J, McNally J, Osinusi A, Brainard DM, McHutchison JG, Mazzotta F, Tran TT, Gordon SC, Patel K, Reau N, Mangia A, Sulkowski M; ASTRAL-2 Investigators; ASTRAL-3 Investigators. Sofosbuvir and Velpatasvir for HCV Genotype 2 and 3 Infection. *N Engl J Med* 2015; **373**: 2608-2617 [PMID: 26575258 DOI: 10.1056/NEJMoa1512612]

14 **Nelson DR**, Cooper JN, Lalezari JP, Lawitz E, Pockros PJ, Gitlin N, Freilich BF, Younes ZH, Harlan W, Ghalib R, Oguchi G, Thuluvath PJ, Ortiz-Lasanta G, Rabinovitz M, Bernstein D, Bennett M, Hawkins T, Ravendhran N, Sheikh AM, Varunok P, Kowdley KV, Hennicken D, McPhee F, Rana K, Hughes EA; ALLY-3 Study Team. All-oral 12-week treatment with daclatasvir plus sofosbuvir in patients with hepatitis C virus genotype 3 infection: ALLY-3 phase III study. *Hepatology* 2015; **61**: 1127-1135 [PMID: 25614962 DOI: 10.1002/hep.27726]

15 **Carter W**, Connelly S, Struble K. Reinventing HCV Treatment: Past and Future Perspectives. *J Clin Pharmacol* 2017; **57**: 287-296 [PMID: 27654843 DOI: 10.1002/jcph.830]

16 **González-Grande R**, Jiménez-Pérez M, González Arjona C, Mostazo Torres J. New approaches in the treatment of hepatitis C. *World J Gastroenterol* 2016; **22**: 1421-1432 [PMID: 26819511 DOI: 10.3748/wjg.v22.i4.1421]

17 **Duan Z**, Jia JD, Hou J, Lou L, Tobias H, Xu XY, Wei L, Zhuang H, Pan CQ. Current challenges and the management of chronic hepatitis C in mainland China. *J Clin Gastroenterol* 2014; **48**: 679-686 [PMID: 24921215 DOI: 10.1097/MCG.0000000000000109]

18 **Huang JF**, Huang CF, Yeh ML, Dai CY, Yu ML, Chuang WL. Updates in the management and treatment of HCV genotype 3, what are the remaining challenges? *Expert Rev Anti Infect Ther* 2018; **16**: 907-912 [PMID: 30396303 DOI: 10.1080/14787210.2018.1544492]

19 **Dimitroulis D**, Damaskos C, Valsami S, Davakis S, Garmpis N, Spartalis E, Athanasiou A, Moris D, Sakellariou S, Kykalos S, Tsourouflis G, Garmpi A, Delladetsima I, Kontzoglou K, Kouraklis G. From diagnosis to treatment of hepatocellular carcinoma: An epidemic problem for both developed and developing world. *World J Gastroenterol* 2017; **23**: 5282-5294 [PMID: 28839428 DOI: 10.3748/wjg.v23.i29.5282]

20 **Meringer H**, Shibolet O, Deutsch L. Hepatocellular carcinoma in the post-hepatitis C virus era: Should we change the paradigm? *World J Gastroenterol* 2019; **25**: 3929-3940 [PMID: 31413528 DOI: 10.3748/wjg.v25.i29.3929]

21 **Ferrarese A**, Germani G, Gambato M, Russo FP, Senzolo M, Zanetto A, Shalaby S, Cillo U, Zanus G, Angeli P, Burra P. Hepatitis C virus related cirrhosis decreased as indication to liver transplantation since the introduction of direct-acting antivirals: A single-center study. *World J Gastroenterol* 2018; **24**: 4403-4411 [PMID: 30344424 DOI: 10.3748/wjg.v24.i38.4403]

22 **Ioannou GN**, Green PK, Berry K. HCV eradication induced by direct-acting antiviral agents reduces the risk of hepatocellular carcinoma. *J Hepatol* 2017 [PMID: 28887168 DOI: 10.1016/j.jhep.2017.08.030]

23 **ANRS collaborative study group on hepatocellular carcinoma (ANRS CO22 HEPATHER, CO12 CirVir and CO23 CUPILT cohorts)**. Lack of evidence of an effect of direct-acting antivirals on the recurrence of hepatocellular carcinoma: Data from three ANRS cohorts. *J Hepatol* 2016; **65**: 734-740 [PMID: 27288051 DOI: 10.1016/j.jhep.2016.05.045]

24 **Conti F**, Buonfiglioli F, Scuteri A, Crespi C, Bolondi L, Caraceni P, Foschi FG, Lenzi M, Mazzella G, Verucchi G, Andreone P, Brillanti S. Early occurrence and recurrence of hepatocellular carcinoma in HCV-related cirrhosis treated with direct-acting antivirals. *J Hepatol* 2016; **65**: 727-733 [PMID: 27349488 DOI: 10.1016/j.jhep.2016.06.015]

25 **Kim NJ**, Locke CJ, Park H, Magee C, Bacchetti P, Khalili M. Race and Hepatitis C Care Continuum in an Underserved Birth Cohort. *J Gen Intern Med* 2019; **34**: 2005-2013 [PMID: 30238404 DOI: 10.1007/s11606-018-4649-6]

World Journal of Gastroenterology

Submit a Manuscript: https://www.f6publishing.com

World J Gastroenterol 2019 November 28; 25(44): 6561-6570

DOI: 10.3748/wjg.v25.i44.6561

ISSN 1007-9327 (print) ISSN 2219-2840 (online)

SYSTEMATIC REVIEW

Chronic pancreatitis and the heart disease: Still terra incognita?

Sara Nikolic, Ana Dugic, Corinna Steiner, Apostolos V Tsolakis, Ida Marie Haugen Löfman, J-Matthias Löhr, Miroslav Vujasinovic

ORCID number: Sara Nikolic (0000-0003-3751-2619); Ana Dugic (0000-0002-1893-0754); Corinna Steiner (0000-0002-8871-2584); Apostolos V Tsolakis (0000-0002-6784-5572); Ida Marie Haugen Löfman (0000-0002-6648-6846); J-Matthias Löhr (0000-0002-7647-198X); Miroslav Vujasinovic (0000-0002-6496-295X).

Author contributions: Nikolic S and Vujasinovic M contributed to the conception and design of the study, literature review and selection of the eligible studies, analysis and interpretation of data and drafting of the manuscript; Dugic A contributed to literature review, selection of the eligible studies, analysis of data, and critical revision and editing; Steiner C , Tsolakis AV, Haugen Löfman IM, contributed to critical revision and editing; Löhr JM contributed to literature review and analysis, drafting of the manuscript and critical revision and editing.

Conflict-of-interest statement: Vujasinovic M and Löhr JM have worked as speakers for Mylan and Abbott Laboratories. Nikolic S has worked as a speaker for Mylan, Krka, Servier and Ferring. Authors declare no potential conflicts of interest and no financial support regarding presenting the manuscript.

PRISMA 2009 Checklist statement: The authors have read the PRISMA 2009 Checklist, and the manuscript was prepared and revised according to the PRISMA 2009 Checklist.

Sara Nikolic, Miroslav Vujasinovic, Department of Medicine Huddinge, Karolinska Institute, Stockholm 14183, Sweden

Sara Nikolic, Department of Gastroenterology, Division of Internal Medicine, University Medical Centre Maribor, Maribor 2000, Slovenia

Ana Dugic, Department of Medicine, Klinikum Bayreuth, Bayreuth 95445, Germany

Corinna Steiner, Apostolos V Tsolakis, J-Matthias Löhr, Miroslav Vujasinovic, Department for Digestive Diseases, Karolinska University Hospital, Stockholm 14186, Sweden

Apostolos V Tsolakis, Department of Oncology and Pathology, Karolinska Institute, Stockholm 17176, Sweden

Apostolos V Tsolakis, Cancer Centre Karolinska, CCK, Karolinska University Hospital, Stockholm 17176, Sweden

Ida Marie Haugen Löfman, Unit of Cardiology, Heart and Vascular Theme, Karolinska University Hospital Huddinge, Stockholm 14186, Sweden

Ida Marie Haugen Löfman, Department of Medicine Solna, Karolinska Institute, Stockholm 17176, Sweden

J-Matthias Löhr, Department of Clinical Science, Intervention, and Technology (CLINTEC), Karolinska Institute, Stockholm 17176, Sweden

Corresponding author: Miroslav Vujasinovic, MD, PhD, Doctor, Department for Digestive Diseases, Karolinska University Hospital, Hälsovägen 11, Stockholm 14186, Sweden.
miroslav.vujasinovic@sll.se
Telephone:+46-72-4694938

Abstract

BACKGROUND

It has been suggested that chronic pancreatitis (CP) may be an independent risk factor for development of cardiovascular disease (CVD). At the same time, it seems that congestive heart failure (CHF) and CP share the responsibility for the development of important clinical conditions such as sarcopenia, cachexia and malnutrition due to development of cardiac cachexia and pancreatic exocrine insufficiency (PEI), respectively.

AIM

To explore the evidence regarding the association of CP and heart disease, more specifically CVD and CHF.

Manuscript source: Unsolicited manuscript

Received: October 4, 2019
Peer-review started: October 4, 2019
First decision: November 4, 2019
Revised: November 8, 2019
Accepted: November 16, 2019
Article in press: November 16, 2019
Published online: November 28, 2019

P-Reviewer: Armellini E, Sahoo J
S-Editor: Tang JZ
L-Editor: A
E-Editor: Zhang YL

METHODS
A systematic search of MEDLINE, Web of Science and Google Scholar was performed by two independent investigators to identify eligible studies where the connection between CP and CVD was investigated. The search was limited to articles in the English language. The last search was run on the 1st of May 2019. The primary outcomes were: (1) Incidence of cardiovascular event [acute coronary syndrome (ACS), chronic coronary disease, peripheral arterial lesions] in patients with established CP; and (2) Incidence of PEI in patients with CHF.

RESULTS
Out of 1166 studies, only 8 were eligible for this review. Studies regarding PEI and CHF showed an important incidence of PEI as well as associated malabsorption of nutritional markers (vitamin D, selenium, phosphorus, zinc, folic acid, and prealbumin) in patients with CHF. However, after substitution of pancreatic enzymes, it seems that, at least, loss of appetite was attenuated. On the other side, studies investigating cardiovascular events in patients with CP showed that, in CP cohort, there was a 2.5-fold higher incidence of ACS. In another study, patients with alcohol–induced CP with concomitant type 3c diabetes had statistically significant higher incidence of carotid atherosclerotic plaques in comparison to patients with diabetes mellitus of other etiologies. Earlier studies demonstrated a marked correlation between the clinical symptoms in CP and chronic coronary insufficiency. Also, statistically significant higher incidence of arterial lesions was found in patients with CP compared to the control group with the same risk factors for atherosclerosis (hypertension, smoking, dyslipidemia). Moreover, one recent study showed that PEI is significantly associated with the risk of cardiovascular events in patients with CP.

CONCLUSION
Current evidence implicates a possible association between PEI and malnutrition in patients with CHF. Chronic pancreatic tissue hypoxic injury driven by prolonged splanchnic hypoperfusion is likely to contribute to malnutrition and cachexia in patients with CHF. On the other hand, CP and PEI seem to be an independent risk factor associated with an increased risk of cardiovascular events.

Key words: Chronic; Pancreatitis; Pancreatic exocrine insufficiency; Heart failure; Cardiovascular diseases

Core tip: This systematic review explores the studies regarding the connection between chronic pancreatitis (CP) and cardiovascular disease, which seems to be a two-way street. On one hand, congestive heart failure may aid to development of at least mild pancreatic exocrine insufficiency (PEI) that, in return, contributes to development of loss of appetite, cachexia, and malnutrition in patients with heart failure. On the other hand, there is some evidence that CP with concomitant PEI may be an independent risk factor for cardiovascular events in terms of coronary disease, cerebrovascular disease and peripheral atherosclerotic plaques.

Citation: Nikolic S, Dugic A, Steiner C, Tsolakis AV, Haugen Löfman IM, Löhr JM, Vujasinovic M. Chronic pancreatitis and the heart disease: Still terra incognita? *World J Gastroenterol* 2019; 25(44): 6561-6570
URL: https://www.wjgnet.com/1007-9327/full/v25/i44/6561.htm
DOI: https://dx.doi.org/10.3748/wjg.v25.i44.6561

INTRODUCTION

Chronic pancreatitis (CP) is a persistent inflammation of the pancreas with pathological findings of the infiltration of immune cells and the development of fibrosis. Pancreatic exocrine insufficiency (PEI), caused by impaired secretion of

pancreatic digestive enzymes due to loss of intact pancreatic acinar cells, represents one of the most frequent complications of CP[1]. Chronic heart failure describes the complex clinical syndrome where the heart is incapable of maintaining a cardiac output that is adequate to meet metabolic requirements and accommodate venous return[2,3]. There is evidence that CP is associated with an increased risk of cardiovascular diseases (CVD), which may be at least partially explained by sharing many risk factors among these patients[4-7]. Even association between CP and cerebrovascular disease was reported[8]. There is increasing evidence for the involvement of the gastrointestinal (GI) system in congestive heart failure (CHF)[9]. Furthermore, patients with CP and CHF share two other very important clinical conditions: sarcopenia and cachexia[10-13]. Muscle wasting, or sarcopenia, is characterized by loss of muscle mass, loss of muscle strength and impaired functional capacity[10]. The occurrence of malnutrition has been reported as a hallmark of muscle wasting especially in older patients[14,15]. Cardiac cachexia is the clinical entity occurring at the end of the chronic natural course of CHF with complex and multifactorial pathophysiology[16]. Association of PEI in patients with CHF with appetite loss was recently reported[17,18].

MATERIALS AND METHODS

Search strategy and study selection

MEDLINE, Web of Science and Google Scholar databases were searched until May 1, 2019 using the following terms: [(Chronic pancreatitis OR pancreatic exocrine insufficiency) AND (heart failure OR cardiovascular risk OR cardiovascular disease)]. The search was limited to articles in the English language. Eligibility assessment was performed independently by screening the titles and, consequently, the abstracts by 2 reviewers, Nikolic S and Dugic A. All disagreements were resolved by Vujasinovic M and Löhr JM. Review articles, editorials, conference reports, comments on other studies, and animal studies were excluded. Studies on clinical association between CP and heart diseases were included. Of the selected articles, the full texts, as well as the reference lists, were reviewed independently ("snowball-strategy") by three authors (Nikolic S, Dugic A and Vujasinovic M). The selection process of the articles for this review is summarized in Figure 1.

Data collection process and data items

This review was limited to the question of whether there is a connection between CP and CVD in patients older than 18 years at the onset of CVD. The following characteristics were extracted from the publications included: Year of publication, country of origin, study design, number of patients, demographics of patients included and study results.

Interventions made in all of the included studies were diagnostic measures needed for establishing CVD in patients with CP and vice versa. CHF was assessed by echocardiography[3]. Diagnosis of CP was made upon clinical data and pancreatic imaging[1]. Diagnosis of PEI was established by measuring fecal elastase in stool or a C-labeled mixed triglyceride breath test. Control patients were either healthy individuals or were matched with the study group. The exception is the study by de la Iglesia where controls had CP only, whereas the study group had CP and PEI[4].

RESULTS

Study selection

Overall, 1166 citations were retrieved; 1145 were rejected based on title, abstract relevance or duplication; 21 articles were fully reviewed. After further review, an additional 13 full-text articles were excluded due to reasons stated in Figure 1. Final analysis included 8 studies[4-6,17-21]. Characteristics of studies on PEI in patients with CHF are summarized in Table 1. Table 2 shows characteristics of studies on CVD in patients with CP. Figure 2 shows possible association between cardiovascular and pancreatic disease.

Results of the individual studies

Table 1 and Table 2 synthesize the main results of each individual study included in the systematic research.

Outcomes

Three studies assessed the incidence of PEI in patients with CHF as a primary

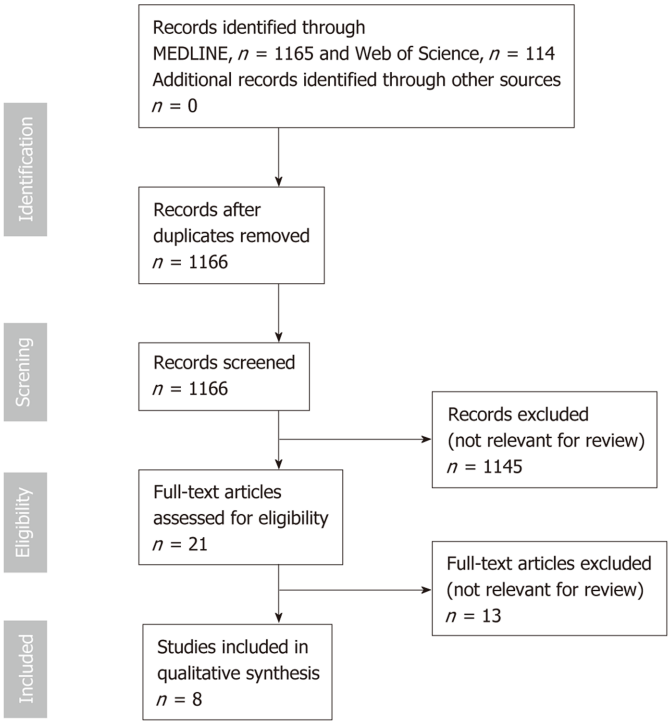

Figure 1 Flow chart on study-selection process.

outcome[17-19] and five studies assessed incidence of cardiovascular complication (acute or chronic coronary lesion, carotid atheroma, peripheral arterial lesion) in patients with CP[4-6,20,21]. Improvement of appetite loss by supplemented pancreatic enzymes was investigated as a secondary outcome in the study by Xia *et al*[17]. The study by de la Iglesia *et al*[4] examined the association of PEI and cardiovascular risk in patients with CP as a primary outcome. The primary outcome measure in most studies was the mean difference between control and patient groups. In studies by Hsu *et al*[6] and Wong *et al*[8], time to vascular event was measured and result represented as a hazard ratio.

DISCUSSION

Congestive heart failure is a progressive disease that causes ischemia and congestion in peripheral tissues and may result in function loss in many organs such as the kidney, liver, stomach and intestine[17]. Nausea and lack of appetite may also occur as blood is shifted from the GI tract to the more vital organs[2]. Susceptibility of the pancreas to ischemic injury in shock, malignant hypertension and after cardiac surgery is well known[22-25]. The splanchnic circulation normally receives approximately 20%-30% of the cardiac output[26,27]. In patients with CHF, the splanchnic circulation is decreased, and if this state is prolonged, tissue damage to the splanchnic organs is possible, especially in pancreas that are highly vascularized organs[22,28].

Pancreatic exocrine insufficiency in patients with heart failure

Appetite loss and malnutrition are well known and highly prevalent in patients with CHF and an important risk factor for morbidity and mortality[29,30]. PEI refers to an insufficient secretion of pancreatic enzymes (acinar function) and/or sodium bicarbonate (ductal function), mostly associated with various pancreatic illnesses but could be associated even with extra pancreatic diseases[1].

Earlier, we performed a prospective study on 87 patients with CHF, using fecal elastase-1 (FE-1) as a diagnostic tool for diagnosis of PEI[18]. The mean time from the confirmation of chronic heart failure to inclusion in the study was 4 years and PEI was diagnosed in 6.9% of patients suggesting a possibility that PEI occurred because of decreased splanchnic circulation in CHF patients. Additionally, the clinical significance of PEI was assessed in this study by using a complete laboratory serum nutritional panel showing decreased levels in one or more nutritional serum markers (vitamin D, selenium, phosphorus, zinc, folic acid, and prealbumin) in all of the

Table 1 Studies on pancreatic exocrine insufficiency in patients with chronic heart failure

Ref.	*n*	Mean age (yr)	Method used	PEI (%)
Xia *et al*[17], 2017, China	All patients: 104 (85.6% males) NYHA I/II: 32 NYHA III: 42 NYHA IV: 30	70.4	FE-1	All patients: *n* = 59 (56.7%) NYHA I-II: Mild/moderate: *n* = 7, severe: *n* = 1; NYHA III: Mild/moderate: *n* = 15, severe: *n* = 14; NYHA IV: Mild/moderate: *n* = 10, severe: *n* = 12
Vujasinovic*et al*[18], 2016, Slovenia	All patients: 87 (64.4% males) NYHA II: 54 NYHA III: 33	74.7	FE-1	All patients: *n* = 6 (6.9%), mild/moderate PEI: *n* = 3, severe PEI: *n* = 3, NYHA II: *n* = 3, NYHA III: *n* = 3
Özcan *et al*[19], 2015, Turkey	All patients: 52 (61,5% males) NYHA I/II: 32 NYHA III/IV: 20	67.5	FE-1	All patients: *n* = 21 (40.4%) NYHA I/II: Mild/moderate PEI: *n* = 3, severe PEI: *n* = 4 NYHA III/IV: Mild/moderate PEI: *n* = 4, severe PEI: *n* = 10

n: Number of patients; FE-1: Fecal elastase-1; PEI: Pancreatic exocrine insufficiency; NYHA: New York Heart Association classification.

patients tested with PEI[18].

Özcan *et al*[19] investigated FE-1 levels (as an indicator of pancreatic exocrine function) and blood ghrelin levels (which affect eating, sleeping, cell proliferation, the cardiovascular system, and carbohydrate energy metabolism in patients with CHF as well as the pancreatic exocrine function) in 52 patients with acute decompensated heart failure and compared them with 31 healthy patients in the control group. The authors reported significant difference in FE-1 levels between the control and NYHA I/II patients *vs* NYHA III/IV group. In patients with advanced heart failure, ten patients (50%) had severe, and four patients (20%) moderate PEI, whereas two- thirds of the controls and patients with mild heart failure had normal pancreatic function. However, there was no statistically significant difference for ghrelin levels[19].

Xia *et al*[17] attempted to detect the association between PEI (measured by FE-1 levels) and CHF-induced appetite, which was tested by the simplified nutritional appetite questionnaire. PEI was diagnosed in 56.7% of 104 patients with CHF and in none within the control group (n = 20) of patients with normal heart function. In the very important second part of this study, patients with CHF and PEI were treated with pancreatic enzyme replacement therapy (PERT) in the form of pancreatin (30000 units per day) and compared with the CHF and PEI patients treated with a placebo. After a 4-wk treatment, pancreatin significantly improved the appetite loss in the treatment group, indicating that PERT can attenuate the appetite loss in CHF and give the strongest evidence so far in the association of PEI with appetite loss in patients with CHF[17].

Cardiovascular risk in patients with CP

The association between CP and CVD has received little attention in the past. In 1975, Tuzhilin *et al*[20] reported a study on cardiovascular lesions in 98 patients with CP and 32 control subjects, analyzing serum amylase, trypsin, trypsin inhibitor, elastase, plasma recalcification time, plasma heparin tolerance, blood fibrinogen level, fibrinolysis activity and capillary permeability to protein and water. They observed a marked correlation between the clinical symptoms in CP and chronic coronary insufficiency, probably because of pancreatic enzymes and their inhibitors that profoundly affected blood coagulability and appear to influence the course of pancreatic inflammation.

In 1982, Gullo *et al*[5] prospectively investigated 54 consecutive CP patients and 54 control subjects for the presence of cardiovascular lesions. Clinical and laboratory evidence of arterial involvement was found in 18 patients (33%) and in 5 controls (9%) ($P < 0.01$), concluding that patients with CP have more frequent cardiovascular lesions that tend to develop at an earlier age, compared to the general population (there were no differences between the two groups for major risk factors like arterial hypertension, smoking habits, or blood lipid abnormalities).

Lee *et al*[21] recently performed an interesting retrospective observational study on 32 patients with alcohol related CP and type 3 c diabetes mellitus (diabetes secondary to pancreatic disease) in whom panoramic (dental) images were taken and compared

Table 2 Studies on cardiovascular diseases in patients with chronic pancreatitis

Ref.	*n*	Mean age (yr)	Results
Tuzhilin *et al*[20], 1975, Union of Soviet Socialist Republics/United States	98	Not reported	Marked correlation between the clinical symptoms in CP and chronic coronary insufficiency Pancreatic enzymes and their inhibitors profoundly affected blood coagulability and appear to influence the course of pancreatic inflammation
Gullo *et al*[5], 1982, Italy	54 49 (90.7%) males	44.2	Arterial lesions were found in 18 patients (33.3%) and in five controls (9.3%) ($P < 0.01$) No differences were found between the two groups for arterial hypertension, smoking habits, or blood lipid abnormalities
Hsu *et al*[6], 2016, Taiwan	17405 14418 (82.8%) males	48.3	The overall incidence of acute coronary syndrome was 2.15-fold higher in the CP cohort than in the non-CP cohort (4.89 *vs* 2.28 per 10,000 person-years) with an adjusted hazard ratio of 1.40 (95% confidence interval 1.20-1.64) Compared with individuals without CP, patients with CP aged ≤ 39 years exhibited the highest risk of acute coronary syndrome CP may become an independent risk factor for acute coronary syndrome
Lee *et al*[21], 2018, United States	32 (100%) males	61.7	Statistically significant association between a diagnosis of alcohol-related CP and diabetes mellitus, and the presence of an atheroma (calcified carotid artery plaques) on the panoramic image, in comparison with the rate manifested by the historical general population cohort (25% *vs* 3%; $P < 0.05$)
de la Iglesia *et al*[4], 2018, Spain	430 340 (79%) males	47.8	Together with known major cardiovascular risk factors like smoking and hypertension, pancreatic exocrine insufficiency is significantly associated with the increased risk of cardiovascular events in patients with CP

CP: Chronic pancreatitis.

to a historical cohort of healthy patients. The prevalence rate of calcified carotid artery plaques (25%) was significantly higher than the rate (3%) in the control group.

Although DM is common in CP and is a well-known risk factor for arteriosclerosis, the link between CP and CVD seems to depend on other mechanisms[31]. Chronic inflammation has been found to be associated with accelerated atherosclerosis and increased risk of CVDs[32]. The pancreatic changes at an advanced age are considered to be related to atherosclerosis (of small vessels)[15]. This concept of "senile pancreatitis" was first described by Ammann *et al*[33] and in most cases has a silent and mild course[34].

In a prospective, longitudinal cohort study, Spanish colleagues evaluated the risk of cardiovascular events and the impact of PEI in a cohort of 430 CP patients with the mean follow-up of 8.6 years[4]. The study demonstrated, for the first time, that PEI is an independent risk factor significantly associated with an increased risk of cardiovascular events.

Hsu *et al*[6] conducted a nationwide retrospective cohort study in Taiwan to determine the risk of acute coronary syndrome (ACS) in patients with CP. In total, 17405 patients with CP and 69620 individuals without CP were followed for 84430 and 417426 person-years showing that overall ACS incidence was 2.15-fold higher in the CP cohort than in the non-CP cohort. Interestingly, the highest risk of ACS was observed in patients aged ≤ 39 years. Here the increased risk was thought to be

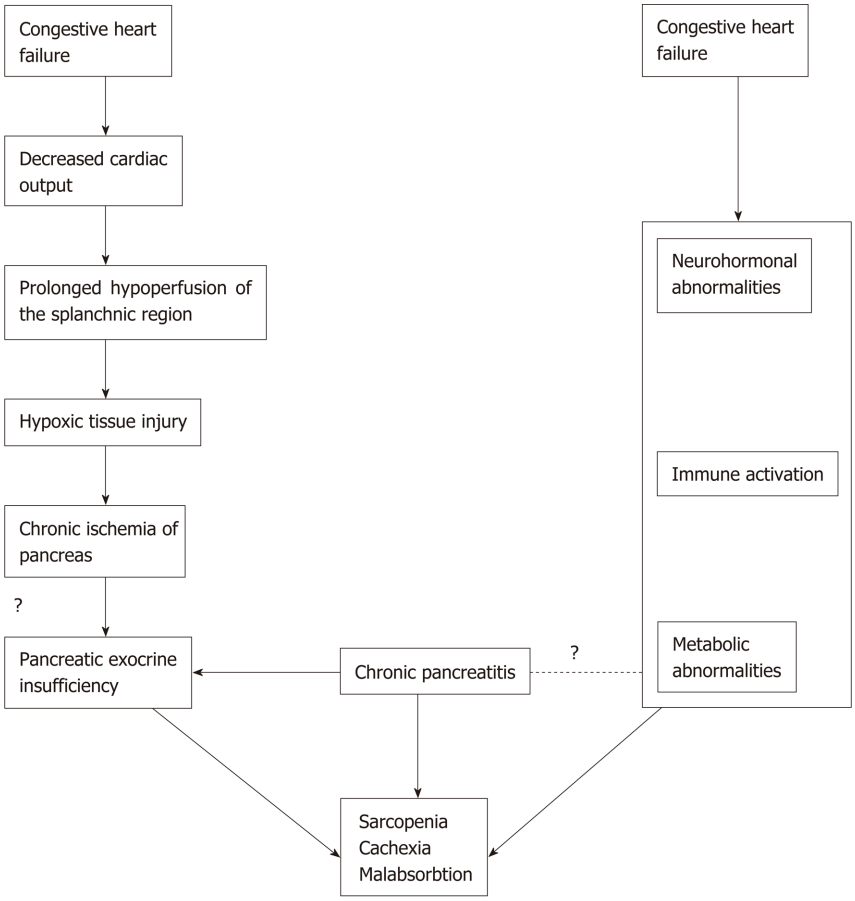

Figure 2 Possible association between cardiovascular and pancreatic disease.

caused by inflammation leading to endothelial dysfunction and progress of unstable plaque. In the similarly conducted retrospective population-based cohort study from Taiwan, Wong *et al*[8] reported association of CP with increased risk of subsequent cerebrovascular disease. The overall incidence of cerebrovascular disease among 16672 patients with CP was 1.24-fold greater than in the non-CP patients.

In conclusion, so far, research on association between heart and pancreas disease has received little attention and its role in pathogenesis is not fully elucidated. However, studies presented in this article indicate an important association that should be further investigated. Patients with CP/pancreatic exocrine insufficiency and chronic heart failure (especially right ventricular dysfunction) share similar clinical symptoms like abdominal pain, anorexia, nausea and bloating[1,2]. Interplay between malnutrition (intake driven) and cachexia (disease driven) can also be seen in both cardiac and pancreatic patients, as well as in sarcopenia (muscle wasting)[1,10,11,16,35]. Current evidence implicates possible association between PEI and malnutrition in patients with CHF. Chronic pancreatic tissue hypoxia and consequent injury is likely to contribute to malnutrition and cachexia in patients with CHF; however, too simplistic of an explanation should be avoided. Future prospective studies on this topic are necessary, especially using diagnostic methods for PEI other than FE-1, like the ^{13}C-trygliceride breath test, secretin enhanced magnetic resonance cholangiopancreatography and serum nutritional markers[1].

On the other side, besides well-known risk factors, CP and PEI seem to be independent risk factors associated with an increased risk of CVD. However, most of the studies so far have been performed on patients with alcohol related CP, and in males. Future studies on CP patients with other etiologies and female patients would be of interest.

ARTICLE HIGHLIGHTS

Research background

Chronic pancreatitis (CP) is a persistent inflammation of the pancreas and with time fibrosis develops. Pancreatic exocrine insufficiency (PEI) due to loss of intact pancreatic acinar cells, represents one of the most frequent complications of CP. Chronic heart failure is a complex clinical syndrome where the heart is incapable of maintaining a cardiac output that is adequate to meet human metabolic requirements. Association between CP and heart disease was reported.

Research motivation

Despite sharing risk factors for atherosclerosis among patients with cardiovascular diseases (CVD) and CP, it has been suggested that CP may be an independent risk factor for development of CVD. At the same time, it seems that congestive heart failure (CHF) and CP share the responsibility for the development of important clinical entities such as sarcopenia, cachexia and malnutrition consequences of cardiac cachexia and PEI, respectively.

Research objectives

The objective of our systematic review was to explore all current evidence regarding the association between CP and heart disease such as CVD and CHF.

Research methods

MEDLINE, Web of Science and Google Scholar were independently searched by two investigators with the aim to identify eligible studies where the connection between CP and CVDs was researched. The primary outcomes were: (1) Incidence of cardiovascular event [acute coronary syndrome (ACS), chronic coronary disease, peripheral arterial lesions] in patients with established CP; and (2) Incidence of PEI in patients with CHF. The primary outcome measure in most studies was the mean difference between control and patient groups.

Research results

Eight studies were eligible for this review. Studies regarding PEI and CHF showed an important incidence of PEI as well as associated malabsorption of nutritional markers (vitamin D, selenium, phosphorus, zinc, folic acid, and prealbumin) in patients with CHF. However, after substitution of pancreatic enzymes, it seems that, at least, loss of appetite was attenuated. On the other side, studies investigating cardiovascular events in patients with CP showed that CP is associated with an increased risk of CVD (a 2.5-fold higher incidence of ACS). Also, CP with concomitant type 3c diabetes had statistically significant higher incidence of carotid atherosclerotic plaques in comparison to patients with diabetes mellitus of other etiologies. When other risk factors for atherosclerosis (hypertension, smoking, and dyslipidemia) were matched, patients with CP had significantly higher incidence of arterial lesions. Moreover, one recent study showed that PEI is significantly associated with the risk of cardiovascular events in patients with CP.

Research conclusions

Chronic pancreatic tissue hypoxic injury driven by prolonged splanchnic hypoperfusion is likely to contribute to malnutrition and cachexia in patients with CHF. On the other hand, CP and PEI seem to be an independent risk factor associated with an increased risk of cardiovascular events.

Research perspectives

Interplay between malnutrition (intake driven) and cachexia (disease driven) can be seen in both cardiac and pancreatic patients, as well as in sarcopenia (muscle wasting) Current evidence implicates possible association between PEI and malnutrition in patients with CHF as well as CP with or without PEI being an independent risk factor for CVD. However, too simplistic explanations should be avoided. Future prospective studies on this topic are necessary, especially using diagnostic methods for PEI other than fecal elastase-1, like the ^{13}C-trygliceride breath test, secretin enhanced magnetic resonance cholangiopancreatography and serum nutritional markers.

REFERENCES

1 **Löhr JM**, Dominguez-Munoz E, Rosendahl J, Besselink M, Mayerle J, Lerch MM, Haas S, Akisik F, Kartalis N, Iglesias-Garcia J, Keller J, Boermeester M, Werner J, Dumonceau JM, Fockens P, Drewes A, Ceyhan G, Lindkvist B, Drenth J, Ewald N, Hardt P, de Madaria E, Witt H, Schneider A, Manfredi R, Brøndum FJ, Rudolf S, Bollen T, Bruno M; HaPanEU/UEG Working Group. United European Gastroenterology evidence-based guidelines for the diagnosis and therapy of chronic pancreatitis (HaPanEU). *United European Gastroenterol J* 2017; **5**: 153-199 [PMID: 28344786 DOI: 10.1177/2050640616684695]

2 **Kemp CD**, Conte JV. The pathophysiology of heart failure. *Cardiovasc Pathol* 2012; **21**: 365-371 [PMID: 22227365 DOI: 10.1016/j.carpath.2011.11.007]

3 **Ponikowski P**, Voors AA, Anker SD, Bueno H, Cleland JG, Coats AJ, Falk V, González-Juanatey JR, Harjola VP, Jankowska EA, Jessup M, Linde C, Nihoyannopoulos P, Parissis JT, Pieske B, Riley JP, Rosano GM, Ruilope LM, Ruschitzka F, Rutten FH, van der Meer P; Authors/Task Force Members; Document Reviewers. 2016 ESC Guidelines for the diagnosis and treatment of acute and chronic heart failure: The Task Force for the diagnosis and treatment of acute and chronic heart failure of the European Society of Cardiology (ESC). Developed with the special contribution of the Heart Failure Association (HFA) of the ESC. *Eur J Heart Fail* 2016; **18**: 891-975 [PMID: 27207191 DOI: 10.1002/ejhf.592]

4 **de la Iglesia D**, Vallejo-Senra N, López-López A, Iglesias-Garcia J, Lariño-Noia J, Nieto-García L, Domínguez-Muñoz JE. Pancreatic exocrine insufficiency and cardiovascular risk in patients with chronic pancreatitis: A prospective, longitudinal cohort study. *J Gastroenterol Hepatol* 2019; **34**: 277-283 [PMID: 30156337 DOI: 10.1111/jgh.14460]
5 **Gullo L**, Stella A, Labriola E, Costa PL, Descovich G, Labò G. Cardiovascular lesions in chronic pancreatitis: a prospective study. *Dig Dis Sci* 1982; **27**: 716-722 [PMID: 7094792 DOI: 10.1007/bf01393767]
6 **Hsu MT**, Lin CL, Chung WS. Increased Risk of Acute Coronary Syndrome in Patients With Chronic Pancreatitis: A Nationwide Cohort Analysis. *Medicine (Baltimore)* 2016; **95**: e3451 [PMID: 27196450 DOI: 10.1097/MD.0000000000003451]
7 **Maisonneuve P**, Lowenfels AB, Müllhaupt B, Cavallini G, Lankisch PG, Andersen JR, Dimagno EP, Andrén-Sandberg A, Domellöf L, Frulloni L, Ammann RW. Cigarette smoking accelerates progression of alcoholic chronic pancreatitis. *Gut* 2005; **54**: 510-514 [PMID: 15753536 DOI: 10.1136/gut.2004.039263]
8 **Wong TS**, Liao KF, Lin CM, Lin CL, Chen WC, Lai SW. Chronic Pancreatitis Correlates With Increased Risk of Cerebrovascular Disease: A Retrospective Population-Based Cohort Study in Taiwan. *Medicine (Baltimore)* 2016; **95**: e3266 [PMID: 27082563 DOI: 10.1097/MD.0000000000003266]
9 **Krack A**, Sharma R, Figulla HR, Anker SD. The importance of the gastrointestinal system in the pathogenesis of heart failure. *Eur Heart J* 2005; **26**: 2368-2374 [PMID: 15980032 DOI: 10.1093/eurheartj/ehi389]
10 **Saitoh M**, Rodrigues Dos Santos M, von Haehling S. Muscle wasting in heart failure : The role of nutrition. *Wien Klin Wochenschr* 2016; **128**: 455-465 [PMID: 27761739 DOI: 10.1007/s00508-016-1100-z]
11 **Olesen SS**, Büyükuslu A, Køhler M, Rasmussen HH, Drewes AM. Sarcopenia associates with increased hospitalization rates and reduced survival in patients with chronic pancreatitis. *Pancreatology* 2019; **19**: 245-251 [PMID: 30665702 DOI: 10.1016/j.pan.2019.01.006]
12 **Singh S**, Midha S, Singh N, Joshi YK, Garg PK. Dietary counseling versus dietary supplements for malnutrition in chronic pancreatitis: a randomized controlled trial. *Clin Gastroenterol Hepatol* 2008; **6**: 353-359 [PMID: 18328440 DOI: 10.1016/j.cgh.2007.12.040]
13 **Midha S**, Singh N, Sachdev V, Tandon RK, Joshi YK, Garg PK. Cause and effect relationship of malnutrition with idiopathic chronic pancreatitis: prospective case-control study. *J Gastroenterol Hepatol* 2008; **23**: 1378-1383 [PMID: 18554234 DOI: 10.1111/j.1440-1746.2008.05459.x]
14 **Htun NC**, Ishikawa-Takata K, Kuroda A, Tanaka T, Kikutani T, Obuchi SP, Hirano H, Iijima K. Screening for Malnutrition in Community Dwelling Older Japanese: Preliminary Development and Evaluation of the Japanese Nutritional Risk Screening Tool (NRST). *J Nutr Health Aging* 2016; **20**: 114-120 [PMID: 26812506 DOI: 10.1007/s12603-015-0555-3]
15 **Löhr JM**, Panic N, Vujasinovic M, Verbeke CS. The ageing pancreas: a systematic review of the evidence and analysis of the consequences. *J Intern Med* 2018; **283**: 446-460 [PMID: 29474746 DOI: 10.1111/joim.12745]
16 **Loncar G**, Springer J, Anker M, Doehner W, Lainscak M. Cardiac cachexia: hic et nunc. *J Cachexia Sarcopenia Muscle* 2016; **7**: 246-260 [PMID: 27386168 DOI: 10.1002/jcsm.12118]
17 **Xia T**, Chai X, Shen J. Pancreatic exocrine insufficiency in patients with chronic heart failure and its possible association with appetite loss. *PLoS One* 2017; **12**: e0187804 [PMID: 29155861 DOI: 10.1371/journal.pone.0187804]
18 **Vujasinovic M**, Tretjak M, Tepes B, Marolt A, Slemenik Pusnik C, Kotnik Kerbev M, Rudolf S. Is pancreatic exocrine insufficiency a result of decreased splanchnic circulation in patients with chronic heart failure? *JOP.J Pancreas (Online)* 2016; **17**: 201-203
19 **Özcan M**, Öztürk GZ, Köse M, Emet S, Aydın Ş, Arslan K, Arman Y, Akkaya V, Tükek T. Evaluation of malnutrition with blood ghrelin and fecal elastase levels in acute decompensated heart failure patients. *Turk Kardiyol Dern Ars* 2015; **43**: 131-137 [PMID: 25782117 DOI: 10.5543/tkda.2015.06606]
20 **Tuzhilin DA**, Dreiling DA. Cardiovascular lesions in pancreatitis. *Am J Gastroenterol* 1975; **63**: 381-388 [PMID: 1146795]
21 **Lee UK**, Chang TI, Polanco JC, Pisegna JR, Friedlander AH. Prevalence of Panoramically Imaged Carotid Atheromas in Alcoholic Patients With Chronic Pancreatitis and Comorbid Diabetes. *J Oral Maxillofac Surg* 2018; **76**: 1929.e1-1929.e7 [PMID: 29859950 DOI: 10.1016/j.joms.2018.05.011]
22 **Warshaw AL**, O'Hara PJ. Susceptibility of the pancreas to ischemic injury in shock. *Ann Surg* 1978; **188**: 197-201 [PMID: 686887 DOI: 10.1097/00000658-197808000-00012]
23 **Feiner H**. Pancreatitis after cardiac surgery; a morphologic study. *Am J Surg* 1976; **131**: 684-688 [PMID: 937646 DOI: 10.1016/0002-9610(76)90178-1]
24 **Hranilovich GT**, Baggenstoss AH. Lesions of the pancreas in malignant hypertension; review of one hundred cases at necropsy. *AMA Arch Pathol* 1953; **55**: 443-456 [PMID: 13039692]
25 **Fernández-del Castillo C**, Harringer W, Warshaw AL, Vlahakes GJ, Koski G, Zaslavsky AM, Rattner DW. Risk factors for pancreatic cellular injury after cardiopulmonary bypass. *N Engl J Med* 1991; **325**: 382-387 [PMID: 1712076 DOI: 10.1056/NEJM199108083250602]
26 **Ralevic V**. Splanchnic circulatory physiology. *Hepatogastroenterology* 1999; **46** Suppl 2: 1409-1413 [PMID: 10431701]
27 **Takala J**. Determinants of splanchnic blood flow. *Br J Anaesth* 1996; **77**: 50-58 [PMID: 8703630 DOI: 10.1093/bja/77.1.50]
28 **Nyman LR**, Wells KS, Head WS, McCaughey M, Ford E, Brissova M, Piston DW, Powers AC. Real-time, multidimensional in vivo imaging used to investigate blood flow in mouse pancreatic islets. *J Clin Invest* 2008; **118**: 3790-3797 [PMID: 18846254 DOI: 10.1172/JCI36209]
29 **Landi F**, Picca A, Calvani R, Marzetti E. Anorexia of Aging: Assessment and Management. *Clin Geriatr Med* 2017; **33**: 315-323 [PMID: 28689565 DOI: 10.1016/j.cger.2017.02.004]
30 **Rahman A**, Jafry S, Jeejeebhoy K, Nagpal AD, Pisani B, Agarwala R. Malnutrition and Cachexia in Heart Failure. *JPEN J Parenter Enteral Nutr* 2016; **40**: 475-486 [PMID: 25634161 DOI: 10.1177/0148607114566854]
31 **Szuszkiewicz-Garcia MM**, Davidson JA. Cardiovascular disease in diabetes mellitus: risk factors and medical therapy. *Endocrinol Metab Clin North Am* 2014; **43**: 25-40 [PMID: 24582090 DOI: 10.1016/j.ecl.2013.09.001]
32 **Steyers CM**, Miller FJ. Endothelial dysfunction in chronic inflammatory diseases. *Int J Mol Sci* 2014; **15**: 11324-11349 [PMID: 24968272 DOI: 10.3390/ijms150711324]
33 **Ammann R**, Sulser H. ["Senile" chronic pancreatitis; a new nosologic entity? Studies in 38 cases.

Indications of a vascular origin and relationship to the primarily painless chronic pancreatitis]. *Schweiz Med Wochenschr* 1976; **106**: 429-437 [PMID: 772803]
34 **Nagai H**, Ohtsubo K. Pancreatic lithiasis in the aged. Its clinicopathology and pathogenesis. *Gastroenterology* 1984; **86**: 331-338 [PMID: 6690361 DOI: 10.1016/0016-5085(84)90419-0]
35 **Aquilani R**, Opasich C, Verri M, Boschi F, Febo O, Pasini E, Pastoris O. Is nutritional intake adequate in chronic heart failure patients? *J Am Coll Cardiol* 2003; **42**: 1218-1223 [PMID: 14522484 DOI: 10.1016/s0735-1097(03)00946-x]

World Journal of Gastroenterology

Submit a Manuscript: https://www.f6publishing.com

World J Gastroenterol 2019 November 28; 25(44): 6571-6578

DOI: 10.3748/wjg.v25.i44.6571

ISSN 1007-9327 (print) ISSN 2219-2840 (online)

CASE REPORT

Primary gastric melanoma: A case report with imaging findings and 5-year follow-up

Jian Wang, Fang Yang, Wei-Qun Ao, Chang Liu, Wen-Ming Zhang, Fang-Yi Xu

ORCID number: Jian Wang (0000-0003-1194-9046); Fang Yang (0000-0003-0688-5690); Wei-Qun Ao (0000-0001-5496-4559); Chang Liu (0000-0001-7374-0972); Wen-Ming Zhang (0000-0002-6494-4575); Fang-Yi Xu (0000-0002-2791-8941).

Author contributions: Wang J and Ao WQ designed the study; Yang F and Liu C performed the research; Zhang WM and Xu FY analyzed the data; Wang J and Ao WQ wrote the manuscript; Ao WQ revised the manuscript.

Supported by the Medical Health Science and Technology Project of Zhejiang Province (2019RC028).

Informed consent statement: Written informed consent was obtained from the patient for publication of this report and any accompanying images.

Conflict-of-interest statement: The authors declare that they have no conflicts of interest.

CARE Checklist (2016) statement: The authors have read the CARE Checklist (2016), and the manuscript was prepared according to the CARE Checklist (2016).

Jian Wang, Wei-Qun Ao, Chang Liu, Department of Radiology, Tongde Hospital of Zhejiang Province, Hangzhou 310012, Zhejiang Province, China

Fang Yang, Department of Pathology, Sir Run Run Shaw Hospital, Zhejiang University, Hangzhou 310016, Zhejiang Province, China

Wen-Ming Zhang, Fang-Yi Xu, Department of Radiology, Sir Run Run Shaw Hospital, Zhejiang University, Hangzhou 310016, Zhejiang Province, China

Corresponding author: Wei-Qun Ao, MD, Doctor, Radiologist, Department of Radiology, Tongde Hospital of Zhejiang Province, No. 234, Gucui Road, Hangzhou 310012, Zhejiang Province, China. 78123858@qq.com
Telephone: +86-18758213025
Fax: +86-571-89972025

Abstract

BACKGROUND

Most melanomas identified in the stomach are metastatic; primary gastric melanoma (PGM) is extremely rare, and the relevant studies are relatively scarce. PGM may be incorrectly diagnosed as other gastric malignant tumor types.

CASE SUMMARY

We describe a rare case of PGM confirmed through long-term clinical observation and pathological diagnosis. A 67-year-old woman presented to our hospital with recurrent chest tightness and chest pain. Digital gastrointestinal radiography revealed a circular shadow in the gastric cardia. Computed tomography (CT) revealed a heterogeneous tumor with uneven enhancement. Enlarged lymph nodes were noted in the lesser curvature of the stomach. On magnetic resonance imaging (MRI), T1- and T2-weighted imaging revealed hyperintensity in and hypointensity in the tumor, respectively, both of which increased substantially after uneven enhancement. Near total gastrectomy was performed, and the tumor was pathologically confirmed to be a gastric melanoma. Because no other possible primary site of malignant melanoma was suspected, a clinical diagnosis of PGM was made. The patient was followed for nearly 5 years, during which she received CT reexamination, but no recurrence or metastasis was observed.

CONCLUSION

Certain imaging characteristics could be revealed in PGM. Imaging examination can be of great value in preoperative diagnosis, differential diagnosis, and follow-up of patients with PGM.

Manuscript source: Unsolicited manuscript

Received: September 19, 2019
Peer-review started: September 19, 2019
First decision: November 4, 2019
Revised: November 6, 2019
Accepted: November 13, 2019
Article in press: November 13, 2019
Published online: November 28, 2019

P-Reviewer: de la Serna I, Gavriilidis P
S-Editor: Tang JZ
L-Editor: Wang TQ
E-Editor: Zhang YL

Key words: Gastric tumors; Melanoma; Tomography; X-ray computed; Computed tomography; Magnetic resonance imaging

Core tip: Primary gastric melanoma (PGM) is extremely rare and has rarely been discussed. This report presents a rare case of PGM, along with the relevant digital gastrointestinal radiography, computed tomography, and magnetic resonance imaging findings of PGM, which have been rarely reported thus far. In this case report, the related literature was reviewed so as to explore the imaging features of PGM.

Citation: Wang J, Yang F, Ao WQ, Liu C, Zhang WM, Xu FY. Primary gastric melanoma: A case report with imaging findings and 5-year follow-up. *World J Gastroenterol* 2019; 25(44): 6571-6578
URL: https://www.wjgnet.com/1007-9327/full/v25/i44/6571.htm
DOI: https://dx.doi.org/10.3748/wjg.v25.i44.6571

INTRODUCTION

Melanoma is a malignant tumor that commonly occurs in tissues where melanocytes reside, such as the skin, oropharynx, eyes, meninges, and anal canal, and is rarely found in the esophagus, stomach, or small intestine[1-3]. Most melanomas identified in the stomach are metastatic; primary gastric melanoma (PGM) is extremely rare and has rarely been discussed[4]. PGM may be misdiagnosed as other gastric malignant tumor types because of its nonspecific characteristics[5], so it is not easy to make this diagnosis via clinical or imaging manifestations. This report describes a pathologically confirmed PGM case with long-term clinical observation. Additionally, the characteristics of digital gastrointestinal (GI) radiography, computed tomography (CT), and magnetic resonance imaging (MRI) were analyzed, and relevant studies were reviewed to improve the understanding of PGM and provide diagnostic evidence and reference values for clinical treatment of this malignancy.

CASE PRESENTATION

Chief complaints

A 67-year-old Chinese woman presented to our hospital with recurrent chest tightness and chest pain.

History of present illness

The patient who presented with recurrent chest tightness and chest pain persisting for more than 15 d was admitted to our hospital. The clinical symptoms were characterized as primary distension pain near the xiphoid process without obvious cause. The patient demonstrated no panting, coughing, hemoptysis, hematemesis, or weight loss. The patient could take food normally.

History of past illness

The patient's past medical history included hyperlipidaemia and coronary heart disease for more than 10 years.

Personal and family history

The patient did not have a history of smoking or consuming alcohol, and the patient's family medical history was negative.

Physical examination

Physical examination revealed normal cognition and reflexes, and the patient was cooperative in the examination. No abnormal pigmentation of the skin or sclerae, enlarged superficial lymph nodes, or head deformities were observed. The patient's heart and lungs were normal; the liver and spleen were not palpable.

Laboratory examinations

A laboratory examination indicated that the levels of the tumor markers CA19-9, CA-

153, CA-125, carcinoembryonic antigen, and alpha-fetoprotein were in the normal range. Blood tests for liver and kidney function and electrolyte levels, sternum compression test, and liver, gallbladder, and spleen ultrasound all demonstrated normal results.

Imaging examinations

The patient underwent digital GI radiography, CT, and MRI examinations during hospitalization. Digital GI radiography indicated a 3.8 cm × 3.8 cm circular shadow in the gastric cardia and fundus (Figure 1). A thickened rigid gastric wall with no peristalsis was detected. Thus, radiography data suggested that the tumor was a malignant gastric tumor. CT revealed an iso-or slight low-density tumor in plain scanning (Figure 2A). The tumor had heterogeneous enhancement in the arterial phase (Figure 2B) but persistent enhancement in the portal venous phase (Figure 2C). Enlarged lymph nodes in the lesser curvature of the stomach were detected. MRI revealed a 4.0 cm × 4.0 cm mass in the gastric cardia. The mass exhibited heterogeneous hyperintensity on T1-weighted imaging (T1WI) (Figure 3A) and hypointensity on T2-weighted imaging (T2WI) (Figure 3B), and the lesions displayed hyperintense signal on diffusion-weighted imaging (DWI) when a *b*-value of 800 s/mm^2 was used. There was slightly uneven enhancement during the arterial phase and continuous enhancement on delayed scans (Figure 3D). Based on these results, the presence of melanin was suspected. Therefore, the tumor was suspected to be melanoma. Endoscopic images demonstrated growth of hyperpigmented lesions affecting the cardia and gastric mucosa, causing swelling and congestion. Endoscopic gastric biopsy confirmed the presence of melanoma in the gastric cardia.

TREATMENT

Near total gastrectomy (D2 lymph node dissection and modified laparoscopic Roux-en-Y anastomosis) was performed in October 2014.

Pathological findings

Gross examination of the surgically resected specimens revealed a 4.0 cm × 4.0 cm dark pigmented neoplasm in the gastric cardia. The tumor was raised and ulcerative. Moreover, metastatic black lymph nodes were noted in the lesser curvature of the stomach. Based on the immunohistochemical detection using monoclonal antibodies against oncoproteins, the tumor was HMB45$^+$, S-100$^+$, CK(P)$^-$, MITF$^+$, A103$^+$, and VM$^+$ (Figure 4B and D).

FINAL DIAGNOSIS

Examinations of the skin, eyes, genital tract, paranasal sinus, anus, vulva, and other regions provided normal results, and no suspected malignant melanoma at any other primary site was detected. Therefore, a clinical diagnosis of PGM was made.

OUTCOME AND FOLLOW-UP

During hospitalization, the patient received treatments for infection prevention, bleeding prevention, pain relief, stomach protection, and nutritional support. Postoperatively, the patient recovered well and was discharged from the hospital.

The patient was followed at 20 and 36 mo after the operation in the outpatient department. The patient was doing well physically, with no abnormal findings on physical examination. The patient underwent CT reexamination; whole-body CT revealed no recurrence or metastasis after near total gastrectomy (Figure 5). In August 2019 (at 58-mo follow-up), the patient underwent another CT at a different hospital, the result of which also demonstrated no recurrence or metastasis.

DISCUSSION

Most melanomas identified in the stomach result from a metastatic disease. PGM is extremely rare, with few cases being described thus far. For the diagnosis of a primary malignant melanoma in the GI tract, the following criteria must be fulfilled[6]: (1) Exclusion of any primary sites of melanoma; (2) No unexplained skin tumors or any other extraintestinal metastases of melaonoma; and (3) Absence of any other intestinal

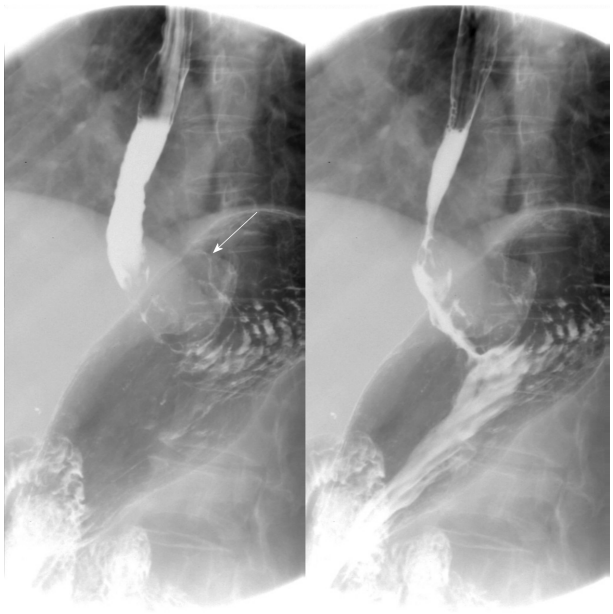

Figure 1 Digital gastrointestinal radiography showed that the tumor was located in the gastric cardia. Thickening and rigidity of the gastric wall with no peristalsis were detected.

mucosal lesions. Gastric melanoma is a rare malignant tumor of the digestive system with a poor overall prognosis and 5-year survival rate of 25%[7]. Late diagnosis and aggressive behavior of mucosal malignant melanoma may contribute to this poor prognosis. Additionally, malignant GI melanoma has predilection of dissemination in early time due to abundant vascular and lymphatic supply of the GI tract[8,9]. The median survival time of primary malignant GI melanoma was 17 mo after operation, whereas that of PGM was only 5 mo[10,11]. Our patient has been followed for nearly 5 years thus far.

Metastatic gastric melanoma are more common than primary ones; PGM are rare in clinic, and the related literature is also relatively scarce[2-5]. Imaging examination is of great value in melanoma diagnosis and reexamination. To date, only three cases have applied CT or MRI examination (Table 1). Bolzacchini *et al*[2] reported a case in which CT and MRI revealed a thickened stomach wall in the lesser curvature of the stomach, and metastasis to the liver and regional lymph nodes. Wang *et al*[11] reported a case of primary advanced esophagogastric melanoma. Digital GI radiography showed a large tumor blocking the esophago-gastric junction. CT revealed a soft mass in the esophagogastric junction with lymph node metastasis in the lesser curvature of the stomach. Yılmaz *et al*[12] reported a PGM case with a synchronous gastric GI stromal tumor, for which CT showed a large, heterogeneous, cystic solid tumor originating from the posterior wall of the stomach. However, digital GI radiography, CT, and MRI results were not reported in the aforementioned cases. Thus, this is the first PGM case report presenting digital GI radiography, CT, and MRI results, along with follow-up records of up to 5 years.

Digital GI radiography revealed that the tumor was located in the gastric cardia, and demonstrated a thickened and rigid gastric wall with an inability to perform peristalsis. These features meet the diagnostic criteria for malignant tumors. CT is an effective method for demonstrating abdominal hollow viscera. In the present case, muscular invasion was observed on CT. The tumor grew with abundant blood supply and demonstrated considerable enhancement in contrast imaging. MRI with a high soft tissue resolution and large field can display gastric tumors and their surrounding structures, observable from all directions. Multiphase dynamic contrast-enhanced MRI can be used to comprehensively evaluate tumor enhancement patterns and characteristics.

Melanoma produces a paramagnetic substance called melanin; melanin-containing melanoma is indicated by hyperintensity on T1WI and hypointensity on T2WI in MRI[1], which is consistent with the patient's results in the present report. PGM is a malignant tumor with abundant blood supply. On DWI, the tumor demonstrated a considerably high signal intensity. In enhanced images, the lesions were notably enhanced. The patient was followed for nearly 5 years, during which she underwent CT reexamination, which revealed no recurrence or metastasis.

Figure 2 Computed tomography images. A: Computed tomography plain scanning revealed an iso-or slight low-density tumor; B: The tumor showed heterogeneous enhancement in the arterial phase; C: Persistent enhancement was found in the portal vein phase.

Thus, digital GI radiography can clearly reveal the shape, location, and size of upper GI tumors. It also can used to dynamically observe gastric wall peristalsis and digestive tract obstruction. Because CT is an effective method for visualizing abdominal hollow viscera, its use in the evaluation of tumor vascularity and invasion-adjacent structures is valuable. CT can be used to evaluate the feasibility of excision of gastric tumors and is a useful and crucial method of monitoring recurrences or metastases during follow-up of patients with PGM. MRI signal intensity can be used to evaluate melanin-containing gastric melanoma. Moreover, MRI can provide additional details that can aid in determining whether a tumor is malignant or benign. Thus, MRI has become the gold standard method for the preoperative diagnosis of melanoma.

CONCLUSION

This report presents a rare case of PGM, along with the relevant digital GI radiography, CT, and MRI findings of PGM, which have been rarely reported thus far. In this case report, the related literature was reviewed so as to explore the imaging features of PGM. This report can be of great value in preoperative diagnosis, differential diagnosis, and follow-up of patients with PGM.

Table 1 Imaging findings of primary gastric melanoma in the literature and our case

Ref.	Modality	Imaging findings
Bolzacchini *et al*[2]	CT, MRI	A thickened stomach wall in the lesser curvature of the stomach, and metastasis to the liver and regional lymph nodes
Wang *et al*[11]	Digital GI radiography	A large tumor blocking the esophago-gastric junction
	CT	A soft mass in the esophago-gastric junction with lymph node metastasis in the lesser curvature of the stomach
Yılmaz *et al*[12]	CT	A large, heterogeneous, cystic solid tumor originating from the posterior wall of the stomach
Our case	Digital GI radiography	A tumor located in the gastric cardia; a thickened and rigid gastric wall with an inability to perform peristalsis
	CT	An iso-or slight low-density tumor in plain scanning, with heterogeneous enhancement in the arterial phase and persistent enhancement in the portal vein phase
	MRI	A mass exhibiting a heterogeneous hyperintensity on T1WI and hypointensity on T2WI; hyperintense signal on DWI; a lesion obviously unevenly enhanced

CT: Computed tomography; MRI: Magnetic resonance imaging; GI: Gastrointestinal; T1WI: T1-weighted imaging; T2WI: T2-weighted imaging; DWI: Diffusion-weighted imaging.

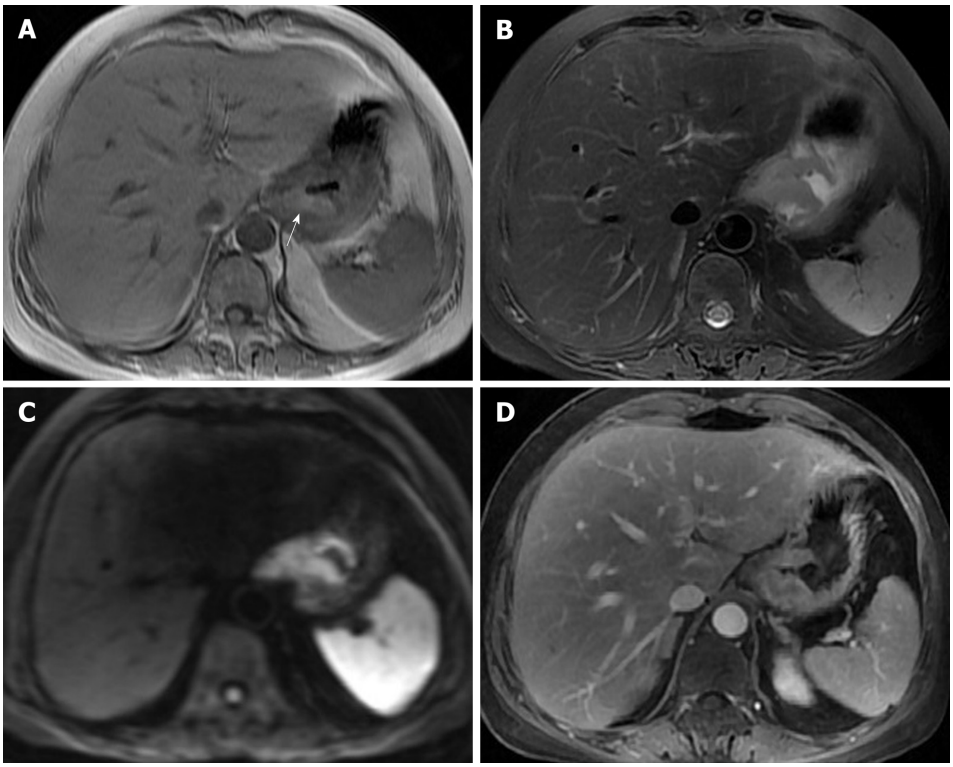

Figure 3 Magnetic resonance imaging images. A: On magnetic resonance imaging (MRI), the mass exhibited a heterogeneous hyperintensity on T1-weighted imaging; B: On MRI, the mass exhibited a heterogeneous hypointensity on T2-weighted imaging; C: Diffusion weighted imaging showed hyperintense signal; D: On enhanced image, the lesion was obviously unevenly enhanced.

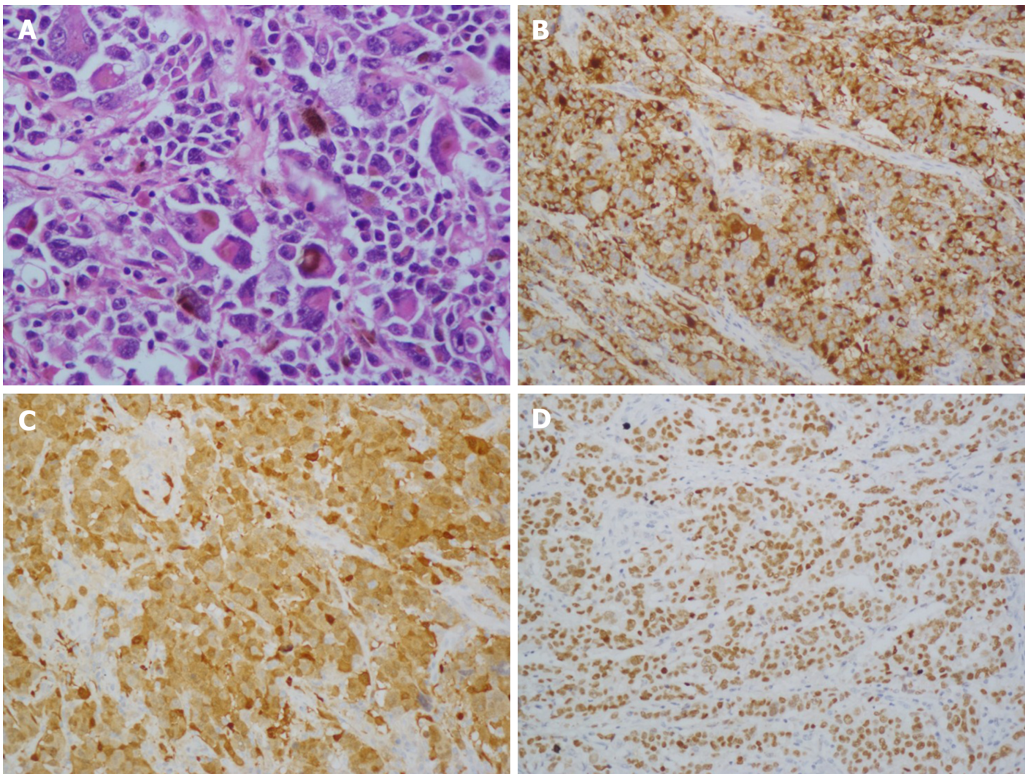

Figure 4 Histological and immunohistochemical images. A: Hematoxylin and eosin staining (× 100) showed that the tumor cells were lymphocyte-like with pigmentation; B-D: Immunohistochemical staining showed that the primary gastric melanoma (PGM) was positive for HMB-45 (B; × 100), S100 (C; × 400), and MITF (D; × 100).

Figure 5 Re-examination 36 mo after total gastrectomy. Computed tomography revealed that no recurrence or metastasis was observed. Surgical sutures were seen (arrow).

REFERENCES

1 **Ao W**, Wang J, Mao G, Yang G, Han X, Jia Y, Cheng Y. Primary hepatic melanoma: A case report of computed tomography and magnetic resonance imaging findings. *Medicine (Baltimore)* 2019; **98**: e16165 [PMID: 31232974 DOI: 10.1097/MD.0000000000016165]
2 **Bolzacchini E**, Marcon I, Bernasconi G, Pinotti G. Primary melanoma of the stomach treated by BRAF inhibitor and immunotherapy. *Dig Liver Dis* 2016; **48**: 974 [PMID: 27158123 DOI: 10.1016/j.dld.2016.04.002]
3 **Augustyn A**, de Leon ED, Yopp AC. Primary gastric melanoma: case report of a rare malignancy. *Rare Tumors* 2015; **7**: 5683 [PMID: 25918612 DOI: 10.4081/rt.2015.5683]
4 **Lamichhane NS**, An J, Liu Q, Zhang W. Primary malignant mucosal melanoma of the upper lip: a case report and review of the literature. *BMC Res Notes* 2015; **8**: 499 [PMID: 26420268 DOI: 10.1186/s13104-015-1459-3]
5 **Goral V**, Ucmak F, Yildirim S, Barutcu S, Ileri S, Aslan I, Buyukbayram H. Malignant melanoma of the stomach presenting in a woman: a case report. *J Med Case Rep* 2011; **5**: 94 [PMID: 21388529 DOI: 10.1186/1752-1947-5-94]

6 **Wong K**, Serafi SW, Bhatia AS, Ibarra I, Allen EA. Melanoma with gastric metastases. *J Community Hosp Intern Med Perspect* 2016; **6**: 31972 [PMID: 27609722 DOI: 10.3402/jchimp.v6.31972]

7 **Chang AE**, Karnell LH, Menck HR. The National Cancer Data Base report on cutaneous and noncutaneous melanoma: a summary of 84,836 cases from the past decade. The American College of Surgeons Commission on Cancer and the American Cancer Society. *Cancer* 1998; **83**: 1664-1678 [PMID: 9781962 DOI: 10.1002/(sici)1097-0142(19981015)83:8<1664::aid-cncr23>3.0.co;2-g]

8 **Castro C**, Khan Y, Awasum M, Belostocki K, Rosenblum G, Belilos E, Carsons S. Case report: primary gastric melanoma in a patient with dermatomyositis. *Am J Med Sci* 2008; **336**: 282-284 [PMID: 18794626 DOI: 10.1097/MAJ.0b013e318159cc21]

9 **Jelincic Z**, Jakic-Razumovic J, Petrovic I, Cavcic AM, Unusic J, Trotic R. Primary malignant melanoma of the stomach. *Tumori* 2005; **91**: 201-203 [PMID: 15948553 DOI: 10.1177/030089160509100219]

10 **Yamamura K**, Kondo K, Moritani S. Primary malignant melanoma of the stomach: report of a case. *Surg Today* 2012; **42**: 195-199 [PMID: 22167480 DOI: 10.1007/s00595-011-0077-5]

11 **Wang L**, Zong L, Nakazato H, Wang WY, Li CF, Shi YF, Zhang GC, Tang T. Primary advanced esophago-gastric melanoma: A rare case. *World J Gastroenterol* 2016; **22**: 3296-3301 [PMID: 27004009 DOI: 10.3748/wjg.v22.i11.3296]

12 **Yılmaz B**, Ekiz F, Altınbas A, Aktaş B, Altıntas S. Synchronous giant gastric gastrointestinal stromal tumor and gastric malignant melanoma. *Endoscopy* 2014; **46** Suppl 1: E574 [PMID: 25409080 DOI: 10.1055/s-0034-1377981]

Published By Baishideng Publishing Group Inc
7041 Koll Center Parkway, Suite 160, Pleasanton, CA 94566, USA
Telephone: +1-925-2238242
E-mail: bpgoffice@wjgnet.com
Help Desk:http://www.f6publishing.com/helpdesk
http://www.wjgnet.com